Modeling and Control of a Cabel Driven Parallel Manipulator Suspended By a Heavy Lift Airship

Fida Ben Abdallah

université PARIS-SACLAY

NNT : 2019SACL009

Thèse de doctorat

Modeling and Control of a Cabel Driven Parallel Manipulator Suspended By a Heavy Lift Airship

Thèse de doctorat de l'Université Paris-Saclay et de l'Ecole Polytechnique de Tunisie
préparée à l'Université d'Evry Val d'Essonne

Ecole doctorale n°580 Sciences et Technologies de l'Information et de la Communication (STIC)
Spécialité de doctorat : Robotique

Thèse présentée et soutenue à Evry, le 12/07/2019, par

FIDA BEN ABDALLAH

Composition du Jury :

Pierre Joli Maître de Conférences HDR à l'Université d'Evry	President du jury
Mohamed Djemai Professeur à l'Université de Valenciennes et Hainaut-Cambrésis	Rapporteur
Mohamed Ali Hammami Professeur à l' Université de Sfax	Rapporteur
Jamel Neji Professeur à l'Ecole Nationale d'Ingénieurs de Tunis	Examinateur
Rabia Sehab Maître de Conférences à l'Ecole Supérieure des Techniques Aeronautiques et de Construction Automobile	Examinatrice
Azgal Abichou Professeur à l'Ecole Polytechnique de Tunisie	Directeur de thèse
Lotfi Beji Maître de Conférences HDR à l'Université d'Evry	Directeur de thèse
Naoufel Azouz Maître de Conférences à l'Université d'Evry	Encadrant

To the memory of my grandmother Jamila
To my dear parents, Mohamed and Farouza
To my sister and my two brothers
To my first beautiful niece, Ella
Withou whom, I am not nothing

"*All truth passes through three stages. First, it is ridiculed. Second, it is violently opposed. Third, it is accepted as being self-evident.*"

Arthur Schopenhauer

Remerciement

Je tiens à exprimer ma sincère reconnaissance à l'ensemble des personnes qui ont participé de près ou de loin à l'élaboration de ce travail. Ces quelques lignes viennent conclure ces quatre années de thèses intenses, pleines d'enseignements, de défis, de difficultés, de joies et de rencontres.

En premier, je remercie très chaleureusement Mme Samia Bouchafa Directrice du laboratoire IBISC pour m'avoir accueilli au sein du laboratoire ainsi que pour son aide et sa disponibilité.

Ensuite, je tiens à adresser mes remerciements aux directeurs de cette thèse, M. Azgal Abichou Professeur à l'école polytechnique de Tunisie et M. Lotfi Beji Maître de conférences HDR à l'université d'Evry, Paris-Saclay pour leurs conseils précieux. Ma reconnaissance va ensuite à mon encadrant M. Naoufel Azouz Maître de conférences à l'université d'Evry, Paris-Saclay pour les nombreuses discussions fructueuses que nous avons eues.

Je remercie M. Pierre Joli, Maître de conférences HDR à l'université d'Evry, Paris-Saclay qui m'a fait l'honneur de présider le jury de soutenance. Je remercie également mes rapporteurs, M. Mohamed Djemai Professeur à l'Université de Valenciennes ainsi que M. Mohamed Ali Hammami Professeur à la faculté des sciences de Sfax pour avoir vaillamment relu ma thèse. De même je remercie M. Jamel Néji Professeur à l'Ecole Nationale d'Ingénieurs de Tunis et Madame Rabia Sehab Maître de conférence à l'ESTACA de Laval pour avoir accepté d'examiner ce travail et faire partie de ce jury.

Cette thèse s'est déroulée dans une ambiance très chaleureuse au sein de laboratoire IBISC. Pour cela, je tiens à remercier également mes amis et collègues doctorants de l'équipe : Majda pour la solidarité, Sara pour nos discussions constructives et son écoute, Yasser pour nos discussions scientifiques. Plus largement, je remercie Rayen, Insaf, Safa, Aylen, Manel, Taha, Suchil, Mohammed et à tous ceux que j'aurais pu oublier pour ces moments de bonne humeur. Tout ça va me manquer ! J'ai eu la chance de pouvoir côtoyer des doctorants et des chercheurs brillants, provenant d'horizons tellement différents. J'espère que nous pourrons nous recroiser dans le futur !

D'une façon plus personnelle, je veux en premier remercier ma famille, qui ont tous aidé à façonner mon chemin et qui m'ont aidé à arriver où j'en suis, pour avoir été ma force durant ces années, et pour avoir toujours été ma lumière au fond du tunnel. Merci à mes chers parents qui ont fait tant de sacrifices pour moi, qui m'ont toujours poussé à donner le meilleur de moi-même et à me dépasser. Je veux aussi remercier ma sœur et mes deux frères, pour m'avoir motivé et encouragé lorsque j'en avais besoin, et que le tunnel semblait ne jamais finir. Merci à mon oncle, qui m'a fait découvrir le monde de la recherche et qui a toujours été là pour me conseiller.

Abstract

In the recent years, researchers have become increasingly interested in the development of radically new and sustainable transportation modes for both passengers and cargo. These challenges have led to study in areas of knowledge that were dormant, such as the potential of using lighter than air aircraft for cargo transportation. The focus of this thesis is the development of a control architecture that can be integrated on autonomous heavy lift airship and thereby enables safe cargo exchange process. Besides, the dynamic model of the heavy lift airship must be clarified before designing a controller. This system makes use of a Cable Driven Parallel Manipulator (CDPM), allowing the airship to load and unload cargo while hovering.

The heavy lift airship is a multi-body systems in which multiple rigid bodies are joined together. During loading and unloading process, the transferred cargo can oscillate due to airship maneuvers. On the other hand, the pendulum-like behavior of suspended load can alter the flight characteristics of the airship. The thesis contributions are presented in two parts. In the first part, we assume that there is no inertial coupling between the airship and CDPM. Hence, our researches concern only the CDPM tacking into account the base mobility at first and then the cable sagging phenomena. The control design should integrate an optimal tension distribution since cables must remain in tension.

In the second part, we address the analysis of the heavy lift airship considering the coupling effect between the suspended payload and the airship. To describe the dynamics coupling, the basic motion of one subsystem is regarded as an external disturbance input for the other one. Hence, the dynamic model of this multi-body system composed of the airship and the CDPM can be modeled as an interconnection of lower order subsystems. We assume that the heavy lift airship is a weakly coupled subsystems. Based on this assumption, we design a decentralized controller, which makes it possible to control the airship and the CDPM independently. Numerical simulation results are presented and stability analysis are provided to confirm the accuracy of our derivations.

Résumé

A l'heure où le monde entier appelle à développer de nouvelles technologies de transport afin de faire face au défi écologique, des projets de dirigeables gros porteurs permettent de relever ce défi. En outre, les dernières avancées technologiques dans le domaine de l'aérospatiale ont permis de résoudre un certain nombre de problèmes responsables de l'hibernation des grands dirigeables pendant plus d'un demi-siècle. Ceci a donné naissance à de nouveaux types de dirigeables gros porteurs.

Dans cette thèse, le modèle dynamique du dirigeable gros porteur est défini afin de concevoir un contrôleur efficient. La particularité du dirigeable présenté est sa capacité de charger et de décharger le fret en vol stationnaire, ce qui permet de réduire l'apport logistique et humain par rapport à des scénarios comportant un atterrissage et permet ainsi l'utilisation de cet engin dans des zones ayant peu ou pas d'infrastructure.

Ce dirigeable est muni d'une grue formée par un robot parallèle à câbles (RPC) permettant d'optimiser le chargement et déchargement. Cette phase étant la plus sensible, car la charge suspendue peut osciller dangereusement notamment sous l'effet du mouvement de dirigeable. Nous avons concentré nos efforts dans cette thèse à l'analyse de cette phase critique. Le dirigeable gros porteur sera représenté par un système multi-corps composé de plusieurs corps reliés entre eux par des articulations.

Les contributions de la thèse sont présentées en deux parties. Dans la première partie, nous supposons qu'il n'y a pas de couplage inertiel entre le dirigeable et le RPC. Ainsi nos recherches ne concernent que le RPC en tenant compte de la mobilité de la base suspendue par des câbles considérés dans un premier temps comme idéaux, puis les phénomènes d'affaissement et de flexibilité des câbles seront pris en compte. La conception de la commande de ce système doit aussi intégrer une répartition optimale de la tension car les câbles doivent à chaque configuration rester tendus.

Dans la deuxième partie, nous abordons l'analyse du système global en considérant l'effet de couplage inertiel entre la charge utile suspendue et le dirigeable. Le modèle dynamique de ce système multicorps formé par le dirigeable et le RPC peut être modélisé comme une interconnexion de sous-systèmes d'ordre inférieur. Nous supposons que le dirigeable gros porteur est un sous-système faiblement couplé. En se basant sur cette hypothèse, un contrôleur décentralisé est proposé permettant de contrôler indépendamment le dirigeable et le RPC. Les résultats des simulations numériques sont présentés et montrent la robustesse de ce contrôleur.

Contents

List of Figures

List of Tables

List of Abbreviations

CDPM	**C**able **D**riven **P**arallel **M**anipulator
MCDPM	**M**obile **C**able **D**riven **P**arallel **M**anipulator
RCDPM	**R**econfigurable **C**able **D**riven **P**arallel **M**anipulator
DOF	**D**gree **O**f **F**reedom
PD	**P**roportional **D**erivative
PID	**P**roportional **I**ntegral **D**erivative
SMC	**S**liding **M**ode **C**ontrol

Nomenclature

We will present here some notations which will be regularly used in this document.

Typeface

italic	Scalar variable
blod	Vector or matrix variable

Subscripts

a	Regarding the airship
p	Regarding the platform
i	Regarding the i^{th} cable
j	Regarding the j^{th} rotor

Operation

$\times$	Cross product
$\dot{()}$	Time derivative relative to a Galilean reference frame
$\mathring{()}$	Time derivative relative to local frame
$()'$	Partial derivative with respect to space

Coordinate systems

$\mathcal{R}_0$	Galilean frame
$\mathcal{R}_A$	Airship body-fixed frame
$\mathcal{R}_P$	Platform body-fixed frame
$\mathcal{R}_i$	Auxiliary frame attached to the i^{th} cable
$\mathcal{R}_j$	Auxiliary frame attached to the j^{th} rotor

A	Gravity center of the airship
B	Buoyancy center of the airship
P	Geometric center of the suspended platform
A_i	Exit cable point for the CDPM
B_i	Attachment cable point for the CDPM
P_i	An arbitrary point along the cable

Matrix

$\boldsymbol{C}$	Centrifugal matrix of the platform w.r.t $\mathcal{R}_0$
$\boldsymbol{C}_P$	Centrifugal matrix of the platform w.r.t $\mathcal{R}_A$
$\boldsymbol{C}_i$	Centrifugal matrix of the i^{th} cable w.r.t $\mathcal{R}_0$
$\boldsymbol{J}$	Jacobian matrix for the conventional CDPM
$\boldsymbol{J}_a$	Transformation matrix for the airship
$\boldsymbol{I}_{P_0}$	Inertia moment matrix of the platform w.r.t $\mathcal{R}_0$
$\boldsymbol{I}_p$	Inertia moment matrix of the platform w.r.t to $\mathcal{R}_P$
$\boldsymbol{I}_m$	Inertia moment matrix of the drums w.r.t to $\mathcal{R}_0$
$\boldsymbol{K}_i$	Stiffness matrix w.r.t $\mathcal{R}_0$
$\boldsymbol{M}_T$	Mass matrix of the airship w.r.t $\mathcal{R}_A$
$\boldsymbol{M}$	Mass matrix of the platform w.r.t $\mathcal{R}_0$
$\boldsymbol{M}_P$	Mass matrix of the platform w.r.t $\mathcal{R}_A$
$\boldsymbol{M}_i$	Mass matrix of the i^{th} cable w.r.t $\mathcal{R}_0$
$\boldsymbol{N}_{ij}$	Diagonal matrix groups cable mode functions $u_{ij}(s,t)$, $v_{ij}(s,t)$ and $w_{ij}(s,t)$
$\boldsymbol{\mathcal{R}}_P^0$	Rotation matrix $(\mathcal{R}_P, \mathcal{R}_0)$
$\boldsymbol{\mathcal{R}}_A^0$	Rotation matrix $(\mathcal{R}_A, \mathcal{R}_0)$
$\boldsymbol{\mathcal{R}}_P^A$	Rotation matrix $(\mathcal{R}_P, \mathcal{R}_A)$
$\boldsymbol{\mathcal{R}}_j^A$	Rotation matrix $(\mathcal{R}_j, \mathcal{R}_A)$
$\boldsymbol{\mathcal{R}}_i^0$	Rotation matrix $(\mathcal{R}_i, \mathcal{R}_0)$
$\boldsymbol{P}_a^{-1}$	Transformation matrix from angular velocities to Euler angles(airship)
$\boldsymbol{S}_a$	Transformation matrix from Euler angles rates to angular velocities (airship)
$\boldsymbol{S}_p$	Transformation matrix from Euler angles rates to angular velocities (platform)
$\boldsymbol{W}$	Force transmission matrix for conventional CDPM
$\boldsymbol{W}_P$	Force transmission matrix for mobile CDPM
$\boldsymbol{W}_m$	Force transmission matrix for CDPM with non-negligible cable mass and elasticity
$\boldsymbol{W}_\rho$	Matrix groups the n_c transmission matrices $\boldsymbol{\Psi}_{P_i}$

Vector

$\boldsymbol{a}_{i0}$	Position of the exit point A_i expressed in $\mathcal{R}_0$
$\boldsymbol{a}_i$	Position of the exit point A_i expressed in $\mathcal{R}_A$
$\boldsymbol{b}_i$	Position of the attachment point B_i expressed in $\mathcal{R}_P$
$\boldsymbol{D}_P$	Disturbance vector due to airship motion
$\boldsymbol{E}_d$	Disturbance vector due to platform motion
$\boldsymbol{e}_1, \boldsymbol{e}_2, \boldsymbol{e}_3$	Inertial frame unit vectors

$\boldsymbol{F}_e$	External wrench acting on the platform geometric center P
$\boldsymbol{f}_{ext}$	External force acting on the platform geometric center P
$\boldsymbol{f}_g$	Gravitational force of the i^{th} cable
$\boldsymbol{f}_i$	Cable force applied on the point P_i
$\boldsymbol{f}_j$	Propulsion force of each rotor
$\boldsymbol{f}_{pro}$	Resultant propulsion force acting on the airship gravity center A
$\boldsymbol{f}_{wb}$	Gravitational and buoyancy force acting on the airship gravity center A
$\boldsymbol{f}_a$	Aerodynamic force acting on the airship gravity center A
$\boldsymbol{f}_c$	Cable force acting on the airship gravity center A
$\boldsymbol{f}_p$	Cable force acting on the the platform geometric center P
$\boldsymbol{G}$	Gravitational force vector of the platform
$\boldsymbol{m}_{ext}$	External moment acting on the platform geometric center P
$\boldsymbol{m}_j$	Propulsion moment of each rotor
$\boldsymbol{m}_{pro}$	Resultant propulsion moment acting on the airship gravity center A
$\boldsymbol{m}_{wb}$	Gravitational and buoyancy moment acting on the airship gravity center A
$\boldsymbol{m}_a$	Aerodynamic moment acting on the airship gravity center A
$\boldsymbol{m}_c$	Cable moment acting on the airship gravity center A
$\boldsymbol{m}_p$	Cable force moment on the the platform geometric center P
$\boldsymbol{l}_i$	Vector along $\overrightarrow{A_iB_i}$
$\dot{\boldsymbol{l}}$	Linear velocity vector of cables
$\boldsymbol{p}$	Position vector of the point P expressed in $\mathcal{R}_A$
$\boldsymbol{q}_{ij}$	Vector groups cable mode coordinate functions $u_{ij}(s,t)$, $v_{ij}(s,t)$ and $w_{ij}(s,t)$
$\boldsymbol{Q}$	Vector of Coriolis and centrifugal terms for the airship
$\boldsymbol{r}_i$	Position vector the point P_i expressed in $\mathcal{R}_0$
$\boldsymbol{t}_i$	Cable tension in the attachment point B_i
$\boldsymbol{T}$	Vector groups the n_c cables tension t_i
$\boldsymbol{T}_\rho$	Vector groups the n_c cables tension component t_{i_x} and t_{i_z}
$\boldsymbol{u}$	Control vector input of the airship
$\boldsymbol{u}_i$	Unit vector of $\boldsymbol{l}_i$ expressed in $\mathcal{R}_A$
$\boldsymbol{v}$	Linear velocity of the point P w.r.t $\mathcal{R}_A$ expressed in $\mathcal{R}_A$
$\boldsymbol{v}_i$	Unit vector of $\boldsymbol{l}_i$ expressed in $\mathcal{R}_0$
$\boldsymbol{\eta}_1^a$	Position of the point A expressed in $\mathcal{R}_0$
$\boldsymbol{\eta}_2^a$	Orientation of the frame $\mathcal{R}_A$ with respect to $\mathcal{R}_0$
$\boldsymbol{\eta}^a$	Generalized coordinate of the airship expressed in $\mathcal{R}_0$
$\boldsymbol{\nu}_1^a$	Linear velocity of the airship w.r.t $\mathcal{R}_0$ expressed in $\mathcal{R}_A$
$\boldsymbol{\nu}_2^a$	Angular velocity of the airship w.r.t $\mathcal{R}_0$ expressed in $\mathcal{R}_A$
$\boldsymbol{\nu}^a$	Generalized coordinate of the airship expressed in $\mathcal{R}_A$
$\boldsymbol{\omega}_a$	Angular velocity of the airship w.r.t $\mathcal{R}_0$ expressed in $\mathcal{R}_0$

$\boldsymbol{\eta}^a$	State vector of the airship
$\dot{\boldsymbol{\chi}}_a$	Airship twist vector expressed $\mathcal{R}_0$
$\boldsymbol{\eta}_1^p$	Position of the point P expressed in $\mathcal{R}_0$
$\boldsymbol{\eta}_2^p$	Orientation of the frame $\mathcal{R}_P$ w.r.t $\mathcal{R}_0$
$\boldsymbol{\eta}^p$	Generalized coordinate of the platform expressed in $\mathcal{R}_0$
$\boldsymbol{\nu}_1^p$	Linear velocity of the platform w.r.t $\mathcal{R}_0$ expressed in $\mathcal{R}_A$
$\boldsymbol{\nu}_2^p$	Angular velocity of the platform w.r.t $\mathcal{R}_0$ expressed in $\mathcal{R}_A$
$\boldsymbol{\omega}_p$	Angular velocity of the platform w.r.t $\mathcal{R}_0$ expressed in $\mathcal{R}_0$
$\dot{\boldsymbol{\chi}}_p = [\dot{\boldsymbol{\eta}}_1^p, \boldsymbol{\omega}_p]^T$	Suspended platform twist vector expressed in $\mathcal{R}_0$
$\ddot{\boldsymbol{\chi}}_p = [\ddot{\boldsymbol{\eta}}_1^p, \dot{\boldsymbol{\omega}}_p]^T$	Absolute acceleration of the point P expressed $\mathcal{R}_0$
$\boldsymbol{\Theta}$	Orientation of the frame $\mathcal{R}_P$ w.r.t $\mathcal{R}_A$
$\boldsymbol{\omega}$	Angular velocity of the platform w.r.t $\mathcal{R}_A$ expressed in $\mathcal{R}_P$
$\mathring{\boldsymbol{\chi}} = [v, \boldsymbol{\omega}]^T$	Relative velocity of the point P w.r.t $\mathcal{R}_A$
$\mathring{\overset{\circ}{\boldsymbol{\chi}}} = [\mathring{\boldsymbol{v}}, \mathring{\boldsymbol{\omega}}]^T$	Relative acceleration of the point P w.r.t $\mathcal{R}_A$
$\boldsymbol{\varphi}$	Joint position vector of engine rotation angle
$\boldsymbol{\Gamma}$	Engine torque input vector acting on the winches
$\boldsymbol{\tau}_{cab}$	Resultant cable wrench acting on the airship gravity center A
$\boldsymbol{\tau}_{pro}$	Resultant propulsion wrench acting on the airship gravity center A
$\boldsymbol{\tau}_{wb}$	Gravitational and buoyancy wrench acting on the airship gravity center A

Scalar

B_u	Airship buoyancy
d_i	Radius of the drum
E	Young's modulus
f_i	Magnitude of cable tension
g	Gravitational acceleration
I_i	Inertia moment of the i^{th} drum
I	kinetic moment of the i^{th} drum
m	Mass of the platform with the load
m_a	Mass of the airship
n	Number of platform degree of freedom
n_c	Number of driving cables
N	Number of modes for each cable
l_i	Cable length
l_{0_i}	Unstrained cable length
T_{tot}	Total kinetic energy
T_a	Kinetic energy of the airship
T_P	Kinetic energy of the platform
t_i	Cable tension at the attachment point B_i

t_{i_x}	Component of the cable tension along x-axis
t_{i_z}	Component of the cable tension along z-axis
S	Cross section area
s_i	Coordinate in the strained cable profile
s_{0_i}	Coordinate in the unstrained cable profile
$\mathcal{V}$	Volume of airship careen
ρ	Mass of cable per unit length
ρ_{air}	Density of the air
φ_i	Angular rotation of the i^{th} cable
ξ_i	Exit position of the i^{th} cable
ε	Deformation of the cable
τ_i	Engine torque

Chapter 1

Introduction

Contents

1.1 Background and Research Motivation

The development of radically new and sustainable transportation modes for both passengers and cargo is absolutely necessary. Actually, more than two-thirds of the world's land area and more than half of the world's population do not have direct access to paved roads or airways so for centuries they have remained isolated. This lack of infrastructure and current environment problem present numerous challenges for the worldwide. The search for an alternative heavy-lifting vehicle on land or sea becomes a priority for many countries. Take the example of Canada, approximately 70 percent of its surface area is inaccessible most of the year. Airplanes and all-weather roads are the only means of transport in Northern Canada. As a result, these transportation and logistics barriers negatively impact on the residents of these regions. For example, the cost of food in the remote communities is 2.5 to 3 times higher than the cost of food in the urban areas of Canada due to the lack of low-cost and reliable freight transport service. Furthermore, the mining industry faces many logistic challenges in remote areas.

In order to transport heavy loads in a precautionary way, the study and development of economical and environmentally friendly air vehicles becomes a priority. One such new transportation system that uses clean and efficient energy are cargo airships, called heavy-lift airship. With unlimited access to isolated locations around the globe, heavy-lift airship enables affordable and safe delivery of cargo that is too heavy for helicopters or too difficult

to transport by land or sea without forward infrastructure or manpower required. Heavy lift airship also burns much less fuel than conventional aircraft. For many projects, the combination of these capabilities makes heavy lift airship the best economic choice and an environmentally friendly alternative to traditional modes of transportation. Many research are conducted to study the airship industry and its enabling technologies. This research effort results in a comprehensive insight to date into the development of a new generation of cargo airships that have the potential to reduce economic barriers for both remote communities and mines.

1.1.1 Advantage of Cargo Airship

The potential for cargo airships to replace conventional heavier-than-air vehicles such as fixed-wing aircraft and helicopters as a lower cost and more sustainable form of air transport is stimulating research. There are several reasons that such cargo airship appears attractive for both civil and military heavy lift application:

High energy efficiency

The inherent nature of airship technology makes it more environmentally sustainable. An airship has the advantage of not requiring large amount of fuel to lift cargo. As a buoyant aircraft, an airship requires only energy for propulsion to move through the air unlike others aircraft that need about half of fuel consumed to just keep the vehicle aloft. For an airship what sustains weight is the physical property of helium gas buoyancy. The engines are only used to drive horizontal shifts. The airship reduces greenhouse gas emissions by up to 90 percent compared to fixed-wing freighters. The resurgence of airships comes as the balance between rapid transportation and lower tax rates. In fact, few products need to be transported at 500 miles per hour and few shippers can afford to pay the costs of jet transport.

Long range and large payload capacity

The vertical takeoff and landing capabilities give the cargo airship an additional advantage over other means of transporting heavy loads. Buoyant lift does not lead to inherent limitations on payload capacity as does dynamic lift. The airship gains one kilogram of lift for every cubic meter of air displaced by a lighter lifting gas. A heavy lit airship can transport several 40 ft cargo containers, offering complementary solutions to current transportation demands and creating delivery solutions that were once previously nonexistent. Due to its long range and large payload capability, the airship is particularly attractive for applications requiring the transport of equipment over land or sea areas that are beyond the range of helicopter. The airship is a paradigm shift for freight transportation in the ice-roads region of northern Canada, possibly as a land bridge across such continents as Africa or as a supply aircraft for all shore activities.

Low cost for infrastructure

Airship basically needs anchoring and gas supply systems to manage the ascent and descent. An airship achieves lift by the displacement of air with lighter than air gas which needs only a prior installation of ballast equipment and mooring towers. Unlike fixed-wing aircrafts which require airports with an extensive runway, airship needs smaller and less sophisticated infrastructure. Its vertical take-off and landing skills eliminate the need for large teams and maneuver infrastructure.

Employing transport airships as part of a multi-modal cargo transportation system reduces freight costs. This benefit is enormous for humanitarian relief operations and developments project in remote areas that rely on air cargo. Nevertheless, one of the drawbacks of airships is the slow speeds in transporting goods across continent compared to heavier-than-air vehicles such as fixed-wing aircraft and helicopters.

1.1.2 Current and Developing Cargo Airship

Modern cargo airships incorporate the latest aeronautical and aerospace technology such as avionics, weather radar, high tech materials (e.g. carbon fiber and light weight materials for the airship skin). The right combination of these technologies creates a mode of freight transportation with significant comparative advantages over rail, air and maritime transportation.

FIGURE 1.1: Cargolifter airship : CL 160

The use of the lighter-than-air vehicle for cargo transport was resumed in 1996 with the CL 160 airship. The latter is designed by the Germany company Cargolifter and can carry 160 tons [1]. Described as a "flying crane", the CL 160 hovers at about 100 m above the ground and a special loading frame, which is fixed during flight to the keel of the airship, is then rigged with four cable winches to the ground. This new and specially developed technology allows the airship to load and unload heavy cargo without touching the ground and almost independently of local infrastructure (See Figure 1.1). Amazon has filed a patent

for flying warehouses that could use a fleet of drones to make deliveries to customers [2]. This flying warehouses is an airship that remains at a high altitude and drones have to pick up items from the airship bay and deliver them to customers. Like Cargolifter and Amazon, several companies are planning to have an operating cargo airship within a few short years.

Flying Whales : The French company Flying Whales will pick up with the LCA60T, a revolutionary cargo airship with a capacity of 60 tons and a length of 150 meters. The cargo is stowed in a cargo hold that is 75 meters long, 8 meters high, and 8 meters wide or suspended by crane. The heavy-lift airship concept is currently being prepared for the market in France and China and is expected to lift off in 2021.

Lockheed Martin Corporation : Lockheed Martin is an American aerospace, defense, security and advanced technologies company with worldwide interests. It is one of the largest and most well-resourced company developing cargo airship technology [3]. More than ten years ago, the Lockheed Martin's team built and flew the technology demonstrator known as the P-791 airship. This cargo airship is a non-rigid hybrid design that depends on aerodynamic lift for buoyancy control. The military canceled the project and Lockheed Martin rebranded the P-791 as SkyTug for civil cargo hauling and sold it to Canadian oil companies. Based on the technology demonstrated by the P-791, Lockheed Martin launched in partnership with Hybrid Enterprises the commercial LMH-1 hybrid airship, scheduled to operate in 2019. A photo of the LMH-1 airship is shown in Figure 1.2.

FIGURE 1.2: Lockheed Martin airship : LMH-1

Worldwide Aeros Corporation : Aeros is an American manufacturer of airships based in Montebello, California. After several organizations failed to deliver lighter-than-air hybrid cargo airships on their NASA and DARPA contracts, Aeros came through and delivered the Aeroscraft, with a lift capability of 66 tons [4]. The Aeroscraft prototype

is 79 meters long and 29.5 meters wide. The structures under airship are landing pads, a type of inflated hovercraft skirt. These landing pads allow the airship to rest on ground, water or ice. The company expects to start flight tests in the near future.

Hybrid Air Vehicles : The British company, Hybrid Air Vehicles, is the successor company of a series of corporations founded originally in 1971 by Roger Munk. In June 2010, Hybrid Air Vehicles was awarded a contract with the United States military to design and build a non-rigid hybrid airship, called the Long Endurance Multi-Intelligence Vehicle (LEMV). Despite a successful test flight in August 2012, the LEMV program faced mounting problems such as the vehicle overweight. Hence, the United States military canceled the program in February 2013 and sold the LEMV airship to its original designer. From its LEMV experience, Hybrid Air Vehicles develops the Airlander 50 airship, with a load capacity of 50 tons [5].

Varialift : Varialift Airships Plc is an airship company based in Great Britain. The latter has so far successfully demonstrated and patented their buoyancy control system [6]. An agreement was signed between Varialift and the French Ministry of Defense in 2016. Varialift Manufacturing France SARL was duly set up in November 2016. They are pursuing development of a 50 tons capacity cargo airship, named ARH50 (See Figure 1.3).

FIGURE 1.3: Varialift Airship : ARH50

Augur Aeronautical Center : The Augur Aeronautical Center is a leading Russian company which is operating in the field of designing and producing lighter-than-air vehicles. The ATLANT airship is designed by RosAeroSystem, a subsidiary of the Augur Aeronautical Center. The ATLANT can carry up to 170 tons of payload (depending on model). Further, it can perform non-stop flights to a distance of 5,000 km. The key

feature of the ATLANT airship is its autonomous operation in all flight modes (including takeoff and landing) without ground crew and ground infrastructure.

Airship do Brasil Industria Aeronautica (ABD) : ADB is a Brazilian private equity firm, belonging to Groups Engevix and Bertolini. It is one of the biggest logistics companies in Brazil involved in cargo shipping, storage facilities, road equipment construction and naval dockyard construction. About 80 of Brazil's roads are unpaved. This presents major problem to cargo transporting vehicles. ABD is planning to develop a cargo airship, with a load capacity of 30 tons, to serve their own transportation needs. Available details are sketchy on ABD 3-30 cargo airship.

1.1.3 Challenge Statement

All the aforementioned heavy-lift airships have internal cargo bays to transport their cargo, with the exception of the CL-160 that has a suspended external load frame. This means that airships require a very large operational footprint to load or offload cargo. Hence, the aforementioned heavy-lift airships are ill-suited for logistics operations in a compact area, like those required in over land or sea areas that are beyond the range of the helicopter, limited to handle a suspended payload of up to 20 tons.

Limiting the operational footprint of these heavy-lift airships is a key issue. In order to overcome the existing difficulties, the airship's loading and unloading phase makes use of a cable driven parallel manipulator (CDPM), allowing it to load and unload without touching the ground. The airship hovers above the ground and a special loading frame, which is fixed during flight to the keel of the airship, is then handled with cables winches to the ground. The choice of the CDPM for handling a heavy load is justified by its potential properties such as large workspace capability, reconfigurability and economical structure and maintenance. However, replacing the rigid links by cables introduces many new challenges in the study. Unlike the rigid links, cables can only apply tensile forces and not compressive forces. Dynamic behavior of the cables is another major challenge in mechanical design and control.

The focus of this research is to enable the composed system to execute tasks that cannot be accomplished by the robots individually. Hence, the airship is used for gross motion of the system, while the CDPM is used for loading and unloading phase. With regard to this topic, we are pioneer in this field. Researchers have only proposed some effective dynamic model and control methods for heavy lift helicopter. However, their approaches can not be used for cargo airships for due to the underlying ratio of densities between the airship and the surrounding fluid. The airship aerodynamics resembles that of submarines more than that of helicopter. Consequently, the airship has a slow dynamic characteristic contrary to the helicopter with speed dynamic characteristic.

Expected heavy lift airship gives rise to various technical problems compared to existing aircrafts. The airship mission is the loading and unloading of the heavy load by means of motorized winches while the airship hovers above the ground. In this phase, the cargo airship

is assimilated to a flying crane that constitutes a complicated pendulum system. Furthermore, the suspension system connects both airship and the payload via cables. The flying crane is modeled as a multi-body system consisting of the airship envelope and the suspended CDPM. The modeling and control of this system is a major challenge.

1.2 Literature Review

The relevant literature for this thesis covers two principle areas: the airship and the cable driven parallel manipulator. Firstly, we present a literature survey of studies regarding to main challenges of airship, which are in two main categories: modeling and control. Then, some terminologies and basic theories used in the study of cable robots are explained.

1.2.1 Autonomous Unmanned Airship

An airship is a lighter-than-air aircraft that utilizes both aerodynamic and aerostatic (static buoyancy) lift. Unlike conventional heavier-than-air vehicles such as fixed-wing aircraft and helicopters, whose lift is aerodynamically generated by the motion of an airfoil through the air, airships stay a loft using a light lifting gas. The engines will only be used to drive horizontal shifts. This distinguishing feature can provide them with long endurance, high payload-to-weight ratio and low fuel consumption.

Airship is the first aircraft to enable controlled and powered flight. In 1784, a French aeronautical theorist, Jean Baptiste Meusnier, proposed a design for an airship of ellipsoid form that is fundamentally the basis of all airships now. The invention of the steam powered engine in the 19th century sparked the beginning of the airship industry, as it was capable of providing the power needed for sustained flight. In 1884, the first fully controllable airship was launched by Charles Renard and Arthur Constantin Krebs.

The golden age of airships began with the early twentieth century. The great German Zeppelins were prominent in intercontinental transport and also as war reinforcement in both the First and Second World War. Airships demonstrated that lighter-than-air technology has the endurance and capability to cross oceans and reach remote areas. But the use of airships declined over time as fixed-wing aircraft became more capable and with the occurrence of several airship accidents, including the 1937 burning of the Hindenburg while flying over New Jersey, USA.

Although the golden age of airships had ended for decades, airships slowly started to gain popularity again because people wanted to find an aircraft with low fuel consumption later the oil crisis in 1973. In the past few years, the development of modern techniques, such lightweight material, optimal design, renewable energy technologies and automatic control have occurred. The latest technological advances in the field of aeronautics have solved many problems that have led to the hibernation of airships for close to a mid-century. This makes it suitable for a wide range of applications in commercial, scientific and military fields like

cargo transportation [7], environmental and urban areas monitoring [8], [9], advertising and tourism [10], stratospheric observation [11] and telecommunications [12].

1.2.1.1 Classification of Cargo Airship

The airship is composed of a gondola to carry the payload, a structure and an envelope. A propulsion system is required to stabilize and move the airship in the surrounding air.

1.2.1.1.1 Conventional and Hybrid Airship Buoyancy control is necessary for ascent, descent, and cargo exchange. Airship hovers in air, following Archimedes' principle: a body surrounded by a fluid receives a lift equal to the weight of the displaced fluid. Since the density of the carrying gas within the hull is less than the density of air, the buoyancy force provides an energy-free form of lift. The airship gains one kilogram of lift for every cubic meter of air displaced by a lighter lifting gas. The lifting capacity of an airship is based on a variable volume of lighter than air gases design that depends on using ballonets. The latters are bags inside the envelope into which air is either forced in or out. Ballonets equipped with blowers and air valves are used for the control of internal pressure changes caused by expanding and contracting lifting gas within the airship. While the airship climbs during flight, the atmospheric pressure decreases and the lifting gas inside the envelope expands. The reverse occurs when the airship descends so the atmospheric pressure increases and the lifting gas inside of the hull contracts. Ballonets are required to adapt the pressure because variables such as temperature, altitude, density and atmospheric pressure affect the state of the lifting gas inside the hull of the airship during flight.

There are two types of air vehicles currently operating that use lighter than air gases for lift : conventional airships that use primarily static lift and hybrid airships that combine static lift and aerodynamic lift. Both vehicle types are based on a variable volume of lighter than air gases. Most airship developers have chosen one of two routes to address load exchange and ground handling issues [13] :

1. *Conventional Airship*: The conventional airship has enough buoyancy to lift itself and the cargo. This airship is always lighter than air and require ground crews and equipment to assist during takeoff and landing. The ground crews must also supply and remove ballast, such as sand or water to compensate the cargo weight. Provision of material to balance cargo changes is a non-trivial problem. For instance, water is suggested as an easily available and appropriate materials, yet the problems that can occur in obtaining water for desert operations should be obvious.

2. *Hybrid Airship*: The hybrid airship combines the lift obtained from buoyancy effects, known as static lift, with that coming from airship's aerodynamic shape, characterized as dynamic lift. Although, the combination of lift sources reduces the ground crews and equipment, hybrid airships require runways for takeoff and landing and burn much more fuel than traditional airships compared to conventional airships.

1.2.1.1.2 Structure Recent developments in new materials and superior connection techniques enable the design and construction of airships with high performance. Hence, stronger materials that can accommodate lighter weight designs like composite materials, new plastics and metal alloys are available. Unlike an airplane, the most flexible component of an airship is its hull. Based on the hull structure, airships fall into three main categories [14] :

1. *Rigid Airship*: A rigid airship's shape can be maintained independent of envelope pressure because the envelope is usually supported by a metal structure. The external support structures are composed of a variety of transverse girders forming approximately circular frames and longitudinal girders running through the length. Transverse girders, usually made of aluminum, are connected by longitudinal girders and are cross-braced with pretensioned metal wires for increased structural strength. Rigid airships are usually constructed with a load-bearing frame which allows them to accommodate all sizes and types of cargoes. Rigid airships generate increased difficulties and challenges in construction and manufacturing due to the high cost of tooling and complicated assembly of structures.

2. *Non-Rigid Airship*: In contrast to rigid airship, a non-rigid airship's shape is sustained by a pressure differential between the lifting gas in the hull and the atmosphere. In other words, it does not have an internal metal frame inside of the hull. An envelope, as the gas containment membrane, encloses the lifting gas and the ballonets. The gondola, engines and cargo space are held by a catenary curtain that is suspended internally from the top of the envelope. Non-rigid configurations are especially suitable for small airships. In comparison with rigid airships, the fabrication cost of non-rigid airships is lower and the manufacturing time cycle is shorter. Non-rigid airships have simple structures and are easy to design, build, and maintain. They over come the issue of weight penalty inherent in the use of rigid structures.

3. *Semi-Rigid airship*: Semi-rigid airships require the internal gas pressure within the envelope to maintain their shape in combination with a rigid keel that holds the engines and cargo space. A rigid keel with an aerodynamic shape runs from nose to tail along the bottom surface of the air vehicle. Semi-rigid airships have some characteristics of rigid airships and non-rigid airships since the keel on the bottom acts as a structural member carrying load. The mutual support between keel and envelope is good for resisting and distributing the bending moments.

Rigid airships must be larger than semi-rigid and non-rigid airships to obtain the same useful cargo lift because more lifting gas is required to overcome the dead-weight of their structure. Contrary to rigid airships, semi-rigid and non-rigid airships pressurize the gas within their envelope above the ambient atmosphere. In fact at higher pressures, the tiny molecules of the lifting gas are pushed out of every pinhole and leaky seam. There is an economic trade-off between the increased weight of a rigid airship and the cost of replacing

helium that leaks. Non-rigid, semi-rigid and rigid airships have their specific advantages and disadvantages. In reality the choice of configuration depends on vehicle size, availability of materials and tentative applications.

1.2.1.2 Airship Dynamic Modeling

The resurgence of airships has created a need for accurate dynamics models and simulation capabilities to analyze their flight behavior and to design their control systems. Unlike conventional heavier-than-air vehicles such as fixed-wing aircraft and helicopters, certain solid-fluid interaction forces can not be neglected such as buoyancy and those related to the inertia of the surrounding air called the added-mass force and moment. The added masses phenomenon is well known for airships and similarly for submarines. When an airship moves in an incompressible and infinite inviscid fluid, the kinetic energy of the fluid produces an effect equivalent to an important increase of the mass and the inertia moments of the body.

Besides the aerodynamic forces and the added mass effect, the airship dynamics are influenced by the gravity force, the buoyancy created by the lifting gas and the actuation forces. Both Nahon [15] and Gomes [16] elaborate a complete dynamic model of the airship in the absence of external disturbances. Furthermore, Azinheira et al. [17] incorporate the wind effects into the nonlinear airship equations motion. As a result, a real airship dynamic model is developed to accurately represent the behavior of the aircraft under the effect of atmospheric turbulence and other disturbances. Linear dynamic models are still used for airships nowadays due to their simplicity and the fact that the models can be calibrated by updating the aerodynamic derivatives obtained from wind-tunnel or flight tests.

Numerous of other airship dynamics models are presented in the literature. Actually, references are categorized into two major topics in this filed: structural analysis of airships and air-structure interaction mainly represented by the added masses phenomena. In the existing airship dynamics models, such as those presented in [18], the aircraft is modeled as a rigid body and the structural flexibility is ignored. However, real airships experience deformations and their structural flexibility can influence the aerodynamic forces and moments. The largest component of a typical modern airship, the hull, is actually an inflated membrane structure. The defection behavior of flexible airships is investigated by using a bending beam model and experiments show that such a model could provide reasonable accuracy [19]. With more recent advances in computational capabilities, finite element analysis has been used for the structural analysis to obtain the static elastic deformation and natural modes. In general, the majority of the above works on flexible airships focus on the computation of their static deformation, stress, aerodynamic forces and natural modes. However, few studies investigated the influence of flexibility on the dynamics characteristics. Bennaceur et al. [20] investigate the motion equations of a flexible airship with a particular focus on the effects of deformation on the inertial force. However, their formulation is limited by assuming the air to be a potential fluid. The use of Lagrangian approach in the dynamic analysis of flexible structures leads to complex relationships when describing deformations and stresses. An

updated Lagrangian method is developed for deformable bodies in large displacements of translation and rotation [21]. The resolution of the dynamic problem is incremental. Body configuration and motion are identified using a moving reference pattern representing the position of the deformable body in the previous step. In the same sense Azouz et al. propose, as a reference configuration, a rigid configuration of the airship that follows the movement of the deformable body without coinciding with it [22]. The disadvantage of this approach is the computation time which seems important to control the system in real time.

1.2.1.3 Airship Control

One of the most important feature of an autonomous airship is its capacity to accomplish different type of tasks with a high level of performance, maneuverability and with less oversight of human operators. The existence of two radically different modes of flight (aerostatic versus aerodynamic flight) complicate the autonomy (control) in addition to the large variability of the models during the different phases of flight (take off, cruise flight, landing). Another challenge stems from the fact that the airship often has parametric uncertainties and external disturbances.

A linearized airship model is introduced as a solution to provide airships with autonomous operation capacity. One important result of the linearization approach is the separation of two independent motions : the motion in the vertical plane, named longitudinal, and the motion in the horizontal plane, named lateral. This decoupling allows the design of independent controllers for the two motions. Based on linearized decoupled models of the airship, The LAAS/CNRS autonomous blimp project [23] proposes a global control strategy including hover and aerodynamic flight. It is achieved by switching between four sub-controllers based on linear and back-stepping solutions one for each of the independent flight phases considered, take-off and landing as well as longitudinal and lateral navigation.

The nonlinear dynamics modeling of airship is developed and summarized in a component form by Khoury [24]. For trajectory tracking control, this kind of formulation is useful to apply numerous control methods such as classical PID, feedback linearization, back-steeping approach and sliding mode control. A path following controller for the AURORA airship is designed where the objective is to make the vehicle follows a set of pre-defined points at a given altitude and velocity [25]. The PID controller for the path following regulation problem consists of a classical inner/outer-loop structure. The inner loop controls the airship heading whose reference signal the output of the outer-loop controller. A global approach based on the back-stepping solution guarantees the airship path-tracking. This controller is designed from the airship nonlinear dynamic model taking into account actuator saturation and being robust to wind disturbances. In addition, the authors of [26] use sliding mode control to perform the trajectory tracking task in $3D$ space for an unmanned blimp. The vehicle motion is split into lateral and longitudinal motion then a sliding mode controller is designed for each motion. Moreover, researcher uses a dynamic inversion or feedback linearization approach to achieve robust control in their autonomous airship of the AURORA project [27].

Robustness tests ere conducted in this research in order to study the nonlinear controller performance in the presence of disturbances and model parameter errors. Furthermore, the authors of [28] and [29] propose a nonlinear trajectory tracking control for airship moving at low speed. The algorithm is described using the transformed equations of motion instead of the classical equations. They use the decomposition of the inertia matrix which contains inertial and geometrical parameters of the vehicle already applied in [30]. The main feature of the proposed algorithm is that the dynamical coupling are included in the control gain matrix. As a result, the controller gives fast system response and it ensures the tracking error convergence. Moreover, the authors of [31] propose a predefined path following controller for small robotic airship based on computer vision-based navigation. In order to keep the airship on a predefined track, a fuzzy flight control system is designed where a geometrical methodology can extract information about orientation and position of the airship needed for the control.

1.2.2 Cable Driven Parallel Manipulator

In the recent years, the field of robotics has grown tremendously as a result of both an improved theoretical understanding of these complex systems and rapid technological advances in computation, communication and miniaturization. Robotic manipulators are classified based on their structural topology. A serial manipulator is an open-loop kinematic chain obtained by consecutively connecting different rigid bodies with joints allowing one degree of freedom between two links. Typically, These couplers are generally translational or revolute joints. A popular application for serial robots in today's industry is the pick-and-place assembly robot, called a SCARA robot [32]. On the other hand, a parallel manipulator is a closed-loop kinematic chain mechanism whose end-effector is linked to the base by several independent kinematic chains. These chains are typically referred to as legs or limbs, while the end effector is commonly called the platform. The prototypical example of a parallel manipulator is the Stewart-Gough platform [33]. The latter consists of six prismatic actuators connecting the base to the moving platform. One particular subset of parallel manipulators that has seen considerable recent research interest is cable-driven parallel manipulator [34].

Cable Driven Parallel Manipulators (CDPM), also called Cable Driven Parallel Robots (CDPR) or cable robots are a special class of parallel robots in which the rigid links are replaced by cables. Typical cable robots are formed simply by multiple cables that connect the movable end-effector to the base instead of articulated legs. The position and orientation of the platform depend on the cables length which can be adjusted by winches fixed at remote positions or mounted on mobile bases. Actually, a CDPM is composed of four basic components. A platform or end-effector, which is positioned within a workspace to fulfill a specific task, cables to control and move the platform, winches which change the cable length and a supporting structure upon which these winches are fastened.

1.2.2.1 Classification of CDPM

A general classification of cable-driven parallel manipulators is introduced in [35]. According to the relationship between the number of driving cables (n_c) and the number of degree of freedom of the end-effector (n), two types of CDPMs can be distinguished

Under-constrained CDPMs : under-constrained CDPMs are equipped with a number of cables less than or equal to the number of degrees of freedom ($n_c \leq n$), allowing the control of only n_c end-effector degrees of freedom. In such a system, the platform may move and deviate from its equilibrium position since it can still preserve some level of freedom once the actuators are locked and the cable lengths are fixed. Despite this, under-constrained CDPMs are implemented over several applications such as measurement, rescue, service and rehabilitation operations.

Over-constrained CDPMs : over-constrained CDPMs are equipped with more cables than the number of degrees of freedom ($n_c \geq n + 1$), allowing the control of all degrees of freedom of the moving platform by cable. Compared to under-constrained CDPMs, this cable robot has the ability to increase the usable workspace and reduce the number of singular configurations. Through adding redundant driving cables, payload are redistributed to more cables and the stiffness can be increased. In addition, safety is reinforced by employing redundant cables. However, the rising risk of cable collision can be a major inconvenience of redundant actuated CDPMs. Anti-collision should be paid more attention in the design and trajectory planing. Examples of over-constrained CDPR are the FALCON robot [36] and the KNTU [37].

1.2.2.2 Advantage and Disadvantage of CDPM

Cable-driven parallel manipulators offer a variety of potential advantages over serial and traditional parallel manipulators. Due to its unique configuration, cable robot bears several attractive features which can be summarized as follows

Large workspace : In literature, the CDPM workspace is defined as the set of postures where a force and torque equilibrium can be obtained with cable tensions remaining within a prescribed range (usually between its minimum and maximum). As cables can be easily released and retracted through winches, the workspace ranges from very small to very large areas (from several centimeters to several hundred meters)

Large payload capacity and energy eficiency : Replacement of the heavy prismatic actuators with relatively light cables provides a high payload-to-weight ratios. Furthermore, their relatively low mass and inertial properties facilitate performance at higher dynamics. Thus, CDPM is suitable for high acceleration applications. For serial robots, the energy consumption is high because each actuator must support not only the payload being maneuvered but also the weight of all the subsequent links and actuators.

Indeed, deformations in each link and positioning errors in the joints accumulate towards the end-effector. The CDPM improves upon these shortcomings as the end-effector weight can be distributed through each of the supporting limbs. Hence, the energy consumption is focused on the end-effector movement and CDPM has a greater positioning accuracy.

Simple structure and low cost : Besides the above advantages, the simple structure of CDPM gives rise to a system that is reconfigurable and less expensive to construct and maintain. Another advantage provided by cables consists in the possibility to easily connect and disconnect them to the end effector which makes CDPM easily assembled, disassembled and transported. Thus, CDPM can be designed in extremely large scale within an acceptable cost to meet different requirements/tasks with cheap components and much shorter time.

Despite their numerous advantages, there are several challenges associated with CDPM.

Cable tension analysis : Replacing the rigid links by cables introduces many new challenges in the study. Unlike the rigid links, the unilateral characteristic of the cables (can pull but not push moving platforms) adds complexity to the modeling and analysis of the system. In order to overcome this constraint, it is possible to design CDPMs with a minimum of one degree of actuation redundancy. In addition, the controller design of CDPMs should integrate an optimal tension distribution to keep cable in tension for the whole manoeuvre. Another related problem is the determination of the workspace. The workspace of CDPRs is not only related to the geometric constrain of CDPMs, but also is limited by the cable tensions.

Behavior of cables : Dynamic behavior of the cables is another major challenge in mechanical design and control. In most studies of CDPM, a non-elastic massless cable model is used [38]. The cables are then considered as straight line segments. Thereby, studies become much easier and the model obtained is quite close to reality. Another aspect considers the elasticity along cable axis and assumes cable as massless spring. However, these assumptions are not accurate enough especially for large working volume applications where the cables must withstand large tensions. Thus a non-negligible cable mass must be taken into account to fit well with the real manipulator. This more realistic cable behavior has lead to study the sagging phenomena, aiming to elaborate the model of a cable shape under the effect of its own weight. A related problem is to analyze the static and dynamic stiffness of CDPMs which has a significant effect on their static and dynamic behaviors.

1.2.2.3 Application of CDPMs

The application of cable driven system has risen significantly. Inspired by the Stewart platform, the NIST RoboCrane has the capacity to lift and precisely manipulate heavy loads over

large volumes with fine control in all six degrees of freedom [39]. Recently, a new cable-driven system for transportation of loads in industrial area has been developed which is called CoGiRo [40]. It is the Europe biggest cable robot driven by 8 cables acting in parallel (See Figure 1.4). The load capacity of the CoGiRo can reach 500 kg, while the total mass of the moving parts of the robot including the end-effector and the driving cables is only about 100 kg.

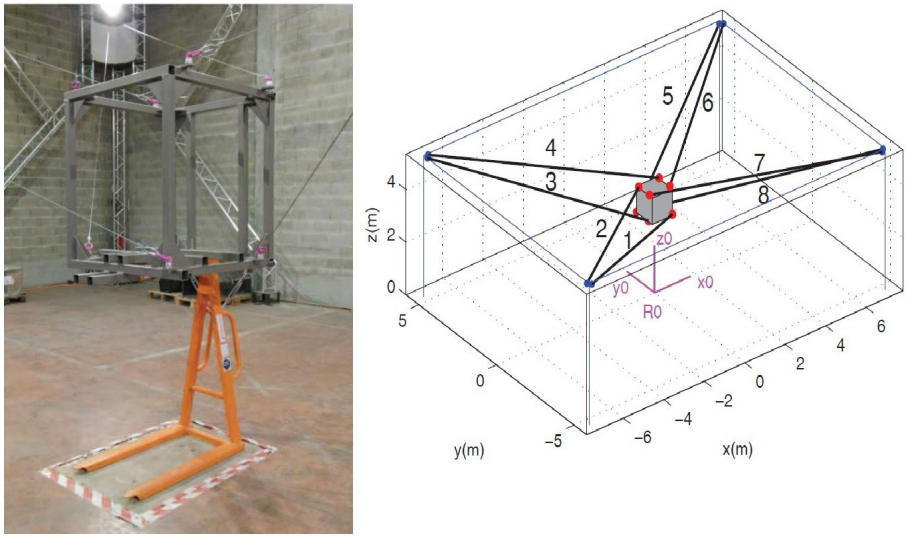

FIGURE 1.4: CoGiRo cable robot

Many researchers have used cable-driven systems to design more efficient medical devices. They are used in rehabilitation and nursing. For example, individuals who are rehabilitating their gait after a stroke could use such a system to help accelerate their recovery. Rosati et al. developed a wire-driven robot for poststroke upper-limb rehabilitation (NeReBot) [41]. Basically, the robot consists of a set of three wires independently driven by three electric motors. The wires are connected to the patient's upper limb by means of a splint and are supported by a transportable frame. By controlling wire length, rehabilitation treatment can help patient in training certain muscle functions in a given workspace.

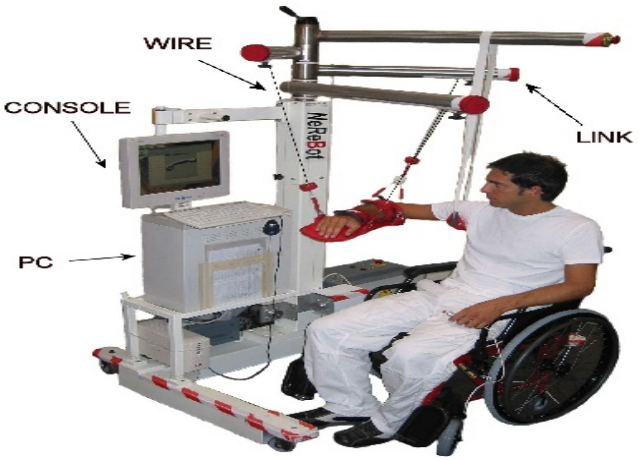

FIGURE 1.5: NeReBot for rehabilitation

Probably the largest planned application for a CDPM is the "Five Hundred Meter Aparture Spherical Telescope" (FAST) to be built in southwest China [42]. As shown in Figure 1.6, The robot consists of a light focus cabin (end-effector) driven by cables and servomechanism plus a parallel robot as secondary adjustable system to carry the most precise parts of the receivers for astronomical observation [43]. This telescope offer astronomers a new window in the sky to study the universe. A rapidly deployable cable robot to augment search and rescue mobile robots is proposed by Merlet [44]. This device can play an important role in rescue operations by providing quickly a heavy lift ability in environment. Pott et al. introduce a family of cable-driven parallel robot called IPAnema that are designed for industrial processes [45]. The last field of applications mentioned is virtual reality simulator where a new cable robot simulator is developed at the Max Planck Institute for Biological Cybernetics [46].

FIGURE 1.6: Five Hundred Meter Aparture Spherical Telescope (FAST)

1.3 Contributions and Thesis Outline

The main objective of this thesis is the development of a control architecture that can be integrated on autonomous heavy lift airship and thereby enables safe cargo exchange process. Besides, the dynamic model of the heavy lift airship must be clarified before designing a controller. The heavy lift airship studied here is composed of a set of rigid solids interconnected by kinematic joints. The work of the heavy-lift airship requires the cooperation of the two subsystems (i.e the airship and cable driven parallel manipulator (CDPM). This novel flying robot is composed of four basic components. (i) A moving platform, which is positioned within a workspace to fulfill a specific task, (ii) cables to control and move the platform, (iii) winches which change the cable length and finally (iv) an airship considered as a supporting structure underneath it these winches are fastened. The modeling of this multi-body system is quite complicated. To make the task less arduous, we have to make some assumptions.

In the first part, we assume that the inertial coupling between the two above subsystems is negligible. For the first case, the airship is controlled at a fixed point. Thus, we limit ourselves to develop the kinematic and dynamic model of a convectional CDPM as well as a robust tracking controller. The second case corresponds to the critical phase where the airship may be subjected to destabilization during hovering. Here, the six-dimensional motions of the airship have a direct impact on handling position of the moving suspended platform connected to the airship via cables. Consequently, we are interested in the modeling and control of a mobile CDPM. For our heavy lift airship, cables have the length of several hundred meters. Therefore, cable mass and elasticity should be included within the models. To better understand the dynamic behavior of CDPM with non-negligible cable mass and elasticity, we investigate this problem latter in 3.

In the second part, the contributions are twofold. First, the dynamic model of this multi-body system is determined by considering the coupling effect between the suspended payload and the airship using Kirchoff equation in 5. Second, the control of this complex system consisting of an airship carrying a payload through a CDPM is a major challenge. The reason is that the systems to be controlled are too large and the problems to be solved are too complex. For this purpose, a decentralized control structure is proposed in 6. The choice of the above control architecture is justified by the weakly coupled of the two subsystems (i.e. airship and cable driven parallel robot) which makes it possible to control the above two subsystems independently. A robust sliding mode control, capable of auto-piloting and controlling the airship, is developed. Furthermore, an inverse dynamic controller is applied to the cable driven parallel robot in order to ensure loading and unloading phase. The feature of the proposed control system, is that the coupled dynamics between the airship and the cable driven parallel robot are explicitly incorporated into control system design, without any simplifying assumption.

The following two parts are divided into chapters.

Chapter 2 This chapter presents the kinematic and dynamic model of both convectional

and mobile CDPM, using Newton-Euler approach. We assume that cables are massless, inextensible and they are always taut. The cables are then considered as straight line segments. This assumption is valid if the ratio of platform to cables masses is large or generally, the compliant displacements of the platform are small. In this preliminary analysis of a mobile CDPM, the suspended platform is taken as the research object and the base motion is regarded as a disturbance. The motion equations show explicitly the interaction between suspended platform and the movable base through cable tensions.

Chapter 3 In this chapter, kinematic and dynamic analysis of large CDPM is addressed, focusing on a more realistic model involving cables with distributed mass and time-varying lengths. For large workspace applications, cables are of relatively large cross-sectional area to withstand a heavy payload and self-weight. The compliance of the driving cables is the major factor that affects the positioning accuracy of CDPM. To solve this problem, the inverse kinematic model is introduced by gathering both the cable catenary equations to the platform static equilibrium equations. This model is used to determine the static pose error of the suspended platform for a given set of unstrained cable lengths. Furthermore, a dynamic structure approach for large CDPM is developed. The dynamic model of the system is characterized by partial differential equations. These equations are converted to a finite number of ordinary differential equations using Ritz's procedure.

Chapter 4 Based on the established dynamic models for CDPM with non-elastic massless cables, a robust trajectory tracking control is developed in this chapter for both conventional and mobile CDPM. The control of the CDPM is not trivial. Compared to parallel robots with rigid arms, the cable forces of a CDPM must be kept in tension in all manoeuvres. This leads to use redundant actuation in order to keep all the driving cables in tension during the CDPM operation. Therefore, the control design must integrate an optimal tension distribution which minimize actuation energy according to the kinematics and dynamic conditions. The stability of the system is analyzed through Lyapunov function. Finally the performance of proposed controller is examined by simulation results.

Chapter 5 This chapter describes the heavy lift airship as a multi-body systems composed of the airship and the suspended CDPM. The dynamic model of this multi-body system can be modeled as an interconnection of lower order subsystems. Specifically, we decompose our system into two isolated subsystems (i.e the airship and the CDPM). By applying Kirchoff equations, we obtain the global dynamic model. The unknown disturbance from the airship motion can be modeled as additive terms in the dynamics of suspended platform and vice-versa.

Chapter 6 In this chapter, a robust control is developed for heavy lift airship. A special focus is done on the critical phase of loading and unloading using CDPM. We assume

that the heavy lift airship is a weakly coupled subsystems. This assumption is exploited to design a decentralized controller, which makes it possible to control the airship and the CDPM independently. In this preliminary study, we chose to apply a sliding mode control to stabilize the airship and a PD computed-torque controller for tracking trajectory during loading and unloading phase. Further, rigorous stability analysis is provided. Finally, numerical simulation results are presented to verify the proposed approach

Chapter 7 Finally, concluding remarks will be given and potential direction for future work will be discussed.

Part I

Modeling and Control of Cable Driven Parallel Manipulator

Chapter 2

Cable Driven Parallel Manipulator with Non-elastic Massless Cables

Contents

2.1 Introduction

A Cable Driven Parallel Robot is a type of parallel manipulator whose rigid links are replaced by cables. The platform motion is generated by an appropriate control of the cable lengths. The platform is manipulated by winches that can extend or retract the cables. These winches may be in fixed locations or mounted on mobile bases. In this chapter we present an introduction to CDPM in order to highlight the different challenges involved with CDPM.

Unlike conventional CDPM with fixed winches, Mobile Cable Driven Parallel Manipulators are a special category of cable driven parallel robots in which the actuators pulling the cables (winches) possess some degrees of freedom to move in space. For both the kinematic and dynamic analyses, the problem can be classified into Conventional CDPM and mobile CDPM. A non-elastic massless cable model is used in this chapter. The cables are then considered as straight line segments.

2.2 Conventional Cable Driven Parallel Manipulator

Most of the past research efforts focus mainly on conventional CDPM. Among them, several studies on large-dimension cable robot have been made. Notable CDPM prototypes which can handle heavy payloads are the early NIST RoboCrane [47], the large dimension CDPM in FAST project [48], [49] , the Marionet crane robot [50] and CoGiRo [51]. The CoGiRo, developed by LIRMM1 and TECNALIA, is a 6-DOF suspended CDPM driven by 8 cables used for the pick-and-place.

The choice of the CDPM for handling a heavy load is justified by its potential properties such as large workspace capability, reconfigurability and economical structure and maintenance. However, replacing the rigid links by cables introduces many new challenges in the study. Unlike the rigid links, cables can only apply tensile forces and not compressive forces. Dynamic behavior of the cables is another major challenge in mechanical design and control. In most studies of CDPM, a non-elastic massless cable model is used [52],[53]. The cables are then considered as straight line segments. Based on numerical and experimental results given in [54], Ottaviano and Castelli prove the suitability of neglecting the cables mass.

2.2.1 Kinematic Modeling

For kinematics model, geometrical property such as positions and its corresponding time derivatives, velocity and acceleration are our concern. The inverse kinematics problem seeks to determine the lengths of the cables given the position and orientation of the suspended platform. However, the reverse calculation leads to the forward kinematic model. The inverse kinematics for parallel structures are easier to compute than the forward kinematics.

2.2.1.1 Jacobian Matrix

In this section, we assume that cables are massless, inextensible and they are always taut which means that the cable forms a perfect straight line between the platform and the base of the CDPM. In order to identify the kinematic relationships between the joint space and the operational space of the system, the following loop-closure equations are developed with corresponding to the i^{th} kinematic chain:

$$\boldsymbol{l}_i = \overrightarrow{A_iB_i} = \boldsymbol{\eta}_1^p + \boldsymbol{\mathcal{R}}_P^0 \boldsymbol{b}_i - \boldsymbol{a}_{i0}, \qquad i \in \{1, 2, ..., n_c\} \tag{2.2.1}$$

For a CDPM having the geometry illustrated in Figure 2.1, there are n_c kinematic closures. In fact, the i^{th} exit point A_i of the cable is connected to a winch whereas the other end is attached to a suspended platform in i^{th} attachment point B_i. $\boldsymbol{l}_i$ is the i^{th} driving cable connecting these two points. The coordinates of n_c exit and attachment points are collected respectively in the vectors $\boldsymbol{a}_{i0}$ and $\boldsymbol{b}_i$. $\boldsymbol{a}_{i0}$ is expressed in the inertial reference frame $\mathcal{R}_0(O, X_0, Y_0, Z_0)$ while $\boldsymbol{b}_i$ is expressed in the platform body-fixed frame $\mathcal{R}_P(P, X_p, Y_p, Z_p)$ having as origin the geometric center of the platform P. We use a parametrization by the

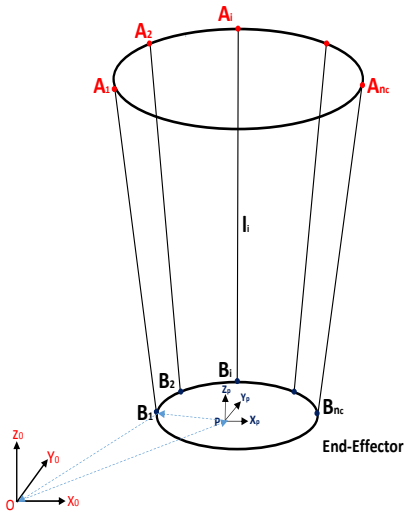

FIGURE 2.1: Representation of the conventional CDPM

Euler angles : yaw, pitch and roll $(\psi_p, \theta_p, \phi_p)$ to describe the suspended platform attitude. $\boldsymbol{\mathcal{R}}_P^0$ is the rotation matrix between the two frames $\mathcal{R}_0$ and $\mathcal{R}_P$:

$$\boldsymbol{\mathcal{R}}_P^0 = \begin{pmatrix} c_{\psi_p} c_{\theta_p} & c_{\psi_p} s_{\theta_p} s_{\phi_p} - s_{\psi_p} c_{\phi_p} & s_{\psi_p} s_{\phi_p} + c_{\psi_p} c_{\phi_p} s_{\theta_p} \\ s_{\psi_p} c_{\theta_p} & c_{\psi_p} c_{\theta_p} + s_{\phi_p} s_{\theta_p} s_{\psi_p} & s_{\theta_p} s_{\psi_p} c_{\phi_p} - c_{\psi_p} s_{\phi_p} \\ -s_{\theta_p} & c_{\theta_p} s_{\phi_p} & c_{\theta_p} c_{\phi_p} \end{pmatrix} \tag{2.2.2}$$

The following shorthand notation for trigonometric function is used: $c_{\theta_p} := \cos\theta_p$, $s_{\theta_p} := \sin\theta_p$, $t_{\theta_p} := \tan\theta_p$. To help the reader to follow modeling of the CDPM, we use standard notations. The italic type indicates a scalar quantity, the boldface indicates a matrix or a vector quantity. The transpose operator is ^{T}. The cross product of two vectors a and b is defined only in three-dimensional space and is denoted by $a \times b$. These notations hold for all the expressions used in this thesis.

Under the established coordinate frames, the generalized coordinates of the suspended platform are expressed by $\boldsymbol{\eta}^p = [\boldsymbol{\eta}_1^p, \boldsymbol{\eta}_2^p]^T$, where the position and orientation of the suspended platform in the inertial frame $\mathcal{R}_0$ can be respectively described by $\boldsymbol{\eta}_1^p = [x_p, y_p, z_p]^T$ and $\boldsymbol{\eta}_2^p = [\phi_p, \theta_p, \psi_p]^T$. Further, we denote by $\dot{\boldsymbol{\chi}}_p = [\dot{\boldsymbol{\eta}}_1^p, \boldsymbol{\omega}_p]^T$ the suspended platform twist (linear and angular velocities) such that the two vectors $\dot{\boldsymbol{\eta}}_1^p = [\dot{x}_p, \dot{y}_p, \dot{z}_p]^T$ and $\boldsymbol{\omega}_p = [\omega_{x_p}, \omega_{y_p}, \omega_{z_p}]^T$ represent respectively the linear and angular velocity of the platform. $\boldsymbol{\omega}_p$ is obtained from the following relation:

$$\boldsymbol{\omega}_p = \begin{pmatrix} c_{\psi_p} c_{\theta_p} & -s_{\psi_p} & 0 \\ s_{\psi_p} c_{\theta_p} & c_{\psi_p} & 0 \\ -s_{\theta_p} & 0 & 1 \end{pmatrix} \begin{pmatrix} \dot{\phi}_p \\ \dot{\theta}_p \\ \dot{\psi}_p \end{pmatrix} = \boldsymbol{S}_p(\boldsymbol{\eta}_2^p)\dot{\boldsymbol{\eta}}_2^p \tag{2.2.3}$$

where $\boldsymbol{S}_p(\boldsymbol{\eta}_2^p)$ is the transformation matrix from Euler angle rates to angular velocities. The relation between $\dot{\boldsymbol{\chi}}_p = [\dot{x}_p, \dot{y}_p, \dot{z}_p, \omega_{x_p}, \omega_{y_p}, \omega_{z_p}]^T$ and $\dot{\boldsymbol{\eta}}^p = [\dot{x}_p, \dot{y}_p, \dot{z}_p, \dot{\phi}_p, \dot{\theta}_p, \dot{\psi}_p]^T$ is:

$$\dot{\boldsymbol{\chi}}_p = \begin{pmatrix} \boldsymbol{I}_{3\times3} & \boldsymbol{0}_{3\times3} \\ \boldsymbol{0}_{3\times3} & \boldsymbol{S}_p(\boldsymbol{\eta}_2^p) \end{pmatrix} \dot{\boldsymbol{\eta}}^p \tag{2.2.4}$$

Note that $[\boldsymbol{\omega}_p]$ is the anti-symmetric tensor corresponding to the cross product associated with $\boldsymbol{\omega}_p$, such that : $\dot{\boldsymbol{\mathcal{R}}}_P^0 = [\boldsymbol{\omega}_p]\boldsymbol{\mathcal{R}}_P^0$.

$$[\boldsymbol{\omega}_p] = \begin{pmatrix} 0 & -\omega_{z_p} & \omega_{y_p} \\ \omega_{z_p} & 0 & -\omega_{x_p} \\ -\omega_{y_p} & \omega_{x_p} & 0 \end{pmatrix} \tag{2.2.5}$$

The Jacobian matrix can be determined by taking the time derivative of each cable length l_i. Note that $\boldsymbol{a}_{i0}$ is the position vector of the exit point of the cable A_i, its derivative with respect to time is zero. Then, we have:

$$l_i^2 = (\boldsymbol{\eta}_1^p + \boldsymbol{\mathcal{R}}_P^0\boldsymbol{b}_i - \boldsymbol{a}_{i0})^T(\boldsymbol{\eta}_1^p + \boldsymbol{\mathcal{R}}_P^0\boldsymbol{b}_i - \boldsymbol{a}_{i0}) \qquad i \in \{1, 2, ..., n_c\} \tag{2.2.6}$$

$$l_i\dot{l}_i = \boldsymbol{l}_i^T(\dot{\boldsymbol{\eta}}_1^p + \dot{\boldsymbol{\mathcal{R}}}_P^0\boldsymbol{b}_i) \qquad i \in \{1, 2, ..., n_c\} \tag{2.2.7}$$

$$l_i\dot{l}_i = \boldsymbol{l_i}^T\dot{\boldsymbol{\eta}}_1^p + \boldsymbol{l}_i^T[\boldsymbol{\omega}_p]\boldsymbol{\mathcal{R}}_P^0\boldsymbol{b}_i \qquad i \in \{1, 2, ..., n_c\} \tag{2.2.8}$$

$$l_i\dot{l}_i = \boldsymbol{l}_i^T\dot{\boldsymbol{\eta}}_1^p + (\boldsymbol{\mathcal{R}}_P^0\boldsymbol{b}_i \times \boldsymbol{l}_i)^T\boldsymbol{\omega}_p \qquad i \in \{1, 2, ..., n_c\} \tag{2.2.9}$$

If we generalize for the n_c cables, the matrix writing becomes:

$$\underbrace{\begin{pmatrix} l_1 & \cdots & 0 \\ \vdots & \ddots & \vdots \\ 0 & \cdots & l_{n_c} \end{pmatrix}}_{\boldsymbol{B}_1} \begin{pmatrix} \dot{l}_1 \\ \vdots \\ \dot{l}_{n_c} \end{pmatrix} = \underbrace{\begin{pmatrix} \boldsymbol{l}_1^T & (\boldsymbol{\mathcal{R}}_P^0\boldsymbol{b}_1 \times \boldsymbol{l}_1)^T \\ \vdots & \vdots \\ \boldsymbol{l}_{n_c}^T & (\boldsymbol{\mathcal{R}}_P^0\boldsymbol{b}_{n_c} \times \boldsymbol{l}_{n_c})^T \end{pmatrix}}_{\boldsymbol{A}_1} \begin{pmatrix} \dot{\boldsymbol{\eta}}_1^p \\ \boldsymbol{\omega}_p \end{pmatrix} \tag{2.2.10}$$

Thus the Jacobian matrix of the system is : $\boldsymbol{J} = \boldsymbol{B}_1^{-1}\boldsymbol{A}_1$. In the case of a conventional CDPM with n_c cables and 6-DOF suspended platform, the Jacobian matrix is:

$$\boldsymbol{J}(\boldsymbol{\chi}_p) = \begin{pmatrix} \frac{1}{l_1}(\boldsymbol{\eta}_1^p + \boldsymbol{\mathcal{R}}_P^0\boldsymbol{b}_1 - \boldsymbol{a}_1)^T & \frac{1}{l_1}(\boldsymbol{\mathcal{R}}_P^0\boldsymbol{b}_1 \times (\boldsymbol{\eta}_1^p - \boldsymbol{a}_1))^T \\ \vdots & \vdots \\ \frac{1}{l_{n_c}}(\boldsymbol{\eta}_1^p + \boldsymbol{\mathcal{R}}_P^0\boldsymbol{b}_{n_c} - \boldsymbol{a}_{n_c})^T & \frac{1}{l_{n_c}}(\boldsymbol{\mathcal{R}}_P^0\boldsymbol{b}_{n_c} \times (\boldsymbol{\eta}_1^p - \boldsymbol{a}_{n_c}))^T \end{pmatrix} \tag{2.2.11}$$

2.2.1.2 Inverse Kinematics

Unlike serial manipulators, inverse kinematics for CDPMs is trivial. The Jacobian matrix $\boldsymbol{J}(\boldsymbol{\chi}_p)$ is defined as the relation between the platform twist $\dot{\boldsymbol{\chi}}_p = [\dot{\boldsymbol{\eta}}_1^p, \boldsymbol{\omega}_p]^T$ and the linear velocities of the driving cables $\dot{\boldsymbol{l}} = [\dot{l}_1, \dot{l}_2, ..., \dot{l}_{n_c}]^T$ such that:

$$\dot{\boldsymbol{l}} = \boldsymbol{J}(\boldsymbol{\chi}_p)\dot{\boldsymbol{\chi}}_p \tag{2.2.12}$$

The n_c motorized winches are used to adjust the cable length. Each winch consists essentially of a movable drum around which a cable is wrapped. In fact any rotation of the drum corresponds to a released or wound cable portion. The relationship between the variation of cable length, δl_i and the variation of motor rotational angle, $\delta\varphi_i$ is:

$$\delta l_i = d_i \delta\varphi_i, \qquad i \in \{1, 2, ..., n_c\} \tag{2.2.13}$$

where d_i is the constant radius of the drum. Let us denote by $\dot{\boldsymbol{\varphi}} = [\dot{\varphi}_1, \dot{\varphi}_2, ..., \dot{\varphi}_{n_c}]^T$ the joint velocity vector of motor rotational angle. The both vectors in operational space $\dot{\boldsymbol{l}}$ and in joint space $\dot{\boldsymbol{\varphi}}$ are connected by the following equation:

$$\dot{\boldsymbol{l}} = \boldsymbol{R}\dot{\boldsymbol{\varphi}} \tag{2.2.14}$$

where $\boldsymbol{R}$ is a diagonal matrix $n_c \times n_c$ defined by $diag(\boldsymbol{R}) = [d_1, d_2, ..., d_{n_c}]^T$. By substituting the equation (2.2.12) into the equation (2.2.14), we obtain the inverse kinematic model:

$$\dot{\boldsymbol{\varphi}} = \boldsymbol{R}^{-1}\boldsymbol{J}(\boldsymbol{\chi}_p)\dot{\boldsymbol{\chi}}_p \tag{2.2.15}$$

2.2.1.3 Forward Kinematics

The forward kinematics can be considered as the dual problem of the inverse kinematics analysis. In fact, this model refers to the determination of position and orientation of the suspended platform given the joint velocity vector of motor rotational angle such that:

$$\dot{\boldsymbol{\chi}}_p = \boldsymbol{J}^+(\boldsymbol{\chi}_p)\boldsymbol{R}\dot{\boldsymbol{\varphi}} \tag{2.2.16}$$

in which, $\boldsymbol{J}^+ = \boldsymbol{J}^T(\boldsymbol{J}\boldsymbol{J}^T)^{-1}$ is the pseudo-inverse of $\boldsymbol{J}$. In general, the forward kinematic produces a coupled nonlinear equations which can result in multiple solutions. This problem is often solved using numerical methods or through the use of additional sensors. Merlet propose interval analysis method to determine several solution for redundant cable robot [55]. Finding all the solutions and selecting one for the system is a problem that is still open today and is not be addressed in this thesis.

2.2.2 Static Modeling

For CDPMs, static analysis becomes essential for proper workspace analysis and control. We assume that the cable is massless and not extensible which means that the cable shape is considered as a straight line. Indeed the tensions, exerted by each cable on the platform at different attachment points B_i, have the same direction as the vector $\overrightarrow{A_iB_i}$. These tensions can be seen as the product between its magnitude, t_i, and the opposite of the corresponding unit vector, named $\boldsymbol{v}_i = \frac{\overrightarrow{A_iB_i}}{\|\overrightarrow{A_iB_i}\|}$. Further, we denoted by $\boldsymbol{F}_e = [\boldsymbol{f}_{ext}, \boldsymbol{m}_{ext}]^T$ the external wrench acting on the suspended platform, where $\boldsymbol{f}_{ext}$ and $\boldsymbol{m}_{ext}$ represent respectively the external force and torque. For suspended platform static equilibrium, the force and torque balance equations are given by:

$$\boldsymbol{f}_{ext} - \sum_{i=1}^{n_c} t_i \boldsymbol{v}_i = 0 \tag{2.2.17}$$

$$\boldsymbol{m}_{ext} - \sum_{i=1}^{n_c} \boldsymbol{\mathcal{R}}_P^0 \boldsymbol{b}_i \times t_i \boldsymbol{v}_i = 0 \tag{2.2.18}$$

Form the loop-closure kinematic equation (2.2.1), we have $\boldsymbol{v}_i = \frac{1}{l_i}(\boldsymbol{\eta}_1^p + \boldsymbol{\mathcal{R}}_P^0 \boldsymbol{b}_i - \boldsymbol{a}_{i0})$. By substituting $\boldsymbol{v}_i$ in the above two equations, we get the suspended platform static equilibrium in matrix form:

$$\boldsymbol{F}_e = \underbrace{-\begin{pmatrix} \frac{1}{l_1}(\boldsymbol{\eta}_1^p + \boldsymbol{\mathcal{R}}_P^0 \boldsymbol{b}_1 - \boldsymbol{a}_1)^T & \cdots & \frac{1}{l_{n_c}}(\boldsymbol{\eta}_1^p + \boldsymbol{\mathcal{R}}_P^0 \boldsymbol{b}_{n_c} - \boldsymbol{a}_{n_c})^T \\ \frac{1}{l_1}(\boldsymbol{\mathcal{R}}_P^0 \boldsymbol{b}_1 \times (\boldsymbol{\eta}_1^p - \boldsymbol{a}_1))^T & \cdots & \frac{1}{l_{n_c}}(\boldsymbol{\mathcal{R}}_P^0 \boldsymbol{b}_{n_c} \times (\boldsymbol{\eta}_1^p - \boldsymbol{a}_{n_c}))^T \end{pmatrix}^T}_{\boldsymbol{W}} \boldsymbol{T} \tag{2.2.19}$$

where the vector $\boldsymbol{T} = [t_1, t_2, ..., t_{n_c}]^T$ is the collection of the n_c cables tension magnitude, t_i and $\boldsymbol{W}$ describes the force transmission matrix. The Jacobian matrix $\boldsymbol{J}$ and the wrench matrix $\boldsymbol{W}$ are essentially the same since one is minus the transpose of the other, such that $\boldsymbol{W} = -\boldsymbol{J}^T$.

Using the principle of virtual work, we obtain the static equilibrium of the CDPM (i.e winches and suspended platform). Let us denote by $\boldsymbol{\Gamma}$ the engine torque input vector that acts on the n_c winches to manipulate the platform via cables used as transmission elements. $\delta\boldsymbol{\varphi}$ represents the virtual displacement vector of motor rotational angle caused by $\boldsymbol{\Gamma}$ whereas $\delta\boldsymbol{\chi}_p$ represents the virtual displacements vector of the suspended platform caused by the external force and moment tensor $\boldsymbol{F}_e$. According to the principle of virtual work, known as D'Alembert's Principle [56], we have:

$$\boldsymbol{\Gamma}^T \delta\boldsymbol{\varphi} + \boldsymbol{F}_e^T \delta\boldsymbol{\chi}_p = 0 \tag{2.2.20}$$

Referring to the kinematic model (2.2.15), the virtual displacements $\delta\boldsymbol{\varphi}$ and $\delta\boldsymbol{\chi}_p$ are related by following relation:

$$\delta\boldsymbol{\varphi} = \boldsymbol{R}^{-1} \boldsymbol{J}(\boldsymbol{\chi}_p) \delta\boldsymbol{\chi}_p \tag{2.2.21}$$

Thus,

$$(\boldsymbol{\Gamma}^T \boldsymbol{R}^{-1} \boldsymbol{J}(\boldsymbol{\chi}_p) + \boldsymbol{F}_e^T)\delta\boldsymbol{\chi}_p = 0 \tag{2.2.22}$$

The above equation holds for any virtual displacement $\delta\boldsymbol{\chi}_p$. Then by eliminating $\delta\boldsymbol{\chi}_p$, we can get $\boldsymbol{\Gamma}^T \boldsymbol{R}^{-1} \boldsymbol{J}(\boldsymbol{\chi}_p) + \boldsymbol{F}_e^T = 0$. By taking transpose of it, yields:

$$\boldsymbol{F}_e = -\boldsymbol{R}^{-1} \boldsymbol{J}^T(\boldsymbol{\chi}_p)\boldsymbol{\Gamma} \tag{2.2.23}$$

It can be shown that the torque input vector $\boldsymbol{\Gamma}$ in joint space are related to the external forces and moments $\boldsymbol{F}_e$ applied on the CDPM suspended platform in operational space. Hence, The statics of cable parallel robot is closely related to the inverse kinematics.

2.2.3 Dynamic Modeling

Using the Newton-Euler approach, the general dynamic model of a CDPM can be divided into two expressions corresponding to the platform dynamics and the dynamics of the n_c winches. These dynamic equations that describe the movement of a CDPM can provide the controller designer with valuable information to design an optimum controller. As already mentioned, we assume that the cables are massless and not extensible. Hence, the cable behavior has no effect.

2.2.3.1 Dynamics of the Actuators

Each winch (actuator) consist of a synchronous servo motor coupled to a planetary gearbox witch is connected to a drum. Winches are usually equipped with a movable drum around it a cable is wrapped. Actually, the engine torque input, τ_i causes the cylindrical drum to rotate by an angle φ_i about its symmetry axis. Then, the rotating drum transmits a tensile force, named t_i, to the cable exit point A_i. Since we assume that cable remains taut during operation this tensile force has the same direction as the vector $\overrightarrow{A_i B_i}$. Applying the Newton-Euler approach, the dynamic equation of the i^{th} winch is:

$$\tau_i = I_i \ddot{\varphi}_i + d_i t_i \tag{2.2.24}$$

where I_i is the inertia moment of the drum, d_i is the constant radius of the drum and $\ddot{\varphi}_i$ is the accelerations of motor rotational angle φ_i. Then we generalize the above equation for the n_c winches, so that we obtain the dynamic model of CDPM actuators given by the following equation:

$$\boldsymbol{\Gamma} = \boldsymbol{I}_m \ddot{\boldsymbol{\varphi}} + \boldsymbol{R}\boldsymbol{T} \tag{2.2.25}$$

The engine torques input vector $\boldsymbol{\Gamma} = [\tau_1, \tau_2, ..., \tau_{n_c}]^T$ that acts on the winches can control all cables length thought tensions $\boldsymbol{T} = [t_1, t_2, ..., t_{n_c}]^T$. Furthermore, $\boldsymbol{I}_m$ is the diagonal inertia moment matrix of drums, such that $diag(\boldsymbol{I}_m) = [I_1, I_2, ..., I_{n_c}]^T$, $\ddot{\boldsymbol{\varphi}} = [\ddot{\varphi}_1, \ddot{\varphi}_2, ..., \ddot{\varphi}_{n_c}]^T$ is the joint accelerations vector of motor rotational angle and $\boldsymbol{R}$ is a diagonal matrix defined by $diag(\boldsymbol{R}) = [d_1, d_2, ..., d_{n_c}]^T$.

2.2.3.2 Dynamics of the Platform

Once the actuators dynamic model is elaborated, we derivate the dynamic model of the CDPM suspended platform by applying Newton-Euler approach. For a CDPM, the position and orientation of the platform depend on the cables length which can be adjusted by motorized winches. The external forces, such as the weight of the platform and its loading, are represented by the vector $mg\boldsymbol{e}_3$ where $\boldsymbol{e}_3$ is a unit vector pointing in the direction of gravity, m is the loaded platform mass and g the gravitational acceleration. The dynamic model of the suspended platform is given by the following relation:

$$m\ddot{\boldsymbol{\eta}}_1^p = mg\boldsymbol{e}_3 - \sum_{i=1}^{n_c} t_i \boldsymbol{v}_i \tag{2.2.26}$$

$$\boldsymbol{I}_{P_0}\dot{\boldsymbol{\omega}}_p + \boldsymbol{\omega}_p \times \boldsymbol{I}_{P_0}\boldsymbol{\omega}_p = -\sum_{i=1}^{n_c} \boldsymbol{\mathcal{R}}_P^0 \boldsymbol{b}_i \times t_i \boldsymbol{v}_i \tag{2.2.27}$$

with $\ddot{\boldsymbol{\chi}}_p = [\dot{\boldsymbol{\eta}}_1^p, \dot{\boldsymbol{\omega}}_p]^T$ is the operational acceleration vector, where $\dot{\boldsymbol{\eta}}_1^p$ and $\dot{\boldsymbol{\omega}}_p$ represent respectively the linear and angular acceleration of the platform in operational space. Remember that for CDPM with massless and not extensible cable, the tensions can be seen as the product between t_i, its magnitude and the corresponding unit vector, named $\boldsymbol{v}_i = \frac{\overrightarrow{A_iB_i}}{\|\overrightarrow{A_iB_i}\|}$. These tensions are collected in the wrench $\boldsymbol{F}_e = -\boldsymbol{J}^T\boldsymbol{T}$ applied at its geometric center P where the vector $\boldsymbol{T} = [t_1, t_2, ..., t_{n_c}]^T$ groups the n_c cables tension t_i and $-\boldsymbol{J}^T$ is the force transmission matrix. $\boldsymbol{I}_{P_0}$ and $\boldsymbol{I}_p$ are the inertia moment matrix of the platform expressed respectively in the inertial reference frame $\mathcal{R}_0$ and platform body-fixed frame $\mathcal{R}_P$, such that $\boldsymbol{I}_{P_0} = \boldsymbol{\mathcal{R}}_P^0 \boldsymbol{I}_p \boldsymbol{\mathcal{R}}_0^P$. The compact dynamic model of the suspended platform is:

$$\boldsymbol{M}(\boldsymbol{\chi}_p)\ddot{\boldsymbol{\chi}}_p + \boldsymbol{C}(\boldsymbol{\chi}_p, \dot{\boldsymbol{\chi}}_p)\dot{\boldsymbol{\chi}}_p = -\boldsymbol{J}^T(\boldsymbol{\chi}_p)\boldsymbol{T} + \boldsymbol{G} \tag{2.2.28}$$

where

$$\boldsymbol{M}(\boldsymbol{\chi}_p) = \begin{pmatrix} m\boldsymbol{I}_{3\times3} & \boldsymbol{0}_{3\times3} \\ \boldsymbol{0}_{3\times3} & \boldsymbol{\mathcal{R}}_P^0 \boldsymbol{I}_p \boldsymbol{\mathcal{R}}_0^P \end{pmatrix}; \quad \boldsymbol{C}(\boldsymbol{\chi}_p, \dot{\boldsymbol{\chi}}_p)\dot{\boldsymbol{\chi}}_p = \begin{pmatrix} \boldsymbol{0}_{3\times1} \\ \boldsymbol{\omega}_p \times \boldsymbol{\mathcal{R}}_P^0 \boldsymbol{I}_p \boldsymbol{\mathcal{R}}_0^P \boldsymbol{\omega}_p \end{pmatrix}; \quad \boldsymbol{G} = [mg\boldsymbol{e}_3, \boldsymbol{0}_{3\times1}]^T$$

$$\boldsymbol{J}^T(\boldsymbol{\chi}_p) = \begin{pmatrix} \frac{1}{l_1}(\boldsymbol{\eta}_1^p + \boldsymbol{\mathcal{R}}_P^0\boldsymbol{b}_1 - \boldsymbol{a}_1)^T & \cdots & \frac{1}{l_{n_c}}(\boldsymbol{\eta}_1^p + \boldsymbol{\mathcal{R}}_P^0\boldsymbol{b}_{n_c} - \boldsymbol{a}_{n_c})^T \\ \frac{1}{l_1}(\boldsymbol{\mathcal{R}}_P^0\boldsymbol{b}_1 \times (\boldsymbol{\eta}_1^p - a_1))^T & \cdots & \frac{1}{l_{n_c}}(\boldsymbol{\mathcal{R}}_P^0\boldsymbol{b}_{n_c} \times (\boldsymbol{\eta}_1^p - \boldsymbol{a}_{n_c}))^T \end{pmatrix}$$

The complete dynamic model is obtained by coupling the two expressions: the dynamic model of the n_c winches (2.2.25) and the dynamic model of the platform (2.2.28):

$$\boldsymbol{\Gamma} = \boldsymbol{I}_m\ddot{\boldsymbol{\varphi}} + \boldsymbol{R}\boldsymbol{T} \tag{2.2.29}$$

$$\boldsymbol{M}(\boldsymbol{\chi}_p)\ddot{\boldsymbol{\chi}}_p + \boldsymbol{C}(\boldsymbol{\chi}_p, \dot{\boldsymbol{\chi}}_p)\dot{\boldsymbol{\chi}}_p = -\boldsymbol{J}^T(\boldsymbol{\chi}_p)\boldsymbol{T} + \boldsymbol{G} \tag{2.2.30}$$

Solving $\boldsymbol{\Gamma}$ from the equation (2.2.29) and substituting into (2.2.30), the resulting expression is not homogeneous. It depends on both operational and joint acceleration vector $\ddot{\boldsymbol{\chi}}_p$ and $\ddot{\boldsymbol{\varphi}}$:

$$\boldsymbol{M}(\boldsymbol{\chi}_p)\ddot{\boldsymbol{\chi}}_p + \boldsymbol{C}(\boldsymbol{\chi}_p, \dot{\boldsymbol{\chi}}_p)\dot{\boldsymbol{\chi}}_p - \boldsymbol{G} = -\boldsymbol{J}^T(\boldsymbol{\chi}_p)\boldsymbol{R}^{-1}(\boldsymbol{\Gamma} - \boldsymbol{I}_m\ddot{\boldsymbol{\varphi}}) \tag{2.2.31}$$

Referring to equation (2.2.15) and by replacing $\ddot{\boldsymbol{\varphi}}$ by $\boldsymbol{R}^{-1}(\boldsymbol{J}(\boldsymbol{\chi}_p)\ddot{\boldsymbol{\chi}}_p + \dot{\boldsymbol{J}}(\boldsymbol{\chi}_p)\dot{\boldsymbol{\chi}}_p)$ in the preceding expression, the complete dynamic model in the operational space becomes:

$$-\boldsymbol{J}^T(\boldsymbol{\chi}_p)\boldsymbol{R}^{-1}\boldsymbol{\Gamma} = \boldsymbol{M}_{eq}(\boldsymbol{\chi}_p)\ddot{\boldsymbol{\chi}}_p + \boldsymbol{C}_{eq}(\boldsymbol{\chi}_p, \dot{\boldsymbol{\chi}}_p)\dot{\boldsymbol{\chi}}_p - \boldsymbol{G} \tag{2.2.32}$$

with

- $\boldsymbol{M}_{eq}(\boldsymbol{\chi}_p) = \boldsymbol{M}(\boldsymbol{\chi}_p) - \boldsymbol{J}^T(\boldsymbol{\chi}_p)\boldsymbol{R}^{-1}\boldsymbol{I}_m\boldsymbol{R}^{-1}\boldsymbol{J}(\boldsymbol{\chi}_p)$.
- $\boldsymbol{C}_{eq}(\boldsymbol{\chi}_p, \dot{\boldsymbol{\chi}}_p) = \boldsymbol{C}(\boldsymbol{\chi}_p, \dot{\boldsymbol{\chi}}_p) - \boldsymbol{J}^T(\boldsymbol{\chi}_p)\boldsymbol{R}^{-1}\boldsymbol{I}_m\boldsymbol{R}^{-1}\dot{\boldsymbol{J}}(\boldsymbol{\chi}_p)$.

2.3 Mobile Cable Driven Parallel Manipulator

Most of the research on payload manipulation via cables focus mainly on two major classes: (i) conventional cable robots with winches fixed in the inertial frame, already presented in the previous section and (ii) towing robots with fixed-length cables on mobile bases. Typically, towing robots is accomplished via cooperative manipulation of a payload suspended via cables by quad-rotors or other unmanned aerial vehicles (UAVs). The use of cables eliminates the need to carry manipulators or grippers on board the quad-rotors, thus allowing to transport heavier objects. Additionally, cables can have a long extension, thus giving more freedom to distribute the quad-rotors. The problem of cooperative aerial transportation has already been addressed in several recent publications. In [57], [58] and [58], quasi-static models have been used to study this problem. However, these approaches are severely limited because they ignore the payload dynamics. In [59], the authors address this limitation by studying the dynamics of cooperative manipulation. The authors prove that the system is differentially flat and give an expression of the flat output, using it, to plan feasible trajectories.

A promising alternative [60] attempts to merge these two approaches together. Thus, the variability of cable lengths is associated to the base mobility. In [61], the authors examined enhancing manipulation capabilities of cable robots by the addition of base mobility to spooling winches (allowing a group of mobile robots to cooperatively manipulate a payload using cables). As a result, cooperating mobile cable robots, called Mobile Cable-Driven Parallel Robots (MCDPRs) becomes a reality. A MCDPR is composed of a conventional CDPR with n_c cables and a n-DOF moving-platform mounted on p mobile bases. The first MCDPR prototype has been designed and built in the context of Echord++ Fastkit project [62]. The targeted application for such MCDPR prototype is logistics. Fastkit addresses an industrial

need for flexible pick-and-place operations while being easy to install, keeping exiting infrastructures and covering large areas. The prototype is composed of eight cables ($n_c = 8$), a six degree-of-freedom moving-platform ($n = 6$) and two mobile bases ($p = 2$).

By appropriately modifying the exit and/or anchor points, the cable robot performance can be improved. In fact, base mobility facilitates the regulation of the tension direction (via active coordination of mobile bases) and allows for better conditioning of the wrench-feasible workspace [63]. However, the idea for introducing mobility into the bases (in the form of gantries, and/or vehicle bases) can significantly enhance the redundancy and complexity into the system which needs to be carefully analyzed and resolved. Some recent works [64] and [65] have considered the static kinematics of MCDPRs, using it to find the optimal actuators configuration according to various metrics. In [66], the developed kinematic model is utilized to determine the available twist set of MCDPRs. It considers the joint velocity limits for cables and the mobile bases. Further in [62], the authors prove that the workspace of the MCDPR depends not only on the tension limits but on the Static equilibrium constraints of the mobile bases. They determine the available wrench set for a planar MCDPR with a point-mass end-effector using both the convex hull and hyperplane shifting method. Then, a new real time tension distribution algorithm is introduced for MCDPRs that takes into account the stability of the mobile bases during the computation of feasible cable tensions [67]. Yet none of these papers fully considers the dynamics of the system showing explicitly the interaction between payload and mobile bases. In this preliminary analysis of a MCDPR, the suspended platform is taken as the research object and the base motion is regarded as a disturbance [68].

2.3.1 Kinematic Modeling

A Mobile Cable Driven Parallel Manipulator is composed of a conventional CDPM with n_c cables and n-DOF moving platform mounted on a mobile base. The kinematic and dynamic analysis of a MCDPM is made with respect to three reference frames (as shown in Figure 2.2), namely an earth-fixed frame $\mathcal{R}_0(O, X_0, Y_0, Z_0)$, a base body-fixed frame $\mathcal{R}_A(A, X_a, Y_a, Z_a)$ having as origin the inertia center of the mobile base A and a platform fixed-frame $\mathcal{R}_P(P, X_p, Y_p, Z_p)$ having as origin the geometric center of the suspended platform P. We use a parametrization by the Euler angles : yaw, pitch and roll $(\psi_a, \theta_a, \phi_a)$ to describe the mobile base attitude. $\boldsymbol{\mathcal{R}}_A^0$ is the rotation matrix between the two frames $\mathcal{R}_0$ and $\mathcal{R}_A$:

$$\boldsymbol{\mathcal{R}}_A^0 = \begin{pmatrix} c_{\psi_a} c_{\theta_a} & c_{\psi_a} s_{\theta_a} s_{\phi_a} - s_{\psi_a} c_{\phi_a} & s_{\psi_a} s_{\phi_a} + c_{\psi_a} c_{\phi_a} s_{\theta_a} \\ s_{\psi_a} c_{\theta_a} & c_{\psi_a} c_{\theta_a} + s_{\phi_a} s_{\theta_a} s_{\psi_a} & s_{\theta_a} s_{\psi_a} c_{\phi_a} - c_{\psi_a} s_{\phi_a} \\ -s_{\theta_a} & c_{\theta_a} s_{\phi_a} & c_{\theta_a} c_{\phi_a} \end{pmatrix} \tag{2.3.1}$$

The following shorthand notation for trigonometric function is used: $c_{\theta_a} := \cos\theta_a$, $s_{\theta_a} := \sin\theta_a$, $t_{\theta_a} := \tan\theta_a$. The general motion of the base can be described by $\boldsymbol{\eta}^a = [\boldsymbol{\eta}_1^a, \boldsymbol{\eta}_2^a]^T$ with

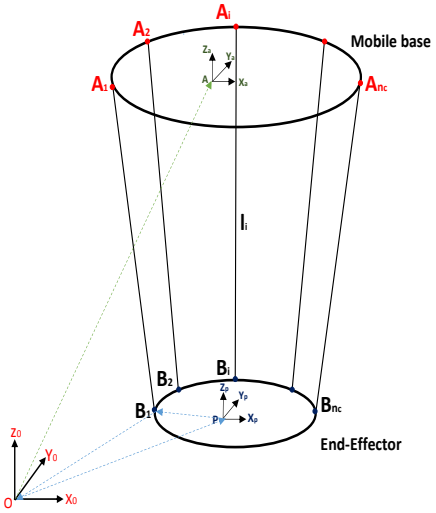

FIGURE 2.2: Representation of the mobile CDPM

respect to the reference frame $\mathcal{R}_0$, where $\boldsymbol{\eta}_1^a = [x_a, y_a, z_a]^T$ and $\boldsymbol{\eta}_2^a = [\phi_a, \theta_a, \psi_a]^T$ denote respectively the position and orientation vector of the base expressed in $\mathcal{R}_0$. The two vectors $\dot{\boldsymbol{\eta}}_1^a = [\dot{x}_a, \dot{y}_a, \dot{z}_a]^T$ and $\boldsymbol{\omega}_a = [\omega_{x_a}, \omega_{y_a}, \omega_{z_a}]^T$ represent respectively the linear and angular velocities of the base with respect to the inertial reference frame $\mathcal{R}_0$. The angular velocity $\boldsymbol{\omega}_a$ can be expressed in terms of Euler angle rates $\dot{\boldsymbol{\eta}}_2^a = [\dot{\phi}_a, \dot{\theta}_a, \dot{\psi}_a]^T$ as follows:

$$\boldsymbol{\omega}_a = \begin{pmatrix} c_{\psi_a} c_{\theta_a} & -s_{\psi_a} & 0 \\ s_{\psi_a} c_{\theta_a} & c_{\psi_a} & 0 \\ -s_{\theta_a} & 0 & 1 \end{pmatrix} \begin{pmatrix} \dot{\phi}_a \\ \dot{\theta}_a \\ \dot{\psi}_a \end{pmatrix} = \boldsymbol{S}_a(\boldsymbol{\eta}_2^a)\dot{\boldsymbol{\eta}}_2^a \tag{2.3.2}$$

The generalized coordinates of the suspended platform are expressed by $\boldsymbol{\eta}^p = [\boldsymbol{\eta}_1^p, \boldsymbol{\eta}_2^p]^T$, where the position and orientation of the suspended platform in the inertial frame $\mathcal{R}_0$ can be respectively described by $\boldsymbol{\eta}_1^p = [x_p, y_p, z_p]^T$ and $\boldsymbol{\eta}_2^p = [\phi_p, \theta_p, \psi_p]^T$. $\boldsymbol{\mathcal{R}}_P^0$ is the rotation matrix between the two frames $\mathcal{R}_0$ and $\mathcal{R}_P$:

$$\boldsymbol{\mathcal{R}}_P^0 = \begin{pmatrix} c_{\psi_p} c_{\theta_p} & c_{\psi_p} s_{\theta_p} s_{\phi_p} - s_{\psi_p} c_{\phi_p} & s_{\psi_p} s_{\phi_p} + c_{\psi_p} c_{\phi_p} s_{\theta_p} \\ s_{\psi_p} c_{\theta_p} & c_{\psi_p} c_{\theta_p} + s_{\phi_p} s_{\theta_p} s_{\psi_p} & s_{\theta_p} s_{\psi_p} c_{\phi_p} - c_{\psi_p} s_{\phi_p} \\ -s_{\theta_p} & c_{\theta_p} s_{\phi_p} & c_{\theta_p} c_{\phi_p} \end{pmatrix} \tag{2.3.3}$$

We denote by $\dot{\boldsymbol{\chi}}_p = [\dot{\boldsymbol{\eta}}_1^p, \boldsymbol{\omega}_p]^T$ the suspended platform twist such that the linear and angular velocity are defined by $\dot{\boldsymbol{\eta}}_1^p = [\dot{x}_p, \dot{y}_p, \dot{z}_p]^T$ and $\boldsymbol{\omega}_p = [\omega_{x_p}, \omega_{y_p}, \omega_{z_p}]^T$ respectively. The angular velocity $\boldsymbol{\omega}_p$ can be expressed in terms of Euler angle rates $\dot{\boldsymbol{\eta}}_2^p = [\dot{\phi}_p, \dot{\theta}_p, \dot{\psi}_p]^T$ as follows:

$$\boldsymbol{\omega}_p = \begin{pmatrix} c_{\psi_p}c_{\theta_p} & -s_{\psi_p} & 0 \\ s_{\psi_p}c_{\theta_p} & c_{\psi_p} & 0 \\ -s_{\theta_p} & 0 & 1 \end{pmatrix} \begin{pmatrix} \dot{\phi_p} \\ \dot{\theta_p} \\ \dot{\psi_p} \end{pmatrix} = \boldsymbol{S}_p(\boldsymbol{\eta}_2^p)\dot{\boldsymbol{\eta}}_2^p \tag{2.3.4}$$

Unlike conventional CDPM with fixed base, a mobile CDPM consists of a suspended platform connected to winches mounted on a mobile base by means of n_c cables acting in parallel. The position of the i^{th} exit point A_i is defined by vector $\boldsymbol{a}_i$ in the local frame fixed to the mobile base $\mathcal{R}_A$, originating from A. The point B_i, where the i^{th} cable is attached to the suspended platform, is defined by vector $\boldsymbol{b}_i$ in platform body-fixed frame $\mathcal{R}_P$, originating from P and $\boldsymbol{l}_i$ is the i^{th} driving cable connecting these two points. The length of the i^{th} cable is denoted by $l_i = \|\overrightarrow{A_iB_i}\|$ and $\boldsymbol{v}_i = \frac{\overrightarrow{A_iB_i}}{\|\overrightarrow{A_iB_i}\|}$ denotes the unit vector along the i^{th} cable. Cables are assumed to be straight and massless. For parallel robot, there are n_c kinematic closures. The vector $\boldsymbol{l}_i$ is expressed in reference frame $\mathcal{R}_0$ as follows:

$$\boldsymbol{l}_i = \overrightarrow{A_iB_i} = \boldsymbol{\eta}_1^p + \boldsymbol{\mathcal{R}}_P^0\boldsymbol{b}_i - \boldsymbol{\eta}_1^a - \boldsymbol{\mathcal{R}}_A^0\boldsymbol{a}_i \qquad i \in \{1,2,...,n_c\} \tag{2.3.5}$$

The kinematic model of mobile CDPM seeks to determine the relationship between the 6-DOF moving platform twists, $\dot{\boldsymbol{\chi}}_p = [\dot{\boldsymbol{\eta}}_1^p, \boldsymbol{\omega}_p]^T$ and both the linear velocities of the driving cables, $\dot{\boldsymbol{l}} = [\dot{l}_1, \dot{l}_2, ..., \dot{l}_{n_c}]^T$ as well as the linear and angular velocities of the mobile base $\dot{\boldsymbol{\chi}}_a = [\dot{\boldsymbol{\eta}}_1^a, \boldsymbol{\omega}_a]^T$. For this purpose, we derive the cable length l_i with respect to time. We have then:

$$l_i^2 = (\boldsymbol{\eta}_1^p + \boldsymbol{\mathcal{R}}_P^0\boldsymbol{b}_i - \boldsymbol{\eta}_1^a - \boldsymbol{\mathcal{R}}_A^0\boldsymbol{a}_i)^T(\boldsymbol{\eta}_1^p + \boldsymbol{\mathcal{R}}_P^0\boldsymbol{b}_i - \boldsymbol{\eta}_1^a - \boldsymbol{\mathcal{R}}_A^0\boldsymbol{a}_i) \tag{2.3.6}$$

$$l_i\dot{l}_i = \boldsymbol{l}_i^T(\dot{\boldsymbol{\eta}}_1^p + \dot{\boldsymbol{\mathcal{R}}}_P^0\boldsymbol{b}_i - \dot{\boldsymbol{\eta}}_1^a - \dot{\boldsymbol{\mathcal{R}}}_A^0\boldsymbol{a}_i) \tag{2.3.7}$$

$$l_i\dot{l}_i = \boldsymbol{l}_i^T(\dot{\boldsymbol{\eta}}_1^p - \dot{\boldsymbol{\eta}}_1^a + [\boldsymbol{\omega}_p]\boldsymbol{\mathcal{R}}_P^0\boldsymbol{b}_i - [\boldsymbol{\omega}_a]\boldsymbol{\mathcal{R}}_A^0\boldsymbol{a}_i) \tag{2.3.8}$$

$$l_i\dot{l}_i + \boldsymbol{l}_i^T\dot{\boldsymbol{\eta}}_1^a + (\boldsymbol{\mathcal{R}}_A^0\boldsymbol{a}_i \times \boldsymbol{l}_i)^T\boldsymbol{\omega}_a = \boldsymbol{l}_i^T\dot{\boldsymbol{\eta}}_1^p + (\boldsymbol{\mathcal{R}}_P^0\boldsymbol{b}_i \times \boldsymbol{l}_i)^T\boldsymbol{\omega}_p \tag{2.3.9}$$

$$\dot{l}_i + \boldsymbol{v}_i^T\dot{\boldsymbol{\eta}}_1^a + (\boldsymbol{\mathcal{R}}_A^0\boldsymbol{a}_i \times \boldsymbol{v}_i)^T\boldsymbol{\omega}_a = \boldsymbol{v}_i^T\dot{\boldsymbol{\eta}}_1^p + (\boldsymbol{\mathcal{R}}_P^0\boldsymbol{b}_i \times \boldsymbol{v}_i)^T\boldsymbol{\omega}_p \tag{2.3.10}$$

where $[\boldsymbol{\omega}_p]$ and $[\boldsymbol{\omega}_a]$ are anti-symmetric tensors corresponding to the cross product of the two vectors $\boldsymbol{\omega}_p$ and $\boldsymbol{\omega}_a$ respectively, such that : $\dot{\boldsymbol{\mathcal{R}}}_P^0 = [\boldsymbol{\omega}_p]\boldsymbol{\mathcal{R}}_P^0$ and $\dot{\boldsymbol{\mathcal{R}}}_A^0 = [\boldsymbol{\omega}_a]\boldsymbol{\mathcal{R}}_A^0$. If we generalize for the n_c cables, the matrix writing becomes:

$$\begin{pmatrix} \dot{l}_1 \\ : \\ \dot{l}_{n_c} \end{pmatrix} + \underbrace{\begin{pmatrix} \boldsymbol{v}_1^T & (\boldsymbol{\mathcal{R}}_A^0 \boldsymbol{a}_1 \times \boldsymbol{v}_1)^T \\ : & : \\ \boldsymbol{v}_{n_c}^T & (\boldsymbol{\mathcal{R}}_A^0 \boldsymbol{a}_{n_c} \times \boldsymbol{v}_{n_c})^T \end{pmatrix}}_{\boldsymbol{J}_1} \begin{pmatrix} \dot{\boldsymbol{\eta}}_1^a \\ \boldsymbol{\omega}_a \end{pmatrix} = \underbrace{\begin{pmatrix} \boldsymbol{v}_1^T & (\boldsymbol{\mathcal{R}}_P^0 \boldsymbol{b}_1 \times \boldsymbol{v}_1)^T \\ : & : \\ \boldsymbol{v}_{n_c}^T & (\boldsymbol{\mathcal{R}}_P^0 \boldsymbol{b}_{n_c} \times \boldsymbol{v}_{n_c})^T \end{pmatrix}}_{\boldsymbol{J}} \begin{pmatrix} \dot{\boldsymbol{\eta}}_1^p \\ \boldsymbol{\omega}_p \end{pmatrix} \tag{2.3.11}$$

Then, the suspended platform twist $\dot{\boldsymbol{\chi}}_p$ of the mobile CDPM is defined as follows:

$$\boldsymbol{J}\dot{\boldsymbol{\chi}}_p = \dot{\boldsymbol{l}} + \boldsymbol{J}_1 \dot{\boldsymbol{\chi}}_a \tag{2.3.12}$$

$$\dot{\boldsymbol{\chi}}_p = \boldsymbol{J}^+ \dot{\boldsymbol{l}} + \boldsymbol{J}^+ \boldsymbol{J}_1 \dot{\boldsymbol{\chi}}_a \tag{2.3.13}$$

in which, $\boldsymbol{J}^+ = \boldsymbol{J}^T(\boldsymbol{J}\boldsymbol{J}^T)^{-1}$ is the pseudo-inverse of Jacobian matrix $\boldsymbol{J}$. As it is shown in the above equation, the suspended platform twist can be expressed in two terms. The first one, $\boldsymbol{J}^+\dot{\boldsymbol{l}}$ is caused by the variation of cable length and the second term, $\boldsymbol{J}^+\boldsymbol{J}_1\dot{\boldsymbol{\chi}}_a$ is the twist due to the motion of the base. For a conventional CDPM with fixed base, the platform twist is $\dot{\boldsymbol{\chi}}_p = \boldsymbol{J}^+\dot{\boldsymbol{l}}$.

2.3.1.1 Velocity and Acceleration of the Suspended Platform

In this section, we analyze the motion of the 6-DOF suspended platform relative to both the inertial reference frame $\mathcal{R}_0$ and the local frame $\mathcal{R}_A$ attached to the mobile base of the CDPM. The vector $\boldsymbol{p} = [x, y, z]^T$ represents the relative position of the platform geometric center P with respect to $\mathcal{R}_A$, originating from A. The orientation vector of the platform body-fixed frame $\mathcal{R}_P$ with respect to $\mathcal{R}_A$ is $\boldsymbol{\Theta} = [\phi, \theta, \psi]^T$. $\boldsymbol{\mathcal{R}}_P^A$ is the rotation matrix between the two local frames $\mathcal{R}_A$ and $\mathcal{R}_P$.

$$\boldsymbol{\mathcal{R}}_P^A = \begin{pmatrix} c_\psi c_\theta & c_\psi s_\theta s_\phi - s_\psi c_\phi & s_\psi s_\phi + c_\psi c_\phi s_\theta \\ s_\psi c_\theta & c_\psi c_\theta + s_\phi s_\theta s_\psi & s_\theta s_\psi c_\phi - c_\psi s_\phi \\ -s_\theta & c_\theta s_\phi & c_{\theta_a} c_\phi \end{pmatrix} \tag{2.3.14}$$

The following shorthand notation for trigonometric function is used: $c_\theta := \cos\theta$, $s_\theta := \sin\theta$, $t_\theta := \tan\theta$. The platform body-fixed frame $\mathcal{R}_P$ is rotating with respect to the local frame $\mathcal{R}_A$ with an angular velocity $\boldsymbol{\omega}$ witch can be expressed in terms of Euler angle rates $\dot{\boldsymbol{\Theta}} = [\dot{\phi}, \dot{\theta}, \dot{\psi}]^T$ as follows:

$$\boldsymbol{\omega} = \begin{pmatrix} c_\psi c_\theta & -s_\psi & 0 \\ s_\psi c_\theta & c_\psi & 0 \\ -s_\theta & 0 & 1 \end{pmatrix} \begin{pmatrix} \dot{\phi} \\ \dot{\theta} \\ \dot{\psi} \end{pmatrix} = \boldsymbol{S}(\boldsymbol{\Theta})\dot{\boldsymbol{\Theta}} \tag{2.3.15}$$

where $\boldsymbol{S}$ is the transformation matrix from Euler angle rates to angular velocities. We introduce the notation $\frac{d\overrightarrow{OM}}{dt}\rceil^C_{\rfloor G}$ to represent the linear velocity vector of a point M with respect to the frame G, expressed in a frame C and $\overrightarrow{\omega}\rceil^C_{\rfloor B/G}$ represents the angular velocity vector

of a frame B with respect to a frame G, expressed in a frame C. The superposed dot, $\dot{\boldsymbol{w}}$, denotes the time derivative relative to a Galilean reference frame $\mathcal{R}_0$ whereas the superposed ring, $\mathring{\boldsymbol{w}}$, denotes the time derivative relative to local frame. The notation holds for all the vectors used in this section. The expression of the linear velocity of the platform geometric center P expressed into the inertial reference frame $\mathcal{R}_0$ is given by:

$$\frac{d\overrightarrow{OP}}{dt}\rfloor^{\mathcal{R}_0}_{\mathcal{R}_0} = \frac{d\overrightarrow{OA}}{dt}\rfloor^{\mathcal{R}_0}_{\mathcal{R}_0} + \frac{d\overrightarrow{AP}}{dt}\rfloor^{\mathcal{R}_0}_{\mathcal{R}_A} + \overrightarrow{\omega}\rfloor^{\mathcal{R}_0}_{\mathcal{R}_A/\mathcal{R}_0} \times \overrightarrow{AP} \tag{2.3.16}$$

As it is known, the vectors $\frac{d\overrightarrow{OA}}{dt}\rfloor^{R_0}_{R_0}$ and $\overrightarrow{\omega}\rfloor^{\mathcal{R}_A}_{\mathcal{R}_A/\mathcal{R}_0}$ correspond to the absolute linear and angular velocities of the mobile base, defined respectively as $\dot{\boldsymbol{\eta}}_1^a$ and $\boldsymbol{\nu}_2^a$. $\frac{d\overrightarrow{AP}}{dt}\rfloor^{R_A}_{R_A}$ corresponds to the relative linear velocity of the platform geometric center P expressed into the base body-fixed frame $\mathcal{R}_A$, denoted as $\boldsymbol{v}$. We multiply the two latter vectors $\boldsymbol{\nu}_2^a$ and $\boldsymbol{v}$ by the rotation matrix $\boldsymbol{\mathcal{R}}_A^0$ to get the expression of $\dot{\boldsymbol{\eta}}_1^p$ in the inertial reference frame $\mathcal{R}_0$. By substituting these expressions in the above equation (2.3.16), we have:

$$\dot{\boldsymbol{\eta}}_1^p = \dot{\boldsymbol{\eta}}_1^a + \boldsymbol{\mathcal{R}}_A^0\boldsymbol{v} + (\boldsymbol{\mathcal{R}}_A^0\boldsymbol{\nu}_2^a \times \boldsymbol{\mathcal{R}}_A^0\boldsymbol{p}) \tag{2.3.17}$$

$$\dot{\boldsymbol{\eta}}_1^p = \dot{\boldsymbol{\eta}}_1^a + \boldsymbol{\mathcal{R}}_A^0(\boldsymbol{v} + \boldsymbol{\nu}_2^a \times \boldsymbol{p}) \tag{2.3.18}$$

By differentiating the equation (2.3.16) with respect to time, the linear acceleration of the platform geometric center P expressed in the inertial reference frame $\mathcal{R}_0$ is given by the following expressions:

$$\frac{d^2\overrightarrow{OP}}{dt^2}\rfloor^{\mathcal{R}_0}_{\mathcal{R}_0} = \frac{d^2\overrightarrow{OA}}{dt^2}\rfloor^{\mathcal{R}_0}_{\mathcal{R}_0} + \frac{d}{dt}\left\{\frac{d\overrightarrow{AP}}{dt}\rfloor^{\mathcal{R}_0}_{\mathcal{R}_A} + \overrightarrow{\omega}\rfloor^{\mathcal{R}_0}_{\mathcal{R}_A/\mathcal{R}_0} \times \overrightarrow{AP}\right\} \tag{2.3.19}$$

$$\begin{aligned}\frac{d^2\overrightarrow{OP}}{dt^2}\rfloor^{\mathcal{R}_0}_{\mathcal{R}_0} = \frac{d^2\overrightarrow{AP}}{dt^2}\rfloor^{\mathcal{R}_0}_{\mathcal{R}_A} + 2\overrightarrow{\omega}\rfloor^{\mathcal{R}_0}_{\mathcal{R}_A/\mathcal{R}_0} \times \frac{d\overrightarrow{AP}}{dt}\rfloor^{\mathcal{R}_0}_{\mathcal{R}_A} \\ + \left\{\frac{d^2\overrightarrow{OA}}{dt^2}\rfloor^{\mathcal{R}_0}_{\mathcal{R}_0} + \frac{d\overrightarrow{\omega}}{dt}\rfloor^{\mathcal{R}_0}_{\mathcal{R}_A/\mathcal{R}_0} \times \overrightarrow{AP} + \overrightarrow{\omega}\rfloor^{\mathcal{R}_0}_{\mathcal{R}_A/\mathcal{R}_0} \times (\overrightarrow{\omega}\rfloor^{\mathcal{R}_0}_{\mathcal{R}_A/\mathcal{R}_0} \times \overrightarrow{AP})\right\}\end{aligned} \tag{2.3.20}$$

Note that $\frac{d^2\overrightarrow{OA}}{dt^2}\rfloor^{\mathcal{R}_0}_{\mathcal{R}_0}$ and $\frac{d\overrightarrow{\omega}}{dt}\rfloor^{\mathcal{R}_A}_{\mathcal{R}_A/\mathcal{R}_0}$ correspond to the absolute linear and angular acceleration of the mobile base, defined respectively as $\ddot{\boldsymbol{\eta}}_1^a$ and $\dot{\boldsymbol{\nu}}_2^a$. Further, $\frac{d^2\overrightarrow{AP}}{dt^2}\rfloor^{R_A}_{R_A}$ represents the relative linear acceleration of the platform geometric center P expressed into the base body-fixed frame $\mathcal{R}_A$, denoted as $\mathring{\boldsymbol{v}}$. By substituting these expressions in the above equation (2.3.20), we get:

$$\ddot{\boldsymbol{\eta}}_1^p = \boldsymbol{\mathcal{R}}_A^0(\mathring{\boldsymbol{v}} + 2\boldsymbol{\nu}_2^a \times \boldsymbol{v}) + \ddot{\boldsymbol{\eta}}_1^a + \boldsymbol{\mathcal{R}}_A^0\left\{\dot{\boldsymbol{\nu}}_2^a \times \boldsymbol{p} + \boldsymbol{\nu}_2^a \times (\boldsymbol{\nu}_2^a \times \boldsymbol{p})\right\} \tag{2.3.21}$$

The expression of the absolute angular velocity of the suspended platform expressed in inertial reference frame $\mathcal{R}_0$ is:

$$\overrightarrow{\omega}^{]\mathcal{R}_0}_{]\mathcal{R}_P/\mathcal{R}_0} = \overrightarrow{\omega}^{]\mathcal{R}_0}_{]\mathcal{R}_P/\mathcal{R}_A} + \overrightarrow{\omega}^{]\mathcal{R}_0}_{]\mathcal{R}_A/\mathcal{R}_0} \tag{2.3.22}$$

$$\overrightarrow{\omega}^{]\mathcal{R}_P}_{]\mathcal{R}_P/\mathcal{R}_0} = \boldsymbol{\mathcal{R}}^0_A \overrightarrow{\omega}^{]\mathcal{R}_A}_{]\mathcal{R}_P/\mathcal{R}_A} + \boldsymbol{\mathcal{R}}^0_A \overrightarrow{\omega}^{]\mathcal{R}_A}_{]\mathcal{R}_A/\mathcal{R}_0} \tag{2.3.23}$$

As already stated, $\overrightarrow{\omega}^{]\mathcal{R}_A}_{]\mathcal{R}_A/\mathcal{R}_0}$ represents the angular velocity of the mobile base expressed in local frame $\mathcal{R}_A$, defined as $\boldsymbol{\nu}^a_1$. $\boldsymbol{\omega}$ is the relative angular velocity of the suspended platform expressed in local mobile frame $\mathcal{R}_A$ which corresponds to $\overrightarrow{\omega}^{]\mathcal{R}_A}_{]\mathcal{R}_P/\mathcal{R}_A}$. Substituting these expressions in the above equation (2.3.23), we get:

$$\boldsymbol{\omega}_p = \boldsymbol{\mathcal{R}}^0_A(\boldsymbol{\omega} + \boldsymbol{\nu}^a_2) \tag{2.3.24}$$

By differentiating the equation (2.3.24) with respect to time, the angular acceleration of the platform expressed in the inertial reference frame $\mathcal{R}_0$ is given by the following expression:

$$\dot{\boldsymbol{\omega}}_p = \boldsymbol{\mathcal{R}}^0_A(\mathring{\boldsymbol{\omega}} + \dot{\boldsymbol{\nu}}^a_2) + \dot{\boldsymbol{\mathcal{R}}}^0_A(\boldsymbol{\omega} + \boldsymbol{\nu}^a_2) \tag{2.3.25}$$

$$\dot{\boldsymbol{\omega}}_p = \boldsymbol{\mathcal{R}}^0_A(\mathring{\boldsymbol{\omega}} + \dot{\boldsymbol{\nu}}^a_2 + \boldsymbol{\nu}^a_2 \times \boldsymbol{\omega}) \tag{2.3.26}$$

2.3.2 Dynamic Modeling

In this section, we describe the dynamic equations showing explicitly the interaction between suspended platform and the movable base through the cable tensions. In this preliminary analysis of a mobile CDPM, the suspended platform is taken as the research object and the base motion is regarded as a disturbance. The dynamic model is built by considering both the force and torque balance equations of the suspended platform. We assume that the cables are massless and not extensible.

2.3.2.1 Force Balance Equation

The tension in each cable is denoted by $\boldsymbol{t}_i = t_i \boldsymbol{v}_i$, where $\boldsymbol{v}_i$ corresponds to the unit vector along the i^{th} cable and t_i is the tension magnitude. If gravity and cables tension are considered as the only forces acting on the platform, the force balance equation at the moving platform geometric center P can be formulated as follows:

$$m\ddot{\boldsymbol{\eta}}^p_1 = mg\boldsymbol{e}_3 - \sum_{i=1}^{n_c} t_i \boldsymbol{v}_i \tag{2.3.27}$$

where $\ddot{\boldsymbol{\eta}}^p_1$ is the linear acceleration of the platform. The gravity force is represented by the vector $mg\boldsymbol{e}_3$ where $\boldsymbol{e}_3$ is a unit vector pointing in the direction of gravity, m is the loaded

platform mass and g the gravitational acceleration. By substituting the linear acceleration $\ddot{\boldsymbol{\eta}}_1^p$ from (2.3.21) into the above equation (2.3.27), we get:

$$m\boldsymbol{\mathcal{R}}_A^0\left[\mathring{\boldsymbol{v}}+\boldsymbol{\mathcal{R}}_0^A\ddot{\boldsymbol{\eta}}_1^a+2\boldsymbol{\nu}_2^a\times\boldsymbol{v}+\dot{\boldsymbol{\nu}}_2^a\times\boldsymbol{p}+\boldsymbol{\nu}_2^a\times(\boldsymbol{\nu}_2^a\times\boldsymbol{p})\right]=mg\boldsymbol{e}_3-\sum_{i=1}^{n_c}t_i\boldsymbol{v}_i \tag{2.3.28}$$

We multiply the above equation by $\boldsymbol{\mathcal{R}}_0^A$:

$$m\left[\mathring{\boldsymbol{v}}+\boldsymbol{\mathcal{R}}_0^A\ddot{\boldsymbol{\eta}}_1^a+2\boldsymbol{\nu}_2^a\times\boldsymbol{v}+\dot{\boldsymbol{\nu}}_2^a\times\boldsymbol{p}+\boldsymbol{\nu}_2^a\times(\boldsymbol{\nu}_2^a\times\boldsymbol{p})\right]=mg\boldsymbol{\mathcal{R}}_0^A\boldsymbol{e}_3-\sum_{i=1}^{n_c}t_i\boldsymbol{\mathcal{R}}_0^A\boldsymbol{v}_i \tag{2.3.29}$$

We denote by $\boldsymbol{u}_i$ the unit vector along the i^{th} cable , such that $\boldsymbol{u}_i=\boldsymbol{\mathcal{R}}_0^A\boldsymbol{v}_i$:

$$m\mathring{\boldsymbol{v}}+m\left[\boldsymbol{\mathcal{R}}_0^A\ddot{\boldsymbol{\eta}}_1^a+2\boldsymbol{\nu}_2^a\times\boldsymbol{v}+\dot{\boldsymbol{\nu}}_2^a\times\boldsymbol{p}+\boldsymbol{\nu}_2^a\times(\boldsymbol{\nu}_2^a\times\boldsymbol{p})\right]=mg\boldsymbol{\mathcal{R}}_0^A\boldsymbol{e}_3-\sum_{i=1}^{n_c}t_i\boldsymbol{u}_i \tag{2.3.30}$$

2.3.2.2 Torque Balance Equation

Similar to the force balance, only gravity and cables tension act on the suspended platform. Thus, the torque balance equation at the moving platform geometric center P can be formulated as follows:

$$\boldsymbol{I}_{P_0}\dot{\boldsymbol{\omega}}_p+\boldsymbol{\omega}_p\times\boldsymbol{I}_{P_0}\boldsymbol{\omega}_p=-\sum_{i=1}^{n_c}\boldsymbol{\mathcal{R}}_P^0\boldsymbol{b}_i\times t_i\boldsymbol{v}_i \tag{2.3.31}$$

in which $\dot{\boldsymbol{\omega}}_p$ is the angular acceleration of $\mathcal{R}_P$ relative to $\mathcal{R}_0$ expressed in $\mathcal{R}_0$ and $\boldsymbol{I}_{P_0}$ is the inertia matrix of the suspended platform with respect to inertial reference frame $\mathcal{R}_0$, such that $\boldsymbol{I}_{P_0}=\boldsymbol{\mathcal{R}}_P^0\boldsymbol{I}_p\boldsymbol{\mathcal{R}}_0^P$, where $\boldsymbol{I}_p$ is the inertia matrix of the suspended platform with respect to the local frame $\mathcal{R}_P$. $\boldsymbol{b}_i$ is the position vector of the point B_i, where the i^{th} cable is attached to the suspended platform. By substituting the angular velocity and acceleration $\boldsymbol{\omega}_p$ and $\dot{\boldsymbol{\omega}}_p$ respectively, given by the expressions (2.3.24) and (2.3.26), into the above equation (2.3.31), we get:

$$\boldsymbol{I}_{P_0}\boldsymbol{\mathcal{R}}_A^0\left[\mathring{\boldsymbol{\omega}}+\dot{\boldsymbol{\nu}}_2^a+(\boldsymbol{\nu}_2^a\times\boldsymbol{\omega})\right]+\boldsymbol{\mathcal{R}}_A^0(\boldsymbol{\omega}+\boldsymbol{\nu}_2^a)\times\boldsymbol{I}_{P_0}\boldsymbol{\mathcal{R}}_A^0(\boldsymbol{\omega}+\boldsymbol{\nu}_2^a)=-\sum_{i=1}^{n_c}\boldsymbol{\mathcal{R}}_P^0\boldsymbol{b}_i\times t_i\boldsymbol{v}_i \tag{2.3.32}$$

By substituting the inertia matrix $\boldsymbol{I}_{P_0}=\boldsymbol{\mathcal{R}}_P^0\boldsymbol{I}_p\boldsymbol{\mathcal{R}}_0^P$ into the latter equation, we get:

$$\boldsymbol{\mathcal{R}}_P^0\boldsymbol{I}_p\boldsymbol{\mathcal{R}}_A^P\left[\mathring{\boldsymbol{\omega}}+\dot{\boldsymbol{\nu}}_2^a+(\boldsymbol{\nu}_2^a\times\boldsymbol{\omega})\right]+\boldsymbol{\mathcal{R}}_A^0(\boldsymbol{\omega}+\boldsymbol{\nu}_2^a)\times\boldsymbol{\mathcal{R}}_P^0\boldsymbol{I}_p\boldsymbol{\mathcal{R}}_A^P(\boldsymbol{\omega}+\boldsymbol{\nu}_2^a)=-\sum_{i=1}^{n_c}\boldsymbol{\mathcal{R}}_P^0\boldsymbol{b}_i\times t_i\boldsymbol{v}_i \tag{2.3.33}$$

We multiply the latter equation by $\boldsymbol{\mathcal{R}}_0^A$:

$$\boldsymbol{\mathcal{R}}_P^A \boldsymbol{I}_p \boldsymbol{\mathcal{R}}_A^P \left[\mathring{\boldsymbol{\omega}} + \dot{\boldsymbol{\nu}}_2^a + (\boldsymbol{\nu}_2^a \times \boldsymbol{\omega})\right] + (\boldsymbol{\omega} + \boldsymbol{\nu}_2^a) \times \boldsymbol{\mathcal{R}}_P^A \boldsymbol{I}_p \boldsymbol{\mathcal{R}}_A^P (\boldsymbol{\omega} + \boldsymbol{\nu}_2^a) = -\sum_{i=1}^{n_c} \boldsymbol{\mathcal{R}}_P^A \boldsymbol{b}_i \times t_i \boldsymbol{\mathcal{R}}_0^A \boldsymbol{v}_i \quad (2.3.34)$$

We denote by $\boldsymbol{u}_i$ the unit vector along the i^{th} cable, such that $\boldsymbol{u}_i = \boldsymbol{\mathcal{R}}_0^A \boldsymbol{v}_i$:

$$\begin{aligned}\boldsymbol{\mathcal{R}}_P^A \boldsymbol{I}_p \boldsymbol{\mathcal{R}}_A^P \mathring{\boldsymbol{\omega}} + \boldsymbol{\omega} \times \boldsymbol{\mathcal{R}}_P^A \boldsymbol{I}_p \boldsymbol{\mathcal{R}}_A^P \boldsymbol{\omega} + \boldsymbol{\mathcal{R}}_P^A \boldsymbol{I}_p \boldsymbol{\mathcal{R}}_A^P \left[\dot{\boldsymbol{\nu}}_2^a + (\boldsymbol{\nu}_2^a \times \boldsymbol{\omega})\right] \\ + \boldsymbol{\nu}_2^a \times \boldsymbol{\mathcal{R}}_P^A \boldsymbol{I}_p \boldsymbol{\mathcal{R}}_A^P (\boldsymbol{\omega} + \boldsymbol{\nu}_2^a) + \boldsymbol{\omega} \times \boldsymbol{\mathcal{R}}_P^A \boldsymbol{I}_p \boldsymbol{\mathcal{R}}_A^P \boldsymbol{\nu}_2^a = -\sum_{i=1}^{n_c} \boldsymbol{\mathcal{R}}_P^A \boldsymbol{b}_i \times t_i \boldsymbol{u}_i \quad (2.3.35)\end{aligned}$$

Gathering both force and torque balance equation, we get:

$$m\mathring{\boldsymbol{v}} + m\left[\boldsymbol{\mathcal{R}}_0^A \ddot{\boldsymbol{\eta}}_1^a + 2\boldsymbol{\nu}_2^a \times \boldsymbol{v} + \dot{\boldsymbol{\nu}}_2^a \times \boldsymbol{p} + \boldsymbol{\nu}_2^a \times (\boldsymbol{\nu}_2^a \times \boldsymbol{p})\right] = mg\boldsymbol{\mathcal{R}}_0^A \boldsymbol{e}_3 - \sum_{i=1}^{n_c} t_i \boldsymbol{u}_i \quad (2.3.36)$$

$$\begin{aligned}\boldsymbol{\mathcal{R}}_P^A \boldsymbol{I}_p \boldsymbol{\mathcal{R}}_A^P \mathring{\boldsymbol{\omega}} + \boldsymbol{\omega} \times \boldsymbol{\mathcal{R}}_P^A \boldsymbol{I}_p \boldsymbol{\mathcal{R}}_A^P \boldsymbol{\omega} + \boldsymbol{\mathcal{R}}_P^A \boldsymbol{I}_p \boldsymbol{\mathcal{R}}_A^P \left[\dot{\boldsymbol{\nu}}_2^a + (\boldsymbol{\nu}_2^a \times \boldsymbol{\omega})\right] \\ + \boldsymbol{\nu}_2^a \times \boldsymbol{\mathcal{R}}_P^A \boldsymbol{I}_p \boldsymbol{\mathcal{R}}_A^P (\boldsymbol{\omega} + \boldsymbol{\nu}_2^a) + \boldsymbol{\omega} \times \boldsymbol{\mathcal{R}}_P^A \boldsymbol{I}_p \boldsymbol{\mathcal{R}}_A^P \boldsymbol{\nu}_2^a = -\sum_{i=1}^{n_c} \boldsymbol{\mathcal{R}}_P^A \boldsymbol{b}_i \times t_i \boldsymbol{u}_i \quad (2.3.37)\end{aligned}$$

The two latter equations can be combined in one matrix equation:

$$\begin{aligned}\underbrace{\begin{pmatrix} m\boldsymbol{I}_3 & \boldsymbol{0}_{3\times3} \\ \boldsymbol{0}_{3\times3} & \boldsymbol{\mathcal{R}}_P^A \boldsymbol{I}_p \mathcal{R}_A^P \end{pmatrix}}_{\boldsymbol{M}_P} \begin{pmatrix} \mathring{\boldsymbol{v}} \\ \mathring{\boldsymbol{\omega}} \end{pmatrix} + \underbrace{\begin{pmatrix} \boldsymbol{0}_{3\times1} \\ \boldsymbol{\omega} \times \boldsymbol{\mathcal{R}}_P^A \boldsymbol{I}_p \mathcal{R}_A^P \boldsymbol{\omega} \end{pmatrix}}_{\boldsymbol{C}_P \mathring{\boldsymbol{\chi}}} + \underbrace{\begin{pmatrix} -mg\boldsymbol{\mathcal{R}}_0^A \boldsymbol{e}_3 \\ \boldsymbol{0}_{3\times1} \end{pmatrix}}_{\boldsymbol{G}_P} \\ + \underbrace{\begin{pmatrix} \boldsymbol{D}_{\eta_1^a} \\ \boldsymbol{D}_{\eta_2^a} \end{pmatrix}}_{\boldsymbol{D}_P} = \underbrace{-\begin{pmatrix} \boldsymbol{u}_1 & \cdots & \boldsymbol{u}_{n_c} \\ \boldsymbol{\mathcal{R}}_P^A \boldsymbol{b}_1 \times \boldsymbol{u}_1 & \cdots & \boldsymbol{\mathcal{R}}_P^A \boldsymbol{b}_{n_c} \times \boldsymbol{u}_{n_c} \end{pmatrix}}_{\boldsymbol{W}_P} \boldsymbol{T}\end{aligned}$$

with:

- $\boldsymbol{D}_{\eta_1^a} = m\left[\boldsymbol{\mathcal{R}}_0^A \ddot{\boldsymbol{\eta}}_1^a + 2\boldsymbol{\nu}_2^a \times \boldsymbol{v} + \dot{\boldsymbol{\nu}}_2^a \times \boldsymbol{p} + \boldsymbol{\nu}_2^a \times (\boldsymbol{\nu}_2^a \times \boldsymbol{p})\right]$
- $\boldsymbol{D}_{\eta_2^a} = \boldsymbol{\mathcal{R}}_P^A \boldsymbol{I}_p \boldsymbol{\mathcal{R}}_A^P \left[\dot{\boldsymbol{\nu}}_2^a + (\boldsymbol{\nu}_2^a \times \boldsymbol{\omega})\right] + \boldsymbol{\nu}_2^a \times \boldsymbol{\mathcal{R}}_P^A \boldsymbol{I}_p \boldsymbol{\mathcal{R}}_A^P (\boldsymbol{\omega} + \boldsymbol{\nu}_2^a) + \boldsymbol{\omega} \times \boldsymbol{\mathcal{R}}_P^A \boldsymbol{I}_p \boldsymbol{\mathcal{R}}_A^P \boldsymbol{\nu}_2^a$

The base motion acts as a disturbance to the platform. By choosing to express the preceding dynamics equations in the base body-fixed frame $\mathcal{R}_A$, the unknown disturbance due to base motion can be modeled as additive terms in the dynamics of the suspended platform. Further, the latter disturbance term is denoted by the vector $\boldsymbol{D}_P$ where $\boldsymbol{D}_{\eta_1^a}$ and

$\boldsymbol{D}_{\eta_2^a}$ are considered respectively as the disturbance along both the platform transition and rotation motion. The compact dynamic model of the platform is given by the following expression:

$$\boldsymbol{M}_P(\boldsymbol{\chi})\overset{\circ\circ}{\boldsymbol{\chi}} + \boldsymbol{C}_P(\boldsymbol{\chi},\overset{\circ}{\boldsymbol{\chi}})\overset{\circ}{\boldsymbol{\chi}} + \boldsymbol{G}_P(\boldsymbol{\chi}) + \boldsymbol{D}_P(\boldsymbol{\chi},\overset{\circ}{\boldsymbol{\chi}},\ddot{\boldsymbol{\eta}}^a,\dot{\boldsymbol{\eta}}^a) = \boldsymbol{W}_P(\boldsymbol{\chi})\boldsymbol{T} \tag{2.3.38}$$

in which, $\overset{\circ\circ}{\boldsymbol{\chi}} = [\overset{\circ}{\boldsymbol{v}},\overset{\circ}{\boldsymbol{\omega}}]$ is the operational acceleration of the platform expressed in the mobile frame attached to the base $\mathcal{R}_A$. $\boldsymbol{M}_P$ is the mass matrix, $\boldsymbol{C}_P$ is the matrix of Coriolis and centrifugal terms and $\boldsymbol{G}_P$ is the gravitational force. $\boldsymbol{D}_P$ represents the disturbance term due to base motion. The vector $\boldsymbol{T} = [t_1, t_2, ..., t_{n_c}]^T$ groups the n_c cables tension t_i and $\boldsymbol{W}_P$ is the force transmission matrix.

2.4 Conclusion

In this chapter, we have investigated the motion equations of both convectional and mobile CDPM, using Newton-Euler approach. The addition of base mobility provides greater flexibility, but it requires careful investigation. The kinematic and dynamic modeling play an important role in the movement analysis of a CDPM and is the foundation to design a robust controller. For both motion equations, A non-elastic massless cable model is used. Subsequently an extension is made for non-negligible cable mass in the next chapter.

Chapter 3

Cable Driven Parallel Manipulator with Non-negligible Cable Mass and Elasticity

Contents

3.1 Introduction

Despite their numerous advantages, there are several challenges associated with CDPMs. The compliance of the driving cables is the major factor that affects the positioning accuracy of CDPMs. In most studies, a non-elastic massless cable model is used. The cables are then considered as straight line segments. Another aspect considers the elasticity along cable axis and assumes cable as massless spring [69],[70]. The basic assumption of the spring model is that the effect of cable weight on the static cable profile is negligible. The strained cable length depends on the cable tension and the cable elasticity. Therefore, spring cable model is efficient for low-density and thin cables. If the cable weight is significant compared with the external load, a non-negligible cable mass must be taken into account to fit well with the real manipulator. This more realistic cable behavior leads to study the sagging phenomena. The above model considers both the cable elasticity and the effect of cable weight on the static

cable profile. This model is studied and used in civil engineering since 1930s [71]. However, it is quite new in the analysis of CDPMs [72].

3.2 Inverse Kinematic Modeling

In most studies of CDPMs with non-negligible cable mass and elasticity, the kinematic analysis leads to a system of non-linear equations [73]. In this system, the robot kinematics and the mobile platform static equilibrium are coupled. In [74]. Kozak et al present a methodology to compute numerically the inverse kinematics of the manipulator and then study the sagging effects on the stiffness of the mechanism. The stiffness concept as discussed by [75] is used in order to model the robot's behavior. For CDPMs using massless spring cable model, the platform pose error can be calculated by its static Cartesian stiffness matrix. The latter relates the force and torque applied on the mobile platform to its corresponding linear and angular displacement. Stiffness is needed in order to maintain positional accuracy of CDPMs and attenuate vibration to ensure the system safety.

3.2.1 Static cable modeling

Considering the physical cable characteristics, the compliance of cables mainly has two sources. One is the axial stiffness of the cables that is associated with the elastic material modulus and the cable structure. The other is the sag-introduced flexibility which comes from the effect of cable weight on the static cable profile. The sag-introduced flexibility corresponds to the gravitational potential energy stored in the cable. The static sagging cable model, also known as elastic catenary model, describes the static profile of a cable by a set of non-linear equations. According to Irvine [71], this model exists for a long time and is mainly used in civil engineering. However, it is necessary to briefly introduce this model using our coordinate system and variables.

To get the cable static model, it is necessary to place in the plane $\mathcal{P}_i$ containing A_i and B_i. Thus, an additional axis frame $\mathcal{R}_i(A_i, X_i, Z_i)$ that lies in the vertical plane $\mathcal{P}_i$ needs to be established. This frame shares the vector Z_0 with the frame $\mathcal{R}_0$. Axis X_i, orthogonal to Z_i, is chosen so that the x-coordinate B_{ix} of B_i in frame $\mathcal{R}_i$ is positive. Thus, to transform $\mathcal{R}_0$ into the frame attached to the plane $\mathcal{P}_i$, one single rotation of angle β_i around Z_0 is needed. The rotation angle can be computed as $\beta_i = \arctan(\frac{y_{\overrightarrow{A_iB_i}}}{x_{\overrightarrow{A_iB_i}}})$, where $x_{\overrightarrow{A_iB_i}}$ and $y_{\overrightarrow{A_iB_i}}$ are the components of vector $\overrightarrow{A_iB_i}$ expressed in the frame $\mathcal{R}_{B_i}$(having as origin B_i and whose axises are parallel to the axises of the global frame $\mathcal{R}_0$). The rotation matrix $\boldsymbol{\mathcal{R}}_i^0$ between the global frame $\mathcal{R}_0$ and the local frame $\mathcal{R}_i$ is:

$$\boldsymbol{\mathcal{R}}_i^0 = \begin{pmatrix} c_{\beta_i} & -s_{\beta_i} & 0 \\ s_{\beta_i} & c_{\beta_i} & 0 \\ 0 & 0 & 1 \end{pmatrix} = [\boldsymbol{p}_{i_1}; \boldsymbol{p}_{i_2}; \boldsymbol{p}_{i_3}] \tag{3.2.1}$$

where the vectors $\boldsymbol{p}_{i_1}$, $\boldsymbol{p}_{i_2}$ and $\boldsymbol{p}_{i_3}$ are the three column vectors of the rotation matrix $\boldsymbol{\mathcal{R}}_i^0$. One of the cable-ends is fixed and an external tension $\boldsymbol{t}_i$ is applied to the other end. With the effect of both external tension and gravity, the shape of the cable between points A_i and B_i is not a straight line but a sagging curve in the plane $\mathcal{P}_i$. Assume that all cables have the same Young's modulus E, cross section area S and mass per unit length ρ. P_i is an arbitrary point along the strained cable. The position of P_i is denoted by Cartesian coordinates x_i and z_i. The variable s_i represents the arc length of the cable as measured from the exit point A_i to the point P_i, whereas the variable s_{0_i} will be used to denote the unstrained length of that cable segment. s_{0_i} varies from 0 to l_{0_i}. Further, $\boldsymbol{r}_i(s_{0_i})$ represents the position vector of a cable element ds_{0_i} located at s_{0_i}. To compute the static displacement of the i^{th} cable, we assume that the unstrained length of the cable l_{0_i} and the tension applied to the cable end $\boldsymbol{t}_i$ are known. From this starting point, we briefly reproduce Irvine's derivation using our coordinate system and variables. Firstly, the shape of the cable must satisfy the geometric constraint around the point P_i:

$$\left(\frac{dx_i}{ds_i}\right)^2 + \left(\frac{dz_i}{ds_i}\right)^2 = 1 \tag{3.2.2}$$

Secondly, the constraint of the static equilibrium can be written as:

$$f_i \frac{dx_i}{ds_i} = t_{i_x} \tag{3.2.3}$$

$$f_i \frac{dz_i}{ds_i} = t_{i_z} + \rho g(s_{0_i} - l_{0_i}) \tag{3.2.4}$$

where f_i is the cable force applied at point P_i. t_{i_x} and t_{i_z} are the components of $\boldsymbol{t}_i$ along X_i and Z_i axis respectively. Thirdly, the cable force f_i must satisfy Hooke's law:

$$f_i = ES\left(\frac{ds_i}{ds_{0_i}} - 1\right) \tag{3.2.5}$$

Solving for $\frac{dx_i}{ds_i}$ and $\frac{dz_i}{ds_i}$ and substituting into (3.2.2), we find an expression for the cable force as a function of the unstrained path length s_{0_i}:

$$f_i(s_{0_i}) = \sqrt{t_{i_x}^2 + [t_{i_z} + \rho g(s_{0_i} - l_{0_i})]^2} \tag{3.2.6}$$

since both $\frac{dx_i}{ds_i}$ and $\frac{ds_i}{ds_{0_i}}$ can be written as function of f_i by equations (3.2.3) and (3.2.5), $\frac{dx_i}{ds_{0_i}}$ is given by:

$$\frac{dx_i}{ds_{0_i}} = \frac{dx_i}{ds_i}\frac{ds_i}{ds_{0_i}} = \frac{t_{i_x}}{f_i}\left(\frac{f_i}{ES} + 1\right) \tag{3.2.7}$$

Applying the same procedure for $z-$axis:

$$\frac{dz_i}{ds_{0i}} = \frac{dz_i}{ds_i}\frac{ds_i}{ds_{0_i}} = \frac{1}{f_i}\left(t_{i_z} + \rho g(s_{0_i} - l_{0_i})\right)\left(\frac{f_i}{ES} + 1\right) \tag{3.2.8}$$

Substituting the tension expression (3.2.6) back into (3.2.7) and (3.2.8), the following solvable differential equations are obtained:

$$\frac{dx_i}{ds_{0_i}} = \frac{t_{i_x}}{ES} + \frac{t_{i_x}}{\sqrt{t_{i_x}^2 + [t_{i_z} + \rho g(s_{0_i} - l_{0_i})]^2}} \tag{3.2.9}$$

$$\frac{dz_i}{ds_{0_i}} = \frac{t_{i_z}}{ES} + \frac{\rho g(s_{0_i} - l_{0_i})}{ES} + \frac{t_{i_z} + \rho g(s_{0_i} - l_{0_i})}{\sqrt{t_{i_x}^2 + [t_{i_z} + \rho g(s_{0_i} - l_{0_i})]^2}} \tag{3.2.10}$$

Integrating and applying the boundary conditions $x_i(0) = 0$ and $z_i(0) = 0$, we get the following equations (3.2.11) and (3.2.12). These equations describe the profile of the cable under the action of gravity g and cable tensions $[t_{i_x}, t_{i_z}]^T$:

$$x_i(s_{0_i}) = \frac{t_{i_x} s_{0_i}}{ES} + \frac{t_{i_x}}{\rho g}\left\{\sinh^{-1}\left[\frac{t_{i_z} - \rho g(l_{0_i} - s_{0_i})}{t_{i_x}}\right] - \sinh^{-1}\left[\frac{t_{i_z} - \rho g l_{0_i}}{t_{i_x}}\right]\right\} \tag{3.2.11}$$

$$z_i(s_{0_i}) = \frac{t_{iz} s_{0_i}}{ES} + \frac{\rho g}{ES}\left(\frac{s_{0_i}^2}{2} - l_{0_i} s_{0_i}\right) + \frac{1}{\rho g}\left\{\sqrt{t_{i_x}^2 + \left[t_{i_z}^2 + \rho g(s_{0_i} - l_{0_i})\right]^2} - \sqrt{t_{i_x}^2 + [t_{i_z} - \rho g l_{0_i}]^2}\right\} \tag{3.2.12}$$

3.2.2 Kinematic model of CDPM

In this section, the inverse kinematics of CDPM is presented with considering both the cable elasticity and the effect of cable weight on the cable profile. The objective of the inverse kinematic model is to calculate the length of all the driving cables for a given pose of the suspended platform. When cable sag is non-negligible, the inverse kinematics of CDPM becomes quite difficult to compute. In fact, the cables lengths l_{0_i} and the components of the tensions applied at their end point B_i are related and must be determined at the same time.

The first challenge for analyzing a cable-driven robot with sagging cables is to mathematically describe the static displacement (or the shape) of the cables under the influence of gravity. For a suspended CDPM, one of the cable ends A_i is connected to winches mounted on a fixed base and an external tension $\boldsymbol{t}_i$ is applied to the other end B_i. The position of the i^{th} exit point A_i is defined by vector $\boldsymbol{a}_{i0}$ in the inertial reference frame $\mathcal{R}_0(O, X_0, Y_0, Z_0)$. The position of the attachment point B_i is defined by vector $\boldsymbol{b}_i$ in platform body-fixed frame $\mathcal{R}_P(P, X_p, Y_p, Z_p)$, originating from the geometric center of the platform P and $\boldsymbol{l}_i$ is the i^{th} driving cable connecting these two points. The length of the i^{th} cable is denoted by $l_i = \|\overrightarrow{A_iB_i}\|$ and $\boldsymbol{v}_i = \frac{\overrightarrow{A_iB_i}}{\|\overrightarrow{A_iB_i}\|}$ denotes the unit vector along the i^{th} cable. We use a parametrization by the Euler angles : yaw, pitch and roll $(\psi_p, \theta_p, \phi_p)$ to describe the suspended platform attitude. $\boldsymbol{\mathcal{R}}_P^0$ is the rotation matrix between the two local frames $\mathcal{R}_0$ and $\mathcal{R}_P$.

Under the established coordinate frames, the generalized coordinates of the suspended platform are expressed by $\boldsymbol{\eta}^p = [\boldsymbol{\eta}_1^p, \boldsymbol{\eta}_2^p]^T$, where the position and orientation of the suspended

platform in the inertial frame $\mathcal{R}_0$ can be respectively described by $\boldsymbol{\eta}_1^p = [x_p, y_p, z_p]^T$ and $\boldsymbol{\eta}_2^p = [\phi_p, \theta_p, \psi_p]^T$. For parallel robot, there are n_c kinematic closures. The vector $\boldsymbol{l}_i$ is expressed in reference frame $\mathcal{R}_0$ as follows:

$$\boldsymbol{l}_i = \overrightarrow{A_i B_i} = \boldsymbol{\eta}_1^p + \boldsymbol{\mathcal{R}}_P^0 \boldsymbol{b}_i - \boldsymbol{a}_{i0}, \qquad i \in \{1, 2, ..., n_c\} \tag{3.2.13}$$

Let $\boldsymbol{e}_{i_1}$ and $\boldsymbol{e}_{i_3}$ be the unit vectors along the axes of the cable frame $\mathcal{R}_i(A_i, X_i, Z_i)$. The coordinates (x_i^{end}, z_i^{end}) of the ending point B_i of the i^{th} cable in frame $\mathcal{R}_i$ can be obtained from the loop-closure kinematic equation (3.2.13) as follows:

$$x_i^{end} = \boldsymbol{\mathcal{R}}_0^i (\boldsymbol{\eta}_1^p + \boldsymbol{\mathcal{R}}_P^0 \boldsymbol{b}_i - \boldsymbol{a}_{i0}) \boldsymbol{e}_{i_1} \tag{3.2.14}$$

$$z_i^{end} = \boldsymbol{\mathcal{R}}_0^i (\boldsymbol{\eta}_1^p + \boldsymbol{\mathcal{R}}_P^0 \boldsymbol{b}_i - \boldsymbol{a}_{i0}) \boldsymbol{e}_{i_3} \tag{3.2.15}$$

Referring to the static cable sagging model and substituting unstrained arc length s_{0_i} in equations (3.2.11) and (3.2.12) by unstrained cable length l_{0_i}, we get another coordinate expressions of the cable end point B_i in frame $\mathcal{R}_i$:

$$x_i^{end} = \frac{t_{i_x} l_{0_i}}{ES} + \frac{|t_{i_x}|}{\rho g} \left\{ \sinh^{-1}\left[\frac{t_{i_z}}{t_{i_x}}\right] - \sinh^{-1}\left[\frac{t_{i_z} - \rho g l_{0_i}}{t_{i_x}}\right] \right\} \tag{3.2.16}$$

$$z_i^{end} = \frac{t_{i_z} l_{0_i}}{ES} - \frac{\rho g l_{0_i}^2}{2ES} + \frac{1}{\rho g} \left\{ \sqrt{t_{i_x}^2 + t_{i_z}^2} - \sqrt{t_{i_x}^2 + [t_{i_z} - \rho g l_{0_i}]^2} \right\} \tag{3.2.17}$$

Now, let us introduce the platform static equilibrium equations. Unlike a CDPM with massless cables where the tension direction is a long the straight line segment from B_i to A_i, the cable tension of a CDPM with non-negligible cable mass and elasticity has the same direction as the unit vector tangent to the cable at the attachment point B_i. Further, we denoted by $\boldsymbol{F}_e = [\boldsymbol{f}_{ext}, \boldsymbol{m}_{ext}]^T$ the external wrench acting on the suspended platform, where $\boldsymbol{f}_{ext}$ and $\boldsymbol{m}_{ext}$ represent respectively the external force and torque. For suspended platform static equilibrium, the force and torque balance equations are given by:

$$\boldsymbol{f}_{ext} - \sum_{i=1}^{n_c} \boldsymbol{\mathcal{R}}_i^0 \boldsymbol{t}_i = 0 \tag{3.2.18}$$

$$\boldsymbol{m}_{ext} - \sum_{i=1}^{n_c} \boldsymbol{\mathcal{R}}_P^0 \boldsymbol{b}_i \times \boldsymbol{\mathcal{R}}_i^0 \boldsymbol{t}_i = 0 \tag{3.2.19}$$

Thus, the wrench resulting from the tension $\boldsymbol{t}_i$ applied by cable i on the platform at the geometric center of the platform P can be written as follows:

$$\boldsymbol{\Psi}_{P_i} \begin{pmatrix} t_{i_x} \\ t_{i_z} \end{pmatrix} = \begin{pmatrix} \boldsymbol{p}_{i_1} & \boldsymbol{p}_{i_3} \\ \boldsymbol{\mathcal{R}}_P^0 \boldsymbol{b}_i \times \boldsymbol{p}_{i_1} & \boldsymbol{\mathcal{R}}_P^0 \boldsymbol{b}_i \times \boldsymbol{p}_{i_3} \end{pmatrix} \begin{pmatrix} t_{i_x} \\ t_{i_z} \end{pmatrix} \tag{3.2.20}$$

where t_{i_x} and t_{i_z} are the components of cable tension $\boldsymbol{t}_i$ expressed in the local cable frame $\boldsymbol{\mathcal{R}}_i$. The vectors $\boldsymbol{p}_{i_1}$ and $\boldsymbol{p}_{i_3}$ are two of the three column vectors of the rotation matrix $\boldsymbol{\mathcal{R}}_i^0$. Thus the static equilibrium of the n-DOF suspended platform subjected to the action of n_c cables and an external wrench $\boldsymbol{F}_e$ is:

$$\boldsymbol{W}_\rho \boldsymbol{T}_\rho + \boldsymbol{F}_e = 0 \tag{3.2.21}$$

where $\boldsymbol{W}_\rho = (\boldsymbol{\Psi}_{P_1}, \boldsymbol{\Psi}_{P_2}, .., \boldsymbol{\Psi}_{P_{n_c}})$ the matrix that groups the transmission matrices $\boldsymbol{\Psi}_{P_i}$ and $\boldsymbol{T}_\rho = [t_{1_x}, t_{1_z}, t_{2_x}, t_{2_z} ..., t_{nc_x}, t_{nc_z}]^T$ the component vector of forces applied by cables on the platform. To compute the unstrained length of all the driving cables l_{0i}, we assume that the value of the external wrench $\boldsymbol{F}_e$ as well as the position and orientation of the n-DOF suspended platform are known. Equations (3.2.16)-(3.2.17) for $i \in \{1, 2, ..., n_c\}$ and equation (3.2.21) together provide a system of $2n_c + n$ equations. The unknowns in these equations are the n_c unstrained cable length l_{0i} and the $2n_c$ cables tension components (t_{i_x}, t_{i_z}) gathered in the vector $\boldsymbol{T}_\rho$. Finally, the inverse kinematic problem of the CDPM consists of solving the following non-linear equation system where there are $3n_c$ unknowns and $2n_c + n$ equations:

$$x_i^{end} = \frac{t_{i_x} l_{0_i}}{ES} + \frac{|t_{i_x}|}{\rho g} \left\{ \sinh^{-1}\left[\frac{t_{i_z}}{t_{i_x}}\right] - \sinh^{-1}\left[\frac{t_{i_z} - \rho g l_{0_i}}{t_{i_x}}\right] \right\} \tag{3.2.22}$$

$$z_i^{end} = \frac{t_{i_z} l_{0_i}}{ES} - \frac{\rho g l_{0_i}^2}{2ES} + \frac{1}{\rho g} \left\{ \sqrt{t_{i_x}^2 + t_{i_z}^2} - \sqrt{t_{i_x}^2 + [t_{i_z} - \rho g l_{0_i}]^2} \right\} \tag{3.2.23}$$

$$\boldsymbol{W}_\rho \boldsymbol{T}_\rho + \boldsymbol{F}_e = 0 \tag{3.2.24}$$

For CDPMs with redundancy of actuation (more actuators than DOF $(n_c > n)$), there exist different sets of cable lengths and tensions to balance a known wrench applied on a given position of the suspended platform. To make the solution unique, constrained optimization with a cost function which minimize actuation energy can be used. For instance the quadratic programming problem seeks to minimize the sum of the squared tensions in order to guarantee continuity by providing a smooth objective function. Good initial guess is important for the convergence and the efficiency of the optimization method. In this case, the cable lengths and tensions obtained from the ideal inverse kinematic model can be used as a good initial guess for the inverse kinematic model.

3.3 Dynamic Model of the CDPM

3.3.1 Dynamic modeling

To illustrate the dynamic model of a CDPMs with non-negligible cable mass and elasticity, we consider each chain or branch of the system comprises of two parts: (1) a drum and portion of cable wound on it and (2) the deployed portion of cable. We assume that only the

deployed length of the cable has strain while the cable wound on the drum is assumed to be strain free. The equations of motion for this system are derived using Newton's laws.

3.3.1.1 Wound portion of cable

Each cable is wound around a drum with radius d_i and the segment of the cable wound around the drum is assumed to be inextensible. For simplicity, the axis of the drum is chosen to be parallel to the plane of motion along $y-$axis. A guide pulley is employed so that the cable leaves the drum at a fixed position $\xi_i(t)$. Note that $\xi_i(t)$ is a function of time since it changes during winding and unwinding of the cable.

In this model, we assume that the mass center of the cable wound on the drum coincides with the mass center of the drum. Indeed, if we suppose that the thickness of the cable wound on the drum is negligible compared to the radius at which the cable is wound, then we can write the inertia moment of the cable about the $y-$axis as:

$$\rho d_i^3(\varphi_i - \frac{\pi}{2}) \tag{3.3.1}$$

where φ_i is the angular rotation of cable contact point $s_{0_i} = 0$ and ρ is the cable mass per unit length. Note that I_i is the inertia moment of the drum about the $y-$axis, then the combined inertia moment of the drum and the wrapped cable on it about the $y-$axis is given by:

$$I_i + \rho d_i^3(\varphi_i - \frac{\pi}{2}) \tag{3.3.2}$$

To determine the kinetic moment I, we have to multiply the expression of the inertia moment (3.3.2) by the angular velocity $\dot{\varphi}_i$:

$$I = [I_i + \rho d_i^3(\varphi_i - \frac{\pi}{2})]\dot{\varphi}_i \tag{3.3.3}$$

To obtain the dynamic moment, we only have to derive the kinetic moment I with respect to time. Applying the Newton-Euler approach, the dynamic equation of the cable wound on the drum is:

$$[I_i + \rho d_i^3(\varphi_i - \frac{\pi}{2})]\ddot{\varphi}_i + \rho d_i^3\dot{\varphi}_i^2 = \tau_i - f_i(\xi_i)d_i, \quad 0 < s_{0_i} < \xi_i \tag{3.3.4}$$

where the external moments applied on the drum are the externally torque τ_i along the $y-$axis and the cable tension $f_i(\xi_i)$ applied to the cable exit point $\xi_i(t)$.

As already mentioned, we consider only the deployed length of the cable has strain while the cable wound on the drum is assumed to be strain free. Because of this assumption there is a discontinuity in cable elastic elongation at the outlet point where cable leaves the drum. The geometric constraint on the cable motion on the drum is:

$$\xi_i(t) = d_i(\varphi_i - \frac{\pi}{2}) \tag{3.3.5}$$

3.3.1.2 Deployed portion of cable

We denote by ds_{0_i} a cable element located at s_{0_i}, whose position is given by the vector $\boldsymbol{r}_i(s_{0_i})$. The axial forces on the two sides of this element are $\boldsymbol{f}_i(s_{0_i}+ds_{0_i})$ and $\boldsymbol{f}_i(s_{0_i})$ applied respectively in $s_0+ds_{0_i}$ and s_{0_i}. In addition, there is a gravity force $\rho g ds_{0_i}$. Since the deployed length of the cable has strain, we get the dynamic equation by applying Newton's law to the element ds_{0_i} as following:

$$\boldsymbol{f}_i(s_{0_i}+ds_{0_i})-\boldsymbol{f}_i(s_{0_i})+\rho g\boldsymbol{e}_3 ds_{0_i}=\rho\ddot{\boldsymbol{r}}_i(s_{0_i})ds_{0_i} \tag{3.3.6}$$

where $\boldsymbol{e}_3$ is the unit vector along the direction of gravity. On making $ds_{0_i}\longrightarrow 0$, the resulting governing equations are:

$$\frac{\delta\boldsymbol{f}_i(s_{0_i})}{\delta s_{0_i}}+\rho g\boldsymbol{e}_3=\rho\ddot{\boldsymbol{r}}_i(s_{0_i}) \tag{3.3.7}$$

The tangent to the cable at a point s_i is given by $\hat{\boldsymbol{t}}(s_i)=\frac{\partial\boldsymbol{r}_i(s_i)}{\partial s_i}$. Define $\eta(s_{0_i})=\frac{\partial s_i}{\partial s_{0_i}}$. From the property of the tangent, we obtain $\hat{\boldsymbol{t}}(s_{0_i})\hat{\boldsymbol{t}}(s_{0_i})=1$. This results in $\boldsymbol{r}_i'(s_{0_i})\boldsymbol{r}_i'(s_{0_i})=\eta^2(s_{0_i})$ where $\boldsymbol{r}_i'(s_{0_i})=\frac{\partial\boldsymbol{r}_i(s_{0_i})}{\partial s_{0_i}}$. Therefore, $\eta(s_{0_i})=\|\boldsymbol{r}_i'(s_{0_i})\|=\frac{\partial s_i}{\partial s_{0_i}}$. From the definition of strain, $\varepsilon=\frac{\partial s_i}{\partial s_{0_i}}-1=\|\boldsymbol{r}_i'(s_{0_i})\|-1$. The axial force $\boldsymbol{f}_i$, on point P_i, is along the unit vector tangent to the cable and its expression is given by:

$$\boldsymbol{f}_i(s_{0_i})=\frac{ES(\|\boldsymbol{r}_i'(s_{0_i})\|-1)\boldsymbol{r}_i'(s_{0_i})}{\|\boldsymbol{r}_i'(s_{0_i})\|} \tag{3.3.8}$$

Substituting the expression $\boldsymbol{f}_i(s_{0_i})$ from the equation (3.3.8) back into (3.3.7), we obtain:

$$\left[\frac{ES(\|\boldsymbol{r}_i'(s_{0i},t)\|-1)\boldsymbol{r}_i'(s_{0i},t)}{\|\boldsymbol{r}_i'(s_{0_i},t)\|}\right]'+\rho g\boldsymbol{e}_3=\rho\ddot{\boldsymbol{r}}_i(s_{0_i},t),\quad \xi_i<s_{0_i}<l_{0_i} \tag{3.3.9}$$

3.3.1.3 Suspended Platform

The external forces, such as the weight of the platform and its loading, are represented by the vector $mg\boldsymbol{e}_3$ where $\boldsymbol{e}_3$ is a unit vector pointing in the direction of gravity, m is the loaded platform mass and g the gravitational acceleration. The dynamic model of the suspended platform is given by the following relation:

$$m\ddot{\boldsymbol{\eta}}_1^p=mg\boldsymbol{e}_3-\sum_{i=1}^{n_c}\boldsymbol{t}_i \tag{3.3.10}$$

$$\boldsymbol{I}_{P_0}\dot{\boldsymbol{\omega}}_p+\boldsymbol{\omega}_p\times\boldsymbol{I}_{P_0}\boldsymbol{\omega}_p=-\sum_{i=1}^{n_c}\boldsymbol{\mathcal{R}}_P^0\boldsymbol{b}_i\times\boldsymbol{t}_i \tag{3.3.11}$$

with $\ddot{\boldsymbol{\chi}}_p=[\dot{\boldsymbol{\eta}}_1^p,\dot{\boldsymbol{\omega}}_p]^T$ is the operational acceleration vector, where $\dot{\boldsymbol{\eta}}_1^p$ and $\dot{\boldsymbol{\omega}}_p$ represent respectively the linear and angular acceleration of the platform in operational space. The

vector $\boldsymbol{T} = [t_1, t_2, ..., t_{n_c}]^T$ groups the n_c cables tension t_i. Hence, the compact dynamic model of the suspended platform is:

$$\boldsymbol{M}(\boldsymbol{\chi}_p)\ddot{\boldsymbol{\chi}}_p + \boldsymbol{C}(\boldsymbol{\chi}_p, \dot{\boldsymbol{\chi}}_p)\dot{\boldsymbol{\chi}}_p = \boldsymbol{W}_m(\boldsymbol{\chi}_p)\boldsymbol{T} + \boldsymbol{G} \tag{3.3.12}$$

where

$$\boldsymbol{M}(\boldsymbol{\chi}_p) = \begin{pmatrix} m\boldsymbol{I}_{3\times3} & \boldsymbol{0}_{3\times3} \\ \boldsymbol{0}_{3\times3} & \boldsymbol{I}_{P_0} \end{pmatrix}; \quad \boldsymbol{C}(\boldsymbol{\chi}_p, \dot{\boldsymbol{\chi}}_p)\dot{\boldsymbol{\chi}}_p = \begin{pmatrix} \boldsymbol{0}_3 \\ \boldsymbol{\omega}_p \times \boldsymbol{I}_{P_0}\boldsymbol{\omega}_p \end{pmatrix}; \quad \boldsymbol{G} = [mg\boldsymbol{e}_3, \boldsymbol{0}_3]^T$$

$$\boldsymbol{W}_m(\boldsymbol{\chi}_p) = \begin{pmatrix} \frac{\boldsymbol{r}'_1}{\|\boldsymbol{r}'_1\|} & \cdots & \frac{\boldsymbol{r}'_{n_c}}{\|\boldsymbol{r}'_{n_c}\|} \\ \boldsymbol{\mathcal{R}}_P^0\boldsymbol{b}_1 \times \frac{\boldsymbol{r}'_1}{\|\boldsymbol{r}'_1\|} & \cdots & \boldsymbol{\mathcal{R}}_P^0\boldsymbol{b}_{n_c} \times \frac{\boldsymbol{r}'_{n_c}}{\|\boldsymbol{r}'_{n_c}\|} \end{pmatrix}$$

3.3.2 Solution of Dynamic Equation

The suspended platform is demanded to track a desired trajectory. Since we focus on the cable dynamic effect, a typical translational CDPM driven by n_c long flexible cables where the suspended platform is reduced to a point mass is considered. Since cable length is convenient to adjust in order to move the suspended platform, here the cable length variation is employed as the input parameter. The dynamics of the deployed cables and the platform can be achieved by solving (3.3.9) and (3.3.10) given as follows:

$$\left[\frac{ES(\|\boldsymbol{r}'_i(s_{0i},t)\| - 1)\boldsymbol{r}'_i(s_{0i},t)}{\|\boldsymbol{r}'_i(s_{0_i},t)\|}\right]' + \rho g\boldsymbol{e}_3 = \rho\ddot{\boldsymbol{r}}_i(s_{0_i},t), \quad \xi_i < s_{0_i} < l_{0_i} \tag{3.3.13}$$

$$m\ddot{\boldsymbol{r}}_i(l_{0i},t) = mg\boldsymbol{e}_3 - \sum_{i=1}^{n_c} \frac{ES(\|\boldsymbol{r}'_i(l_{0i},t)\| - 1)\boldsymbol{r}'_i(l_{0i},t)}{\|\boldsymbol{r}'_i(l_{0_i},t)\|}, \quad s_{0_i} = l_{0_i} \tag{3.3.14}$$

In order to solve the dynamic equations, the partial differential (3.3.13) has to be converted into ordinary differential equations. This is achieved using Ritz's procedure. In this way, the infinite dimensional problem is transformed into a finite dimensional one, thus traditional numerical integration methods can be readily utilized. The configuration of the i^{th} cable can be approximately expressed as the linear combination of mode functions and the corresponding mode coordinates in the following way:

$$\boldsymbol{r}_i(s,t) = \sum_{j=1}^{N} \boldsymbol{N}_{ij}(s,t)\boldsymbol{q}_{ij}(t) \tag{3.3.15}$$

where $\boldsymbol{N}_{ij}(s,t) = diag(u_{ij}(s,t), v_{ij}(s,t), w_{ij}(s,t))$ such that $u_{ij}(s,t)$, $v_{ij}(s,t)$ and $w_{ij}(s,t)$ are the mode functions employed in the x, y, and z directions for the i^{th} cable, respectively $\phi_{ij}(t)$, $\varphi_{ij}(t)$ and $\omega_{ij}(t)$ are the mode coordinates associated with these mode functions. The vector $\boldsymbol{q}_{ij}(t) = [\phi_{ij}(t), \varphi_{ij}(t), \omega_{ij}(t)]^T$ groups these mode coordinates. N is the number of mode functions involved. Since the length of the deployed cable depends on time t, the mode

functions also depend on time, which makes the problem involving variable-length cables more complex. The derivatives of $\boldsymbol{r}_i(s,t)$ with respect to arc length s and time t can be expressed in terms of mode functions and mode coordinates as:

$$\boldsymbol{r}_i'(s,t) = \sum_{j=1}^{N} \boldsymbol{N}_{ij}' \boldsymbol{q}_{ij} \tag{3.3.16}$$

The velocity and acceleration of point P_i can be obtained as:

$$\dot{\boldsymbol{r}}_i(s,t) = \sum_{j=1}^{N} \dot{\boldsymbol{N}}_{ij} \boldsymbol{q}_{ij} + \boldsymbol{N}_{ij} \dot{\boldsymbol{q}}_{ij} \tag{3.3.17}$$

$$\ddot{\boldsymbol{r}}_i(s,t) = \sum_{j=1}^{N} \ddot{\boldsymbol{N}}_{ij} \boldsymbol{q}_{ij} + 2\dot{\boldsymbol{N}}_{ij} \dot{\boldsymbol{q}}_{ij} + \boldsymbol{N}_{ij} \ddot{\boldsymbol{q}}_{ij} \tag{3.3.18}$$

By left-multiplying (3.3.13) by the diagonal matrix $\boldsymbol{N}_{ij}^T$, we get:

$$-\rho \boldsymbol{N}_{ij}^T \ddot{\boldsymbol{r}}_i + \boldsymbol{N}_{ij}^T \left[\frac{ES(\|\boldsymbol{r}_i'(s_{0i},t)\| - 1)\boldsymbol{r}_i'(s_{0i},t)}{\|\boldsymbol{r}_i'(s_{0_i},t)\|} \right]' + \rho g \boldsymbol{N}_{ij}^T \boldsymbol{e}_3 = 0 \tag{3.3.19}$$

From the definition of strain $\varepsilon = \frac{(\|\boldsymbol{r}_i'(s_{0i},t)\|-1)}{\|\boldsymbol{r}_i'(s_{0_i},t)\|}$, we have:

$$-\rho \boldsymbol{N}_{ij}^T \ddot{\boldsymbol{r}}_i + \boldsymbol{N}_{ij}^T \left[ES\varepsilon \boldsymbol{r}_i' \right]' + \rho g \boldsymbol{N}_{ij}^T \boldsymbol{e}_3 = 0 \tag{3.3.20}$$

Since, the dynamic of the drum and the wound cables is not studied, we consider ξ_i null. Now we integrate the above equation from $\xi_i = 0$ to l_i and we get the following expressions:

$$-\rho \int_0^{l_i} \boldsymbol{N}_{ij}^T \ddot{\boldsymbol{r}}_i ds_i + \int_0^{l_i} \boldsymbol{N}_{ij}^T \left[ES\varepsilon \boldsymbol{r}_i' \right]' ds_i + \rho g \int_0^{l_i} \boldsymbol{N}_{ij}^T \boldsymbol{e}_3 ds_i = 0 \tag{3.3.21}$$

$$-\rho \int_0^{l_i} \boldsymbol{N}_{ij}^T \ddot{\boldsymbol{r}}_i ds_i - \int_0^{l_i} ES\varepsilon \boldsymbol{N}_{ij}'^T \boldsymbol{r}_i' ds_i + \rho g \int_0^{l_i} \boldsymbol{N}_{ij}^T \boldsymbol{e}_3 ds_i = 0 \tag{3.3.22}$$

Due to the closed-loop chain of the CDPM, the mode coordinates of all cables are not independent. The independent unknowns adopted in this work are: all mode coordinates for the first cable and the $(N-1)$ modes coordinates for the rest $n_c - 1$ cables. Hence, we have $(3n_cN - 3n_c + 3)$ independent unknown mode coordinates. Referring to (3.3.16) and (3.3.18), we limit ourself to $N-1$ modes resulting in the following equations:

$$-\rho \int_0^{l_i} \sum_{j=1}^{N-1} \boldsymbol{N}_{ij}^T \left[\ddot{\boldsymbol{N}}_{ij} \boldsymbol{q}_{ij} + 2\dot{\boldsymbol{N}}_{ij} \dot{\boldsymbol{q}}_{ij} + \boldsymbol{N}_{ij} \ddot{\boldsymbol{q}}_{ij} \right] ds_i - \int_0^{l_i} \sum_{j=1}^{N-1} ES\varepsilon \boldsymbol{N}_{ij}'^T \boldsymbol{N}_{ij}' \boldsymbol{q}_{ij} ds_i + \rho g \int_0^{l_i} \boldsymbol{N}_{ij}^T \boldsymbol{e}_3 ds_i = 0 \tag{3.3.23}$$

$$\sum_{j=1}^{N-1}\rho\int_0^{l_i}\boldsymbol{N}_{ij}^T\boldsymbol{N}_{ij}ds_i\quad\ddot{\boldsymbol{q}}_{ij}+\sum_{j=1}^{N-1}2\rho\int_0^{l_i}\boldsymbol{N}_{ij}^T\dot{\boldsymbol{N}}_{ij}ds_i\quad\dot{\boldsymbol{q}}_{ij}+$$
$$\sum_{j=1}^{N-1}\left[\rho\int_0^{l_i}\boldsymbol{N}_{ij}^T\ddot{\boldsymbol{N}}_{ij}ds_i+ES\varepsilon\int_0^{l_i}\boldsymbol{N}_{ij}'^T\boldsymbol{N}_{ij}'ds_i\right]\quad\boldsymbol{q}_{ij}=\rho g\int_0^{l_i}\boldsymbol{N}_{ij}^T\boldsymbol{e}_3ds_i \tag{3.3.24}$$

$$\sum_{j=1}^{N-1}\left[\boldsymbol{M}_{ij}\quad\ddot{\boldsymbol{q}}_{ij}+\boldsymbol{C}_{ij}\quad\dot{\boldsymbol{q}}_{ij}+\boldsymbol{K}_{ij}\quad\boldsymbol{q}_{ij}\right]=\boldsymbol{g}_i \tag{3.3.25}$$

where $\boldsymbol{M}_{ij}=\rho\int_0^{l_i}\boldsymbol{N}_{ij}^T\boldsymbol{N}_{ij}ds_i$, $\boldsymbol{C}_{ij}=2\rho\int_0^{l_i}\boldsymbol{N}_{ij}^T\dot{\boldsymbol{N}}_{ij}ds_i$, $\boldsymbol{K}_{ij}=\int_0^{l_i}\boldsymbol{N}_{ij}^T\ddot{\boldsymbol{N}}_{ij}ds_i+\int_0^{l_i}\boldsymbol{N}_{ij}'^T\boldsymbol{N}_{ij}'ds_i$ and $\boldsymbol{f}_{gi}=\rho g\int_0^{l_i}\boldsymbol{N}_{ij}^T\boldsymbol{e}_3ds_i$. The above equation (3.3.25), can be written in matrix form as follows:

$$\boldsymbol{M}_i\ddot{\boldsymbol{q}}_i+\boldsymbol{C}_i\dot{\boldsymbol{q}}_i+\boldsymbol{K}_i\boldsymbol{q}_i=\boldsymbol{f}_{gi} \tag{3.3.26}$$

in which $\boldsymbol{q}_i=[\boldsymbol{q}_{i_1};\boldsymbol{q}_{i_2};...;\boldsymbol{q}_{i_{N-1}}]^T$ groups all the $N-1$ mode coordinates for the i^{th} cable. $\boldsymbol{M}_i=diag([\boldsymbol{M}_{ij}]_{1\leqslant j\leqslant N-1})$ is the mass matrix, $\boldsymbol{C}_i=diag([\boldsymbol{C}_{ij}]_{1\leqslant j\leqslant N-1})$ is the centrifuge matrix, and $\boldsymbol{K}_i==diag([\boldsymbol{K}_{ij}]_{1\leqslant j\leqslant N-1})$ is the stiffness matrix. If we generalize for n_c cables, we have:

$$\boldsymbol{M}_c\ddot{\boldsymbol{q}}+\boldsymbol{C}_c\dot{\boldsymbol{q}}+\boldsymbol{K}_c\boldsymbol{q}=\boldsymbol{f}_g \tag{3.3.27}$$

where $\boldsymbol{q}=[\boldsymbol{q}_1;\boldsymbol{q}_2;...;\boldsymbol{q}_{n_c}]^T$ and $\boldsymbol{M}_c=diag([\boldsymbol{M}_i]_{1\leqslant i\leqslant n_c})$, $\boldsymbol{C}_c=diag([\boldsymbol{C}_i]_{1\leqslant i\leqslant n_c})$ and $\boldsymbol{K}_c=diag([\boldsymbol{K}_i]_{1\leqslant i\leqslant n_c})$ are block matrices. $\boldsymbol{f}_g=[\boldsymbol{f}_{g1},\boldsymbol{f}_{g2},...,\boldsymbol{f}_{gn_c}]^T$. Now assigning $s_{0_i}=l_{0_i}$ in (3.3.16) and (3.3.18) and substituting them into (3.3.14), we can achieve the dynamic equation of the platform in terms of mode coordinates, resulting in the following equations:

$$m\ddot{\boldsymbol{N}}_{i_N}\boldsymbol{q}_{i_N}+2m\dot{\boldsymbol{N}}_{i_N}\dot{\boldsymbol{q}}_{i_N}+m\boldsymbol{N}_{i_N}\ddot{\boldsymbol{q}}_{i_N}=mg\boldsymbol{e}_3-\sum_{i=1}^{n_c}ES\varepsilon\boldsymbol{N}'_{i_N}\boldsymbol{q}_{i_N} \tag{3.3.28}$$

$$m\boldsymbol{N}_{i_N}\ddot{\boldsymbol{q}}_{i_N}+2m\dot{\boldsymbol{N}}_{i_N}\dot{\boldsymbol{q}}_{i_N}+\left(m\ddot{\boldsymbol{N}}_{i_N}+ES\sum_{i=1}^{n_c}\varepsilon\boldsymbol{N}'_{i_N}\right)\boldsymbol{q}_{i_N}=mg\boldsymbol{e}_3 \tag{3.3.29}$$

The differential equations of the cables,(3.3.27), and that of the suspended platform, (3.3.29), provide the necessary equations to determine the $(3n_cN-3n_c+3)$ independent unknown mode coordinates. The dependent unknowns $3n_c-3$ modes coordinates can be determined from the following relation:

$$\boldsymbol{r}_i(l_{0_i},t)=\boldsymbol{\eta}_1^p+\boldsymbol{\mathcal{R}}_P^0\boldsymbol{b}_i,\qquad i\in\{1,2,...,n_c\} \tag{3.3.30}$$

3.4 Numerical Example

The overall objective of this study is to evaluate the effects of cable mass and elasticity on the static stiffness of the CDPM. The difference between the suspended platform pose (position and orientation) obtained through the sagging cable model and the reference pose obtained through the ideal cable model defines the static pose error of the CDPM $\Delta\boldsymbol{\chi}_p$. As already mentioned, the both virtual displacements $\delta\boldsymbol{\varphi}$ and $\delta\boldsymbol{\chi}_p$ are related by following relation:

$$\delta\boldsymbol{\varphi} = \boldsymbol{R}^{-1}\boldsymbol{J}\delta\boldsymbol{\chi}_p \tag{3.4.1}$$

where $\delta\boldsymbol{\varphi}$ represents the virtual displacement vector of motor rotational angle whereas $\delta\boldsymbol{\chi}_p$ represents the virtual displacements vector of the suspended platform caused by the external force and moment tensor. $\boldsymbol{J}$ is the Jacobian matrix and $\boldsymbol{R}$ is a diagonal matrix that groups the n_c drum radius. As already stated, any rotation of the drum corresponds to a released or wound cable portion. The relationship between the variation of unstrained cable length, $\delta\boldsymbol{l}$ and $\delta\boldsymbol{\varphi}$ is $\delta\boldsymbol{l} = \boldsymbol{R}\delta\boldsymbol{\varphi}$, then we have:

$$\delta\boldsymbol{\chi}_p = \boldsymbol{J}^{+}\delta\boldsymbol{l} \tag{3.4.2}$$

in which, $\boldsymbol{J}^{+} = \boldsymbol{J}^{T}(\boldsymbol{J}\boldsymbol{J}^{T})^{-1}$ is the pseudo-inverse of $\boldsymbol{J}$. For a given position and orientation of the suspended platform, a set of unstrained cable length l_{0_i} can be obtained through the inverse kinematic model. Two different cable models can be used for inverse kinematic model : (i) the ideal cable model where the cable is considered to be an inextensible straight line, (ii) the sagging cable model where the elastic catenary is employed considering both the cable elasticity and the effect of cable weight on the static cable profile. The difference between the cable length, l_{0_i}, obtained through the sagging cable model and the cable length,l_i, obtained through the ideal cable model defines the deflection of the i^{th} cable, namely $\Delta l_i = l_{0_i} - l_i$. In this way, $\Delta\boldsymbol{l} = [\Delta l_1, \Delta l_2, ..., \Delta l_{n_c}]^T$ is a vector consisting of all the n_c cable deflections. Hence, the platform pose error $\Delta\boldsymbol{\chi}_p$ can be defined as follows:

$$\Delta\boldsymbol{\chi}_p = \boldsymbol{J}^{+}\Delta\boldsymbol{l} \tag{3.4.3}$$

This relation gives the variation of the platform pose error due to the deformation of cables length. This variation of the platform can be defined as an index for the static stiffness evaluation.

To achieve the above objectives, simulation experiments are conducted on a suspended CDPM, called CoGiRo **cogiro2013**. The CoGiRo is a redundantly actuated CDPM developed by LIRMM and Tecnalia. The dimensions of this prototype are about 15 m in length, 11 m in width and 5 m in high giving a potential workspace of 677 m^3. The mobile platform is a cube with 1 m side length and a total mass of 79 kg. The base and platform cable attachment points are listed in Table 3.1. Winches are capable of pulling the 10 mm diameter

cables at up to 4150 N. Assume that all cables have the same Young's modulus $E = 100$ GPa and mass per unit length $\rho = 0.346$ kg/m.

TABLE 3.1: The base and platform cable attachment points

	x_{a_i}	y_{a_i}	z_{a_i}		x_{b_i}	y_{b_i}	z_{b_i}
a_1	-7.5	-5.5	6	b_1	0.5	-0.5	0
a_2	-7.5	-5.5	6	b_2	-0.5	0.5	1
a_3	-7.5	5.5	6	b_3	-0.5	-0.5	0
a_4	-7.5	5.5	6	b_4	0.5	0.5	1
a_5	7.5	5.5	6	b_5	-0.5	0.5	0
a_6	7.5	5.5	6	b_6	0.5	-0.5	1
a_7	7.5	-5.5	6	b_7	0.5	0.5	0
a_8	7.5	-5.5	6	b_8	-0.5	-0.5	1

CoGiRo is supposed to perform pick-and-place tasks. In this simulation, we consider two cases. In Case A, the platform mass is 79 kg whereas in Case B, the platform mass goes up to 200 kg. The inertial parameters of the platform are given in Table 3.2.

TABLE 3.2: Platform inertia parameters

	Platform mass (kg)	Platform moment inertia matrix (kgm^2)					
		XX	YY	ZZ	XY	XZ	YZ
Case A	79	62	60	22	-0.32	-0.02	4.5
Case B	200	132	130	45	00	-3	-2

The Figures 3.1 and 3.2 show the variation of the pose error of a CDPM with sagging cables along the vertical direction over the sub-workspace caused by axial cable elasticity with respectively a fixed external load of 79 kg and 200 kg. The sub-workspace is defined by $-3m < x < 3m$, $-3m < y < 3m$ and $Z = 3m$. As illustrated in Figures 3.1 and 3.2, the static pose error of the suspended platform varies significantly with the robot posture. The pose error tends to decrease as the distance from the platform to the Y-axis becomes larger.

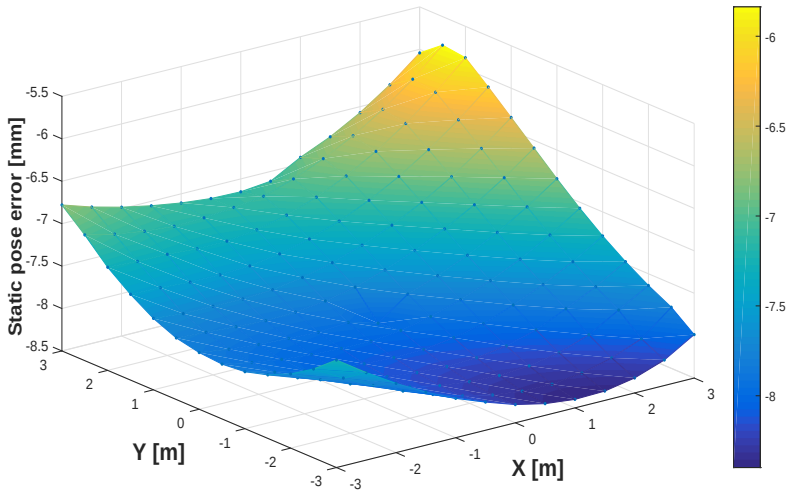

FIGURE 3.1: Static pose error of the platform for CDPM with sagging cables along the vertical direction over the sub-workspace for 79 kg external load

As shown in Figures 3.1 and 3.2, the static pose error calculated for a 200 kg external load is lower than that calculated for the one of 79 kg. In general, the pose error is smallest near the center of the sub-workspace, while it becomes bigger near the edge of the workspace. The simulation results show that the static positioning accuracy along the vertical direction is not that important in both cases.

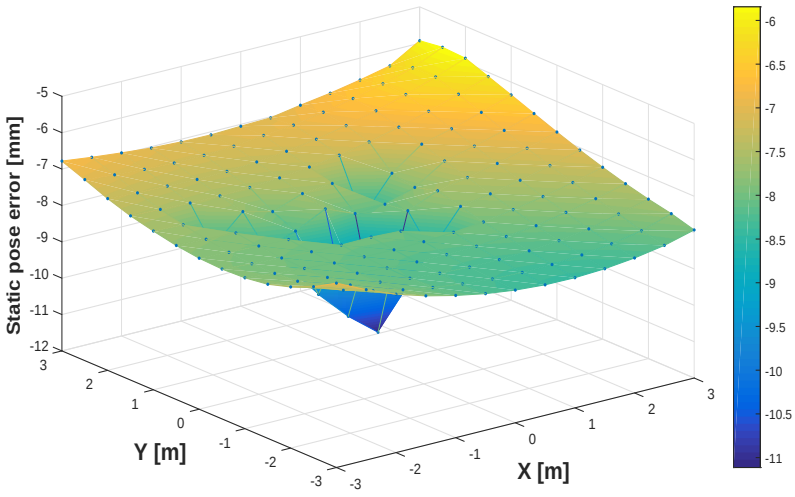

FIGURE 3.2: Static pose error of the platform for CDPM with sagging cables along the vertical direction over the sub-workspace for 200 kg external load

3.5 Conclusion

Driven a manipulator by cables have significant advantages, but it involves many technical challenges. The stiffness of a CDPM is one of the most critical ones because unexpected cable vibration always occurs due to the cable stiffness influenced by its elasticity and mass. The overall objective of this chapter is to study the static and dynamic positioning accuracy especially for a suspended pick-and-place CDPM. Although the sagging cable model is more accurate than the massless cable models, it is more complex in computation. This drawback represents a big challenge for real-time applications. Further, a numerical example is given to evaluate the effects of cable mass and elasticity on the static stiffness of the CDPM. The simulation results show that the static positioning accuracy along the vertical direction is not important. Based on this latter results, a non-elastic massless cable model is used to design a robust controller in the next chapter to accurately pick up and lay down load.

Chapter 4

Robust Trajectory Tracking Control of Cable-Driven Parallel Manipulator

Contents

4.1 Introduction

One of the most important feature of a CDPMs is its capacity to accomplish different type of tasks with a high level of performance, maneuverability and with less oversight of human operators. This chapter aims to design a robust controller for stable tracking control for both conventional CDPM and mobile CDPM. First, a dual-space feedforward control scheme is proposed with a joint space PD corrector for conventional CDPM. Then, Sliding Mode Controller (SMC) based on switching theory and Lyapunov's theory is elaborated for mobile CDPM. Results demonstrate that the application of the proposed controller leads to high accuracy in the trajectory tracking while cables remain always in tension .

4.2 Redundancy of the CDPM

The control of the CDPM is not trivial. Compared to parallel robots with rigid arms, the cable forces of a CDPM must be kept in tension in all manoeuvres. Therefore, the components of the tension vector must remain strictly positives. If the command requires a cable to push when it is not capable, the platform will be unable to reach the desired position and the CDPM will not be controllable.

In order to overcome this constraint while controlling all the degrees of freedom (DOF) of the platform, it is possible to design CDPMs with redundancy of actuation (more actuators than DOF ($n_c > n$) with n the number of DOF and n_c the number of driven cables). Redundant actuation is usually used to keep all the driving cables in tension during the movement of CDPMs. This type of redundancy refers to the use of more actuators than are strictly necessary at least with one degree of actuation redundancy. For redundant manipulators, there exist an infinite number of tension distributions to balance a given wrench applied on the end-effector. Therefore, the control design must integrate an optimal tension distribution which minimize actuation energy according to the kinematics and dynamic conditions. As a consequence, it is important to note that actuation redundancy does not only provide fault tolerance if one of the actuators fail, but also eliminates singularities and thus increase the usable workspace.

Extensive research on tension distribution algorithms are carried out to resolve the actuation redundancy present in most CDPMs. Each of these approaches have different characteristics and varying computational cost. If the sum of all tensions is used as the objective function, then the optimization of tension distribution becomes a linear programming problem. Furthermore, the L2-norm, which results in a quadratic programming problem, seeks to minimize the sum of the squared tensions in order to guarantee continuity by providing a smooth objective function. Another important issue is the determination the lower or upper tension limits. In fact, in order to keep all the cables in tension, positive lower and upper boundary of cable forces are used as constraints in tension distribution algorithms such that cable forces are bounded between minimal and maximal tension values for redundant CDPMs. The upper boundary is notably given by the maximal admissible cable strain whereas the lower boundary is usually set as the lowest acceptable tension with the goal of avoiding slack cables. The value for the lower-boundary of cable forces is chosen arbitrarily and usually the same for all driving cables [38]. In some case, operation at a fixed lower tension limits tends to cause cable sag and decreases cable stiffness. An important cable sag can even cause the end-effector to become under-constrained which means that some driving cables may not have adequate tensions to make robot under control. Indeed, some other driving cables may have more than enough tension to maintain the cable sag low, which is a waste of motor torque and energy consumption. Thus the drawback of fixed lower-boundary emerges.

Usually an optimizer uses iterative algorithms which leads to non-predictable worst-case runtime and requires a large number of iterations to converge. Hence, those aforementioned

methods are not applicable within a real-time controller. Let us note that redundancy resolution turns out to be challenging when the computation has to be done in real time. To get the challenge, a non-iterative efficient methods have been proposed in order to find a feasible tension distribution. Mikelsons et al. propose such a method in which the barycenter of the polytope of feasible tension distributions is determined [76]. However, this method requires the computation of all the vertices of this polytope which takes a lot of time. It is based on geometric considerations applied to the two-dimensional convex polytope of feasible cable tension distribution. This polytope is defined as the intersection between the set of inequality constraints on the cable tension values and the affine space of tension solutions to the mobile platform static or dynamic equilibrium.

Lamaury et al. elaborate a fast algorithm aiming at a real-time implementation of the barycentric approach [51]. The proposed algorithm is dedicated to CDPM with two degree of redundancy. The idea consists essentially in computing a first vertex of this polygon and finding the others by moving from one vertex to the next one while following the polygon one-dimensional boundary which is made of straight line segments. Once all the polygon vertices are determined, the barycenter (centroid) is simply obtained by well-known closed-form formulas. Therefore, the barycentric approach provides a tension distribution set point far from the boundaries of the polytope of feasible tension distributions.

The vast majority of the published works use optimization algorithms in order to obtain an optimal tension distribution [77],[78] . The use of the optimization algorithm has the major advantage of minimizing the tensions of the cables and therefore the energy absorbed by the motors. In this chapter, the problem of tension distribution is formulated as a quadratic programming method as follows:

Compute: $\min \left[\|\boldsymbol{T}\| = (\Sigma_{i=1}^{n_c} t_i^2)^{\frac{1}{2}} \right]$ such as $\boldsymbol{WT} = \boldsymbol{F}_e$ and $0 < t_{imin} \leq t_i \leq t_{imax} \qquad i = \{1, ..., n_c\}$

For redundant manipulators, there exist an infinite number of tension distributions $\boldsymbol{T} = \boldsymbol{W}^+ \boldsymbol{F}_e$. Here, $\boldsymbol{W}^+$ is the pseudo-inverse of the force transmission matrix $\boldsymbol{W}$ and $\boldsymbol{F}_e$ is the external wrench applied on the geometric center of the platform. The solution of the above linear programming problem can result into positive or negative tensions of the cables. Since the cables of the CDPM can only work in tension, a constrained optimization technique is proposed in here such that all its components t_i are contained between minimal and maximal tension values t_{imin} and t_{imax}. The maximum t_{imax} is notably given by the maximal admissible cable strain whereas t_{imin} is usually set as the lowest acceptable tension with the goal of avoiding slack cables ($t_{imin} > 0$).

4.3 Conventional Cable Driven Parallel Manipulator

Several control schemes such as PID controller is proposed for cable-driven parallel robots **KHOSRAVI2014**. This technique is the most common control algorithm used in many applications, particularly in the industry, because of its simplicity. However, this controller

demonstrates low robust ability and difficulties in tuning the gains PID corrector in operational space. To overcome such a difficulty, Kawamura et al. propose a Proportional-Derivative Controller (PD) with feedback in the joint space, only the weight of the platform is compensated [79]. The stability of the control law is demonstrated by a Lyapunov function. A similar control scheme (PD corrector in the joint space with feedback linearization) is proposed by Agrawal but with a compensation of the platform dynamics [80]. Other works propose a dual-space feedforward control scheme in operational space with two feedforward terms to compensate both the platform and the winch dynamics [51]. This proposed dual-space feedforward controller relies on a good knowledge of the system parameters. Since some of them can be unknown or may vary during the execution of the task, these controllers can provide erroneous inputs decreasing the tracking and regulation performances. In order to handle such parametric uncertainties and variability, adaptive control is proposed for controlling CDPM [81], [82]. Essentially, the goal of this technique is to tune the controller on-line according to the state of the system. In this section, a dual-space feed-forward control scheme with a joint space PD corrector is introduced. This proposed controller not only guarantees a well tracking performance of the redundantly actuated parallel manipulator, but also enables to easily embed a tension distribution algorithm.

4.3.1 Inverse Dynamics with PD Controller

The ultimate control objective is to move the suspended platform along a prescribed desired trajectory. In this chapter, we do not concern ourselves with the actual trajectory planning problem. The dynamic equations of the CDPM are nonlinear and complex. For this purpose, a dual-space feedforward control scheme, which are based on inverse dynamics, is designed with a joint space PD corrector. To improve the tracking performance of the CDPM, the controller must take into account the dynamic model of the robot in order to compensate the applied forces. Therefore, this technique presumes that the equations of motion as well as all the relevant geometric and inertial parameters of the system are known. We assume that elasticity of cables can be ignored and cables behave as massless rigid strings. Because the technique is model-based, the full robot motion equations of n_c-cable parallel robot with loaded platform and actuators (winches) in operational space are given by (2.2.32):

$$\boldsymbol{J}^T(\boldsymbol{\chi}_p)\boldsymbol{R}^{-1}\boldsymbol{\Gamma} = \boldsymbol{M}_{eq}(\boldsymbol{\chi}_p)\ddot{\boldsymbol{\chi}}_p + \boldsymbol{C}_{eq}(\boldsymbol{\chi}_p,\dot{\boldsymbol{\chi}}_p)\dot{\boldsymbol{\chi}}_p - \boldsymbol{G} \tag{4.3.1}$$

with

- $\boldsymbol{M}_{eq}(\boldsymbol{\chi}_p) = \boldsymbol{M}(\boldsymbol{\chi}_p) + \boldsymbol{J}^T(\boldsymbol{\chi}_p)\boldsymbol{R}^{-1}\boldsymbol{I}_m\boldsymbol{R}^{-1}\boldsymbol{J}(\boldsymbol{\chi}_p)$.
- $\boldsymbol{M}_{eq}(\boldsymbol{\chi}_p,\dot{\boldsymbol{\chi}}_p) = \boldsymbol{C}(\boldsymbol{\chi}_p,\dot{\boldsymbol{\chi}}_p) + \boldsymbol{J}^T(\boldsymbol{\chi}_p)\boldsymbol{R}^{-1}\boldsymbol{I}_m\boldsymbol{R}^{-1}\dot{\boldsymbol{J}}(\boldsymbol{\chi}_p)$.

The state vector of the suspended platform is defined by an operational space vector $\boldsymbol{\chi}_p$ and Γ is the actuator torque input vector. $\boldsymbol{M}(\boldsymbol{\chi}_p)$ is the inertia matrix, $\boldsymbol{C}(\boldsymbol{\chi}_p,\dot{\boldsymbol{\chi}}_p)$ is the matrix of Coriolis and centrifugal and $\boldsymbol{G}$ is the gravitational force vector. The diagonal

matrix $\boldsymbol{I}_m$ denotes the inertia matrix of the actuator and $\boldsymbol{R}$ is a diagonal matrix such that $diag(\boldsymbol{R}) = [d_1, d_2, ..., d_{n_c}]^T$, d_i is the drum radius of i^{th} winch. The Jacobian matrix $\boldsymbol{J}(\boldsymbol{\chi}_p)$ of the CDPM relates the operational velocity of the suspended platform $\dot{\boldsymbol{\chi}}_p$ to the joint velocities of the n_c winches $\dot{\boldsymbol{\varphi}}$, where $\dot{\boldsymbol{\varphi}} = \boldsymbol{R}^{-1}\boldsymbol{J}(\boldsymbol{\chi}_p)\dot{\boldsymbol{\chi}}_p$. The joint velocity vector of motor rotational angle, denoted $\dot{\boldsymbol{\varphi}} = [\dot{\varphi}_1, \dot{\varphi}_2, ..., \dot{\varphi}_{n_c}]^T$ and its time derivative $\ddot{\boldsymbol{\varphi}}$ are assumed to be measured (by means of incremental encoders).

The proposed controller may be implemented with a correction in the operational space. However, a direct measurement of the platform state vector $\boldsymbol{\chi}_p$ across a large workspace is difficult. Consequently, a dual-space feed-forward controller is proposed to take advantages of both space coordinates. Specifically, the designed controller requires the measurements of the joint coordinate vector of motor rotational angle and its derivative in the feedback loop. Further, this inverse dynamic controller uses the reference signals and the measured signals of the state vector from the trajectory generation to compensate the loaded platform dynamics with an operational space feed-forward force vector term. Thus, the control law is given by:

$$\boldsymbol{J}^T(\boldsymbol{\chi}_p)\boldsymbol{R}^{-1}\boldsymbol{\Gamma} = \boldsymbol{M}_{eq}(\boldsymbol{\chi}_p)\ddot{\boldsymbol{\chi}}_{p_d} + \boldsymbol{C}_{eq}(\boldsymbol{\chi}_p, \dot{\boldsymbol{\chi}}_p)\dot{\boldsymbol{\chi}}_{p_d} - \boldsymbol{G} + \boldsymbol{J}^T(\boldsymbol{\chi}_p)\boldsymbol{R}^{-1}(\boldsymbol{K}_p\boldsymbol{e}_\varphi + \boldsymbol{K}_d\dot{\boldsymbol{e}}_\varphi) \quad (4.3.2)$$

Where $\boldsymbol{M}_{eq}(\boldsymbol{\chi}_p)\ddot{\boldsymbol{\chi}}_{p_d} + \boldsymbol{C}_{eq}(\boldsymbol{\chi}_p, \dot{\boldsymbol{\chi}}_p)\dot{\boldsymbol{\chi}}_{p_d} - \boldsymbol{G}$ compensates the loaded platform dynamics and the term $\boldsymbol{J}^T(\boldsymbol{\chi}_p)\boldsymbol{R}^{-1}(\boldsymbol{K}_p\boldsymbol{e}_\varphi + \boldsymbol{K}_d\dot{\boldsymbol{e}}_\varphi)$ tracks the desired trajectory. The two positive definite matrix $\boldsymbol{K}_p$ and $\boldsymbol{K}_d$ denote the gain of a PD corrector. The controller consists in converting the desired platform trajectory $\boldsymbol{\chi}_{p_d}$ and velocity $\dot{\boldsymbol{\chi}}_{p_d}$ into their associated joint positions $\boldsymbol{\varphi}_d$ and velocity $\dot{\boldsymbol{\varphi}}_d$ using the inverse kinematic model. The operational tracking error $\boldsymbol{e}_{\chi_p} = \boldsymbol{\chi}_{p_d} - \boldsymbol{\chi}_p$ is then converted into $\boldsymbol{e}_\varphi = \boldsymbol{\varphi}_d - \boldsymbol{\varphi}$ by means of the pseudo-inverse of the Jacobian matrix in order to apply the PD corrector in the joint space. Thereafter a dual-space feed-forward control scheme (see Figure 4.1) is proposed by integrating a cable tension distribution algorithm ensuring that the control is capable to keep the cable tensions of the CDPM always positive.

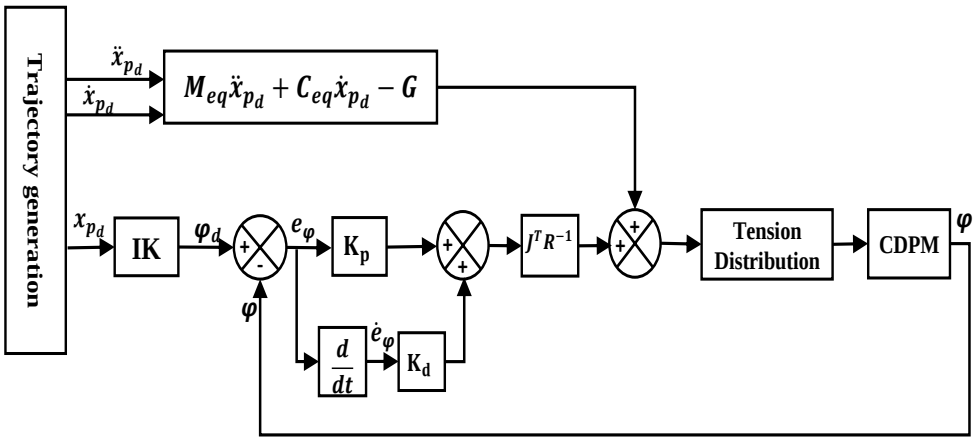

FIGURE 4.1: Dual-space feed-forward control scheme with a joint space PD corrector

4.3.2 Stability Analysis

Referring to the control law given by (4.3.2) and the dynamic model given by (4.3.1), the closed loop system is:

$$\boldsymbol{M}_{eq}(\boldsymbol{\chi}_p)\ddot{\boldsymbol{e}}_{\boldsymbol{\chi}_p} + \boldsymbol{C}_{eq}(\boldsymbol{\chi}_p, \dot{\boldsymbol{\chi}}_p)\dot{\boldsymbol{e}}_{\boldsymbol{\chi}_p} + \boldsymbol{J}^T(\boldsymbol{\chi}_p)\boldsymbol{R}^{-1}(\boldsymbol{K}_p\boldsymbol{e}_\varphi + \boldsymbol{K}_d\dot{\boldsymbol{e}}_\varphi) = 0 \tag{4.3.3}$$

in which, $\boldsymbol{e}_{\chi_p} = \boldsymbol{\chi}_{p_d} - \boldsymbol{\chi}_p$ et $\boldsymbol{e}_\varphi = \boldsymbol{\varphi}_d - \boldsymbol{\varphi}$. Although the dynamic equations of the global system are nonlinear and complex, they have some known properties which are necessary for the controller synthesis and stability analysis:

- *Property* 1 The inertia matrix $\boldsymbol{M}_{eq}(\boldsymbol{\chi}_p)$ is symmetric and positive definite.
- *Property* 2 The matrix $\dot{\boldsymbol{M}}_{eq}(\boldsymbol{\chi}_p) - 2\boldsymbol{C}_{eq}(\boldsymbol{\chi}_p, \dot{\boldsymbol{\chi}}_p)$ is skew symmetric.

Let V be the Lyapunov function for the closed loop system:

$$V = \frac{1}{2}\dot{\boldsymbol{e}}_{\chi_p}^T\boldsymbol{M}_{eq}\dot{\boldsymbol{e}}_{\chi_p} + \frac{1}{2}\boldsymbol{e}_\varphi^T\boldsymbol{K}_p\boldsymbol{e}_\varphi \geq 0 \tag{4.3.4}$$

$\boldsymbol{K}_p$ is chosen as a positive definite diagonal matrix. The time derivative of the Lyapunov function is given by :

$$\dot{V} = \dot{\boldsymbol{e}}_{\chi_p}^T\boldsymbol{M}_{eq}\ddot{\boldsymbol{e}}_{\chi_p} + \frac{1}{2}\dot{\boldsymbol{e}}_{\chi_p}^T\dot{\boldsymbol{M}}_{eq}\dot{\boldsymbol{e}}_{\chi_p} + \dot{\boldsymbol{e}}_\varphi\boldsymbol{K}_p\boldsymbol{e}_\varphi \tag{4.3.5}$$

By substituting $\boldsymbol{M}_{eq}\ddot{\boldsymbol{e}}_{\chi_p}$ from the closed loop system:

$$\dot{V} = \frac{1}{2}\dot{\boldsymbol{e}}_{\chi_p}^T(\dot{\boldsymbol{M}}_{eq}(\boldsymbol{\chi}_p) - 2\boldsymbol{C}_{eq}(\boldsymbol{\chi}_p, \dot{\boldsymbol{\chi}}_p))\dot{\boldsymbol{e}}_{\chi_p} - \dot{\boldsymbol{e}}_{\chi_p}^T\boldsymbol{J}^T(\boldsymbol{\chi}_p)\boldsymbol{R}^{-1}(\boldsymbol{K}_p\boldsymbol{e}_\varphi + \boldsymbol{K}_d\dot{\boldsymbol{e}}_\varphi) + \dot{\boldsymbol{e}}_\varphi^T\boldsymbol{K}_p\boldsymbol{e}_\varphi \tag{4.3.6}$$

Using the inverse kinematic model (2.2.15) and by replacing $\dot{\boldsymbol{e}}_{\varphi}^{T}$ by $\dot{\boldsymbol{e}}_{\chi_p}^{T}\boldsymbol{J}^{T}(\boldsymbol{\chi}_p)\boldsymbol{R}^{-1}$ in the subsequent equation we get:

$$\dot{V} = \frac{1}{2}\dot{\boldsymbol{e}}_{\chi_p}^{T}(\dot{\boldsymbol{M}}_{eq}(\boldsymbol{\chi}_p) - 2\boldsymbol{C}_{eq}(\boldsymbol{\chi}_p, \dot{\boldsymbol{\chi}}_{p_d}))\dot{\boldsymbol{e}}_{\chi_p} - \dot{\boldsymbol{e}}_{\varphi}^{T}\boldsymbol{K}_d\dot{\boldsymbol{e}}_{\varphi} \tag{4.3.7}$$

According to property 2, the first term vanishes and therefore:

$$\dot{V} = -\dot{\boldsymbol{e}}_{\varphi}^{T}\boldsymbol{K}_d\dot{\boldsymbol{e}}_{\varphi} \leq 0 \tag{4.3.8}$$

where $\dot{V} \leq 0$ since $\boldsymbol{K}_d$ is chosen to be positive definite. Referring to LaSalle's Invariance Principle the system is stable. Thus, the motion converges to a maximum invariant set which satisfies $\dot{V} = 0$. This implies that $\dot{\boldsymbol{e}}_{\varphi} = 0$. Due to the kinematic relation $\dot{\boldsymbol{e}}_{\varphi} = \boldsymbol{R}^{-1}\boldsymbol{J}(\boldsymbol{\chi}_p)\dot{\boldsymbol{e}}_{\chi_p}$, $\dot{\boldsymbol{e}}_{\chi_p} = 0$. Substituting these on (4.3.3), we get $\boldsymbol{e}_{\varphi} = 0$. This means that $\boldsymbol{\varphi}$ tends to $\boldsymbol{\varphi}_d$ as time t goes to infinity.

4.3.3 Simulation Results

The overall objective of this study is to evaluate the capability of the proposed controller to move the platform while keeping it stable along the trajectory. To achieve the above objectives, simulation experiments are conducted on a suspended CDPM, called CoGiRo. The CoGiRo prototype is a redundantly actuated CDPM developed by LIRMM and Tecnalia. The dimensions of this prototype are about 15 m in length, 11 m in width and 5 m in high giving a potential workspace of 677 m^3. The mobile platform is a cube with 1 m side length and a total mass of 79 kg. It is capable of manipulating payloads of 300 kg over the entire workspace. The inertial parameters of the platform with and without a typical payload are given in Table 4.2. CoGiRo has 8−actuators with a 6−DOF moving platform. The base and platform cable attachment points are listed in Table 4.1. Winches are capable of pulling the 10 mm diameter cables at up to 4150 N.

TABLE 4.1: The base and platform cable attachment points

	x_{a_i}	y_{a_i}	z_{a_i}		x_{b_i}	y_{b_i}	z_{b_i}
a_1	−7.5	−5.5	6	b_1	0.5	−0.5	0
a_2	−7.5	−5.5	6	b_2	−0.5	0.5	1
a_3	−7.5	5.5	6	b_3	−0.5	−0.5	0
a_4	−7.5	5.5	6	b_4	0.5	0.5	1
a_5	7.5	5.5	6	b_5	−0.5	0.5	0
a_6	7.5	5.5	6	b_6	0.5	−0.5	1
a_7	7.5	−5.5	6	b_7	0.5	0.5	0
a_8	7.5	−5.5	6	b_8	−0.5	−0.5	1

TABLE 4.2: Platform inertia parameters

	Platform mass (kg)	Platform moment inertia matrix (kgm^2)					
		XX	YY	ZZ	XY	XZ	YZ
Without load	79	62	60	22	-0.32	-0.02	4.5
With load	200	132	130	45	00	-3	-2

CoGiRo is supposed to perform pick-and-place tasks. In this simulation study, the desired trajectory given in Table 4.3 is chosen such that the moving platform reaches 5 poses during pick-and-place task. It has been generated by a 5th-order polynomial interpolation given by the following expression:

$$f(t) = h_i \frac{(t_f - t)^5}{(t_f - t)^5 + (t - t_i)^5} + h_d \frac{(t - t_i)^5}{(t - t_i)^5 + (t_f - t)^5} \quad \text{if} \quad t_i \leq t \leq t_f \tag{4.3.9}$$

TABLE 4.3: The desired trajectory of the platform

	x_p	y_p	z_p	ϕ_p	θ_p	ψ_p		x_p	y_p	z_p	ϕ_p	θ_p	ψ_p
p_1	0	0	1.3	0	0	0	p_4	1.4	-0.7	2.5	0	0	0
p_2	0	0	2.5	0	0	0	p_5	0	0	2.5	0	0	0
p_3	-1.1	1.2	2.5	0	0	25	p_6	0	0	1.3	0	0	0

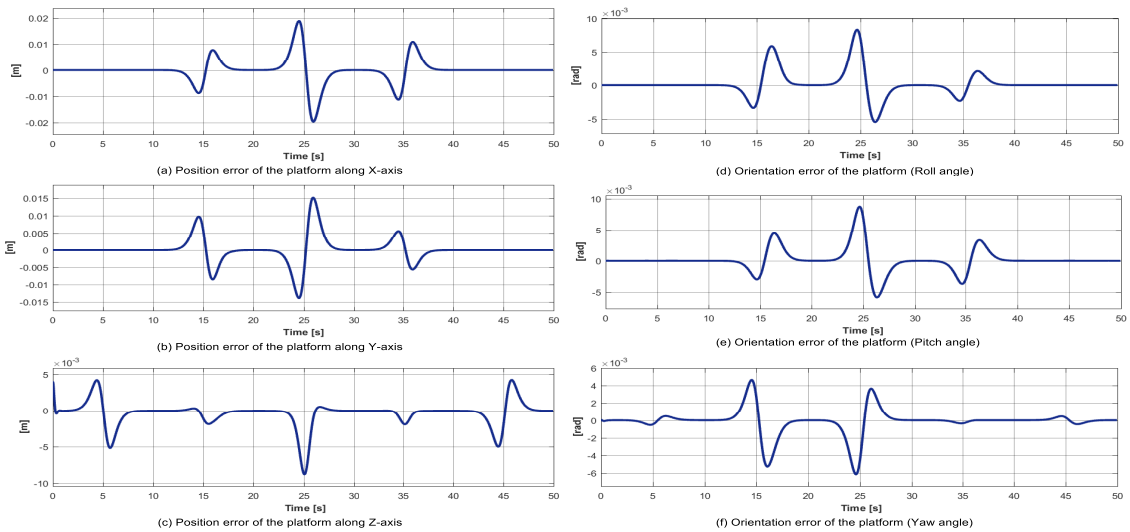

FIGURE 4.2: Position and orientation error of the platform (Case A)

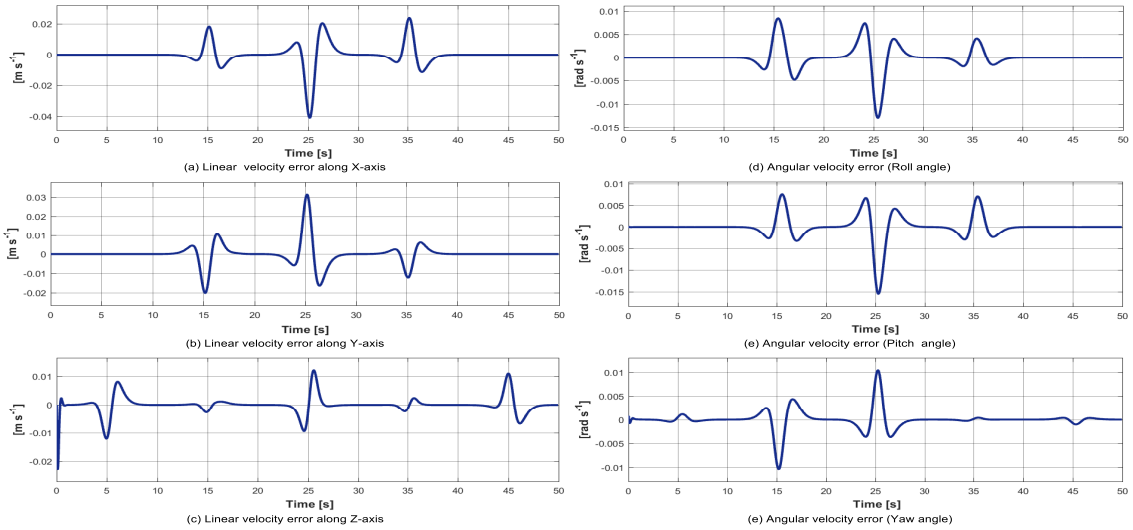

FIGURE 4.3: Linear and angular velocity error of the platform (Case A)

The simulation results show that the proposed controller provides a non-negative and continuous tension distribution along the whole trajectory. As it is shown in Figures 4.2, 4.3, 4.6 and 4.7, position and orientation outputs reach the desired path for both case A and B.

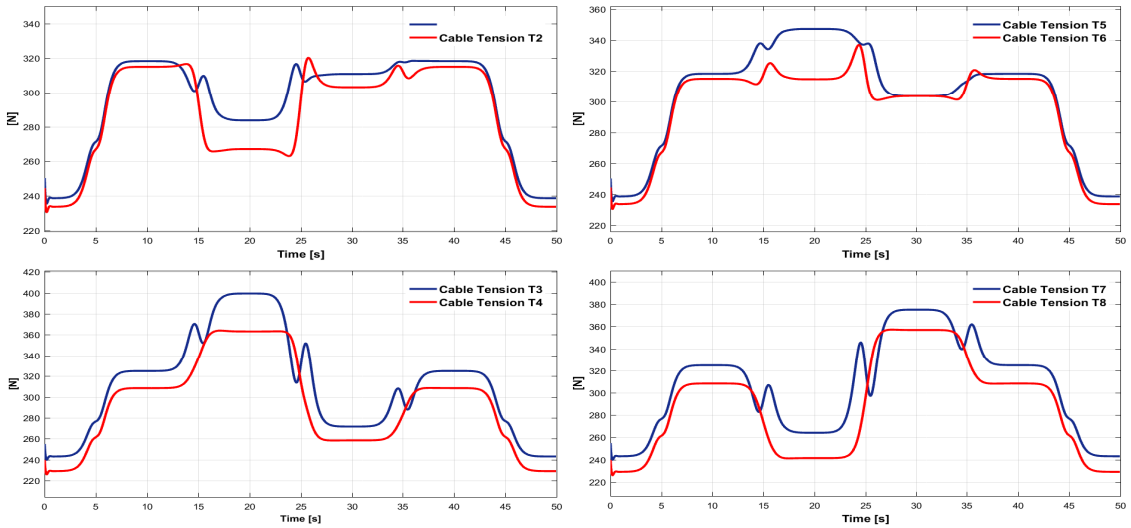

FIGURE 4.4: Cables tension (Case A)

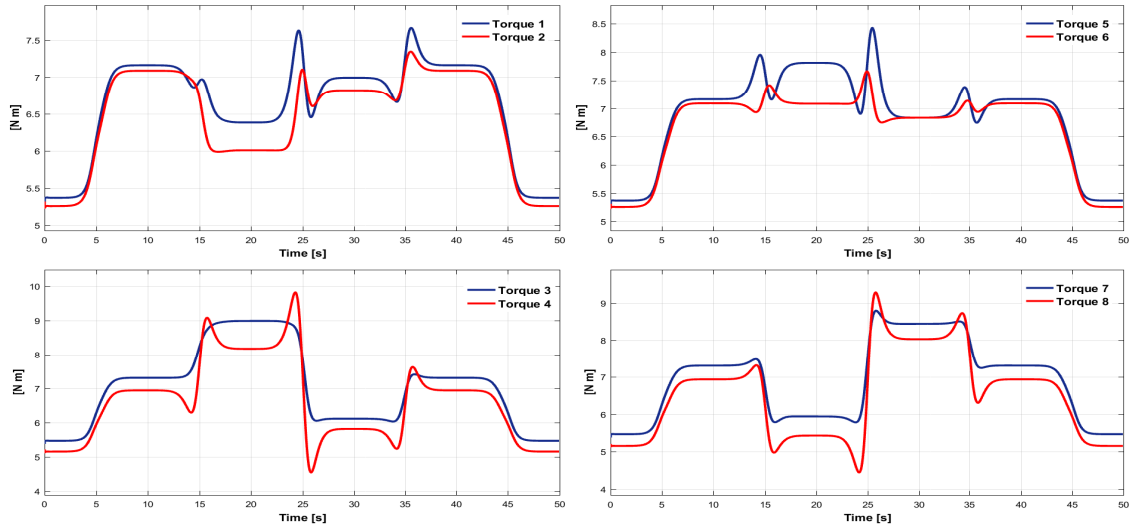

FIGURE 4.5: Winches torque (Case A)

To prove the robustness of the proposed controller, we consider two simulation cases. In Case A, the dual-space feed-forward controller is simulated with no-load platform whereas in Case B, we consider loading the platform at configuration p_1 and releasing the load at configuration p_3. We have to state that the control parameters in our algorithms are all the same in each case (i.e without and with load). For the fast convergence, the gain matrix were selected as $\boldsymbol{K}_p = diag(1.3, 1.3, 3.5, 1.1, 1.1, 1.1)$ and $\boldsymbol{K}_d = diag(0.4, 0.4, 0.4, 0.37, 0.37, 0.37)$.

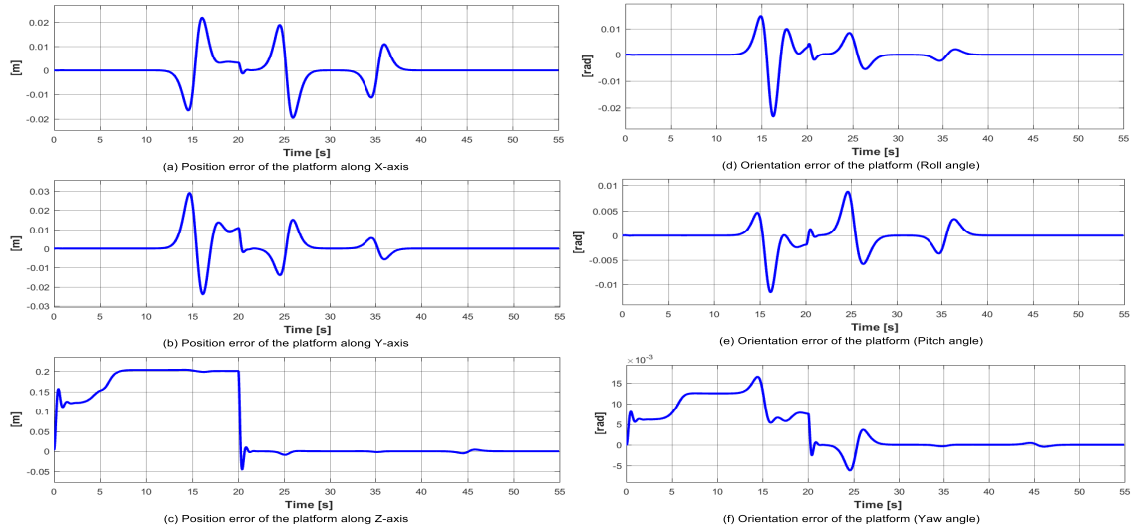

FIGURE 4.6: Position and orientation error of the platform (Case B)

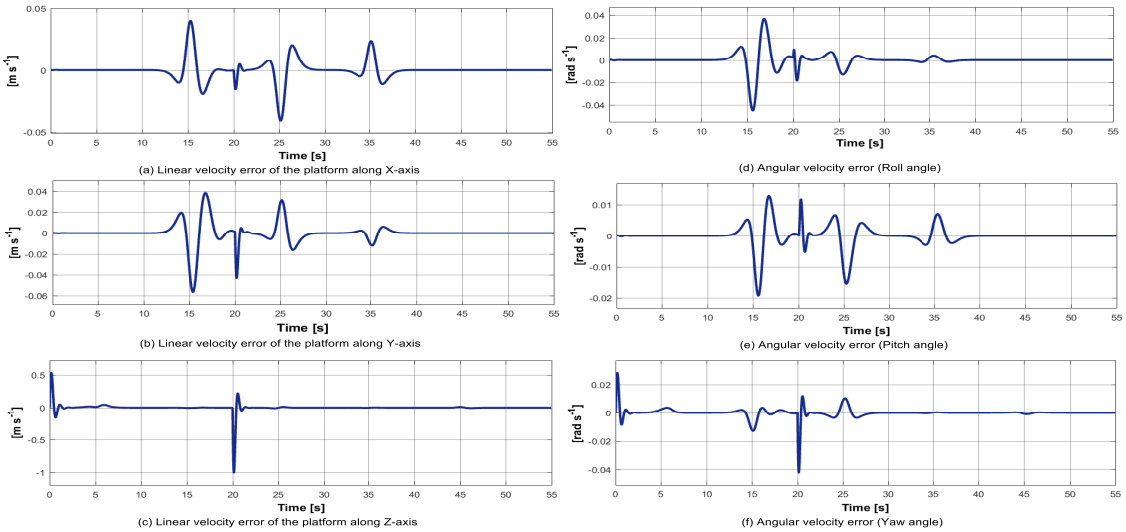

FIGURE 4.7: Linear and angular velocity error of the platform (Case B)

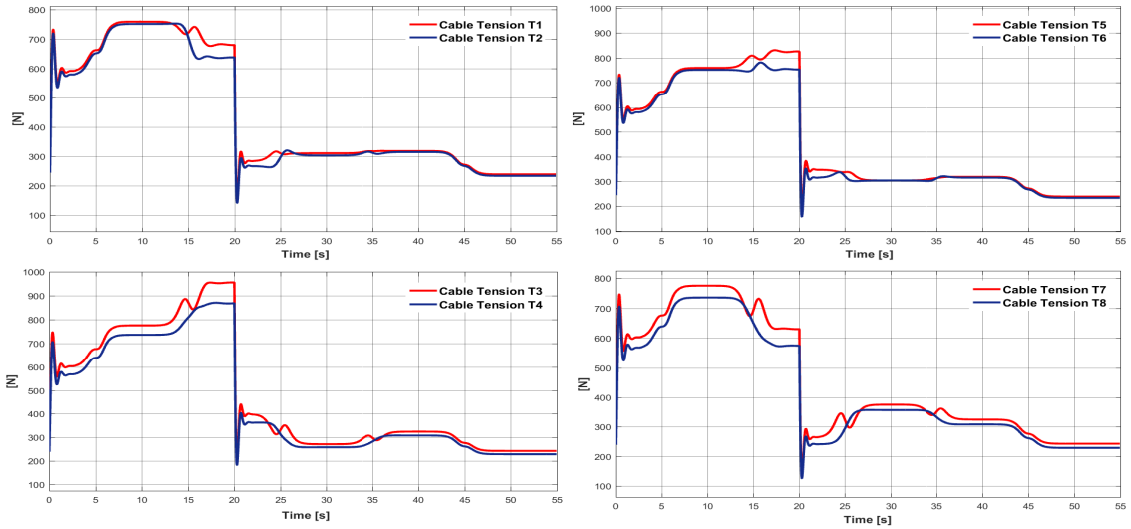

FIGURE 4.8: Cables tension (Case B)

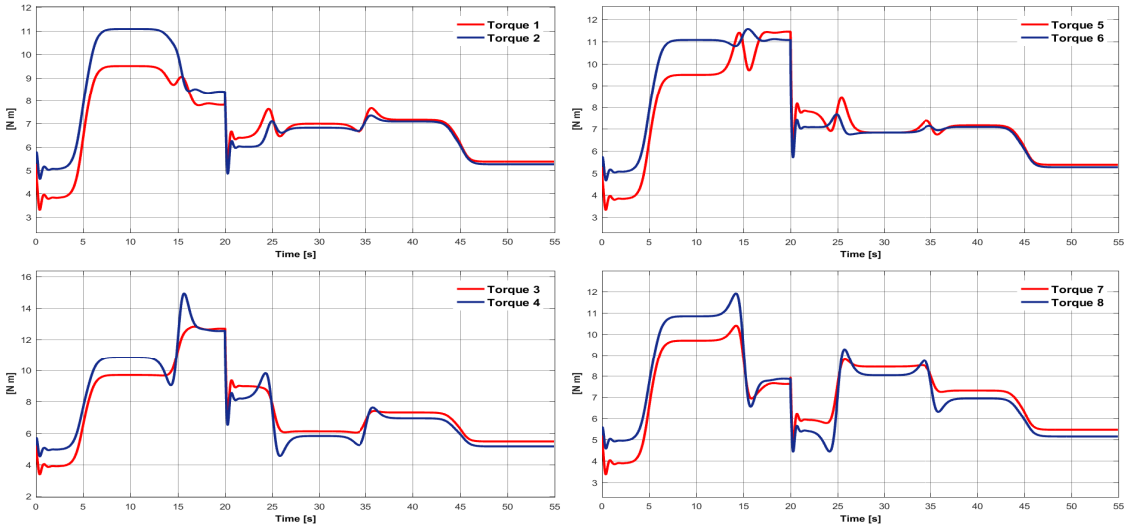

FIGURE 4.9: Winches torque (Case B)

4.4 Mobile Cable Driven Parallel Manipulator

For a mobile CDPM, the position and orientation of the suspended platform depend on the cables length which can be adjusted by motorized winches mounted on a mobile base. In addition to these, the motions of the base have a direct impact on handling position of the suspended platform due to coupling characteristics. The main objective is to develop a robust controller for stable tracking control of mobile CDPM considering the whole dynamics of the system. The well-known control algorithms intended for conventional CDPM with fixed base can be applied only if the base is controlled at a fixed point (stabilization). Few references can be found in the literature regarding mobile cable robots. In fact, all recent works deal with static and kinematic analysis of mobile CDPM [62] and [66]. Further, a real time tension distribution algorithm, that takes into account the dynamic equilibrium of the moving-platform and the static equilibrium of the mobile bases, is introduced by Tahir in [67].

Considering the field of this novel configuration, the main contribution of this chapter is to provide a safe manipulation of the entire system, during an object pick-and-place task. For this purpose, it raises an initial idea that the n_c motorized winches used to adjust cable length should not only manipulate the suspended platform to track a prescribed desired trajectory but also compensate the n-dimensional motions of the base [83]. Such a system would eliminate load oscillation and facilitate pick-and-place task of the mobile CDPM.

4.4.1 Tracking Control of Suspended Platform

In this section, the cables tension is considered as the control input to the robot dynamics. The controller design objective is to find a positive tension vector such that the suspended

platform can follow a predefined desired trajectory. For this purpose, a Sliding Mode Controller (SMC) based on switching theory and Lyapunov's theory is proposed. One of the main features of this approach is that we only need to drive the error to a "switching surface", after which the system is in "sliding mode" and it will not be affected by any modeling uncertainties or disturbances. Therefore, SMC represents an attractive alternative. This technique provides an effective approach for the control problem of systems with nonlinearities and bounded external disturbances [84] and [85]. The dynamic equation of the suspended platform:

$$\boldsymbol{M}_P(\boldsymbol{\chi})\overset{\circ\circ}{\boldsymbol{\chi}} + \boldsymbol{C}_P(\boldsymbol{\chi},\overset{\circ}{\boldsymbol{\chi}})\overset{\circ}{\boldsymbol{\chi}} + \boldsymbol{G}_P(\boldsymbol{\chi}) + \boldsymbol{D}_P(\boldsymbol{\chi},\overset{\circ}{\boldsymbol{\chi}},\ddot{\boldsymbol{\eta}}^a,\dot{\boldsymbol{\eta}}^a) = \boldsymbol{W}_P(\boldsymbol{\chi})\boldsymbol{T} \tag{4.4.1}$$

Remember $\boldsymbol{M}_P$ is the inertia matrix, $\boldsymbol{C}_P$ is the matrix of Coriolis and centrifugal, $\boldsymbol{D}_P$ is the bounded disturbance vector due to base motion and $\boldsymbol{W}_P$ is the force transmission matrix. Let the state vector of the suspended platform be denoted by $\boldsymbol{\chi}$ and $\boldsymbol{T} = [t_1, t_2, ..., t_{n_c}]^T$ that groups the n_c cable tensions represents the control vector input. First of all, we define a sliding surface as follows:

$$\boldsymbol{s} = \overset{\circ}{\boldsymbol{e}}_\chi + \boldsymbol{\Lambda}\boldsymbol{e}_\chi \tag{4.4.2}$$

where $\boldsymbol{\Lambda} = diag(\lambda_1, \lambda_2, ..., \lambda_6)$ with $\lambda_i > 0 \quad i \in \{1, ..., 6\}$. The operational tracking error is defined as $\boldsymbol{e}_\chi = \boldsymbol{\chi}_d - \boldsymbol{\chi}$ and its derivative is $\overset{\circ}{\boldsymbol{e}}_\chi = \overset{\circ}{\boldsymbol{\chi}}_d - \overset{\circ}{\boldsymbol{\chi}}$. To ensure trajectory tracking in operational space, we consider the following control law:

$$\boldsymbol{T} = \boldsymbol{W}_P^+\{\boldsymbol{M}_P(\boldsymbol{\chi})(\boldsymbol{\Lambda}\overset{\circ}{\boldsymbol{e}}_{\boldsymbol{\chi}} + \overset{\circ\circ}{\boldsymbol{\chi}}_d) + \boldsymbol{C}_P(\boldsymbol{\chi},\overset{\circ}{\boldsymbol{\chi}})(\boldsymbol{\Lambda}\boldsymbol{e}_{\boldsymbol{\chi}} + \overset{\circ}{\boldsymbol{\chi}}_d) + \boldsymbol{G}_P(\boldsymbol{\chi}) + \boldsymbol{K}sgn(\boldsymbol{s})\} \tag{4.4.3}$$

where $\boldsymbol{W}_P^+ = \boldsymbol{W}_P^T(\boldsymbol{W}_P\boldsymbol{W}_P^T)^{-1}$ is the pseudo-inverse of the rectangular matrix $\boldsymbol{W}_P$ and $\boldsymbol{K}$ is a positive definite matrix defined as follows :

$$\boldsymbol{K} = \begin{pmatrix} k_1 & & 0 \\ & \ddots & \\ 0 & & k_n \end{pmatrix} \tag{4.4.4}$$

and $sgn(\boldsymbol{s})$ is a signum function defined as follows :

$$sgn(\boldsymbol{s}) = \begin{pmatrix} sgn(s_1) \\ : \\ sgn(s_n) \end{pmatrix} \tag{4.4.5}$$

in which

$$sgn(\boldsymbol{s}) = \begin{cases} +1 & if s_i > 0 \\ -1 & if s_i < 0 \end{cases} \tag{4.4.6}$$

4.4.2 Stability Analysis

Referring to the control law given by (4.3.2) and the dynamic model given by (4.3.1), the closed loop system is:

$$\boldsymbol{M}_P(\boldsymbol{\chi})\dot{\boldsymbol{e}}_{\boldsymbol{\chi}} + \boldsymbol{C}_P(\boldsymbol{\chi},\dot{\boldsymbol{\chi}})\dot{\boldsymbol{e}}_{\boldsymbol{\chi}} - \boldsymbol{D}_P + \boldsymbol{M}_P(\boldsymbol{\chi})\boldsymbol{\Lambda}\dot{\boldsymbol{e}}_{\boldsymbol{\chi}} + \boldsymbol{C}_P(\boldsymbol{\chi},\dot{\boldsymbol{\chi}})\boldsymbol{\Lambda}\boldsymbol{e}_{\boldsymbol{\chi}} = 0 \tag{4.4.7}$$

Although the dynamic equations of the global system are nonlinear and complex, they have some known properties which are necessary for the controller synthesis and stability analysis:

- *Property* 1 The inertia matrix $\boldsymbol{M}_P(\boldsymbol{\chi})$ is symmetric and positive definite.
- *Property* 2 The matrix $\dot{\boldsymbol{M}}_P(\boldsymbol{\chi}) - 2\boldsymbol{C}_P(\boldsymbol{\chi},\dot{\boldsymbol{\chi}})$ is skew symmetric.

The Lyapunov function is defined as follows:

$$V = \frac{1}{2}\boldsymbol{s}^T\boldsymbol{M}_P(\boldsymbol{\chi})\boldsymbol{s} \tag{4.4.8}$$

The time derivative of the Lyapunov function is given by:

$$\dot{V} = \boldsymbol{s}^T(\boldsymbol{M}_P(\boldsymbol{\chi})\dot{\boldsymbol{s}} + \frac{1}{2}\dot{\boldsymbol{M}}_P(\boldsymbol{\chi})\boldsymbol{s}) \tag{4.4.9}$$

$$\dot{V} = \boldsymbol{s}^T\left(\boldsymbol{M}_P(\boldsymbol{\chi})\dot{\boldsymbol{e}}_{\chi} + \boldsymbol{M}_P(\boldsymbol{\chi})\boldsymbol{\Lambda}\dot{\boldsymbol{e}}_{\chi} + \frac{1}{2}\dot{\boldsymbol{M}}_P(\boldsymbol{\chi})\dot{\boldsymbol{e}}_{\chi} + \frac{1}{2}\dot{\boldsymbol{M}}_P(\boldsymbol{\chi})\boldsymbol{\Lambda}\boldsymbol{e}_{\chi}\right) \tag{4.4.10}$$

Solving now for $\boldsymbol{M}_P(\boldsymbol{\chi})\dot{\boldsymbol{e}}_{\chi}$ in (4.4.1) and substituting into the last equation yields:

$$\dot{V} = \boldsymbol{s}^T\left(\boldsymbol{D}_P - \boldsymbol{K}sgn(\boldsymbol{s}) + \frac{1}{2}(\dot{\boldsymbol{M}}_P(\boldsymbol{\chi}) - 2\boldsymbol{C}_P(\boldsymbol{\chi},\dot{\boldsymbol{\chi}}))\dot{\boldsymbol{e}}_{\chi} + \frac{1}{2}(\dot{\boldsymbol{M}}_P(\boldsymbol{\chi}) - 2\boldsymbol{C}_P(\boldsymbol{\chi},\dot{\boldsymbol{\chi}}))\boldsymbol{\Lambda}\boldsymbol{e}_{\chi}\right) \tag{4.4.11}$$

According to property 2, the two latter terms vanish and therefore:

$$\dot{V} = \boldsymbol{s}^T\left(\boldsymbol{D}_P - \boldsymbol{K}sgn(\boldsymbol{s})\right) \tag{4.4.12}$$

As it is known $\boldsymbol{K}\boldsymbol{s}^T sgn(\boldsymbol{s}) = \sum_{i=1}^{n=6} k_i|s_i|$, this leads to:

$$\dot{V} = \boldsymbol{s}^T\boldsymbol{D}_P - \sum_{i=1}^{n=6} k_i|s_i| \tag{4.4.13}$$

Let us note by D_i the component of the disturbance vector $\boldsymbol{D}_P$. Then it is sufficient to choose the terms of positive definite matrix $\boldsymbol{K}$ as follows:

$$k_i \geqslant |D_i| + \eta_i \tag{4.4.14}$$

Where $\eta_i > 0$, therefore,

$$\dot{V} \leqslant -\sum_{i=1}^{n=6} \eta_i|s_i| \tag{4.4.15}$$

To avoid chattering, we replace the $sgn(\boldsymbol{s})$ function by the $sat(\boldsymbol{s})$ function given as:

$$sat(\boldsymbol{s}) = \begin{cases} sgn(s_i) & if \quad |s_i| > \delta \\ \frac{s_i}{\delta} & if \quad |s_i| \leqslant \delta \end{cases} \tag{4.4.16}$$

δ is a constant boundary layer thickness. Hence the control law now looks like:

$$\boldsymbol{T} = \boldsymbol{W}_P^{+}\{\boldsymbol{M}_P(\boldsymbol{\chi})(\boldsymbol{\Lambda}\mathring{\boldsymbol{e}}_\chi + \overset{\circ\circ}{\boldsymbol{\chi}}_d) + \boldsymbol{C}_P(\boldsymbol{\chi},\mathring{\boldsymbol{\chi}})(\boldsymbol{\Lambda}\boldsymbol{e}_\chi + \mathring{\boldsymbol{\chi}}_d) + \boldsymbol{G}_P(\boldsymbol{\chi}) + \boldsymbol{K}sat(\boldsymbol{s})\} \tag{4.4.17}$$

Referring to LaSalle's Invariance Principle the system is stable. Thus, the motion converges to a maximum invariant set which satisfies $\dot{V} = 0$. This implies that $\boldsymbol{s} = 0$. the following equation is derived :

$$\lim_{t\longrightarrow\infty} \boldsymbol{s} = \lim_{t\longrightarrow\infty} (\mathring{\boldsymbol{e}}_\chi + \boldsymbol{\Lambda}\boldsymbol{e}_\chi) = 0 \tag{4.4.18}$$

Witch implies that :

$$\mathring{\boldsymbol{e}}_\chi = \boldsymbol{\Lambda}\boldsymbol{e}_\chi \tag{4.4.19}$$

Thus, the error system is asymptotically stable if $\boldsymbol{\Lambda}$ satisfies the Hurwitz condition. As already mentioned, the asymptotic stability of the suspended platform can not only be provided by the adequate choice of the control law but also a cable tension distribution algorithm should be integrated to ensure that the control is capable to keep the CDPM cable tensions always positive.

4.4.3 Simulation Results

In this section, some numerical simulation are carried on to illustrate the performance of the proposed controller. Simulations concern a suspended CDPM, named CoGiRo. We have to mention that CoGiRo parameters are previously presented in the previous section 4.3.3. Sliding parameters are chosen as $\boldsymbol{\Lambda} = diag(0.7, 0.7, 3.05, 1.05, 1.05, 3.05)$, $\delta = 1$ and $\boldsymbol{K} = diag(0.25, 0.25, 0.37, 0.37, 0.25, 1)$. The resulting simulation is illustrated in Figure 4.10 and Figure 4.11.

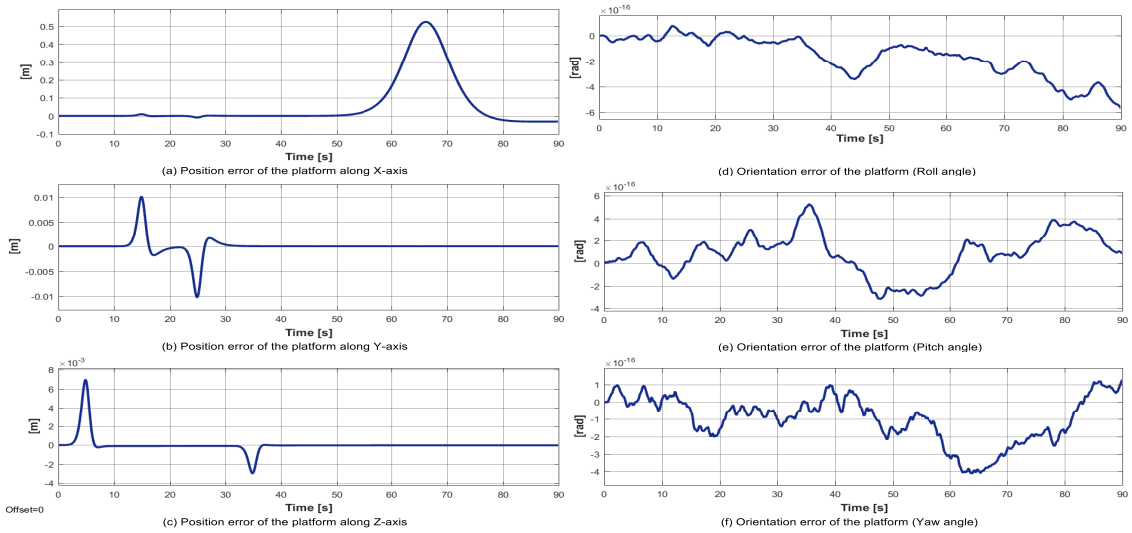

FIGURE 4.10: Position and orientation error of the platform

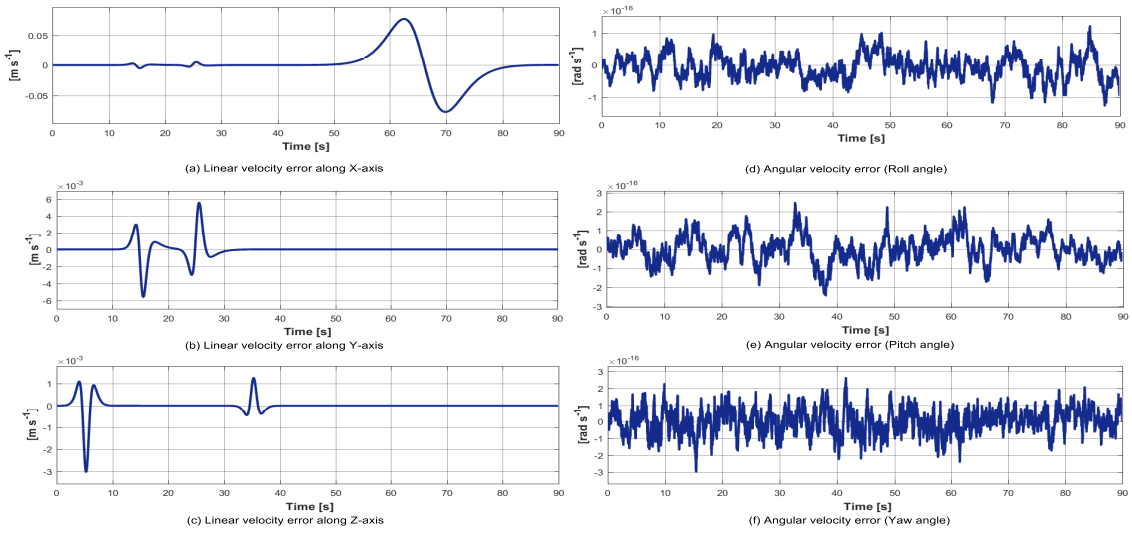

FIGURE 4.11: Linear and angular velocity error of the platform

As it is shown in Figure 4.12, the algorithm developed for the tensions distribution keeps cables in tension for the whole manoeuvre. We can conclude that our objective is largely achieved through the application of sliding mode controller. In fact as can be seen in Figure 4.10, it is clear that thanks to the proposed controller the platform tracks very well the desired trajectory.

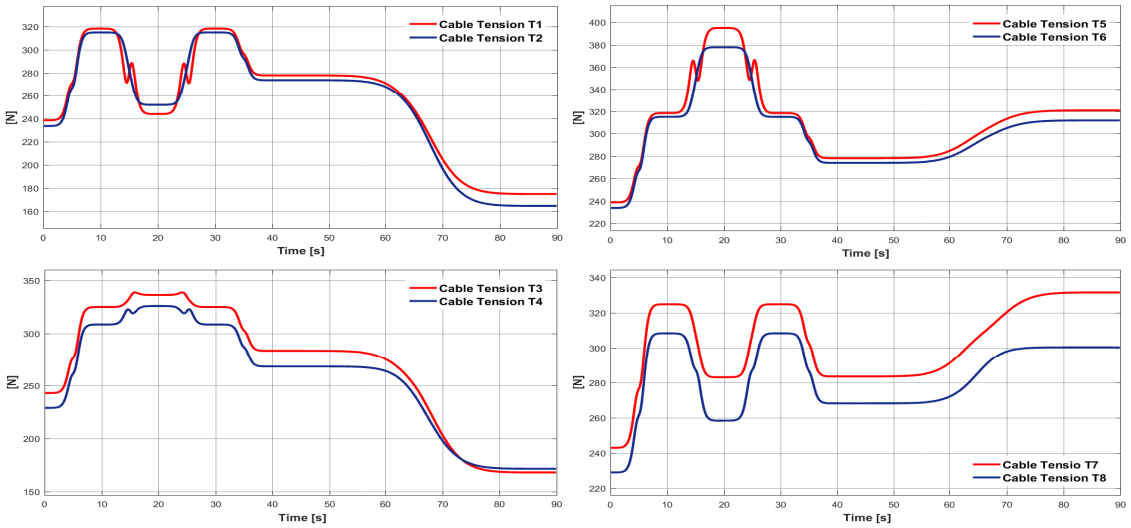

FIGURE 4.12: Cables tension

In this simulation we highlight the capability of our sliding mode controller not only to manipulate the suspended platform in order to track a prescribed desired trajectory but also compensate the motion of the base that ensure safe manipulation of the load.

4.5 Conclusion

For a CDPM with base mobility, a Sliding Mode Controller is proposed to move the suspended platform along a desired trajectory. This technique represents an attractive alternative since it ensures a fast convergence and robustness against disturbance due to base motion. The control design should integrate an optimal tension distribution because cables must remain in tension for this class of robot. The stability of the system is analyzed through Lyapunov function. Finally the performance of proposed controller is examined by simulation results.

Part II

Modeling and Control of Heavy-Lift Airship

Chapter 5

Modeling of Heavy-Lift Airship

Contents

5.1 Introduction

Recently, cargo airships has been specifically designed to be a radically new and sustainable transportation mode for both passengers and cargo. In our study, the heavy lift Airship's loading and unloading phase makes use of a Cable Driven Parallel Manipulator (CDPM). Specifically, the cargo is handled by motorized cable winches, mounted underneath the airship. By this way, the heavy lift airship can load and unload cargo without landing.

The contribution of this chapter consists in the development of the complete model of the heavy lift airship. To the best of our knowledge, we are pioneer in this field. Due to the CDPM dynamics, the modeling of such a multi-body system composed of the airship and the CDPM is more complex than that of the conventional airship. To set up the model, we consider that the airship and the suspended platform are independent. Hence, the heavy lift airship can be modeled as an interconnection of lower order subsystems (i.e the airship and CDPM). In this case, the basic motion of one subsystem is regarded as an external disturbance input for the other one [86].

5.2 Conceptual Design

The heavy lift airship consists of an airship carrying a payload through a Cable Driven Parallel Manipulator (CDPM). The following section gives an overview of the design of our heavy lift airship, including its mechanical components as well as its operating principle.

5.2.1 Composition of the Mechanism

This novel flying robot, the heavy lift airship, is composed of four basic components. (*i*) A moving suspended platform, which is positioned within a workspace to fulfill a specific task, (*ii*) driving cables to control and move the platform, (*iii*) winches which change the cable length and finally (*iv*) an airship considered as a supporting structure underneath which these winches are fastened.

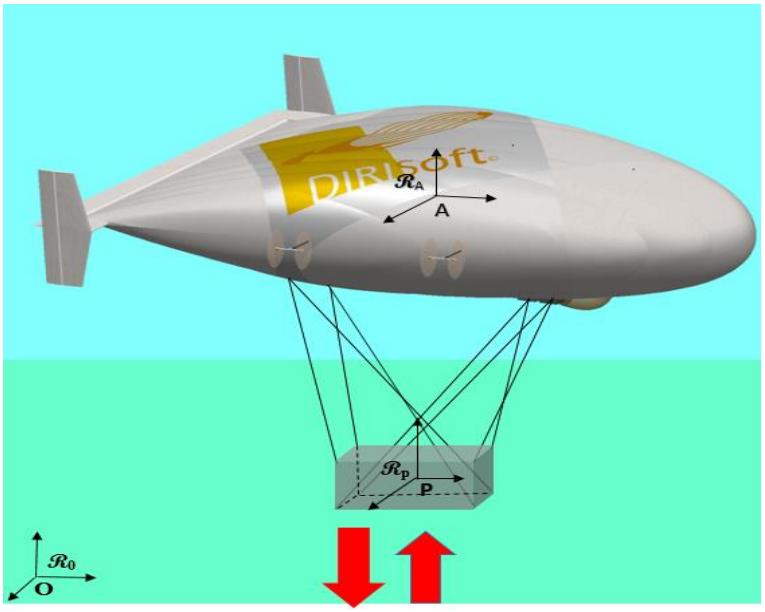

FIGURE 5.1: Loading and unloading of the heavy-lift airship

(i) **Moving suspended platform :** A 6-DOF platform is suspended by eight identical cables. One end of each cable is attached to the mobile platform at point B_i, and the

other end is connected to a mobile point A_i. The position and orientation of the moving platform depend on the cables length which can be adjusted by motorized winches mounted on the airship. In fact, cables are considered as as transmission elements.

(ii) **Driving cables :** For cable driven parallel manipulator, each cable connects the winch mounted on the airship (supporting structure) to the mobile platform. The eight identical cables are considered as straight line segment for the kinematic and dynamic analysis. The supporting structure have no orientation constrains at the connected points with the cables, which means the cables can rotate about any direction at the connected points with the supporting structure. Hence, the connection between cable and the supporting structure can be viewed as a universal joint, whereas the connection between cable and the moving platform is spherical. Moreover, the cable can elongate along its direction, which can be treated as a prismatic joint. Therefore, the kinematic structure of the cable may be considered as universal-prismatic-spherical (commonly denoted as UPS), in which only the prismatic joint is actuated.

(iii) **Motorized winches :** Eight motorized winches, mounted underneath the airship, are used to adjust the length or tension in cables. Each winch consist of a synchronous servo motor coupled to a planetary gearbox witch is connected to a drum having a diameter that can store wound portion of cable. The maximum size of the workspace is primary given by the capacity of the winch's drum. Tiny winches can have a stroke of some millimeters while industrial large scale winches can coil several kilometers of cable.

(iv) **Airship :** In our study, we use the characteristics of the airship $MC500$ developed by the French network DIRISOFT. This airship is a collection of aerodynamic profiles, with symmetry around the $x-z$ axis. Each transverse section of the careen parallel to the plan $y-z$ gives roughly an ellipse. The MC$-$500 is an experimental reduced scale prototype for a set of great innovating airships including cargo airships.

5.2.2 Operating Mechanism

During loading and unloading phase, the heavy-lift airship requires the cooperation of two subsystems (i.e the Airship and Cable Driven Parallel Manipulator). Specifically, the airship hovers above the ground and a special loading frame, which is fixed during flight to the keel of the airship, is then rigged with eight cable winches to the ground. Associating airship and cable driven parallel manipulator, this new design offers novel possibilities for heavy-lift airship to load and unload cargo without landing.

(i) **Propulsion :** The propulsion of the $MC500$ airship is provided by four electric rotors. Each rotor can swivel in two directions. A rotation of angle β_i around the $y-$ axis and a rotation of angle γ_i around $z-$ axis. Therefore the airship have twelve actuators :

The four propulsion forces $\boldsymbol{f}_i$, the four angles of inclination β_i and the four orientation angles γ_i.

(ii) **Cable tensions for loading and unloading :** Eight motorized winches are used to adjust cable lengths or tensions t_i in order to control and move the platform. The cables of a CDPM can only pull and not push on the mobile platform and their tension t_i are contained between minimal and maximal tension values t_{imin} and t_{imax}. The maximum t_{imax} is notably given by the maximal admissible cable strain whereas t_{imin} is usually set as the lowest acceptable tension with the goal of avoiding slack cables, $t_{imin} > 0$. For this purpose, we use eight cables to manipulate the suspended platform in the full six dimensional task space, thus resulting in two redundant cables that can be used to better distribute the tensions.

5.3 Kinematic Modeling

5.3.1 Coordinate Systems

The kinematic and dynamic analysis of the composed system consisting of the airship and the cable driven parallel manipulators require a representative parametrization which implies a significant benefit in the motion equations (see figure 5.1). In fact, the analysis of the global system motion is made with respect to three frames, namely an earth-fixed reference frame $\mathcal{R}_0(O, X_0, Y_0, Z_0)$, an airship body-fixed frame $\mathcal{R}_A(A, X_a, Y_a, Z_a)$, having as origin the gravity center of the airship A and a platform body-fixed frame $\mathcal{R}_P(P, X_p, Y_p, Z_p)$ having as origin the geometric center of the CDPM suspended platform P.

(a) **Inertial reference axis :** An inertial axis system is needed as a point of reference for the airship's position and orientation, namely an earth-fixed frame $\mathcal{R}_0(O, X_0, Y_0, Z_0)$. The origin O is fixed on an arbitrary point on the earth. The **x**-axis is positive towards the north, while the **y**-axis is positive towards the east and is subject to right-hand rule. The **z**-axis lies in the direction of the gravity vector and is positive towards the center of the earth.

(b) **Airship body axis :** For convenience, the motion equations for a 6-DOF air vehicle are usually derived in the body frame. An airship body-fixed frame $\mathcal{R}_A(A, X_a, Y_a, Z_a)$ is centered at the airship gravity center A. The $\mathbf{x}_a$-axis is coincident with the symmetry axis of the envelope, the $\mathbf{x}_a\mathbf{z}_a$-plane coincides with the longitudinal plane of symmetry of the airship where the $\mathbf{z}_a$-axis increasing downward and the positive $\mathbf{y}_a$-axis is determined by the right hand rule. It is reasonable to assume both the center of volume B and the center of gravity A lie on the axis of symmetry of the envelope. The transformation from the inertial reference frame $\mathcal{R}_0$ to the local frame $\mathcal{R}_A$, fixed to the airship, is achieved by the following sequence of rotations starting from the Earth fixed inertial frame:

(i) First a rotation around the z-axis of yaw angle ψ_a (positive direction).

(ii) Then a rotation around Y_1-axis, the new **y**-axis resulting from the previous rotation, of pitch angle θ_a (positive direction).

(iii) Last a rotation around the resulting **x**-axis of roll angle ϕ_a (positive direction).

Where the roll ϕ_a, pitch θ_a and yaw ψ_a angles are commonly referred to as Euler angles. The complete transformation from the inertial frame $\mathcal{R}_0$ to the local frame $\mathcal{R}_A$ is then given by the rotation matrix $\mathcal{R}_A^0$, expressed as function of the Euler angles $[\phi_a, \theta_a, \psi_a]^T$:

$$\boldsymbol{\mathcal{R}}_A^0 = \begin{pmatrix} c_{\psi_a} c_{\theta_a} & c_{\psi_a} s_{\theta_a} s_{\phi_a} - s_{\psi_a} c_{\phi_a} & s_{\psi_a} s_{\phi_a} + c_{\psi_a} c_{\phi_a} s_{\theta_a} \\ s_{\psi_a} c_{\theta_a} & c_{\psi_a} c_{\theta_a} + s_{\phi_a} s_{\theta_a} s_{\psi_a} & s_{\theta_a} s_{\psi_a} c_{\phi_a} - c_{\psi_a} s_{\phi_a} \\ -s_{\theta_a} & c_{\theta_a} s_{\phi_a} & c_{\theta_a} c_{\phi_a} \end{pmatrix} \tag{5.3.1}$$

The following shorthand notation for trigonometric function is used: $c_\theta := \cos\theta$, $s_\theta := \sin\theta$, $t_\theta := \tan\theta$. The notation holds for all the transformation matrix used in this manuscript.

(c) **Platform body axis :** To describe the platform's position and its orientation with regards to both the inertial and airship body-fixed frame, an additional axis needs to be established on the CDPM mobile platform. Thus, we define a platform body-fixed frame $\mathcal{R}_P(P, X_p, Y_p, Z_p)$ having as origin the geometric center of the platform P. We choose the orientation of $\mathcal{R}_P$ to be given by a space-three rotation sequence:

(i) First a rotation around the $\mathbf{z}_a$-axis of yaw angle ψ.

(ii) Then a rotation around Y_1-axis, the new $\mathbf{y}_a$-axis resulting from the previous rotation, of pitch angle θ.

(iii) Last a rotation around the resulting $\mathbf{x}_a$-axis of roll angle ϕ.

We use a parametrization by Euler angles : yaw, pitch and roll to describe the suspended platform attitude in regard to $\mathcal{R}_A$. The rotation matrix $\boldsymbol{\mathcal{R}}_P^A$ between the two local frames $\mathcal{R}_P$ and $\mathcal{R}_A$ is:

$$\boldsymbol{\mathcal{R}}_P^A = \begin{pmatrix} c_\psi c_\theta & c_\psi s_\theta s_\phi - s_\psi c_\phi & s_\psi s_\phi + c_\psi c_\phi s_\theta \\ s_\psi c_\theta & c_\psi c_\theta + s_\phi s_\theta s_\psi & s_\theta s_\psi c_\phi - c_\psi s_\phi \\ -s_\theta & c_\theta s_\phi & c_\theta c_\phi \end{pmatrix} \tag{5.3.2}$$

5.3.2 Airship

The vehicle's motion in space is defined by several coordinates which can be classified into two categories: ones expressed in the reference frame and others in mobile body-fixed frame. Under the established coordinate frames, the general motion of the lighter than air vehicle can be described by $\boldsymbol{\eta}^a = [\boldsymbol{\eta}_1^a, \boldsymbol{\eta}_2^a]^T$ with respect to the reference frame $\mathcal{R}_0$, where $\boldsymbol{\eta}_1^a = [x_a, y_a, z_a]^T$

and $\boldsymbol{\eta}_2^a = [\phi_a, \theta_a, \psi_a]^T$ denote respectively the position and orientation vector of the airship expressed in $\mathcal{R}_0$.

Let us denote by $\dot{\boldsymbol{\eta}}_1^a = [\dot{x}_a, \dot{y}_a, \dot{z}_a]^T$ the linear velocity of the airship inertia center A with respect to reference frame and expressed in $\mathcal{R}_0$, while $\boldsymbol{\nu}_1^a = [u, v, w]^T$ is the linear velocity of the airship inertia center A with respect to reference frame $\mathcal{R}_0$ expressed in the airship body-fixed frame $\mathcal{R}_A$. The transformation of the velocity vector from the local frame to the reference frame is done using the rotation matrix $\boldsymbol{\mathcal{R}}_A^0$. Thus, the two vectors $\dot{\boldsymbol{\eta}}_1^a$ and $\boldsymbol{\nu}_1^a$ are connected by the following relation:

$$\begin{pmatrix} \dot{x}_a \\ \dot{y}_a \\ \dot{z}_a \end{pmatrix} = \boldsymbol{\mathcal{R}}_A^0 \begin{pmatrix} u \\ v \\ w \end{pmatrix} \tag{5.3.3}$$

The vector $\dot{\boldsymbol{\eta}}_2^a = [\dot{\phi}_a, \dot{\theta}_a, \dot{\psi}_a]^T$ designates the angular velocity with respect to the reference frame and expressed in $\mathcal{R}_0$, whereas the vector $\boldsymbol{\nu}_2^a = [p, q, r]^T$ is the angular velocity with respect to the reference frame $\mathcal{R}_0$ and expressed in the airship body-fixed frame $\mathcal{R}_A$.

$$\begin{pmatrix} \dot{\phi}_a \\ \dot{\theta}_a \\ \dot{\psi}_a \end{pmatrix} = \underbrace{\begin{pmatrix} 1 & s_{\phi_a} t_{\theta_a} & c_{\phi_a} t_{\theta_a} \\ 0 & c_{\phi_a} & -s_{\phi_a} \\ 0 & \frac{s_{\phi_a}}{c_{\theta_a}} & \frac{c_{\phi_a}}{c_{\theta_a}} \end{pmatrix}}_{\boldsymbol{P}_a^{-1}(\boldsymbol{\eta}_2^a)} \begin{pmatrix} p \\ q \\ r \end{pmatrix} \tag{5.3.4}$$

where $\boldsymbol{P}_a^{-1}(\boldsymbol{\eta}_2^a)$ is the transformation matrix from angular velocities to Euler angle rates. The kinematics equations of an airship can be expressed in the following way:

$$\begin{pmatrix} \dot{\boldsymbol{\eta}}_1^a \\ \dot{\boldsymbol{\eta}}_2^a \end{pmatrix} = \underbrace{\begin{pmatrix} \boldsymbol{\mathcal{R}}_A^0(\boldsymbol{\eta}_2^a) & \mathbf{0}_{3\times3} \\ \mathbf{0}_{3\times3} & \boldsymbol{P}_a^{-1}(\boldsymbol{\eta}_2^a) \end{pmatrix}}_{\boldsymbol{J}_a} \begin{pmatrix} \boldsymbol{\nu}_1^a \\ \boldsymbol{\nu}_2^a \end{pmatrix} \tag{5.3.5}$$

The first line in the above equation can be regarded as a linear velocity transformation, while the second line presents an angular velocity transformation. The transformation matrix $\boldsymbol{J}_a$ transforms $\boldsymbol{\nu}^a = [\boldsymbol{\nu}_1^a, \boldsymbol{\nu}_2^a]^T$, expressed in the airship body-fixed frame $\mathcal{R}_A$, into $\boldsymbol{\eta}^a = [\boldsymbol{\eta}_1^a, \boldsymbol{\eta}_2^a]^T$, expressed in the reference frame $\mathcal{R}_0$ and is defined as:

$$\boldsymbol{J}_a = \begin{pmatrix} \boldsymbol{\mathcal{R}}_A^0(\boldsymbol{\eta}_2^a) & \mathbf{0}_{3\times3} \\ \mathbf{0}_{3\times3} & \boldsymbol{P}_a^{-1}(\boldsymbol{\eta}_2^a) \end{pmatrix} \tag{5.3.6}$$

Thus, the compact kinematic model of an airship can be written as:

$$\dot{\boldsymbol{\eta}}^a = \boldsymbol{J}_a \boldsymbol{\nu}^a \tag{5.3.7}$$

5.3.3 Suspended platform

For this novel flying mechanism, the airship is used as the supporting structure of the CDPM and a 6 DOF platform is suspended via n_c cables as transmission element. The general motion of suspended platform with respect to the reference frame $\mathcal{R}_0$ can be described by $\boldsymbol{\nu}^p = [\boldsymbol{\nu}_1^p, \boldsymbol{\nu}_2^p]^T$, where $\boldsymbol{\nu}_1^p$ and $\boldsymbol{\nu}_2^p$ represent respectively the linear and angular velocity of the platform expressed in airship body-fixed frame $\mathcal{R}_A$. The expression of $\boldsymbol{\nu}_1^p$ is:

$$\frac{d\overrightarrow{OP}}{dt}\Big]^{\mathcal{R}_A}_{\mathcal{R}_0} = \frac{d\overrightarrow{OA}}{dt}\Big]^{\mathcal{R}_A}_{\mathcal{R}_0} + \frac{d\overrightarrow{AP}}{dt}\Big]^{\mathcal{R}_A}_{\mathcal{R}_A} + \overrightarrow{\omega}\Big]^{\mathcal{R}_A}_{\mathcal{R}_A/\mathcal{R}_0} \times \overrightarrow{AP} \tag{5.3.8}$$

We introduce the notation $\frac{d\overrightarrow{OM}}{dt}\Big]^{C}_{G}$ to represent the linear velocity vector of a point M with respect to the frame G, expressed in a frame C and $\overrightarrow{\omega}\Big]^{C}_{B/G}$ represents the angular velocity vector of a frame B with respect to a frame G, expressed in a frame C. The notation holds for all the vectors used in this section. As it is known, $\boldsymbol{\nu}_1^a$ is the absolute linear velocity of the airship inertia center A with respect to $\mathcal{R}_0$ expressed in $\mathcal{R}_A$ which corresponds to $\frac{d\overrightarrow{OA}}{dt}\Big]^{\mathcal{R}_A}_{\mathcal{R}_0}$ and $\boldsymbol{\nu}_2^a$ is the absolute angular velocity expressed in the body fixed frame $\mathcal{R}_A$ which corresponds to $\overrightarrow{\omega}\Big]^{\mathcal{R}_A}_{\mathcal{R}_A/\mathcal{R}_0}$. By substituting these expressions in the above equation (5.3.8), we get:

$$\boldsymbol{\nu}_1^p = \boldsymbol{\nu}_1^a + \boldsymbol{v} + \boldsymbol{\nu}_2^a \times \boldsymbol{p} \tag{5.3.9}$$

where $\boldsymbol{p} = [x, y, z]^T$ and $\boldsymbol{v} = [\dot{x}, \dot{y}, \dot{z}]^T$ denote the relative position and linear velocity of the platform geometric center P expressed in the airship body-fixed frame $\mathcal{R}_A$. The time derivative of the above equation gives the linear acceleration defines as follows:

$$\begin{aligned}\frac{d^2\overrightarrow{OP}}{dt^2}\Big]^{\mathcal{R}_A}_{\mathcal{R}_0} = \frac{d^2\overrightarrow{AP}}{dt^2}\Big]^{\mathcal{R}_A}_{\mathcal{R}_A} + 2\overrightarrow{\omega}\Big]^{\mathcal{R}_A}_{\mathcal{R}_A/\mathcal{R}_0} \times \frac{d\overrightarrow{AP}}{dt}\Big]^{\mathcal{R}_A}_{\mathcal{R}_A} \\ + \left\{ \frac{d^2\overrightarrow{OA}}{dt^2}\Big]^{\mathcal{R}_A}_{\mathcal{R}_0} + \frac{d\overrightarrow{\omega}}{dt}\Big]^{\mathcal{R}_A}_{\mathcal{R}_A/\mathcal{R}_0} \times \overrightarrow{AP} + \overrightarrow{\omega}\Big]^{\mathcal{R}_A}_{\mathcal{R}_A/\mathcal{R}_0} \times (\overrightarrow{\omega}\Big]^{\mathcal{R}_A}_{\mathcal{R}_A/\mathcal{R}_0} \times \overrightarrow{AP}) \right\}\end{aligned} \tag{5.3.10}$$

Note that $\frac{d^2\overrightarrow{OA}}{dt^2}\Big]^{\mathcal{R}_A}_{\mathcal{R}_0}$ and $\frac{d\overrightarrow{\omega}}{dt}\Big]^{\mathcal{R}_A}_{\mathcal{R}_A/\mathcal{R}_0}$ correspond to the absolute linear and angular acceleration of the mobile base, defined respectively as $\dot{\boldsymbol{\nu}}_1^a$ and $\dot{\boldsymbol{\nu}}_2^a$. Further, $\frac{d^2\overrightarrow{AP}}{dt^2}\Big]^{R_A}_{R_A}$ represents the relative linear acceleration of the platform geometric center P expressed into the base body-fixed frame $\mathcal{R}_A$, denoted as $\mathring{\boldsymbol{v}}$. By substituting these expressions in the above equation (5.3.10), we get:

$$\dot{\boldsymbol{\nu}}_1^p = \mathring{\boldsymbol{v}} + \dot{\boldsymbol{\nu}}_1^a + 2\boldsymbol{\nu}_2^a \times \boldsymbol{v} + \dot{\boldsymbol{\nu}}_2^a \times \boldsymbol{p} + \boldsymbol{\nu}_2^a \times (\boldsymbol{\nu}_2^a \times \boldsymbol{p}) \tag{5.3.11}$$

The expression of the absolute angular velocity of the suspended platform expressed in airship body-fixed frame $\mathcal{R}_A$ is:

$$\overrightarrow{\omega}^{]\mathcal{R}_A}_{]\mathcal{R}_P/\mathcal{R}_0} = \overrightarrow{\omega}^{]\mathcal{R}_A}_{]\mathcal{R}_P/\mathcal{R}_A} + \overrightarrow{\omega}^{]\mathcal{R}_A}_{]\mathcal{R}_A/\mathcal{R}_0} \tag{5.3.12}$$

The absolute angular velocity $\boldsymbol{\nu}_2^p$ of the platform body frame $\mathcal{R}_A$ is equal to the absolute angular velocity $\boldsymbol{\nu}_2^a$ of the airship body-frame $\mathcal{R}_A$ plus the relative angular velocity $\boldsymbol{\omega}$ of platform body-frame $\mathcal{R}_P$ with respect to airship body-frame $\mathcal{R}_A$. Hence, the expression of $\boldsymbol{\nu}_2^p$ is given by:

$$\boldsymbol{\nu}_2^p = \boldsymbol{\nu}_2^a + \boldsymbol{\omega} \tag{5.3.13}$$

Derivate the angular velocity $\boldsymbol{\nu}_2^p$ with respect to time, we obtain the angular acceleration defined by:

$$\dot{\boldsymbol{\nu}}_2^p = \dot{\boldsymbol{\nu}}_2^a + \mathring{\boldsymbol{\omega}} + \boldsymbol{\nu}_2^a \times \boldsymbol{\omega} \tag{5.3.14}$$

In the following section, we will examine the external forces and moments acting on the heavy-lift airship.

5.4 Forces Analysis

To set up the dynamic model, the forces applied on the system should be determined. In our study, the resulting force applied on the airship is a sum of the forces generated by the four rotors $\boldsymbol{f}_j$, the gravitational and buoyancy force $\boldsymbol{f}_{wb}$ and cable tensions $\boldsymbol{f}_c$. We denote by $\boldsymbol{m}_j$,$\boldsymbol{m}_{wb}$ and $\boldsymbol{m}_c$ external torques due to the applied forces $\boldsymbol{f}_j$,$\boldsymbol{f}_{wb}$ et $\boldsymbol{f}_c$ respectively. In first study, we try to evaluate the behavior of the airship in the case of low velocity or while hovering. In these cases, the effect of aerodynamic forces can be neglected. Hence, the resultant force $\boldsymbol{\tau}_{a_1}$ and torque $\boldsymbol{\tau}_{a_2}$ can be written as:

$$\boldsymbol{\tau}_{a_1} = \sum_{j=1}^{4} \boldsymbol{f}_j + \boldsymbol{f}_{wb} + \boldsymbol{f}_c \tag{5.4.1}$$

$$\boldsymbol{\tau}_{a_2} = \sum_{j=1}^{4} \boldsymbol{m}_j + \boldsymbol{m}_{wb} + \boldsymbol{m}_c \tag{5.4.2}$$

5.4.1 Propulsion

The propulsion of the $MC500$ airship is provided by four electric engines driving rotors (see Figure 5.2). Each rotor is attached to an auxiliary frame $\mathcal{R}_j(P_j, X_j, Y_0, Z_j)$, where the origin point P_j is the rotor position and $\boldsymbol{\mathcal{R}}_j^A$ denote the rotation matrix between the local frame $\mathcal{R}_j$ and the airship body-fixed frame $\mathcal{R}_A$:

$$\boldsymbol{\mathcal{R}}_j^A = \begin{pmatrix} c_{\gamma_j} c_{\beta_j} & -s_{\gamma_j} c_{\beta_j} & s_{\beta_j} \\ s_{\gamma_j} & s_{\gamma_j} & 0 \\ -c_{\gamma_j} s_{\beta_j} & s_{\gamma_j} s_{\beta_j} & c_{\beta_j} \end{pmatrix} \quad j \in \{1, ..., 4\} \tag{5.4.3}$$

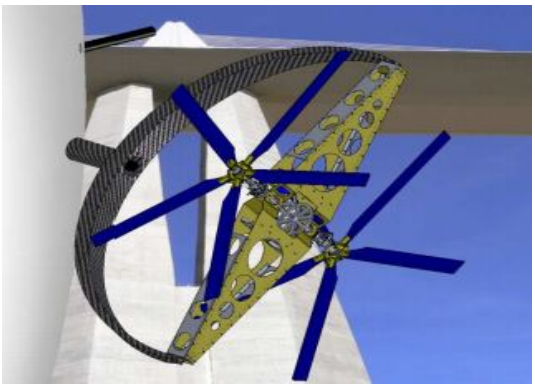

FIGURE 5.2: Rotor of the airship $MC500$

Each rotor has two parallel contrarotating propellers to avoid any aerodynamic torque. The rotor can swivel in two directions. A rotation of angle β_j around the Y_0 axis and a rotation of angle γ_j around Z_j-axis. If we suppose that the intensity of the rotor thrust force is $\|\boldsymbol{f}_j\|$ having as direction the unitary vector $\boldsymbol{e}_j$ along the X_j-axis, then the forces produced by each rotor in the inertia center A will be defined by [87]:

$$\boldsymbol{f}_j = \boldsymbol{\mathcal{R}}_j^A \|\boldsymbol{f}_j\| \boldsymbol{e}_j \quad j \in \{1,...,4\} \tag{5.4.4}$$

$$\boldsymbol{f}_j = \begin{pmatrix} \|\boldsymbol{f}_j\| c_{\gamma_j} c_{\beta_j} \\ \|\boldsymbol{f}_j\| s_{\gamma_j} \\ -\|\boldsymbol{f}_j\| c_{\gamma_j} s_{\beta_j} \end{pmatrix} \quad j \in \{1,...,4\} \tag{5.4.5}$$

The positions P_j of the rotors in the local reference frame are $P_1 = [a, b_1, c]^T$, $P_2 = [a, -b_1, c]^T$, $P_3 = [-a, b_3, c]^T$, and $P_4 = [-a, b_3, c]^T$. The resultant torque vector applied by each rotor on the airship is:

$$\boldsymbol{m}_j = \boldsymbol{f}_j \times \overrightarrow{P_j A} \quad j \in \{1,...,4\} \tag{5.4.6}$$

Thus,

$$For \quad P_1 = \begin{pmatrix} a \\ b_1 \\ c \end{pmatrix}, \quad \boldsymbol{m}_1 = \|\boldsymbol{f}_1\| \begin{pmatrix} c.s_{\gamma_1} + b_1.c_{\gamma_1}.s_{\beta_1} \\ -c.c_{\gamma_1}.c_{\beta_1} - a.c_{\gamma_1}.s_{\beta_1} \\ b_1.c_{\gamma_1}.c_{\beta_1} - a.s_{\gamma_1} \end{pmatrix}$$

$$For \quad P_2 = \begin{pmatrix} a \\ -b_1 \\ c \end{pmatrix}, \quad \boldsymbol{m}_2 = \|\boldsymbol{f}_2\| \begin{pmatrix} c.s_{\gamma_2} - b_1.c_{\gamma_2}.s_{\beta_2} \\ -c.c_{\gamma_2}.c_{\beta_2} - a.c_{\gamma_2}.s_{\beta_2} \\ -b_1.c_{\gamma_2}.c_{\beta_2} - a.s_{\gamma_2} \end{pmatrix}$$

$$For \quad P_3 = \begin{pmatrix} -a \\ b_3 \\ c \end{pmatrix}, \quad \boldsymbol{m}_3 = -\|\boldsymbol{f}_3\| \begin{pmatrix} c.s_{\gamma_3} + b_3.c_{\gamma_3}.s_{\beta_3} \\ -c.c_{\gamma_3}.c_{\beta_3} - a.c_{\gamma_3}.s_{\beta_3} \\ b_3.c_{\gamma_3}.c_{\beta_3} - a.s_{\gamma_3} \end{pmatrix}$$

$$For \quad P_4 = \begin{pmatrix} a \\ -b_3 \\ c \end{pmatrix}, \quad \boldsymbol{m}_4 = \|\boldsymbol{f}_4\| \begin{pmatrix} c.s_{\gamma_4} - b_3.c_{\gamma_4}.s_{\beta_4} \\ -c.c_{\gamma_4}.c_{\beta_4} - a.c_{\gamma_4}.s_{\beta_4} \\ -b_3.c_{\gamma_4}.c_{\beta_4} - a.s_{\gamma_4} \end{pmatrix}$$

To simplify the force and moment expressions, we denote by $f_j = \|\boldsymbol{f}_j\| c_{\gamma_j} c_{\beta_j}$, $g_j = \|\boldsymbol{f}_j\| s_{\gamma_j}$ and $h_j = -\|\boldsymbol{f}_j\| c_{\gamma_j} s_{\beta_j}$ the three components of the thrust vector $\boldsymbol{f}_j$ such that $\boldsymbol{f}_j = [f_j, g_j, h_j]^T \quad j \in \{1, ..., 4\}$. Hence, The resultant force $\boldsymbol{f}_{pro}$ and torque $\boldsymbol{m}_{pro}$ vector applied by the four rotors on the airship are:

$$\boldsymbol{f}_{pro} = \begin{pmatrix} \sum_{j=1}^{4} f_j \\ \sum_{j=1}^{4} g_j \\ \sum_{j=1}^{4} h_j \end{pmatrix} \tag{5.4.7}$$

$$\boldsymbol{m}_{pro} = \begin{pmatrix} c\sum_{j=1}^{4} g_j + b_1(h_1 - h_2) + b_3(h_3 - h_4) \\ -c\sum_{j=1}^{4} f_j + a(h_4 - h_3 - h_1 - h_2) \\ b_1(f_1 - f_2) + b_3(f_3 - f_4) + a(g_4 + g_3 - g_1 - g_2) \end{pmatrix} \tag{5.4.8}$$

5.4.2 Aerodynamic Forces

Like others flying objects, the airships are subjected to aerodynamic forces due to the fluid viscosity. These forces have significant influence on airship dynamics. In [88], the authors add a term related to the cross-flow drag to correct the effects of viscosity for an inclined body of revolution. Indeed, wind tunnel tests have shown that strong aerodynamic interaction effects exist between the hull and the fins of airships. The author of [89] elaborate an aerodynamics prediction methods using efficiency factors to account the interaction between the hull and the fins. These factors are estimated from wind-tunnel test. The aerodynamic model presented here is developed using the procedure outlined by [23]. This model includes expressions for axial force and moment on an axis symmetric airship. The effect of these aerodynamic forces $\boldsymbol{f}_a$ and moments $\boldsymbol{m}_a$ are presented as follows:

$$\boldsymbol{f}_a = (F_{a_1}, F_{a_2}, F_{a_3}) \tag{5.4.9}$$

$$\boldsymbol{m}_a = (M_{a_1}, M_{a_2}, M_{a_3}) \tag{5.4.10}$$

F_{a_1}, F_{a_2} and F_{a_3} are drag, sideforce, and lift, respectively. M_{a_1}, M_{a_2} and M_{a_3} are roll moment, pitch moment, and yaw moment, respectively. These axis forces and moments are expressed as follows in the airship body-fixed frame $\mathcal{R}_A$:

$$\begin{cases} F_{a_1} = \frac{1}{2}\rho_{air} S_{ref} v_a^2 C_X \\ F_{a_2} = \frac{1}{2}\rho_{air} S_{ref} v_a^2 C_Y \\ F_{a_3} = \frac{1}{2}\rho_{air} S_{ref} v_a^2 C_Z \\ M_{a_1} = \frac{1}{2}\rho_{air} L_{ref} S_{ref} v_a^2 C_L \\ M_{a_2} = \frac{1}{2}\rho_{air} L_{ref} S_{ref} v_a^2 C_M \\ M_{a_3} = \frac{1}{2}\rho_{air} L_{ref} S_{ref} v_a^2 C_N \end{cases} \tag{5.4.11}$$

$\boldsymbol{v}_a = \boldsymbol{\nu}_1^a - \boldsymbol{v}_w$ is the airship's aerodynamic translational velocity where $\boldsymbol{\nu}_1^a$ and $\boldsymbol{v}_w$ represent respectively the linear airship's velocity and the wind's velocity with respect to the reference frame $\mathcal{R}_0$ expressed in $\mathcal{R}_A$ (note that in case of no wind $\boldsymbol{v}_a = \boldsymbol{\nu}_1^a$). S_{ref} is a reference section of the airship, for example the medium transverse section, L_{ref} can be chosen as the length of the airship and ρ_{air} is the density of the air. Indeed, C_X, C_Y, C_Z, C_L, C_M and C_N are the aerodynamic coefficients which are computed from wind tunnel experiments. These aerodynamic coefficients are function of several parameters such as the Reynolds number, the angle of attack and the angle of side-slip. More details of the computation of these aerodynamic efforts for an ellipsoidal airship can be seen in [90]. As already mentioned, we try to evaluate the behavior of the airship in the case of low velocity or while hovering. In these cases, the effect of these forces can be neglected.

5.4.3 Gravity and Buoyancy

An important characteristic of the airships is the buoyancy B_u. This force represents a natural static lift, corresponding roughly to 1Kg for each m^3 of helium involved in the careen. We suppose here that this force is applied in the buoyancy center B different from the gravity center A:

$$B_u = \rho_{air} \mathcal{V} g \tag{5.4.12}$$

Where $\mathcal{V}$ is the volume of the careen, ρ_{air} is the density of the air, and g the gravity acceleration. In the airship body-fixed frame $\mathcal{R}_A$, the composite effect of gravity and buoyancy is denoted by $\boldsymbol{f}_{wb}$ as follows:

$$\boldsymbol{f}_{wb} = (m_a g - B_u) \boldsymbol{\mathcal{R}}_A^{0T} \boldsymbol{e}_3 \tag{5.4.13}$$

Where $\boldsymbol{e}_3$ is a unit vector pointing in the direction of gravity, $\boldsymbol{\mathcal{R}}_A^0$ is the rotation matrix and m_a is the airship mass. That leads to:

$$\boldsymbol{f}_{wb} = \begin{pmatrix} -(m_a g - B_u) s_{\theta_a} \\ (m_a g - B_u) s_{\phi_a} c_{\theta_a} \\ (m_a g - B_u) c_{\phi_a} c_{\theta_a} \end{pmatrix} \tag{5.4.14}$$

The moment due to the weight and buoyancy is:

$$\boldsymbol{m}_{wb} = B_u (\boldsymbol{\mathcal{R}}_A^{0T} \boldsymbol{e}_3 \times \overrightarrow{BA}) \tag{5.4.15}$$

The center of volume B and the center of gravity A lie on the axis of symmetry of the envelope, where $\overrightarrow{BA} = [0, 0, -z_B]^T$. The moment vector is given by:

$$\boldsymbol{m}_{wb} = \begin{pmatrix} -B_u z_B s_{\phi_a} c_{\theta_a} \\ -B_u z_B s_{\theta_a} \\ 0 \end{pmatrix} \tag{5.4.16}$$

5.4.4 Cable Tensions

Remember that our flying cable crane, the heavy lift airship, consists of a suspended platform connected to an airship via n_c cables. The i^{th} cable is attached at one end to a point A_i on the airship (moving anchor) and at the other end it is attached to a point B_i on the payload. The coordinates of these points are collected respectively in the vectors $\boldsymbol{a}_i$ and $\boldsymbol{b}_i$. $\boldsymbol{a}_i$ is expressed in airship body-fixed frame $\mathcal{R}_A$ while $\boldsymbol{b}_i$ is expressed in platform body-fixed frame $\mathcal{R}_P$.

We assume that the cable sag is very small and not extensible which means that the cable shape can be seen as a straight line. So the tensions exerted by cables have the same direction as the vector $\overrightarrow{A_i B_i}$ and can be defined by the line segment between the cord end point A_i and B_i as follows:

$$\overrightarrow{A_i B_i} = \boldsymbol{p} + \boldsymbol{\mathcal{R}}_P^A \boldsymbol{b}_i + \boldsymbol{a}_i, \qquad i \in \{1, ..., n_c\} \tag{5.4.17}$$

where $\boldsymbol{p}$ is the relative position vector of the platform geometric center P and $\boldsymbol{\mathcal{R}}_P^A$ is the rotation matrix between the two local frames $\mathcal{R}_A$ and $\mathcal{R}_P$. We denote by $\boldsymbol{u}_i = \frac{\overrightarrow{A_i B_i}}{\|\overrightarrow{A_i B_i}\|}$ the unit vector along the i^{th} cable expressed in airship body-fixed frame $\mathcal{R}_A$. It is interesting to note that the airship motion affects the direction of the cables tensions by moving the cable exit point A_i thus making the suspended platform unstable. In the same way, the platform motion changes the direction of the cables tensions by moving the cable attachment point B_i.

By using cables as transmission elements, we introduce the two force transmission matrices between airship and CDPM suspended platform as follows:

1. **Airship force transmission matrix :** The cable tension vector $\boldsymbol{f}_{c_i}$, applied by each cable on the airship at different exit points A_i, can be seen as the product between the cable tension magnitude t_i and the corresponding unit vector collinear to $\overrightarrow{A_iB_i}$:

$$\boldsymbol{f}_{c_i} = t_i \boldsymbol{u}_i \quad i \in \{1, ..., n_c\} \tag{5.4.18}$$

The resultant torque vector applied by each cable on the airship at different mobile exit points A_i expressed in airship body-fixed frame $\mathcal{R}_A$ is:

$$\boldsymbol{m}_{c_i} = \boldsymbol{f}_{c_i} \times \overrightarrow{A_iA}, \quad i \in \{1, ..., n_c\} \tag{5.4.19}$$

$$\boldsymbol{m}_{c_i} = t_i \boldsymbol{u}_i \times -\boldsymbol{a}_i, \quad i \in \{1, ..., n_c\} \tag{5.4.20}$$

These tensions are collected in a wrench $[\boldsymbol{f}_c, \boldsymbol{m}_c]^T$ applied at the airship gravity center A. Its expression is given by the following relation:

$$\boldsymbol{f}_c = \sum_{i=1}^{n_c} t_i \boldsymbol{u}_i \tag{5.4.21}$$

$$\boldsymbol{m}_c = \sum_{i=1}^{n_c} \boldsymbol{a}_i \times -\boldsymbol{u}_i t_i \tag{5.4.22}$$

Or in matrix form, where $\boldsymbol{T} = [t_1, t_2, ..., t_{n_c}]^T$ groups the n_c cable tensions t_i:

$$\begin{pmatrix} \boldsymbol{f}_c \\ \boldsymbol{m}_c \end{pmatrix} = \underbrace{\begin{pmatrix} \boldsymbol{u}_1 & \cdots & \boldsymbol{u}_{n_c} \\ \boldsymbol{a}_1 \times -\boldsymbol{u}_1 & \cdots & \boldsymbol{a}_{n_c} \times -\boldsymbol{u}_{n_c} \end{pmatrix}}_{\boldsymbol{W}_C} \boldsymbol{T} \tag{5.4.23}$$

$\boldsymbol{W}_C$ describes the force transmission matrix from suspended platform to airship:

$$\boldsymbol{W}_C = \begin{pmatrix} \boldsymbol{u}_1 & \cdots & \boldsymbol{u}_{n_c} \\ \boldsymbol{a}_1 \times -\boldsymbol{u}_1 & \cdots & \boldsymbol{a}_{n_c} \times -\boldsymbol{u}_{n_c} \end{pmatrix} \tag{5.4.24}$$

2. **Platform force transmission matrix :** Similar to the airship, the cable tension vector, $\boldsymbol{f}_{p_i}$ applied by each cable on the platform at different attachment points B_i, can be seen as the product between the cable tension magnitude, t_i, and the corresponding unit vector opposite to $\overrightarrow{A_iB_i}$:

$$\boldsymbol{f}_{p_i} = -t_i \boldsymbol{u}_i \quad i \in \{1, ..., n_c\} \tag{5.4.25}$$

The resultant torque vector applied by each cable on the platform at different attachment points B_i expressed in airship body-fixed frame $\mathcal{R}_A$ is:

$$\boldsymbol{m}_{p_i} = \boldsymbol{f}_{p_i} \times \overrightarrow{B_i P}, \quad i \in \{1, ..., n_c\} \tag{5.4.26}$$

$$\boldsymbol{m}_{p_i} = -\boldsymbol{\mathcal{R}}_P^A \boldsymbol{b}_i \times \boldsymbol{u}_i t_i, \quad i \in \{1, ..., n_c\} \tag{5.4.27}$$

These tensions are collected in a wrench $[\boldsymbol{f}_p, \boldsymbol{m}_p]^T$ applied at the geometric center P. Its expression is given by the following relation:

$$\boldsymbol{f}_p = -\sum_{i=1}^{n_c} t_i \boldsymbol{u}_i \tag{5.4.28}$$

$$\boldsymbol{m}_p = -\sum_{i=1}^{n_c} \boldsymbol{\mathcal{R}}_P^A \boldsymbol{b}_i \times \boldsymbol{u}_i t_i \tag{5.4.29}$$

hence,

$$\begin{pmatrix} \boldsymbol{f}_p \\ \boldsymbol{m}_p \end{pmatrix} = \underbrace{-\begin{pmatrix} \boldsymbol{u}_1 & \cdots & \boldsymbol{u}_{n_c} \\ \boldsymbol{\mathcal{R}}_P^A \boldsymbol{b}_1 \times \boldsymbol{u}_1 & \cdots & \boldsymbol{\mathcal{R}}_P^A \boldsymbol{b}_{n_c} \times \boldsymbol{u}_{n_c} \end{pmatrix}}_{\boldsymbol{\mathcal{W}}_P} \boldsymbol{T} \tag{5.4.30}$$

where the vector $\boldsymbol{T} = [t_1, t_2, ..., t_{n_c}]^T$ is the collection of the n_c cable tensions t_i and $\boldsymbol{\mathcal{W}}_P$ describes the force transmission matrix from airship to suspended platform:

$$\boldsymbol{\mathcal{W}}_P = -\begin{pmatrix} \boldsymbol{u}_1 & \cdots & \boldsymbol{u}_{n_c} \\ \boldsymbol{\mathcal{R}}_P^A \boldsymbol{b}_1 \times \boldsymbol{u}_1 & \cdots & \boldsymbol{\mathcal{R}}_P^A \boldsymbol{b}_{n_c} \times \boldsymbol{u}_{n_c} \end{pmatrix} \tag{5.4.31}$$

5.5 Airship Mass Matrix

The airship mass matrix incorporates all masses and inertias of the airship, including the virtual terms associated with the fact that we are dealing with a buoyant vehicle. The dynamics of an airship are markedly different from traditional aircraft with significant effects from added mass and inertia. Hence, The airship 6×6 mass matrix $\boldsymbol{M}_T$ is composed of the standard mass matrix $\boldsymbol{M}_b$ as well as the additional added mass matrix $\boldsymbol{M}_a$. Therefore:

$$\boldsymbol{M}_T = \boldsymbol{M}_a + \boldsymbol{M}_b \tag{5.5.1}$$

5.5.1 Standard Mass Matrix

The standard mass matrix is given by:

$$\boldsymbol{M}_b = \begin{pmatrix} m_a & 0 & 0 & 0 & 0 & 0 \\ 0 & m_a & 0 & 0 & 0 & 0 \\ 0 & 0 & m_a & 0 & 0 & 0 \\ 0 & 0 & 0 & I_{xx} & 0 & I_{xz} \\ 0 & 0 & 0 & 0 & I_{yy} & 0 \\ 0 & 0 & 0 & I_{zx} & 0 & I_{zz} \end{pmatrix} \tag{5.5.2}$$

where m_a is the total physical mass of the airship and I_{xx}, I_{yy} and I_{zz} are the inertia moments with respect to the indexed axes such as:

$$I_{xx} = \sum_i (z_i^2 + y_i^2); \quad I_{yy} = \sum_i (x_i^2 + z_i^2); \quad I_{zz} = \sum_i (x_i^2 + y_i^2)$$

The non-diagonal terms are such that : $I_{xz,zx} = \sum_i x_i z_i$

5.5.2 Added Mass Matrix

When an airship moves in an incompressible and infinite inviscid fluid, the kinetic energy of the particles of air produces an effect equivalent to an important increase of the mass and inertia of the airship. Many theoretical works on the computation of added masses for conventional airships are based on potential flow theory [91] and [92]. Other comparable theoretical approaches like the decomposition of the airship surface into finite elements are applied to determine the added-mass terms [93] and [94]. Furthermore, these coefficients can be derived by an energy approach in terms of Kirchhoff equations [95] and [96]. The added mass matrix $\boldsymbol{M}_a$ of a rigid body airship includes the contributions of both the hull and the fins, thus:

$$\boldsymbol{M}_a = \boldsymbol{M}_{a_{hull}} + \boldsymbol{M}_{a_{fins}} \tag{5.5.3}$$

Considering that the velocity potential of the air surrounding the airship obeys the Laplace's equation, the added masses matrix of the hull will be determined by means of the velocity potential flow theory. The analytical method for calculating the added mass factors can be found in [87]. $\boldsymbol{M}_{a_{hull}}$ is defined as follows:

$$\boldsymbol{M}_{a_{hull}} = \begin{pmatrix} M_{ah11} & 0 & 0 & 0 & 0 & 0 \\ 0 & M_{ah22} & 0 & 0 & 0 & 0 \\ 0 & 0 & M_{ah33} & 0 & 0 & 0 \\ 0 & 0 & 0 & M_{ah44} & 0 & M_{ah46} \\ 0 & 0 & 0 & 0 & M_{ah55} & 0 \\ 0 & 0 & 0 & M_{ah46} & 0 & M_{ah66} \end{pmatrix} \tag{5.5.4}$$

The non-zero elements in the added-mass matrix of the fins are obtained by integrating the 2-D added mass of the cross section over the fin area. Due to the small size of the fin area, extra-diagonal terms are negligible and only the diagonal elements needs to be calculated. Hence, the added mass matrix of fins $\boldsymbol{M}_{a_{fins}}$ is given by:

$$\boldsymbol{M}_{a_{fins}} = \begin{pmatrix} M_{af11} & 0 & 0 & 0 & 0 & 0 \\ 0 & M_{af22} & 0 & 0 & 0 & 0 \\ 0 & 0 & M_{af33} & 0 & 0 & 0 \\ 0 & 0 & 0 & M_{af44} & 0 & 0 \\ 0 & 0 & 0 & 0 & M_{af55} & 0 \\ 0 & 0 & 0 & 0 & 0 & M_{af66} \end{pmatrix} \tag{5.5.5}$$

The whole symmetric block-diagonal mass matrix $\boldsymbol{M}_T$ can be written in this form [87]:

$$\boldsymbol{M}_T = \boldsymbol{M}_a + \boldsymbol{M}_b = \begin{pmatrix} \boldsymbol{M}_{TT} & 0 \\ 0 & \boldsymbol{M}_{RR} \end{pmatrix} = \begin{pmatrix} M_{11} & 0 & 0 & 0 & 0 & 0 \\ 0 & M_{22} & 0 & 0 & 0 & 0 \\ 0 & 0 & M_{33} & 0 & 0 & 0 \\ 0 & 0 & 0 & M_{44} & 0 & M_{46} \\ 0 & 0 & 0 & 0 & M_{55} & 0 \\ 0 & 0 & 0 & M_{46} & 0 & M_{66} \end{pmatrix} \tag{5.5.6}$$

5.6 Dynamic Modeling

The motion of a rigid body in a fluid is often investigated by having recourse to Kirchhoff equations. The main feature of Kirchhoff equations is that they describe the motion of a rigid body in an ideal fluid. Furthermore they are written in a form which resembles that of Lagrange equations once we replace the generalized coordinates and their time derivatives with velocity and angular velocity. The derivation of Kirchhoff equations traces back to Kirchhoff [97] and perhaps the main reference to the subject in the literature is [95]. Moreover, a recent paper presents the connection between Kirchhoff and Euler equations of rigid body dynamics [98]. The authors establish the conservation laws arising from given external forces. Revisiting the derivation of Kirchhoff equations provides a deeper understanding of the subject.

The heavy lift airship is a multi-body systems in which multiple rigid bodies are joined together. The dynamic model of this multi-body system composed of the airship and the CDPM can be modeled as an interconnection of lower order subsystems. Specifically, we decompose our system into two isolated subsystems (i.e the airship and the CDPM). By applying Kirchhoff equations, we obtain the motion equation. This method involves two steps. The first one is to formulate the expression of kinetic energy T_{tot}. The second one consists of applying Kirchhoff equations as follows:

$$\frac{d}{dt}\left(\frac{\delta T_{tot}}{\delta \boldsymbol{\nu}_1}\right) + \boldsymbol{\nu}_2 \times \frac{\delta T_{tot}}{\delta \boldsymbol{\nu}_1} = \boldsymbol{\tau}_1 \tag{5.6.1}$$

$$\frac{d}{dt}\left(\frac{\delta T_{tot}}{\delta \boldsymbol{\nu}_2}\right) + \boldsymbol{\nu}_2 \times \frac{\delta T_{tot}}{\delta \boldsymbol{\nu}_2} + \boldsymbol{\nu}_1 \times \frac{\delta T_{tot}}{\delta \boldsymbol{\nu}_1} = \boldsymbol{\tau}_2 \tag{5.6.2}$$

where the force $\boldsymbol{\tau}_1$ and moment $\boldsymbol{\tau}_2$ are expressed in the body-fixed frame. The vectors $\boldsymbol{\nu}_1$ and $\boldsymbol{\nu}_2$ represent respectively the body-fixed linear and angular velocity. We have to note that Kirchhoff equations do not include the gravitational forces and is valid in any reference frame, inertial and body-fixed as long as independent generalized coordinates are used.

For this approach, the two subsystems, the airship and the movable suspended platform of the CDPM, are viewed independently. In this section, we develop a 12-DOF mathematical model for the heavy lift airship. These 12-DOF consist of 6-DOF for the airship's rigid body and 6-DOF of the suspended platform where cables are massless, inextensible and they are always taut. The advantage of this approach is that the interconnection between the airship and the suspended platform is clearly presented and the modeling of the airship can refer to the conventional airship model which is available in many reference. The dynamics of the $MC500$ is firstly derived and then those of the suspended platform of the CDPM is derived based on the force analysis done in the previous section.

5.6.1 Airship Dynamic Modeling

In most dynamics models of aircraft, the vehicles are modeled as a rigid-body with three translation and three rotation degree of freedoms [99] and [100]. The Newton-Euler description is used extensively in many studies of rigid aircraft [16]. This choice is mainly motivated by the easiness to build control or stabilization algorithms based on this model. This approach considers the effect of time-varying mass and inertia properties. An alternative approach of the Newton-Euler formulation applies Lagrangian mechanics [101]. The Lagrangian approach involves three energy terms with first the energy of the vehicle motion itself, second the energy of the air around the airship due to the relative velocities and third the energy added to the buoyancy air. Unfortunately, we cannot use the Lagrange equation directly to formulate the equations of motion in the body-fixed frame. However, this problem can be circumvented by applying Kirchhoff equations [102]. This model is written originally for marine vehicles [103]. It is modified later to take into account the specificity of the airship [104] and [105].

For convenience, the motion equations for a 6-DOF air vehicle are usually derived in the body-fixed frame. The airship dynamic modeling is deduced from Kirchhoff equations. The modeling is based on the following hypotheses:

(i) In order to apply the mechanical theory of a rigid body, aeroelastic phenomena are neglected, the hull is considered as a solid.

(ii) The mass of the airship and its volume are considered as constant. This strong hypothesis neglects the variation of mass induced by the inflation of air ballonets inside the hull.

(iii) The center of volume B and the center of gravity A lie on the symmetry axis of the airship envelope.

(iv) During hovering flight of the airship, the aerodynamic forces are neglected.

(v) As the Mach number is low for an airship, the fluid viscosity, which depends on the temperature, can be considered constant. As a consequence the Prandtl number is neglected and the density of air is not locally modified by the airship motion.

The motion of the airship can be described by its inertial velocity $\boldsymbol{\nu}^a = [\boldsymbol{\nu}_1^a, \boldsymbol{\nu}_2^a]^T$ including the inertial linear $\boldsymbol{\nu}_1^a$ and angular $\boldsymbol{\nu}_2^a$ velocities (expressed in airship body-fixed frame $\mathcal{R}_A$). Thus, the expression of the kinetic energy of the airship T_a is defined as:

$$T_a = \frac{1}{2}\boldsymbol{\nu}_1^{aT}\boldsymbol{M}_{TT}\boldsymbol{\nu}_1^a + \frac{1}{2}\boldsymbol{\nu}_2^{aT}\boldsymbol{M}_{RR}\boldsymbol{\nu}_2^a \tag{5.6.3}$$

Once the kinetic energy is defined, we can apply Kirchhoff equations such that the forces and moments are referred to the airship body-fixed axes. The airship motion is usually represented by a set of kinematics and dynamic equations that describe its evolution in a 6-DOF space:

$$\underbrace{\begin{pmatrix} \boldsymbol{M}_{TT} & \boldsymbol{0}_{3\times3} \\ \boldsymbol{0}_{3\times3} & \boldsymbol{M}_{RR} \end{pmatrix}}_{\boldsymbol{M}_T} \begin{pmatrix} \dot{\boldsymbol{\nu}}_1^a \\ \dot{\boldsymbol{\nu}}_2^a \end{pmatrix} + \underbrace{\begin{pmatrix} \boldsymbol{\nu}_2^a \times \boldsymbol{M}_{TT}\boldsymbol{\nu}_1^a \\ \boldsymbol{\nu}_2^a \times \boldsymbol{M}_{RR}\boldsymbol{\nu}_2^a + \boldsymbol{\nu}_1^a \times \boldsymbol{M}_{TT}\boldsymbol{\nu}_1^a \end{pmatrix}}_{\boldsymbol{Q}} = \begin{pmatrix} \boldsymbol{\tau}_{a_1} \\ \boldsymbol{\tau}_{a_2} \end{pmatrix} \tag{5.6.4}$$

As already mentioned, $\boldsymbol{\tau}_{a_1}$ and $\boldsymbol{\tau}_{a_2}$ represent respectively the resultant force and torque applied on the airship such that $\boldsymbol{\tau}_{a_1} = \boldsymbol{f}_{pro} + \boldsymbol{f}_{wb} + \boldsymbol{f}_c$ and $\boldsymbol{\tau}_{a_2} = \boldsymbol{m}_{pro} + \boldsymbol{m}_{wb} + \boldsymbol{m}_c$. We suppose that $\boldsymbol{\tau}_{_{pro}} = [\boldsymbol{f}_{pro}, \boldsymbol{m}_{pro}]^T$ is the propulsion wrench generated by the four rotors, $\boldsymbol{\tau}_{wb} = [\boldsymbol{f}_{wb}, \boldsymbol{m}_{wb}]^T$ is the gravitational and buoyancy wrench as well as $\boldsymbol{\tau}_{_{cab}} = [\boldsymbol{f}_c, \boldsymbol{m}_c]^T$ is the effort caused by cable tensions applied on the airship in each exit point A_i. Hence, the model can be described by two equations. The first characterizes the system dynamics with respect to $\mathcal{R}_A$, while the second represents the kinematic link between the frames $\mathcal{R}_A$ and $\mathcal{R}_0$:

$$\boldsymbol{M}_T\dot{\boldsymbol{\nu}}^a + \boldsymbol{Q}(\boldsymbol{\nu}^a) = \boldsymbol{\tau}_{_{cab}} + \boldsymbol{\tau}_{_{pro}} + \boldsymbol{\tau}_{wb} \tag{5.6.5}$$

$$\dot{\boldsymbol{\eta}}^a = \boldsymbol{J}_a(\boldsymbol{\eta}_2^a)\boldsymbol{\nu}^a \tag{5.6.6}$$

The two vectors $\boldsymbol{\nu}^a = [u, v, w, p, q, r]^T$ and $\boldsymbol{\eta}^a = [x_a, y_a, z_a, \phi_a, \theta_a, \psi_a]^T$ represent respectively the velocity and position vector of the airship. $\boldsymbol{M}_T$ is the inertia matrix including the aerodynamic virtual inertia (added mass) and the vector $\boldsymbol{Q}$ contains the nonlinear forces and moments due to centrifugal and Coriolis forces. $\boldsymbol{\tau}_{_{pro}}$, $\boldsymbol{\tau}_{wb}$ and $\boldsymbol{\tau}_{_{cab}}$ represent the external forces and moments applied on the airship.

5.6.2 Suspended Platform Dynamic Modeling

Once the airship dynamic model is elaborated, we derivate the dynamic model of the CDPM suspended platform. At present, the research on heavy lift airship is still basically in the exploration phase. In [80], authors present a dynamics model of a helicopter carrying a payload

through a cable suspended robot, using Newton-Euler approach. The cable robot is introduced for fine motion, while the gross motion is left to the helicopter. Further, the problem of cooperative aerial transportation has already been addressed in several recent publications where the payload is suspended by cables from multiple quad-rotors [106]. Because of the similar structure, the helicopter carrying a payload and the flying cable robot can provide references for the research of heavy lift airship.

In [107], authors develop the full dynamics of the a cooperative aerial transportation. They are inspired by the literature on Reconfigurable Cable-Driven Parallel Robot (RCDPRs). For this class of robot, the geometric structure can be changed by appropriately modifying the exit or attachment points of CDPR. Following the modeling convention of RCDPRs, authors are able to describe explicitly the interaction between payload and quadrotors through the cable tensions. Different from previous works, we elaborate the dynamic model of the CDPM suspended platform using the Kirchhoff equations. To develop the mathematical models of the heavy lift airship, we have to make some assumptions:

(i) The cables are massless and stiff so that the inertias and spring stiffness of cables will have no effect. Furthermore, cables are always taut which means that they are always under tension.

(ii) The suspended platform via cables is taken as the research object. Therefore, the inertia/dynamics of motors that drive cables is ignored.

(iii) For low speed flight of the airship, the aerodynamic effects of the suspended platform are ignored.

(iv) The airship motion acts as a disturbance to the cable robot.

The six-dimensional motion of the suspended platform can be described by its velocity vector $\boldsymbol{\nu}^p = [\boldsymbol{\nu}_1^p, \boldsymbol{\nu}_2^p]^T$ including the linear and angular velocity (expressed in the airship body-fixed frame $\mathcal{R}_A$) denoted respectively by $\boldsymbol{\nu}_1^p$ and $\boldsymbol{\nu}_2^p$. Hence, the kinetic energy of the suspended platform T_p is given by:

$$T_p = \frac{1}{2}\boldsymbol{\nu}_1^{pT}\boldsymbol{\mathcal{M}}_P\boldsymbol{\nu}_1^p + \frac{1}{2}\boldsymbol{\nu}_2^{pT}\boldsymbol{\mathcal{I}}_P\boldsymbol{\nu}_2^p \tag{5.6.7}$$

where $\boldsymbol{\mathcal{M}}_P$ and $\boldsymbol{\mathcal{I}}_P$ are respectively the inertia mass and moment matrix of the suspended platform expressed in the local frame $\mathcal{R}_A$. By applying Kirchoff equations, the partial derivative of the kinetic energy T_p relative to $\boldsymbol{\nu}_1^p$ and $\boldsymbol{\nu}_2^p$:

$$\frac{\partial T_p}{\partial \boldsymbol{\nu}_1^p} = \boldsymbol{\mathcal{M}}_P\boldsymbol{\nu}_1^p \tag{5.6.8}$$

$$\frac{\partial T_p}{\partial \boldsymbol{\nu}_2^p} = \boldsymbol{\mathcal{I}}_P\boldsymbol{\nu}_2^p \tag{5.6.9}$$

As mentioned in [98], the time derivative is applied with respect to the local frame $\mathcal{R}_P$ in Kirchhoff equations. Hence, for any vector function $\overrightarrow{u}$ of time t we have $\frac{d\overrightarrow{u}}{dt}\rfloor_{\mathcal{R}_P} = \frac{d\overrightarrow{u}}{dt}\rfloor_{\mathcal{R}_0} - \overrightarrow{\omega}_{\rfloor\mathcal{R}_P/\mathcal{R}_0} \times \overrightarrow{u}$ (see B.1). Here, $\overrightarrow{\omega}_{\rfloor\mathcal{R}_P/\mathcal{R}_0}$ corresponds to $\boldsymbol{\nu}_2^p$. Now taking the time derivative gives:

$$\frac{d}{dt}\left(\frac{\partial T_p}{\partial \boldsymbol{\nu}_1^p}\right) = \boldsymbol{\mathcal{M}}_P\dot{\boldsymbol{\nu}}_1^p - \boldsymbol{\mathcal{M}}_P\boldsymbol{\nu}_2^p \times \boldsymbol{\nu}_1^p \tag{5.6.10}$$

$$\frac{d}{dt}\left(\frac{\partial T_p}{\partial \boldsymbol{\nu}_2^a}\right) = \boldsymbol{\mathcal{I}}_P\dot{\boldsymbol{\nu}}_2^p \tag{5.6.11}$$

For the suspended platform, $\boldsymbol{\tau}_{p_1}$ and $\boldsymbol{\tau}_{p_2}$ represent respectively the resultant force and torque applied on the geometric center of the platform P. We consider the weight of the platform, represented by the vector $mg\boldsymbol{e}_3$ and the n_c cable tensions t_i, having as direction the unit vector along the i^{th} cable $\boldsymbol{u}_i$, as external efforts applied on the platform. Thus, the expression of $\boldsymbol{\tau}_{p_1}$ and $\boldsymbol{\tau}_{p_2}$ is given by:

$$\boldsymbol{\tau}_{p_1} = mg\boldsymbol{\mathcal{R}}_0^A\boldsymbol{e}_3 - \sum_{i=1}^{n_c} t_i\boldsymbol{u}_i \tag{5.6.12}$$

$$\boldsymbol{\tau}_{p_2} = -\sum_{i=1}^{n_c} \boldsymbol{\mathcal{R}}_P^A\boldsymbol{b}_i \times t_i\boldsymbol{u}_i \tag{5.6.13}$$

where $\boldsymbol{e}_3$ is a unit vector pointing in the direction of gravity, $\boldsymbol{\mathcal{R}}_0^A$ is the rotation matrix, m is the platform mass and g is the gravity acceleration. Referring to Kirchoff equations and summing up all the previous terms from (5.6.8) to (5.6.13), we get both force and moment equations:

$$\boldsymbol{\mathcal{M}}_P\dot{\boldsymbol{\nu}}_1^p - \boldsymbol{\mathcal{M}}_P\boldsymbol{\nu}_2^p \times \boldsymbol{\nu}_1^p + \boldsymbol{\nu}_2^p \times \boldsymbol{\mathcal{M}}_P\boldsymbol{\nu}_1^p = mg\boldsymbol{\mathcal{R}}_0^A\boldsymbol{e}_3 - \sum_{i=1}^{n_c} t_i\boldsymbol{u}_i \tag{5.6.14}$$

$$\boldsymbol{\mathcal{I}}_P\dot{\boldsymbol{\nu}}_2^p + \boldsymbol{\nu}_2^p \times \boldsymbol{\mathcal{I}}_P\boldsymbol{\nu}_2^p + \boldsymbol{\nu}_1^p \times \boldsymbol{\mathcal{M}}_P\boldsymbol{\nu}_1^p = -\sum_{i=1}^{n_c} \boldsymbol{\mathcal{R}}_P^A\boldsymbol{b}_i \times t_i\boldsymbol{u}_i \tag{5.6.15}$$

We have to note that $\boldsymbol{\mathcal{M}}_P$ is a diagonal matrix defined by $\boldsymbol{\mathcal{M}}_P = m\boldsymbol{I}_{3\times3}$, so that the term $\boldsymbol{\nu}_1^p \times \boldsymbol{\mathcal{M}}_P\boldsymbol{\nu}_1^p$ is null since $\boldsymbol{\nu}_1^p \times \boldsymbol{\nu}_1^p = 0$ as well as the term $\boldsymbol{\nu}_2^p \times \boldsymbol{\mathcal{M}}_P\boldsymbol{\nu}_1^p - \boldsymbol{\mathcal{M}}_P\boldsymbol{\nu}_2^p \times \boldsymbol{\nu}_1^p$ is equal to zero. $\boldsymbol{\mathcal{I}}_P$ is the inertia matrix of the suspended platform with respect to the airship body fixed frame $\mathcal{R}_A$, such that $\boldsymbol{\mathcal{I}}_P = \boldsymbol{\mathcal{R}}_P^A\boldsymbol{I}_p\boldsymbol{\mathcal{R}}_A^P$, where $\boldsymbol{I}_p$ is the inertia matrix of the suspended platform with respect to the local frame $\mathcal{R}_P$. Hence, the latter equations are simplified as follows:

$$m\dot{\boldsymbol{\nu}}_1^p = mg\boldsymbol{\mathcal{R}}_0^A\boldsymbol{e}_3 - \sum_{i=1}^{n_c} t_i\boldsymbol{u}_i \tag{5.6.16}$$

$$\boldsymbol{\mathcal{R}}_P^A\boldsymbol{I}_p\boldsymbol{\mathcal{R}}_A^P\dot{\boldsymbol{\nu}}_2^p + \boldsymbol{\nu}_2^p \times \boldsymbol{\mathcal{R}}_P^A\boldsymbol{I}_p\boldsymbol{\mathcal{R}}_A^P\boldsymbol{\nu}_2^p = -\sum_{i=1}^{n_c} \boldsymbol{\mathcal{R}}_P^A\boldsymbol{b}_i \times t_i\boldsymbol{u}_i \tag{5.6.17}$$

We replace both linear and angular velocities by their expressions $\boldsymbol{\nu}_1^p = \boldsymbol{\nu}_1^a + \boldsymbol{v} + \boldsymbol{\nu}_2^a \times \boldsymbol{p}$ and $\boldsymbol{\nu}_2^p = \boldsymbol{\nu}_2^a + \boldsymbol{\omega}$ respectively. Then, we substitute similarly the linear and angular acceleration by their expressions $\dot{\boldsymbol{\nu}}_1^p = \mathring{\boldsymbol{v}} + \dot{\boldsymbol{\nu}}_1^a + 2\boldsymbol{\nu}_2^a \times \boldsymbol{v} + \dot{\boldsymbol{\nu}}_2^a \times \boldsymbol{p} + \boldsymbol{\nu}_2^a \times (\boldsymbol{\nu}_2^a \times \boldsymbol{p})$ and $\dot{\boldsymbol{\nu}}_2^p = \dot{\boldsymbol{\nu}}_2^a + \mathring{\boldsymbol{\omega}} + \boldsymbol{\nu}_2^a \times \boldsymbol{\omega}$ respectively in the above equations. Thus, we have:

$$m\left[\mathring{\boldsymbol{v}} + \dot{\boldsymbol{\nu}}_1^a + 2\boldsymbol{\nu}_2^a \times \boldsymbol{v} + \dot{\boldsymbol{\nu}}_2^a \times \boldsymbol{p} + \boldsymbol{\nu}_2^a \times (\boldsymbol{\nu}_2^a \times \boldsymbol{p})\right] = mg\boldsymbol{\mathcal{R}}_0^A \boldsymbol{e}_3 - \sum_{i=1}^{n_c} t_i \boldsymbol{u}_i \tag{5.6.18}$$

$$\boldsymbol{\mathcal{R}}_P^A \boldsymbol{I}_p \boldsymbol{\mathcal{R}}_A^P (\dot{\boldsymbol{\nu}}_2^a + \mathring{\boldsymbol{\omega}} + \boldsymbol{\nu}_2^a \times \boldsymbol{\omega}) + (\boldsymbol{\nu}_2^a + \boldsymbol{\omega}) \times \boldsymbol{\mathcal{R}}_P^A \boldsymbol{I}_p \boldsymbol{\mathcal{R}}_A^P (\boldsymbol{\nu}_2^a + \boldsymbol{\omega}) = -\sum_{i=1}^{n_c} \boldsymbol{\mathcal{R}}_P^A \boldsymbol{b}_i \times t_i \boldsymbol{u}_i \tag{5.6.19}$$

This leads to:

$$m\mathring{\boldsymbol{v}} + m(\dot{\boldsymbol{\nu}}_1^a + 2\boldsymbol{\nu}_2^a \times \boldsymbol{v} + \dot{\boldsymbol{\nu}}_2^a \times \boldsymbol{p} + \boldsymbol{\nu}_2^a \times (\boldsymbol{\nu}_2^a \times \boldsymbol{p})) = mg\boldsymbol{\mathcal{R}}_0^A \boldsymbol{e}_3 - \sum_{i=1}^{n_c} t_i \boldsymbol{u}_i \tag{5.6.20}$$

$$\begin{aligned} &\boldsymbol{\mathcal{R}}_P^A \boldsymbol{I}_p \boldsymbol{\mathcal{R}}_A^P \mathring{\boldsymbol{\omega}} + \boldsymbol{\omega} \times \boldsymbol{\mathcal{R}}_P^A \boldsymbol{I}_p \boldsymbol{\mathcal{R}}_A^P \boldsymbol{\omega} + \boldsymbol{\mathcal{R}}_P^A \boldsymbol{I}_p \boldsymbol{\mathcal{R}}_A^P (\dot{\boldsymbol{\nu}}_2^a + \boldsymbol{\nu}_2^a \times \boldsymbol{\omega}) \\ &\quad + \boldsymbol{\nu}_2^a \times \boldsymbol{\mathcal{R}}_P^A \boldsymbol{I}_p \boldsymbol{\mathcal{R}}_A^P (\boldsymbol{\nu}_2^a + \boldsymbol{\omega}) + \boldsymbol{\omega} \times \boldsymbol{\mathcal{R}}_P^A \boldsymbol{I}_p \boldsymbol{\mathcal{R}}_A^P \boldsymbol{\nu}_2^a = -\sum_{i=1}^{n_c} \boldsymbol{\mathcal{R}}_P^A \boldsymbol{b}_i \times t_i \boldsymbol{u}_i \end{aligned} \tag{5.6.21}$$

By selecting appropriate coordinates, the unknown disturbance from the airship motion can be modeled as additive terms in the dynamics of suspended platform. We can combine both force and moment equations such as:

$$\begin{aligned} &\underbrace{\begin{pmatrix} m\boldsymbol{I}_3 & \boldsymbol{0}_{3\times 3} \\ \boldsymbol{0}_{3\times 3} & \boldsymbol{\mathcal{R}}_P^A \boldsymbol{I}_p \boldsymbol{\mathcal{R}}_A^P \end{pmatrix}}_{\boldsymbol{M}_P} \begin{pmatrix} \mathring{\boldsymbol{v}} \\ \mathring{\boldsymbol{\omega}} \end{pmatrix} + \underbrace{\begin{pmatrix} \boldsymbol{0}_{3\times 1} \\ \boldsymbol{\omega} \times \boldsymbol{\mathcal{R}}_P^A \boldsymbol{I}_p \boldsymbol{\mathcal{R}}_A^P \boldsymbol{\omega} \end{pmatrix}}_{\boldsymbol{C}_P \dot{\boldsymbol{\chi}}} + \underbrace{\begin{pmatrix} -mg\boldsymbol{\mathcal{R}}_0^A \boldsymbol{e}_3 \\ \boldsymbol{0}_{3\times 1} \end{pmatrix}}_{\boldsymbol{G}_P} \\ &\qquad + \underbrace{\begin{pmatrix} \boldsymbol{D}_{\boldsymbol{\nu}_1^a} \\ \boldsymbol{D}_{\boldsymbol{\nu}_2^a} \end{pmatrix}}_{\boldsymbol{D}_P} = \underbrace{-\begin{pmatrix} \boldsymbol{u}_1 & \cdots & \boldsymbol{u}_{n_c} \\ \boldsymbol{\mathcal{R}}_P^A \boldsymbol{b}_1 \times \boldsymbol{u}_1 & \cdots & \boldsymbol{\mathcal{R}}_P^A \boldsymbol{b}_{n_c} \times \boldsymbol{u}_{n_c} \end{pmatrix}}_{\boldsymbol{W}_P} \boldsymbol{T} \end{aligned} \tag{5.6.22}$$

with:

$$\boldsymbol{D}_{\boldsymbol{\nu}_1^a} = m\left[\dot{\boldsymbol{\nu}}_1^a + 2\boldsymbol{\nu}_2^a \times \boldsymbol{v} + \dot{\boldsymbol{\nu}}_2^a \times \boldsymbol{p} + \boldsymbol{\nu}_2^a \times (\boldsymbol{\nu}_2^a \times \boldsymbol{p})\right]$$

$$\boldsymbol{D}_{\boldsymbol{\nu}_2^a} = \boldsymbol{\mathcal{R}}_P^A \boldsymbol{I}_p \boldsymbol{\mathcal{R}}_A^P (\dot{\boldsymbol{\nu}}_2^a + \boldsymbol{\nu}_2^a \times \boldsymbol{\omega}) + \boldsymbol{\nu}_2^a \times \boldsymbol{\mathcal{R}}_P^A \boldsymbol{I}_p \boldsymbol{\mathcal{R}}_A^P (\boldsymbol{\nu}_2^a + \boldsymbol{\omega}) + \boldsymbol{\omega} \times \boldsymbol{\mathcal{R}}_P^A \boldsymbol{I}_p \boldsymbol{\mathcal{R}}_A^P \boldsymbol{\nu}_2^a$$

The above dynamic model shows explicitly the interaction between suspended platform and movable airship through the expression of the two additive terms $\boldsymbol{D}_{\boldsymbol{\nu}_1^a}$ and $\boldsymbol{D}_{\boldsymbol{\nu}_2^a}$ that

depend essentially on airship acceleration vector $[\boldsymbol{\nu}_1^a, \boldsymbol{\nu}_2^a]^T$. Knowing that $\overset{\circ\circ}{\boldsymbol{\chi}} = [\mathring{\boldsymbol{v}}, \mathring{\boldsymbol{\omega}}]^T$, the compact dynamic model of the suspended platform is given by the following expression:

$$\boldsymbol{M}_P(\boldsymbol{\chi})\overset{\circ\circ}{\boldsymbol{\chi}} + \boldsymbol{C}_P(\boldsymbol{\chi}, \mathring{\boldsymbol{\chi}})\mathring{\boldsymbol{\chi}} + \boldsymbol{G}_P(\boldsymbol{\chi}) + \boldsymbol{D}_P(\boldsymbol{\chi}, \mathring{\boldsymbol{\chi}}, \boldsymbol{\nu}^a, \dot{\boldsymbol{\nu}}^a) = \boldsymbol{W}_P\boldsymbol{T} \tag{5.6.23}$$

where $\boldsymbol{M}_P$ is the inertia matrix, $\boldsymbol{C}_P$ is the matrix of Coriolis and centrifugal terms, $\boldsymbol{D}_P$ is the disturbance vector due to airship motion and $\boldsymbol{W}_P$ is the force transmission matrix.

5.7 Conclusion

In this chapter, we introduce firstly the concept of the heavy lift airship. A special focus is done on the critical phase of loading and unloading using CDPM. Different from the conventional airship, the developed model intends to include the motion of the CDPM rigidly linked to the airship. On the other side, the airship motion leads to an imprecise dynamics modeling and cable tension determination. The proposed approach corresponds to consider the airship and the CDPM platform as two independent subsystems. The dynamic model is derived using Kirchhoff equations. This explicit dynamic model describes clearly the internal motions of the system. Based on the kinematic and dynamic model, a robust controller is developed to ensure safe cargo handling in the next chapter.

Chapter 6

Control of Heavy-Lift Airship

Contents

6.1 Introduction

The work of the heavy lift airship requires the cooperation of the two subsystems (i.e the airship and CDPM). Specifically, the airship hovers above the ground and a special loading frame, which is fixed during flight to the keel of the airship, is then rigged with eight cables to the ground. Due to the inertial coupling between the airship and the platform, the suspended platform may sway with large amplitudes that may generate dangerous configurations to the system. On the other side, the suspended CDPM suffers from various external disturbances, especially the persistent and unpredictable airship motion. In this chapter, our ultimate control objective is to provide protection for the safety of the heavy lift airship during loading and unloading phase.

As already mentioned, the dynamic model of the global system is modeled as an interconnection of lower order subsystems (i.e the airship and the CDPM). We assume that the heavy lift airship is a weakly coupled subsystems. This assumption is exploited to design a decentralized controller, which makes it possible to control the airship and the CDPM independently. Base on this assumption, we elaborate a robust controller for each subsystem.

The main goal of the decomposition is the reduction of computational complexity. This control architecture serves as effective tool to overcome specific difficulties arising in large-scale complex systems such as high dimensionality, information structure constraints, uncertainty and delays.

In this chapter, a robust sliding mode control, capable of auto-piloting and controlling the airship, is firstly developed. Secondly, a PD computed-torque control is applied on the CDPM in order to ensure loading and unloading phase. The feature of the proposed control system is that the unknown disturbance terms of the airship motion in the suspended platform dynamic are explicitly incorporated into control system design without any simplifying assumption and vice versa. Furthermore, numerical simulation results are presented and a stability analysis is provided to confirm the accuracy of our derivations.

6.2 Stabilization of the Airship

For the stabilization control of airships, linear control methods and a back-stepping control approach have been used. In [108] a back-stepping control approach is designed for each navigation phases from takeoff to landing. Due to the decoupling properties, an equilibrium state is reached at the end of each flight phase. In [109], the stabilization problem is solved with an explicit homogeneous time-varying control law through a detailed analysis of the blimp dynamic model. In this research, a time-varying stabilization is developed by combining an averaging scheme and a back-stepping approach. A proof of the stability of the closed loop system is provided. However, they are effective only around the equilibrium state since these controllers are based on the airships linearized model. The author of [110] studies the stability problem of nonlinear dynamical control systems. he considers a continuous-time dynamical systems whose nominal part is stable and whose perturbed part is norm-bounded by a positive function. Further, nonlinear dynamic inversion control is applied to the autonomous airship due to its ability to remain valid at nonstandard flight regimes [111]. In [87], a q-LPV approach is used to asymptotically stabilize an unconventional airship based on the non-linear dynamic model.

6.2.1 State Representation

In order to elaborate an efficient control strategies, it is necessary to develop the simplest possible mathematical model that adequately predicts the responses of the physical system to all inputs. The airship motion is usually represented by a set of kinematics (5.6.6) and dynamic equations (5.6.5) that describe its evolution in a six degrees of freedom (6−DOF) space:

$$\boldsymbol{M}_T\dot{\boldsymbol{\nu}}^a + \boldsymbol{Q}(\boldsymbol{\nu}^a) = \boldsymbol{\tau}_{cab} + \boldsymbol{\tau}_{pro} + \boldsymbol{\tau}_{wb} \tag{6.2.1}$$

$$\dot{\boldsymbol{\eta}}^a = \boldsymbol{J}_a(\boldsymbol{\eta}_2^a)\boldsymbol{\nu}^a \tag{6.2.2}$$

The two vectors $\boldsymbol{\nu}^a = [u, v, w, p, q, r]^T$ and $\boldsymbol{\eta}^a = [x_a, y_a, z_a, \phi_a, \theta_a, \psi_a]^T$ represent respectively the velocity and position vector of the airship. $\boldsymbol{M}_T$ is the inertia matrix including the aerodynamic virtual inertia (added mass) and the vector $\boldsymbol{Q}$ contains the nonlinear forces and moments due to centrifugal and Coriolis forces. $\boldsymbol{\tau}_{pro} = [\boldsymbol{f}_{pro}, \boldsymbol{m}_{pro}]^T$ is the propulsion wrench generated by the four rotors and $\boldsymbol{\tau}_{wb} = [\boldsymbol{f}_{wb}, \boldsymbol{m}_{wb}]^T$ is the gravitational and buoyancy wrench. $\boldsymbol{\tau}_{cab} = [\boldsymbol{f}_c, \boldsymbol{m}_c]^T$ is the effort caused by cable tension applied on the airship in each exit point A_i. $\boldsymbol{\tau}_{cab}$ is represented by the force vector $\boldsymbol{f}_c = [F_{c_1}, F_{c_2}, F_{c_3}]^T$ and moment vector $\boldsymbol{m}_c = [M_{c_1}, M_{c_2}, M_{c_3}]^T$. Let us note M_{ij} the terms of the inertia matrix $\boldsymbol{M}_T$. It should be mentioned that the mass matrix coupling terms M_{45} and M_{56} are null. Thus, the airship dynamic model can be written as follows after some mathematical analysis done by [87]:

$$
\begin{cases}
\dot{u} = \frac{1}{M_{11}} \sum_{j=1}^{4} \|\boldsymbol{f}_j\| c_{\gamma_j} c_{\beta_j} - \frac{(m_a g - B_u)}{M_{11}} s_{\theta_a} - \frac{M_{33}}{M_{11}} qw + \frac{M_{22}}{M_{11}} vr + \frac{1}{M_{11}} F_{c_1} \\
\\
\dot{v} = \frac{1}{M_{22}} \sum_{j=1}^{4} \|\boldsymbol{f}_j\| s_{\gamma_j} - \frac{(m_a g - B_u)}{M_{22}} s_{\phi_a} c_{\theta_a} + \frac{M_{33}}{M_{22}} pw - \frac{M_{11}}{M_{22}} ur + \frac{1}{M_{22}} F_{c_2} \\
\\
\dot{w} = -\frac{1}{M_{33}} \sum_{j=1}^{4} \|\boldsymbol{f}_j\| c_{\gamma_j} s_{\beta_j} - (m_a g - B_u) c_{\phi_a} c_{\theta_a} + \frac{M_{11}}{M_{33}} uq - \frac{M_{22}}{M_{33}} vp + \frac{1}{M_{33}} F_{c_3} \\
\\
\dot{p} = -\alpha_1 c \sum_{j=1}^{4} \|\boldsymbol{f}_j\| s_{\gamma_j} + \alpha_2 b_1 (\|\boldsymbol{f}_1\| c_{\gamma_1} s_{\beta_1} - \|\boldsymbol{f}_2\| c_{\gamma_2} s_{\beta_2}) \\
+\alpha_2 b_3 (\|\boldsymbol{f}_3\| c_{\gamma_3} s_{\beta_3} - \|\boldsymbol{f}_4\| c_{\gamma_4} s_{\beta_4}) + \alpha_3 a (\|\boldsymbol{f}_4\| s_{\gamma_4} + \|\boldsymbol{f}_3\| s_{\gamma_3} - \|\boldsymbol{f}_1\| s_{\gamma_1} - \|\boldsymbol{f}_2\| s_{\gamma_2}) \\
-\alpha_1 B_u z_B s_{\phi_a} c_{\theta_a} - \alpha_4 pq + \alpha_5 qr + \alpha_6 uv - \alpha_7 vw + \alpha_1 M_{c_1} - \alpha_3 M_{c_3} \\
\\
\dot{q} = \frac{1}{M_{55}} c \sum_{j=1}^{4} \|\boldsymbol{f}_j\| c_{\gamma_j} c_{\beta_j} + \frac{1}{M_{55}} a (\|\boldsymbol{f}_4\| c_{\gamma_4} s_{\beta_4} + \|\boldsymbol{f}_3\| c_{\gamma_3} s_{\beta_3} - \|\boldsymbol{f}_1\| c_{\gamma_1} s_{\beta_1} - \|\boldsymbol{f}_2\| c_{\gamma_2} s_{\beta_2}) \\
-\frac{B_u z_B}{M_{55}} s_{\theta_a} + \alpha_{10} p^2 + \alpha_{11} pr + \alpha_{10} r^2 - \alpha_{12} vw + \frac{1}{M_{55}} M_{c_2} \\
\\
\dot{r} = \alpha_3 c \sum_{j=1}^{4} \|\boldsymbol{f}_j\| s_{\gamma_j} + \alpha_6 b_1 (\|\boldsymbol{f}_1\| c_{\gamma_1} s_{\beta_1} - \|\boldsymbol{f}_2\| c_{\gamma_2} s_{\beta_2}) + \alpha_6 b_3 (\|\boldsymbol{f}_3\| c_{\gamma_3} s_{\beta_3} - \|\boldsymbol{f}_4\| c_{\gamma_4} s_{\beta_4}) \\
-\alpha_7 a (\|\boldsymbol{f}_4\| s_{\gamma_4} + \|\boldsymbol{f}_3\| s_{\gamma_3} - \|\boldsymbol{f}_1\| s_{\gamma_1} - \|\boldsymbol{f}_2\| s_{\gamma_2}) + \alpha_3 B_u z_B s_{\phi_a} c_{\theta_a} + \alpha_8 pq + \alpha_4 qr \\
-\alpha_{13} uv - \alpha_{14} vw - \alpha_3 M_{c_1} - \alpha_7 M_{c_3}
\end{cases}
\tag{6.2.3}
$$

where

$$\begin{cases} \alpha_1 = \frac{M_{66}}{M_{44}M_{66}-M_{46}^2} \\ \alpha_2 = \frac{M_{46}-M_{66}}{M_{44}M_{66}-M_{46}^2} \\ \alpha_3 = \frac{M_{46}}{M_{44}M_{66}-M_{46}^2} \\ \alpha_4 = \frac{M_{46}(M_{44}-M_{55}+M_{66})}{M_{44}M_{66}-M_{46}^2} \\ \alpha_5 = \frac{M_{55}M_{66}-M_{46}^2+M_{66}^2}{M_{44}M_{66}-M_{46}^2} \\ \alpha_6 = \frac{M_{66}(M_{a33}-M_{22})}{M_{44}M_{66}-M_{46}^2} \\ \alpha_7 = \frac{M_{46}(M_{a22}-M_{11})}{M_{44}M_{66}-M_{46}^2} \end{cases} \quad \begin{cases} \alpha_8 = \frac{M_{46}-M_{44}}{M_{44}M_{66}-M_{46}^2} \\ \alpha_9 = \frac{M_{44}}{M_{44}M_{66}-M_{46}^2} \\ \alpha_{10} = \frac{M_{44}}{M_{44}} \\ \alpha_{11} = \frac{M_{66}-M_{44}}{M_{55}} \\ \alpha_{12} = \frac{M_{11}-M_{33}}{M_{55}} \\ \alpha_{13} = \frac{M_{46}^2(M_{a22}-M_{11})}{M_{66}(M_{44}M_{66}-M_{46}^2)} \\ \alpha_{14} = \frac{M_{46}(M_{a33}-M_{22})}{M_{44}M_{66}-M_{46}^2} \end{cases}$$

As already mentioned, the $MC500$ airship has twelve actuators: the four propulsion forces $\boldsymbol{f}_j$, the four angles of inclination β_j and the four orientation angles γ_j. To stabilize the airship, we consider $\boldsymbol{u} = [u_1, u_2, u_3, u_4, u_5, u_6]^T$ as the control input vector expressed by a function $\boldsymbol{u} = f(\boldsymbol{f}_j, \beta_j, \gamma_j)$ where $\boldsymbol{f}_j$,β_j and γ_j are the actual input of each rotor. The function f transforms the real control input $\boldsymbol{f}_j$,β_j and γ_j into the virtual control input $\boldsymbol{u}$ form defined as:

$$\begin{cases} u_1 = \frac{1}{M_{11}} \sum_{j=1}^{4} f_j \\ u_2 = \frac{1}{M_{22}} \sum_{j=1}^{4} g_j \\ u_3 = -\frac{1}{M_{33}} \sum_{j=1}^{4} h_j \\ u_4 = -\alpha_1 c \sum_{j=1}^{4} g_j + \alpha_2 b_1 (h_1 - h_2) + \alpha_2 b_3 (h_3 - h_4) + \alpha_3 a (g_4 + g_3 - g_1 - g_2) \\ u_5 = \frac{1}{M_{55}} c \sum_{j=1}^{4} f_j + \frac{1}{M_{55}} a (h_4 + h_3 - h_1 - h_2) \\ u_6 = \alpha_3 c \sum_{j=1}^{4} g_j + \alpha_6 b_1 (h_1 - h_2) + \alpha_6 b_3 (h_3 - h_4) - \alpha_9 a (g_4 + g_3 - g_1 - g_2) \end{cases} \tag{6.2.4}$$

where $f_j = \|\boldsymbol{f}_j\| c_{\gamma_j} c_{\beta_j}$, $g_j = \|\boldsymbol{f}_j\| s_{\gamma_j}$ and $h_j = -\|\boldsymbol{f}_j\| c_{\gamma_j} s_{\beta_j}$. The explicit expression of the airship dynamic model can be written as follows:

$$\begin{cases} \dot{u} = u_1 - \frac{(m_a g - B_u)}{M_{11}} s_{\theta_a} - \frac{M_{33}}{M_{11}} qw + \frac{M_{22}}{M_{11}} vr + \frac{1}{M_{11}} F_{c_1} \\ \dot{v} = u_2 - \frac{(m_a g - B_u)}{M_{22}} s_{\phi_a} c_{\theta_a} + \frac{M_{33}}{M_{22}} pw - \frac{M_{11}}{M_{22}} ur + \frac{1}{M_{22}} F_{c_2} \\ \dot{w} = u_3 - (m_a g - B_u) c_{\phi_g} c_{\theta_a} + \frac{M_{11}}{M_{33}} uq - \frac{M_{22}}{M_{33}} vp + \frac{1}{M_{33}} F_{c_3} \\ \dot{p} = u_4 - \alpha_1 B_u z_B s_{\phi_a} c_{\theta_a} - \alpha_4 pq + \alpha_5 qr + \alpha_6 uv - \alpha_7 vw + \alpha_1 M_{c_1} - \alpha_3 M_{c_3} \\ \dot{q} = u_5 - \frac{B_u z_B}{M_{55}} s_{\theta_a} + \alpha_{10} p^2 + \alpha_{11} pr + \alpha_{10} r^2 - \alpha_{12} vw + \frac{1}{M_{55}} M_{c_2} \\ \dot{r} = u_6 + \alpha_3 B_u z_B s_{\phi_a} c_{\theta_a} + \alpha_8 pq + \alpha_4 qr - \alpha_{13} uv - \alpha_{14} vw - \alpha_3 M_{c_1} - \alpha_7 M_{c_3} \end{cases} \tag{6.2.5}$$

By denoting $\boldsymbol{\nu}^a = [u, v, w, p, q, r]^T$ as the airship velocity vector and $\boldsymbol{u} = [u_1, u_2, u_3, u_4, u_5, u_6]^T$ as the control input vector, we get the airship dynamic model expressed as follows in a compact form:

$$\dot{\boldsymbol{\nu}}^a = \boldsymbol{A}\boldsymbol{\nu}^a + \boldsymbol{u} + \boldsymbol{E}_d \tag{6.2.6}$$

Where

$$\boldsymbol{A} = \begin{pmatrix} 0 & \frac{M_{22}}{M_{11}} r & -\frac{M_{33}}{M_{11}} q & 0 & 0 & 0 \\ -\frac{M_{11}}{M_{22}} r & 0 & \frac{M_{33}}{M_{22}} p & 0 & 0 & 0 \\ \frac{M_{11}}{M_{33}} q & -\frac{M_{22}}{M_{33}} p & 0 & 0 & 0 & 0 \\ 0 & \alpha_6 u - \alpha_7 w & 0 & 0 & \alpha_4 p + \alpha_5 r & 0 \\ 0 & 0 & \alpha_{12} v & \alpha_{10} p + \alpha_{11} r & 0 & \alpha_{10} r \\ 0 & -\alpha_{13} u - \alpha_{14} w & 0 & 0 & \alpha_8 p + \alpha_4 r & 0 \end{pmatrix} \tag{6.2.7}$$

and

$$\boldsymbol{E}_d = \begin{pmatrix} \frac{1}{M_{11}}[F_{c_1} - (m_a g - B_u)s_{\theta_a}] \\ \frac{1}{M_{22}}[F_{c_2} - (m_a g - B_u)s_{\phi_a} c_{\theta_a}] \\ \frac{1}{M_{33}} F_{c_3} - (m_a g - B_u)c_{\phi_a} c_{\theta_a} \\ \alpha_1 M_{c_1} - \alpha_3 M_{c_3} - \alpha_1 B_u z_B s_{\phi_a} c_{\theta_a} \\ \frac{1}{M_{55}}[M_{c_2} - B_u z_B s_{\theta_a}] \\ -\alpha_3 M_{c_1} - \alpha_7 M_{c_3} + \alpha_3 B_u z_B s_{\phi_a} c_{\theta_a} \end{pmatrix} \tag{6.2.8}$$

We add the effort applied by cables on the airship in each exit point A_i to the gravitational and buoyancy effort. The above result is considered as a disturbance effort that is represented by the vector $\boldsymbol{E}_d$. Indeed, $\boldsymbol{\chi}^a = [u, v, w, p, q, r, x_a, y_a, z_a, \phi_a, \theta_a, \psi_a]^T$ represents the vector state and $\boldsymbol{u}$ is the control input vector. Finally, the dynamic (6.2.1) and kinematic (6.2.2) model of the airship can be expressed in state representation form used later for control synthesis:

$$\begin{cases} \dot{\boldsymbol{\nu}}^a = \boldsymbol{A}(\boldsymbol{\nu}^a)\boldsymbol{\nu}^a + \boldsymbol{u} + \boldsymbol{E}_d \\ \dot{\boldsymbol{\eta}}^a = \boldsymbol{J}_a(\boldsymbol{\eta}_2^a)\boldsymbol{\nu}^a \\ \boldsymbol{\chi}^a = \begin{pmatrix} \boldsymbol{\nu}^a \\ \boldsymbol{\eta}^a \end{pmatrix} \end{cases} \tag{6.2.9}$$

6.2.2 Stabilization Control

Our proposed idea consists of developing a stabilization control in such a way that stabilizes the hovering flight of an airship, while being robust against disturbance due to cable tension. The desired stabilization corresponds to a control system objective where both the velocity state $\boldsymbol{\nu}^a$ and the position state $\boldsymbol{\eta}^a$ are regulated to zero. The present section proposes a control scheme for airship stabilization using Sliding Mode Control (SMC). It is a class of nonlinear, variable structure method, presenting on the concept of changing the controller structure in order to obtain the desired response [112]. The main feature of SMC is that it can switch the control law very fast to drive the system states from any initial state onto a user-specified sliding surface, and to maintain the states on the surface for all subsequent time. Because of this feature, SMC is a powerful control technique yielding high robustness to model uncertainty and external disturbances [113]. A possible drawback is that the control signal tends to switch around the zero error region giving a high frequency input to the control

actuator, called chattering. SMC has been widely applied to the design of many practical control system, such as servo system, robot manipulators, and flight control systems, etc.

Motivated by the above studies, a SMC is proposed to deal with the positioning control problem of an airship in the presence of parametric uncertainty and external disturbance, since SMC not only provides a robust and accurate response, but also makes the system response insensitive to changes in the system parameters and platform disturbances. Before the controller is formulated, some reasonable assumptions have to be made : i) The cable tension, the buoyancy and the gravity, represented by the disturbance vector $\boldsymbol{E}_d$ are bounded ii) the state vector $\boldsymbol{\chi}^a = [\boldsymbol{\nu}^a, \boldsymbol{\eta}^a]^T$ is measurable. We choose the sliding surface to be:

$$\boldsymbol{s} = \boldsymbol{\nu}^a + \boldsymbol{\Lambda}\boldsymbol{\eta}^a \tag{6.2.10}$$

where $\boldsymbol{\Lambda} = diag(\lambda_1, \lambda_2, ..., \lambda_6)$ with $\lambda_i > 0 \quad i \in \{1, ..., 6\}$. The Lyapunov function is defined as follow:

$$V = \frac{1}{2}\boldsymbol{s}^T\boldsymbol{s} \tag{6.2.11}$$

The time derivative of the Lyapunov function is given by:

$$\dot{V} = \boldsymbol{s}^T\dot{\boldsymbol{s}} \tag{6.2.12}$$

$$\dot{V} = \boldsymbol{s}^T(\dot{\boldsymbol{\nu}}^a + \boldsymbol{\Lambda}\dot{\boldsymbol{\eta}}^a) \tag{6.2.13}$$

By substituting $\dot{\boldsymbol{\nu}}^a$ and $\dot{\boldsymbol{\eta}}^a$ from equations (6.2.9) in the previous equation (6.2.13) we get

$$\dot{V} = \boldsymbol{s}^T\left(\boldsymbol{A}\boldsymbol{\nu}^a + \boldsymbol{u} + \boldsymbol{E}_d + \boldsymbol{\Lambda}\boldsymbol{J}_a\boldsymbol{\nu}^a\right) \tag{6.2.14}$$

To ensure the payload asymptotic stability, we must choose a control law that satisfies the condition $\dot{V} \leqslant 0$. Hence, we select the control law as:

$$\boldsymbol{u} = -\left[(\boldsymbol{A} + \boldsymbol{\Lambda}\boldsymbol{J}_a)\boldsymbol{\nu}^a + \boldsymbol{K} \quad sgn(\boldsymbol{s})\right] \tag{6.2.15}$$

where $\boldsymbol{K}$ is a positive definite matrix defined as follows:

$$\boldsymbol{K} = \begin{pmatrix} k_1 & & 0 \\ & \ddots & \\ 0 & & k_n \end{pmatrix} \tag{6.2.16}$$

and $sgn(\boldsymbol{s})$ is a signum function defined as follows:

$$sgn(\boldsymbol{s}) = \begin{pmatrix} sgn(s_1) \\ : \\ sgn(s_n) \end{pmatrix} \tag{6.2.17}$$

in which

$$sgn(\boldsymbol{s}) = \begin{cases} +1 & if s_i > 0 \\ -1 & if s_i < 0 \end{cases} \tag{6.2.18}$$

As it is known $\boldsymbol{K}\boldsymbol{s}^T sgn(\boldsymbol{s}) = \sum_{i=1}^{n=6} k_i |s_i|$, so we obtain:

$$\dot{V} = \boldsymbol{s}^T [\boldsymbol{E}_d - \boldsymbol{K} \quad sgn(\boldsymbol{s})] \tag{6.2.19}$$

$$\dot{V} = \boldsymbol{s}^T \boldsymbol{E}_d - \sum_{i=1}^{n=6} k_i |s_i| \tag{6.2.20}$$

Let us note by E_i the component of the disturbance vector $\boldsymbol{E}_d$. Then it is sufficient to choose the terms of positive definite matrix $\boldsymbol{K}$ as follow:

$$k_i \geqslant |E_i| + \eta_i \tag{6.2.21}$$

where $\eta_i > 0$, therefore,

$$\dot{V} \leqslant - \sum_{i=1}^{n=6} \eta_i |s_i| \tag{6.2.22}$$

To avoid chattering, we replace the $sgn(\boldsymbol{s})$ function by the $sat(\boldsymbol{s})$ function given as :

$$sat(\boldsymbol{s}) = \begin{cases} sgn(s_i) & if \quad |s_i| > \delta \\ \frac{s_i}{\delta} & if \quad |s_i| \leqslant \delta \end{cases} \tag{6.2.23}$$

δ is a constant boundary layer thickness. Hence the control law now looks like:

$$\boldsymbol{u} = - [(\boldsymbol{A} + \boldsymbol{\Lambda}\boldsymbol{J}_a)\boldsymbol{\nu}^a + \boldsymbol{K} \quad sat(\boldsymbol{s})] \tag{6.2.24}$$

The proposed controller (6.2.15) consists of three components. Term $-\boldsymbol{K} \quad sat(\boldsymbol{s})$ guarantees the system reaches and remains on the sliding surface and a compensation term $-(\boldsymbol{A} + \boldsymbol{\Lambda}\boldsymbol{J}_a)\boldsymbol{\nu}^a$. Referring to LaSalle's Invariance Principle the system is stable. Thus, the motion converges to a maximum invariant set which satisfies $\dot{V} = 0$. This implies that $\boldsymbol{s} = 0$. the following equation is derived:

$$\lim_{t \longrightarrow \infty} \boldsymbol{s} = \lim_{t \longrightarrow \infty} (\boldsymbol{\nu}^a + \boldsymbol{\Lambda}\boldsymbol{\eta}^a) = 0 \tag{6.2.25}$$

By substituting $\boldsymbol{\nu}^a = \boldsymbol{J}_a^{-1}\dot{\boldsymbol{\eta}}^a$ in the previous equation:

$$\lim_{t \longrightarrow \infty} \boldsymbol{J}_a^{-1}\dot{\boldsymbol{\eta}}^a + \boldsymbol{\Lambda}\boldsymbol{\eta}^a = 0 \tag{6.2.26}$$

This leads to:

$$\dot{\boldsymbol{\eta}}^a = -\boldsymbol{J}_a \boldsymbol{\Lambda} \boldsymbol{\eta}^a \tag{6.2.27}$$

Hence, it is clear that the position can asymptotically converge to zero if we select $\boldsymbol{\Lambda}$ such that the matrix product $-\boldsymbol{J}_a\boldsymbol{\Lambda}$ satisfies the Hurwitz condition. Therefore, SMC provides an effective approach for the control problem of systems with nonlinearities and bounded external disturbances. As already mentioned, the airship $MC500$ has twelve actuators : the four propulsion forces $\boldsymbol{f}_j$, the four angles of inclination β_j and the four orientation angles γ_j. To control the airship, we have to compute the values of real actuators ($\boldsymbol{f}_j, \beta_j$ and γ_j) by a control allocation algorithm.

6.2.3 Simulation Results

The first proposed scenario consists of state stabilization problem simulated on the unconventional airship $MC500$. We test the proposed framework in numerical simulations that are developed using Matlab/Simulink. The airship parameters are defined in Table 6.1. The inertia mass and moment matrix around the principal axes of inertia are listed respectively in Tables 6.2 and 6.3. The chosen airship equilibrium values are $[0;0;0;0;0;0]^T$ for the six attitude/position vector and $[0;0;0;0;0;0]^T$ for speed.

TABLE 6.1: Characteristic of the airship $MC500$

Parameter		Value
Airship mass	$m_a\ (kg)$	500
Airship volume	$V(m^3)$	500
Density of the air	$\rho_{air}\ (kgm^{-3})$	1.3
Position of volume center	$(0,0,-z_B)\ (m)$	$(0,0,-0.5)$
Position of rotor P_1	$(a,b_1,c)\ (m)$	$(2.5,5.4,2)$
Position of rotor P_2	$(a,-b_1,c)\ (m)$	$(2.5,-5.4,2)$
Position of rotor P_3	$(-a,b_3,c)\ (m)$	$(-2.5,6.5,2)$
Position of rotor P_4	$(-a,-b_3,c)\ (m)$	$(-2.5,-6.5,2)$

TABLE 6.2: Inertia mass matrix

Inertia mass matrix	M_{11}	M_{22}	M_{33}
Value (kg)	607	655	715

TABLE 6.3: Inertia moment matrix

Inertia moment matrix	M_{44}	M_{55}	M_{66}	M_{46}
Value (kgm^2)	11023	11231	19341	203

The simulation is initialized with some small deviations from the equilibrium. The initial position along X-axis is $3m$ instead of 0. The airship attitude is increased by 11 degree from the equilibrium for each Euler angle, whereas the airship initial velocity states are null. The controller is designed to hover the airship back to the steady state from the initial state. As can be seen in Figure 6.1 and Figure 6.2, it is clear that thanks to the sliding mode controller, the airship still be controlled at a fixed equilibrium point.

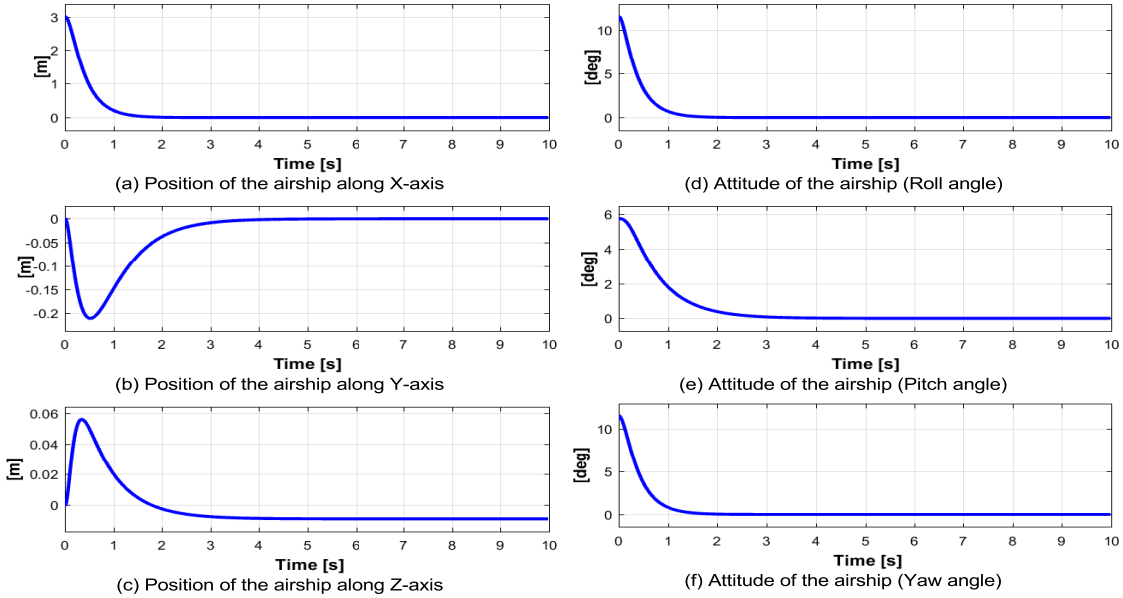

FIGURE 6.1: Convergence of position and orientation of the airship to the equilibrium point

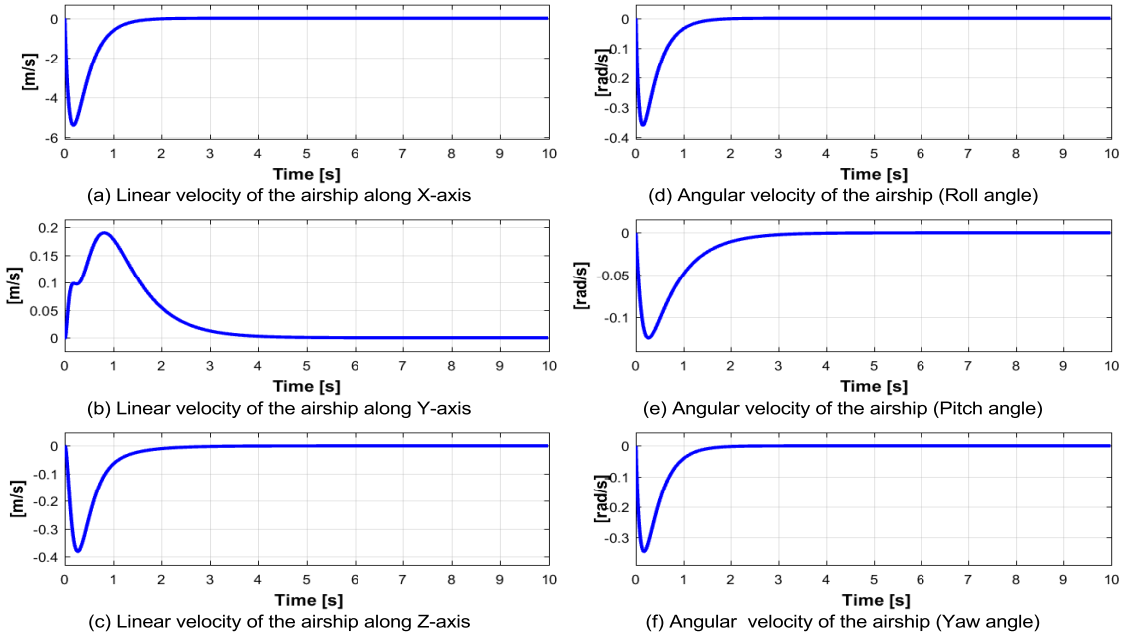

FIGURE 6.2: Convergence of linear and angular velocity of the airship

In order to validate the robustness of the proposed controller, it is interesting to stabilize the hovering flight of the airship in the presence of disturbance. In the case of a heavy hift airship, the forces applied by cables on the airship are considered as disturbance. During loading and unloading phase, the airship stabilization behavior can be affected by the eight cables tensions applied in each exit points A_i. These suspension points have as coordinates $\boldsymbol{a}_i$ listed in the Table 6.4. Note that each pair of winches is installed at each corner of a rectangle. To handle the suspended platform with a total mass of $m = 100\ kg$ from origin to a desired position along the vertical axis, we need only to activate four winches. As shown in Figure 6.3, the four cables tensions remain fairly stable about 50 N, whereas the others ones rise to 400 N.

TABLE 6.4: Cable suspension points

	x_{a_i}	y_{a_i}	z_{a_i}		x_{a_i}	y_{a_i}	z_{a_i}
a_1	-2.5	-1.5	0	a_5	2.5	1.5	0
a_2	-2.5	-1.5	0	a_6	2.5	1.5	0
a_3	2.5	-1.5	0	a_7	-2.5	1.5	0
a_4	2.5	-1.5	0	a_8	-2.5	1.5	0

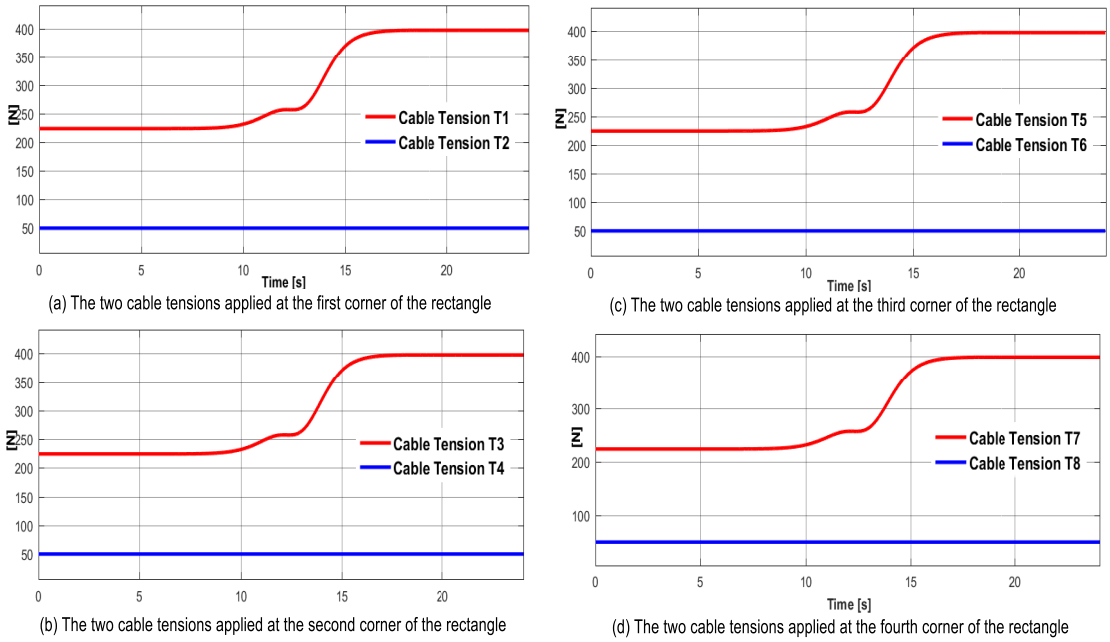

FIGURE 6.3: Cable tensions applied on the airship

As in the previous simulations scenario, the developed sliding mode controller has successfully stabilized the airship while being robust against disturbance caused by external cable tensions (shown in Figure 6.3). We have to state that the control parameters in our algorithms are all the same in each case(i.e without and with disturbance). Sliding parameters are chosen as $\boldsymbol{\Lambda} = diag(9,4,10,11,7,9)$, $\boldsymbol{K} = diag(4,2,2,3,1.5,3)$ and $\delta = 1$. The resulting simulation is illustrated in Figure 6.4 and Figure 6.5. In those figures, the dashed blue line describes the convergence of airship state vector taking into account the effect of cable tensions, while the red line denotes the results given from the first simulation without disturbance. We should mentioned that cable tensions do not really affect the airship stabilization behavior.

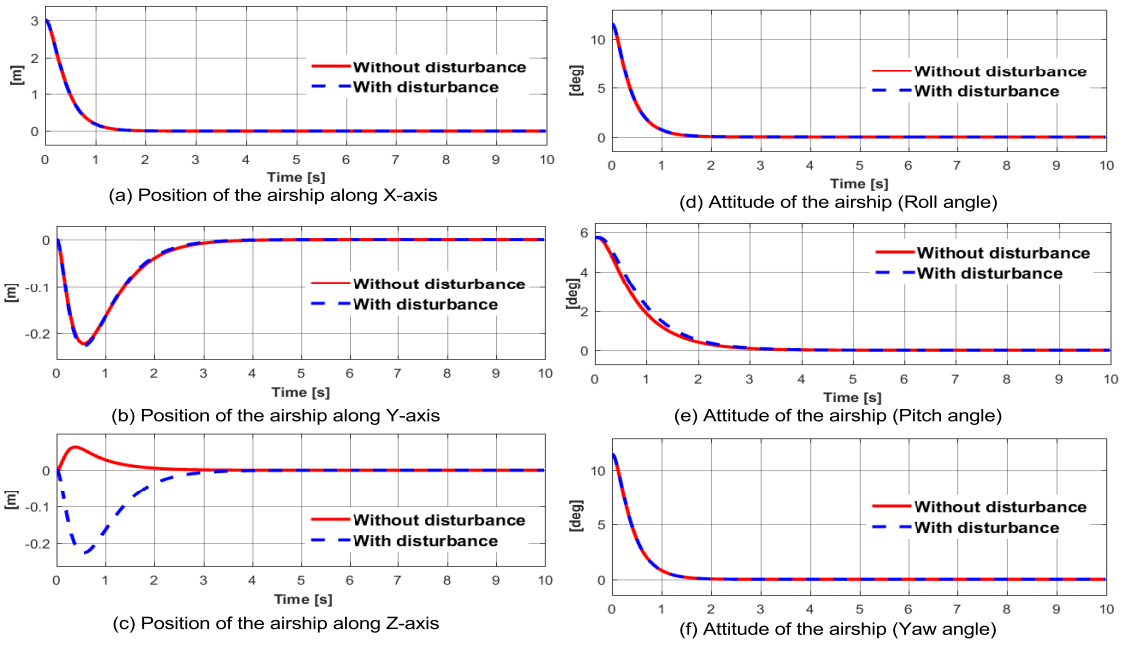

FIGURE 6.4: Position and orientation of the airship with and without disturbance

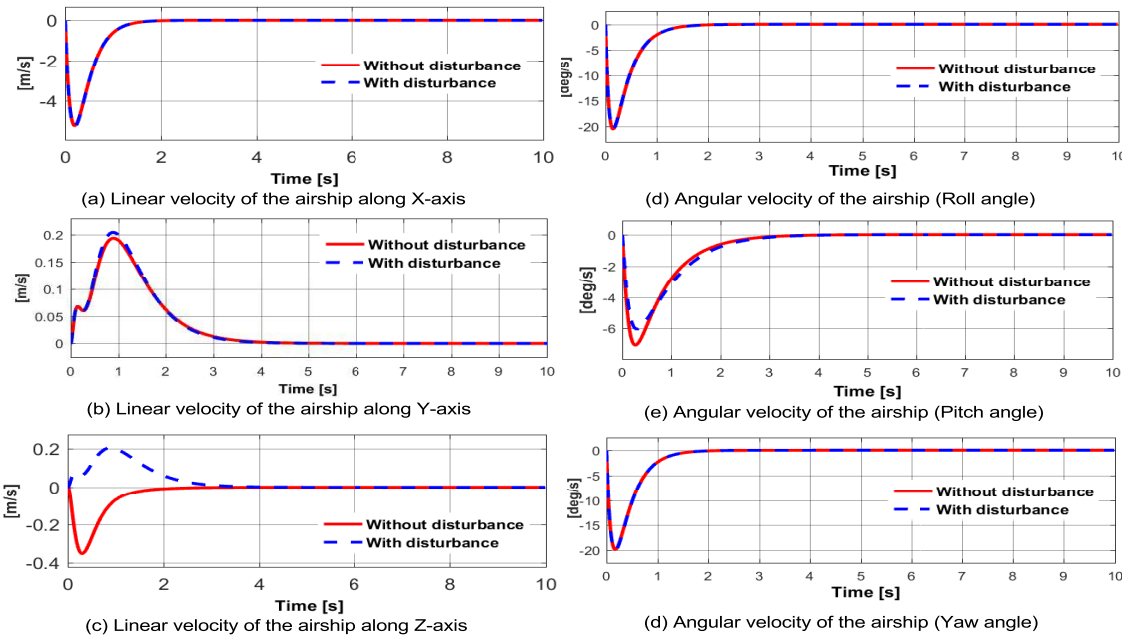

FIGURE 6.5: Linear and angular velocity of the airship with and without disturbance

6.3 Tracking Controller for Loading and Unloading

During loading and unloading process, the transferred cargo can oscillate due to airship maneuvers. This pendulum-like behavior brings a lot of troubles to the handling operation

such as instability and hence must be avoided. In this field, a two time scale control method is proposed by Agrawal in order to control the helicopter and the cable robot independently [80]. In a time separation control scheme, the helicopter state variables are partitioned into two carefully chosen sets, translation constitutes slow dynamics while orientaion with fast dynamics. This scheme is realized by implementing a hierarchical structure of controllers. The slower high level controller runs at a sampling time period Δ_{Th}, an order of magnitude slower than the sampling time of the lower level faster controller Δ_{Tl}. Therefore at the slow time scale, the fast states have already reached their steady state values. Then, a robust controller is designed for the cable robot where the disturbance due to the helicopter motion is modeled as additive terms in the dynamics of the cable robot. By operating the cable system in the slow time scale, the disturbance term can be simplified so that its bounds are determined in a state independent form. Further, the authors of [114] use a new Lyapunov function to obtain a global uniform asymptotic stability of some perturbed systems.

For heavy lift airship, it is interesting to note that the six-dimensional motions of the airship have a direct impact on handling position of the moving suspended platform. In fact, the airship motion affects the direction of the cables tensions by moving the cable exit point A_i, thus making the suspended platform unstable. For loading and unloading phase, we assume that the ultimate control objective is to move the suspended platform along a prescribed desired trajectory. In this chapter, we do not concern ourselves with the actual trajectory planning problem. Computed torque is a special application of feedback linearizion of nonlinear systems, which has gained popularity in modern systems theory. In order to integrate a robust control that can ensure the loading and unloading of the heavy lift airship, we chose to apply the proportional-plus derivative (PD) computed-torque controller. This technique allows us to conveniently derive very effective robot controllers.

6.3.1 PD Computed-Torque Control

It is important to realize that computed-torque depends on the inversion of the robot dynamics. Because the technique is model-based, the following motion equation of the suspended platform (5.6.23) is needed:

$$\boldsymbol{M}_P(\boldsymbol{\chi})\overset{\circ\circ}{\boldsymbol{\chi}} + \boldsymbol{C}_P(\boldsymbol{\chi},\mathring{\boldsymbol{\chi}})\mathring{\boldsymbol{\chi}} + \boldsymbol{G}_P(\boldsymbol{\chi}) + \boldsymbol{D}_P(\boldsymbol{\chi},\mathring{\boldsymbol{\chi}},\boldsymbol{\nu}^a,\dot{\boldsymbol{\nu}}^a) = \boldsymbol{W}_P\boldsymbol{T} \tag{6.3.1}$$

Remember $\boldsymbol{M}_P$ is the inertia matrix, $\boldsymbol{C}_P$ is the matrix of Coriolis and centrifugal terms, $\boldsymbol{D}_P$ is the bounded disturbance vector due to airship motion and $\boldsymbol{W}_P$ is the force transmission matrix. $\boldsymbol{\chi}$ is the state vector and $\boldsymbol{T} = [t_1, t_2, ..., t_{n_c}]^T$ that groups the n_c cable tensions represents the control vector input. In order to integrate a robust control that can ensure the loading and unloading of the heavy lift airship along a prescribed desired trajectory $\boldsymbol{\chi}_d$, we chose to apply the proportional-plus derivative (PD) Computed-torque control, well known in the field of parallel robots. This technique presumes that the equations of motion of the system as well as all the relevant geometric and inertial parameters are known. Defining the

auxiliary control input function by:

$$\boldsymbol{u}_t = \overset{\circ\circ}{\boldsymbol{\chi}}_d + \boldsymbol{M}_P^{-1}\left(\boldsymbol{C}_P\overset{\circ}{\boldsymbol{\chi}} + \boldsymbol{G}_P - \boldsymbol{W}_P\boldsymbol{T}\right) \tag{6.3.2}$$

The feedback linearizing transformation (6.3.2) may be inverted to yield:

$$\boldsymbol{T} = \boldsymbol{W}_P^{+}\left(\boldsymbol{M}_P(\overset{\circ\circ}{\boldsymbol{\chi}}_d - \boldsymbol{u}_t) + \boldsymbol{C}_P\overset{\circ}{\boldsymbol{\chi}} + \boldsymbol{G}_P\right) \tag{6.3.3}$$

To ensure trajectory tracking in operational space, we define respectively a tracking error and its derivative by $\boldsymbol{e} = \boldsymbol{\chi}_d - \boldsymbol{\chi}$ and $\overset{\circ}{\boldsymbol{e}} = \overset{\circ}{\boldsymbol{\chi}}_d - \overset{\circ}{\boldsymbol{\chi}}$. We select the auxiliary control signal $\boldsymbol{u}_t$ as a PD feedback:

$$\boldsymbol{u}_t = -\boldsymbol{K}_P\boldsymbol{e} - \boldsymbol{K}_D\overset{\circ}{\boldsymbol{e}} \tag{6.3.4}$$

where the two positive define matrix $\boldsymbol{K}_P$ and $\boldsymbol{K}_D$ denote the gain of a PD feedback. The control vector input $\boldsymbol{T} = [t_1, t_2, ..., t_{n_c}]^T$ that groups the n_c tension cables becomes:

$$\boldsymbol{T} = \boldsymbol{\mathcal{W}}_P^{+}\left(\boldsymbol{M}_P(\overset{\circ\circ}{\boldsymbol{\chi}}_d + \boldsymbol{K}_P\boldsymbol{e} + \boldsymbol{K}_D\overset{\circ}{\boldsymbol{e}}) + \boldsymbol{C}_P\overset{\circ}{\boldsymbol{\chi}} + \boldsymbol{G}_P\right) \tag{6.3.5}$$

6.3.2 Stability Analysis

Referring to the control law given by (6.3.3) and the dynamic model given by (6.3.1), the closed loop system will then be:

$$\boldsymbol{M}_P\overset{\circ\circ}{\boldsymbol{\chi}} + \boldsymbol{C}_P\overset{\circ}{\boldsymbol{\chi}} + \boldsymbol{G}_P + \boldsymbol{D}_P = \boldsymbol{M}_P(\overset{\circ\circ}{\boldsymbol{\chi}}_d - \boldsymbol{u}_t) + \boldsymbol{C}_P\overset{\circ}{\boldsymbol{\chi}} + \boldsymbol{G}_P \tag{6.3.6}$$

Thus,

$$\overset{\circ\circ}{\boldsymbol{e}} - \boldsymbol{u}_t = \boldsymbol{M}_P^{-1}\boldsymbol{D}_P \tag{6.3.7}$$

The disturbance function is defined by:

$$\boldsymbol{w} = \boldsymbol{M}_P^{-1}\boldsymbol{D}_P \tag{6.3.8}$$

By Substituting the two equations (6.3.4) and (6.3.8) into (6.3.7), the tracking error dynamics can be written as follows:

$$\overset{\circ\circ}{\boldsymbol{e}} + \boldsymbol{K}_D\overset{\circ}{\boldsymbol{e}} + \boldsymbol{K}_P\boldsymbol{e} = \boldsymbol{w} \tag{6.3.9}$$

The two diagonal matrices $\boldsymbol{K}_P$ and $\boldsymbol{K}_D$ are chosen to be positive definite. Thus, the error system is asymptotically stable as long as the disturbance $\boldsymbol{w}$ tends to zero. By referring to the disturbance vector expression $\boldsymbol{\mathcal{D}}_P = [\boldsymbol{D}_{\boldsymbol{\nu}_1^a}, \boldsymbol{D}_{\boldsymbol{\nu}_2^a}]$, we notice that $\boldsymbol{w}$ depends on airship acceleration $[\dot{\boldsymbol{\nu}}_1^a, \dot{\boldsymbol{\nu}}_2^a]^T$ and airship velocity $[\boldsymbol{\nu}_1^a, \boldsymbol{\nu}_2^a]^T$. Thus, our proposed idea is to design a controller that steers the airship to remain at a fixed point in such a way that the acceleration

and velocity of the airship tends to zero. The above results lead to the characterization of the asymptotic stability of the tracking error $\boldsymbol{e}$ since $\boldsymbol{w}$ is null.

6.3.3 Simulation Results

One hazardous task in an airship mission is the loading and unloading of the heavy load by means of motorized winches while the airship hovers above the ground. Simulation experiments are conducted on a reduced scale prototype of the suspended mobile CDPM. We use $n_c = 8$ cables to manipulate a suspended platform in the full $n = 6$ dimensional task space, thus resulting in two redundant cables that can be used to better distribute the tensions. The suspended platform is a cube with a total mass of $m = 100\ kg$. Its inertia moment matrix is $\boldsymbol{I}_p = diag(78, 78, 27)$ expressed in the platform-body fixed frame $\mathcal{R}_P$. The airship and platform cable attachment points are given in Table 6.5, where each pair of winches is installed at each corner of the rectangle and cube.

TABLE 6.5: The airship and platform cable attachment points

	x_{a_i}	y_{a_i}	z_{a_i}		x_{b_i}	y_{b_i}	z_{b_i}
a_1	-2.5	-1.5	0	b_1	0.2	-0.2	0
a_2	-2.5	-1.5	0	b_2	-0.2	0.2	0.4
a_3	2.5	-1.5	0	b_3	-0.2	-0.2	0
a_4	2.5	-1.5	0	b_4	0.2	0.2	0.4
a_5	2.5	1.5	0	b_5	-0.2	0.2	0
a_6	2.5	1.5	0	b_6	0.2	-0.2	0.4
a_7	-2.5	1.5	0	b_7	0.2	0.2	0
a_8	-2.5	1.5	0	b_8	-0.2	-0.2	0.4

To show the effectiveness of the proposed control algorithm, we suppose that the load is at the origin and has to track the following reference trajectory along the vertical axis to reach a desired position $(0, 0, h_d)$ at a specific time t_f see Figure 6.6. It is generated by a 5th-order polynomial interpolation given by the following expression:

$$z_d(t) = \begin{cases} h_d \frac{t^5}{t^5 + (t_f - t)^5}, & \text{if} \quad 0 \leq t \leq t_f \\ h_d, & \text{if} \quad t > t_f \end{cases} \tag{6.3.10}$$

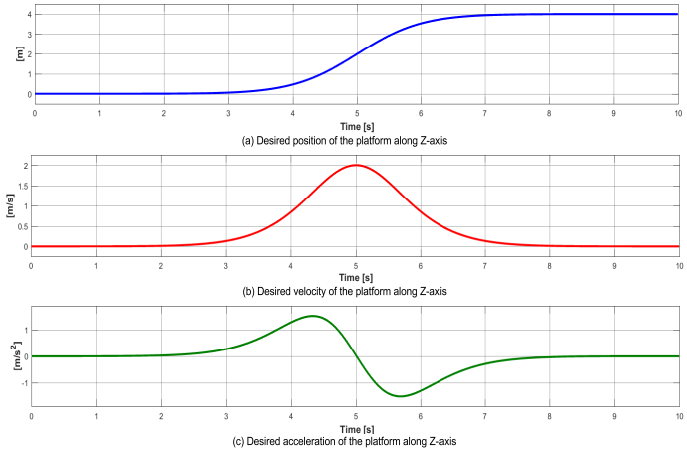

FIGURE 6.6: Desired trajectory of the suspended platform

It is interesting to note that the airship motion, even though it does not visibly affect payload, it affects the direction of the cables tensions, thus making the suspended platform unstable. Due to the inertial coupling between the two subsystem (i.e airship and CDPM), the airship acceleration for stabilization, shown in Figure 6.7, can destabilize the suspended platform during the loading and unloading process.

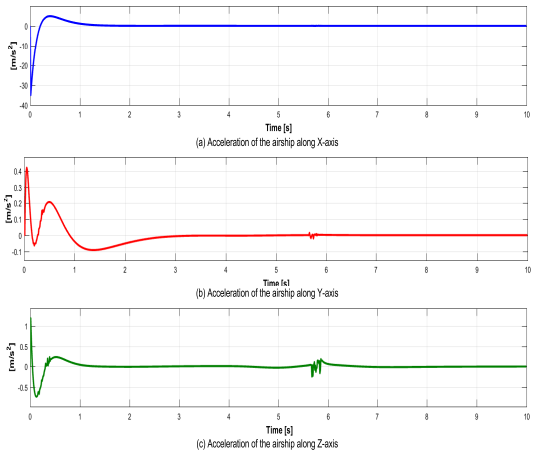

FIGURE 6.7: Acceleration of the airship while hover stabilization

we see that our control algorithm for cable robot is able to achieve good tracking performance even with disturbance due to the airship motion. For the fast convergence, the gain matrix are selected as $\boldsymbol{K}_P = diag(3,3,3,3,3,3)$ and $\boldsymbol{K}_D = diag(1,1,1,1,1,1)$. As it is shown in Figure 6.8, position and orientation outputs of the suspended CDPM platform track the desired values very well.

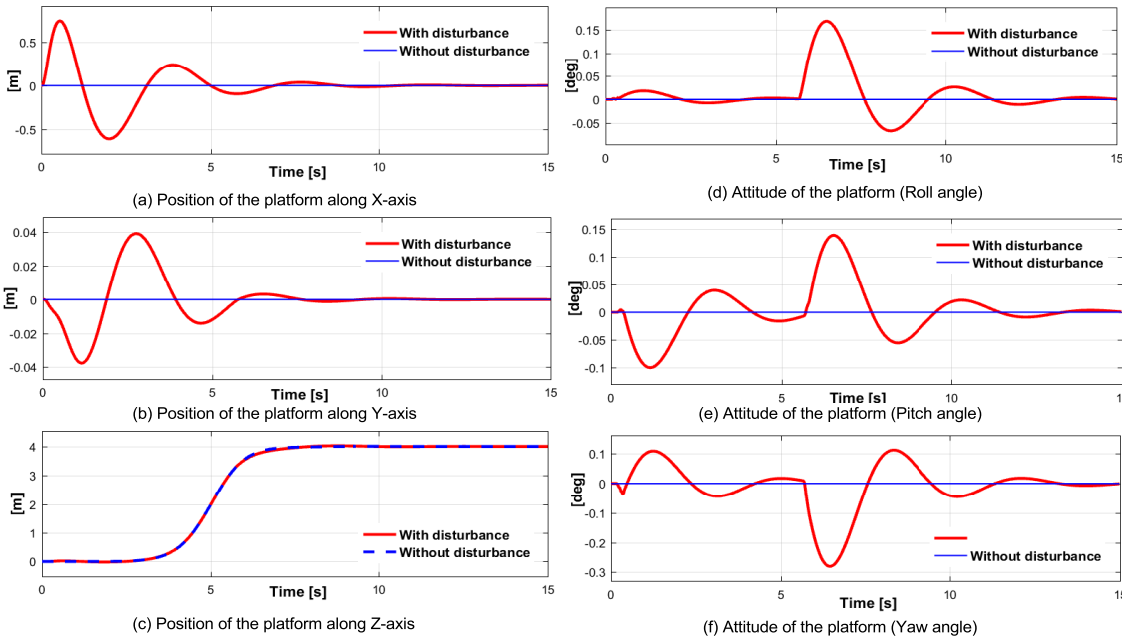

FIGURE 6.8: Position and orientation of the platform with PD computed torque controller

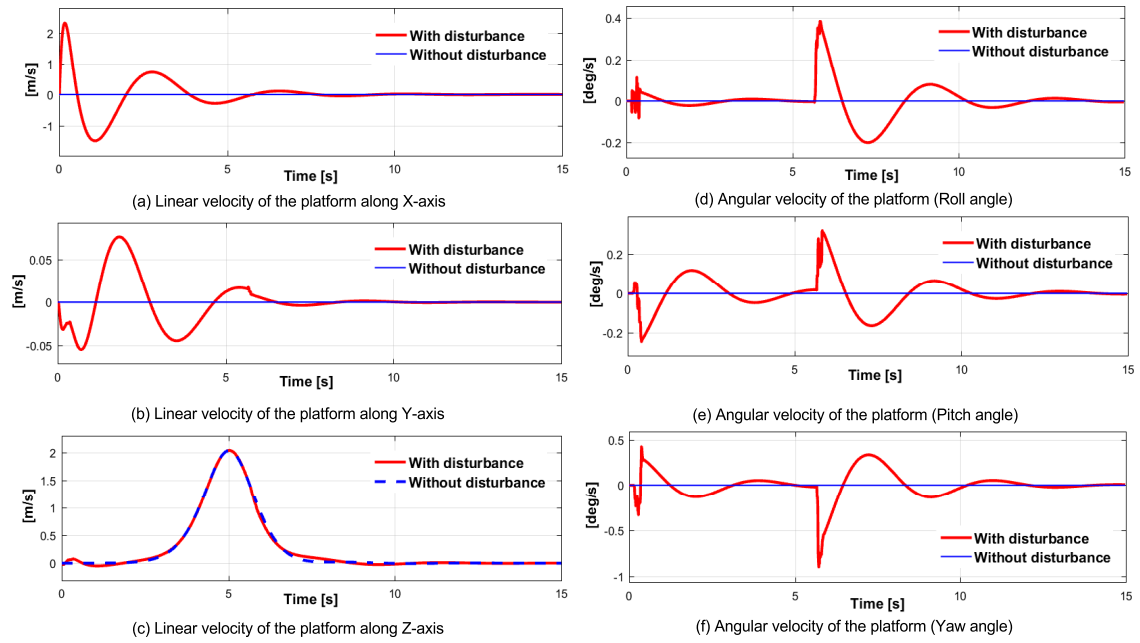

FIGURE 6.9: Linear and angular velocity of the platform with PD computed torque controller

In this simulation we highlight the capability of our controller not only to manipulate the suspended platform in order to track a prescribed desired trajectory but also to keep cables in tension for the whole manoeuvre that ensure safe loading and unloading process. As it is shown in Figure 6.10, the algorithm developed for the tension distributions gives strictly positive cable tensions.

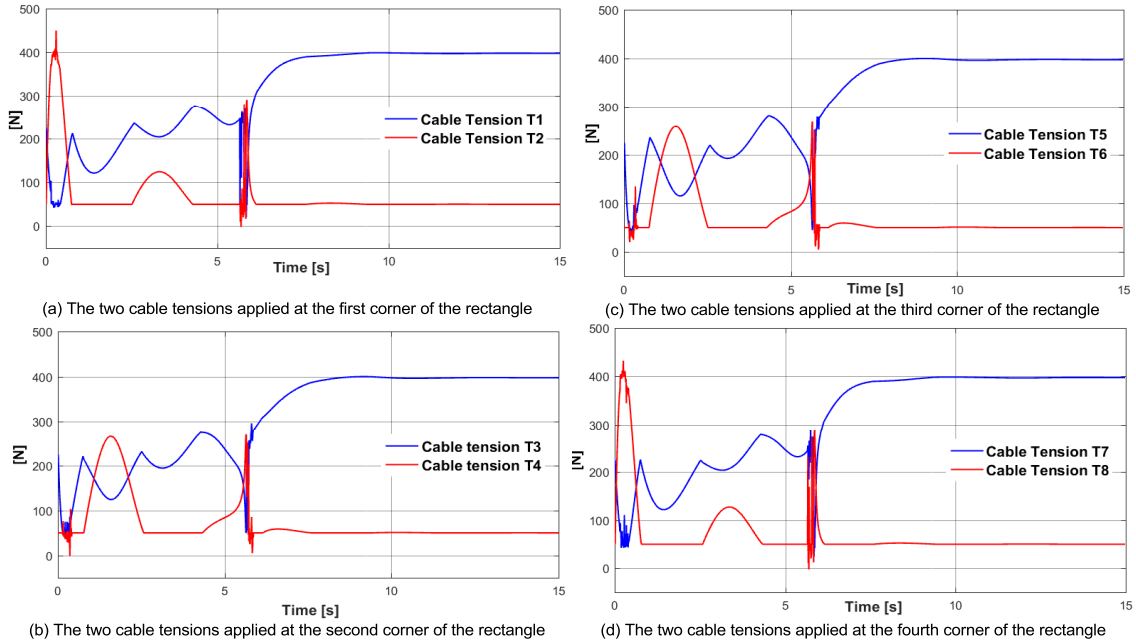

(a) The two cable tensions applied at the first corner of the rectangle

(c) The two cable tensions applied at the third corner of the rectangle

(b) The two cable tensions applied at the second corner of the rectangle

(d) The two cable tensions applied at the fourth corner of the rectangle

FIGURE 6.10: Cable tensions distribution for handling payload along the Z-axis

6.4 Conclusion

The heavy lift airship consists of two subsystems (i.e. airship and CDPM) which cooperate each other for load and unload cargo. In order to control the airship and the CDPM independently, a decentralized control architecture is proposed. The scenario studied corresponds to the critical case where the suspended platform may be subjected to external disturbances due to airship maneuvers during loading and unloading phase. This motion can generate the payload swing which can be detrimental to the safety of the assembly. For this purpose a sliding mode control is developed to remain the airship at a fixed point while a PD computed-torque control. This controller is applied to the eight motorized winches used to adjust cables length in order to track a prescribed desired trajectory. Such a system would eliminate load oscillation and facilitate point-to-point transport without the airship touching the ground and almost independently of local infrastructure.

Chapter 7

General Conclusion

This research has performed the design, modeling and control of a heavy lift airship during loading and unloading phase. This system makes use of a Cable Driven Parallel Manipulator (CDPM), allowing the airship to load and unload cargo without touching the ground. The proposed flying crane has the potential to transport heavy loads in a precautionary way. With unlimited access to isolated locations around the globe, heavy lift airship presents an eco-friendly alternative to existing modes of transportation. One of the most significant challenges facing heavy lift airship is to enable safe cargo exchange process.

To develop the mathematical models of the heavy lift airship, we have to make some assumptions. In the first part, we assume that there is no inertial coupling between the airship and CDPM. Hence, our research concerns only the CDPM tacking into account the base mobility in first time and then the cable characteristics. Contrary to the first assumption, the inertial coupling between the two above subsystems (airship and CDPM) is considered in the second part. In this context, the modeling of such a multi-body system composed of the airship and the CDPM is more complex than that of the conventional airship. The elaborated mathematical models have been used to design the control systems of heavy lift airship.

The main contributions of this thesis are revisited as follows :

- **Mobile Cable Driven Parallel Manipulator**

  Unlike conventional CDPM, a mobile CDPM consists of a suspended platform connected to winches mounted on a mobile base by means of n_c non-elastic massless cables acting in parallel. First of all, the kinematic and dynamic models of a mobile CDPM are introduced in details. For the kinematic modeling, the suspended platform twist depends on the variation of cable length and the motion of the base. Latter, we describe the dynamic equations showing explicitly the interaction between suspended platform and the movable base. In fact, the unknown disturbance due to base motion can be modeled as additive terms in the dynamics of the suspended platform. Based on the above kinematic and dynamic models, a sliding mode controller is proposed for stable tracking control of mobile CDPM. Such a system would not only manipulate the suspended platform to track a prescribed desired trajectory but also compensate the n-dimensional motions of the base. This controller is applied to the eight motorized

winches used to adjust cables length in order to track a prescribed desired trajectory. The control design should integrate an optimal tension distribution since cables must remain in tension. Thus, the simulation results show that the proposed controller provides a non-negative and continuous tension distribution along the whole trajectory.

- **Cable Driven Parallel Manipulator with Non-negligible Cable Mass and Elasticity**

  Based on the static and dynamic cable models, the static and dynamic models of CDPM considering the effect of cable sag are introduced. The sagging cable model considers the effect of cable mass and elasticity. This more realistic cable behavior has lead to analyze the static positioning accuracy of CDPM, especially for large workspace application. To achieve this purpose, the inverse kinematic model is presented through both the cable catenary equations and the platform static equilibrium equations. Further, a dynamic structure approach for large CDPM is developed. Through this dynamic model, we can evaluate the influence of cable mass towards the dynamic behavior of CDPM.

- **Heavy Lift Airship**

  In the second part, the heavy lift airship is considered as a multi-body systems in which multiple rigid bodies are joined together. To set up the model, we consider that the airship and the suspended platform are independent. Specifically, we decompose our system into two isolated subsystems (i.e the airship and the CDPM). By applying Kirchhoff equations, we obtain the motion equations. We assume that the heavy-lift airship is a weakly coupled subsystems. Based on this assumption, a decentralized controller is proposed to control the airship and the CDPM independently. Firstly, a sliding mode controller is developed to remain the airship at a fixed point in the presence of external disturbances. In this context, the proposed controller should stabilize the hovering flight of the airship, while being robust against disturbance due to platform motion during loading and unloading process. Secondly, the transferred cargo has to follow a preplanned desired trajectory and keep moving forward even if there is disturbances caused by airship maneuvers while hovering over the ground. For this purpose, a PD computed-torque control is applied to the cable driven parallel robot in order to enable safe cargo handing. The position and orientation error of the suspended platform is asymptotically stable as long as the disturbance due the airship motion tends to zero.

Based on the above conclusions, perspectives for future works can be made as follows :

- All algorithms, introduced in this work, have been validated in simulations. Therefore, an experimental validation should be carried out to confirm simulation results.
- The proposed dynamic model of heavy lift airship takes into consideration only non-elastic and massless cables, which is restrictive and does not depict the reality. It will be interesting to consider both cable mass and elasticity.

- In this work, all state variables are assumed to be measurable, which could not be the case in real systems. Then, it becomes necessary to develop an state observer to overcome such problem.

Appendix A

Orientation of Rigid Bodies

When analyzing the motion of an aerial vehicles in 6-DOF, it is convenient to define two coordinate frames. The first one is fixed, known as earth-fixed frame and denoted as $\mathcal{R}_0(O, X_0, Y_0, Z_0)$. This axis system is regarded as an inertial reference frame in which Newton's laws of motion are valid. The second frame, $\mathcal{R}_m(O', X_m, Y_m, Z_m)$ is attached to the aerial vehicle and constrained to move with it. The moving coordinate frame $\mathcal{R}_m$ is called the body-fixed reference frame.

A.1 Rotation Matrix

The transformation from the inertial reference frame $\mathcal{R}_0(O, X_0, Y_0, Z_0)$ to the body-fixed reference frame. $\mathcal{R}_m(O', X_m, Y_m, Z_m)$ is achieved by the following sequence of rotations starting from the Earth fixed inertial frame:

1. The coordinate system X_0, Y_0, Z_0 is rotated a yaw angle ψ about the Z_0 axis. This yields the coordinate system X', Y', Z_0

$$\begin{pmatrix} x \\ y \\ z \end{pmatrix} = \underbrace{\begin{pmatrix} c_\psi & -s_\psi & 0 \\ s_\psi & c_\psi & 0 \\ 0 & 0 & 1 \end{pmatrix}}_{R_{z,\psi}} \begin{pmatrix} x' \\ y' \\ z \end{pmatrix} \tag{A.1.1}$$

2. Then coordinate system X', Y', Z_0 is rotated a pitch angle θ about the Y' axis. This yields the coordinate system X_m, Y', Z'.

$$\begin{pmatrix} x' \\ y' \\ z \end{pmatrix} = \underbrace{\begin{pmatrix} c_\theta & 0 & s_\theta \\ 0 & 1 & 0 \\ -s_\theta & 0 & c_\theta \end{pmatrix}}_{R_{y,\theta}} \begin{pmatrix} x_m \\ y' \\ z' \end{pmatrix} \tag{A.1.2}$$

3. Finally Then coordinate system X_m, Y', Z' is rotated a roll angle ϕ about the X_m axis. This yields the coordinate system X_m, Y_m, Z_m.

$$\begin{pmatrix} x_m \\ y' \\ z' \end{pmatrix} = \underbrace{\begin{pmatrix} 1 & 0 & 0 \\ 0 & c_\phi & -s_\phi \\ 0 & s_\phi & c_\phi \end{pmatrix}}_{R_{x,\phi}} \begin{pmatrix} x_m \\ y_m \\ z_m \end{pmatrix} \tag{A.1.3}$$

Where the roll ϕ, pitch θ and yaw ψ angles are commonly referred to as Euler angles. The rotation sequence is written as

$$\mathcal{R}_0^m = R_{z,\psi} R_{y,\theta} R_{x,\phi} \tag{A.1.4}$$

Hence, the complete transformation from the mobile frame $\mathcal{R}_m$ to the inertial reference frame $\mathcal{R}_0$ is given by the rotation matrix $\mathcal{R}_m^0$, expressed as function of the Euler angles (ϕ,θ,ψ) and defined as follows :

$$\mathcal{R}_m^0 = \begin{pmatrix} c_\psi c_\theta & -s_\psi c_\phi + c_\psi s_\theta s_\phi & s_\psi s_\phi + c_\psi c_\phi s_\theta \\ s_\psi c_\theta & c_\psi c_\theta + s_\phi s_\theta s_\psi & -c_\psi s_\phi + s_\theta s_\psi c_\phi \\ -s_\theta & c_\theta s_\phi & c_\theta c_\phi \end{pmatrix} \tag{A.1.5}$$

The following shorthand notation for trigonometric function is used: $c_\theta := \cos\theta$, $s_\theta := \sin\theta$, $t_\theta := \tan\theta$. The inverse of a rotation matrix $\mathcal{R}_m^0$ is, by definition, $\mathcal{R}_0^m$ since it transforms coordinates from the inertial reference frame $\mathcal{R}_0$ to the mobile frame $\mathcal{R}_m$. the inverse of a rotation matrix is its transpose :

$$\mathcal{R}_0^m = (\mathcal{R}_m^0)^T \tag{A.1.6}$$

or, without reference to specific frames:

$$\mathcal{R}^{-1} = \mathcal{R} \tag{A.1.7}$$

Each rotation matrix is an orthogonal matrix, since it satisfies the following relation :

$$\mathcal{R}\mathcal{R}^T = I_3 \tag{A.1.8}$$

A.2 Angular velocity transformation

Let us denote by $\omega_m = [\omega_{x_m},\omega_{y_m},\omega_{z_m}]^T$ the body-fixed angular velocity vector expressed in the inertial reference frame $\mathcal{R}_0$, defined as follows :

$$\omega_m = \begin{pmatrix} 0 \\ 0 \\ \dot{\psi} \end{pmatrix} + R_{z,\psi} \begin{pmatrix} 0 \\ \dot{\theta} \\ 0 \end{pmatrix} + R_{z,\psi} R_{y,\theta} \begin{pmatrix} \dot{\phi} \\ 0 \\ 0 \end{pmatrix} \tag{A.2.1}$$

witch implies that :

$$\omega_m = \begin{pmatrix} c_\psi c_\theta \dot{\phi} - s_\psi \dot{\theta} \\ s_\psi c_\theta \dot{\phi} + c_\psi \dot{\theta} \\ \dot{\psi} - s_\theta \dot{\phi} \end{pmatrix} \tag{A.2.2}$$

$$\begin{pmatrix} \omega_{x_m} \\ \omega_{y_m} \\ \omega_{z_m} \end{pmatrix} = \underbrace{\begin{pmatrix} c_\psi c_\theta & -s_\psi & 0 \\ s_\psi c_\theta & c_\psi & 0 \\ -s_\theta & 0 & 1 \end{pmatrix}}_{S_m(\eta_2^m)} \begin{pmatrix} \dot{\phi} \\ \dot{\theta} \\ \dot{\psi} \end{pmatrix} \tag{A.2.3}$$

Hence, the body-fixed angular velocity vector $\omega_m = [\omega_{x_m}, \omega_{y_m}, \omega_{z_m}]^T$ and the Euler rate vector $\dot{\eta}_2^m = [\dot{\phi}, \dot{\theta}, \dot{\psi}]^T$ are related through the following expression :

$$\omega_m = S_m(\eta_2^m)\dot{\eta}_2^m \tag{A.2.4}$$

Where $S_m(\eta_2^m)$ is the transformation matrix from Euler angle rates to angular velocity. Further, we denote by $\nu_2^m = [p, q, r]^T$ the body-fixed angular velocity vector expressed in the body-fixed frame $\mathcal{R}_m$. This vector can be written as follows :

$$\nu_2^m = R_{x,\phi}^{-1} R_{y,\theta}^{-1} \begin{pmatrix} 0 \\ 0 \\ \dot{\psi} \end{pmatrix} + R_{x,\phi}^{-1} \begin{pmatrix} 0 \\ \dot{\theta} \\ 0 \end{pmatrix} + \begin{pmatrix} \dot{\phi} \\ 0 \\ 0 \end{pmatrix} \tag{A.2.5}$$

This leads to

$$\nu_2^m = \begin{pmatrix} \dot{\phi} - s_\theta \dot{\psi} \\ s_\phi c_\theta \dot{\psi} + c_\phi \dot{\theta} \\ c_\phi c_\theta \dot{\phi} - s_\phi \dot{\theta} \end{pmatrix} \tag{A.2.6}$$

$$\begin{pmatrix} p \\ q \\ r \end{pmatrix} = \underbrace{\begin{pmatrix} 1 & 0 & -s_\theta \\ 0 & c_\phi & s_\phi c_\theta \\ 0 & -s_\phi & c_\phi c_\theta \end{pmatrix}}_{P_m(\eta_2^m)} \begin{pmatrix} \dot{\phi} \\ \dot{\theta} \\ \dot{\psi} \end{pmatrix} \tag{A.2.7}$$

Hence, the body-fixed angular velocity vector $\nu_2^m = [p, q, r]^T$ and the Euler rate vector $\dot{\eta}_2^m = [\dot{\phi}, \dot{\theta}, \dot{\psi}]^T$ are related through the following expression :

$$\nu_2^m = P_m(\eta_2^m)\dot{\eta}_2^m \tag{A.2.8}$$

Where $P_m(\eta_2^m)$ is the transformation matrix from Euler angle rates to angular velocity. By multiplying the previous equation by $P_m^{-1}(\eta_2^m)$, we obtain :

$$\begin{pmatrix} \dot{\phi} \\ \dot{\theta} \\ \dot{\psi} \end{pmatrix} = \underbrace{\begin{pmatrix} 1 & s_\phi t_\theta & c_\phi t_\theta \\ 0 & c_\phi & -s_\phi \\ 0 & \frac{s_\phi}{c_\theta} & \frac{c_\phi}{c_\theta} \end{pmatrix}}_{P_m^{-1}(\eta_2^m)} \begin{pmatrix} p \\ q \\ r \end{pmatrix} \tag{A.2.9}$$

A.3 Rotation matrix time rate

The orthogonality property of the transformation matrix can be used to obtain an expression for that derivative. We can differentiate the equation $\mathcal{R}\mathcal{R}^T = I_3$ to obtain the following expression :

$$\dot{\mathcal{R}}\mathcal{R}^T + \mathcal{R}\dot{\mathcal{R}}^T = 0 \tag{A.3.1}$$

which implies that :

$$\dot{\mathcal{R}}\mathcal{R}^T = -\mathcal{R}\dot{\mathcal{R}}^T = -(\dot{\mathcal{R}}\mathcal{R}^T)^T \tag{A.3.2}$$

A matrix that is equal to the negative of its transpose must be a skew symmetric matrix. It follows that :

$$\dot{\mathcal{R}}\mathcal{R}^T = [\omega_m] \tag{A.3.3}$$

where $[\omega_m]$ a skew symmetric matrix defined by the preceding equation. This skew symmetric matrix defines a vector ω_m, called the angular velocity vector defined in the global coordinate system $\mathcal{R}_0$. It follows from the preceding equation that the time derivative of the transformation matrix is given by :

$$\dot{\mathcal{R}} = [\omega_m]\mathcal{R} \tag{A.3.4}$$

Note that $[\omega_m]$ is the anti-symmetric tensor corresponding to the cross product associated with ω_m and is defined as follows :

$$[\omega_m] = \begin{pmatrix} 0 & -\omega_{z_m} & \omega_{y_m} \\ \omega_{z_m} & 0 & -\omega_{x_m} \\ -\omega_{y_m} & \omega_{x_m} & 0 \end{pmatrix} \tag{A.3.5}$$

Alternatively, we can differentiate the equation $\mathcal{R}^T\mathcal{R} = I_3$ to obtain the following identity:

$$\mathcal{R}^T\dot{\mathcal{R}} = -\dot{\mathcal{R}}^T\mathcal{R} = -(\mathcal{R}^T\dot{\mathcal{R}})^T \tag{A.3.6}$$

which defines another skew symmetric matrix $[\nu_2^m]$ given by

$$\mathcal{R}^T\dot{\mathcal{R}} = [\nu_2^m] \tag{A.3.7}$$

This equation provides another definition for the time derivative of the transformation matrix, given by

$$\dot{\mathcal{R}} = \mathcal{R}[\nu_2^m] \tag{A.3.8}$$

The skew symmetric matrix $[\nu_2^m]$ defines a vector ν_2^m, called the angular velocity vector defined in the body coordinate system.

$$\dot{\mathcal{R}} = \mathcal{R}[\nu_2^m] = [\omega_m]\mathcal{R} \tag{A.3.9}$$

Pre-multiplying and post-multiplying this equation by $\mathcal{R}^T$, we obtain respectively :

$$[\omega_m] = \mathcal{R}[\nu_2^m]\mathcal{R}^T \tag{A.3.10}$$

and

$$[\nu_2^m] = \mathcal{R}^T[\omega_m]\mathcal{R} \tag{A.3.11}$$

Appendix B

Composition of Velocity and Acceleration

B.1 Velocity and acceleration vectors of rotating frame

To describe the relationship between velocity and acceleration vectors from rotating to non-rotating coordinate systems, we consider two frames. The first one is fixed, known as inertial reference frame $\mathcal{R}_0(O, X_0, Y_0, Z_0)$ while the second one is a mobile frame denoted as $\mathcal{R}_m(O', X_m, Y_m, Z_m)$. Let $\overrightarrow{i}'$, $\overrightarrow{j}'$ and $\overrightarrow{k}'$ be the unit vectors along the axes of the rotating coordinate system $\mathcal{R}_m$. $\overrightarrow{U}$ is an arbitrary vector expressed as follows :

$$\overrightarrow{U} = U_x \overrightarrow{i}' + U_y \overrightarrow{j}' + U_z \overrightarrow{k}' \tag{B.1.1}$$

where, U_x, U_y, and U_z denote the components of the vector $\overrightarrow{U}$. Since $\mathcal{R}_m$ is a mobile frame, its associated unit vectors $\overrightarrow{i}'$, $\overrightarrow{j}'$ and $\overrightarrow{k}'$ are function of time. Thus, the time derivative of $\overrightarrow{U}$ with respect to the inertial reference frame $\mathcal{R}_0$ system is given by :

$$\frac{d\overrightarrow{U}}{dt} = \left(\frac{dU_x}{dt}\overrightarrow{i}' + \frac{dU_y}{dt}\overrightarrow{j}' + \frac{dU_z}{dt}\overrightarrow{k}'\right) + \left(U_x\frac{d\overrightarrow{i}'}{dt} + U_y\frac{d\overrightarrow{j}'}{dt} + U_z\frac{d\overrightarrow{k}'}{dt}\right) \tag{B.1.2}$$

The mobile frame $\mathcal{R}_m$ is rotating with respect to the fixed frame $\mathcal{R}_0$ with an angular velocity ω. Hence, the linear velocity of a fixed point M in a rotating frame is given by :

$$\frac{d\overrightarrow{r}}{dt} = \overrightarrow{\omega} \times \overrightarrow{r} \tag{B.1.3}$$

where r is to the position vector of the point M. From the previous equation we can state :

$$\frac{d\overrightarrow{i}'}{dt} = \overrightarrow{\omega} \times \overrightarrow{i}' \tag{B.1.4}$$

$$\frac{d\overrightarrow{j}'}{dt} = \overrightarrow{\omega} \times \overrightarrow{j}' \tag{B.1.5}$$

$$\frac{d\overrightarrow{k}'}{dt} = \overrightarrow{\omega} \times \overrightarrow{k}' \tag{B.1.6}$$

Using Equations B.1.4,B.1.5 andB.1.6, the second term on the right side of Equation B.1.2 becomes :

$$U_x \frac{d\overrightarrow{i}'}{dt} + U_y \frac{d\overrightarrow{j}'}{dt} + U_z \frac{d\overrightarrow{k}'}{dt} = \overrightarrow{\omega} \times \overrightarrow{U} \tag{B.1.7}$$

Besides, as the unit vectors $\overrightarrow{i}', \overrightarrow{j}'$ and $\overrightarrow{k}'$ are constant with respect to the rotating frame. the first term on the right side of Equation B.1.2 corresponds to the derivative of $\overrightarrow{U}$ with respect to $\mathcal{R}_m$. Hence, the transformation relationship of the time derivative from a rotating coordinate system to a fixed one is given by :

$$\frac{d\overrightarrow{U}}{dt}\Big]^{\mathcal{R}_m}_{\rfloor\mathcal{R}_0} = \frac{d\overrightarrow{U}}{dt}\Big]^{\mathcal{R}_m}_{\rfloor\mathcal{R}_m} + \overrightarrow{\omega}]^{\mathcal{R}_m}_{\mathcal{R}_m/\mathcal{R}_0} \times \overrightarrow{U} \tag{B.1.8}$$

Note that $\frac{d\overrightarrow{OM}}{dt}]^{C}_{\rfloor G}$ represents the linear velocity vector of a point M with respect to the frame G, expressed in a frame C and $\overrightarrow{\omega}]^{C}_{B/G}$ represents the angular velocity vector of a frame B with respect to a frame G, expressed in a frame C. The notation holds for all the vectors used in this section.

B.2 Composition of linear velocity and acceleration

Let $\overrightarrow{OM}$ be the position vector of the point M, such that :

$$\overrightarrow{OM} = \overrightarrow{OO'} + \overrightarrow{O'M} \tag{B.2.1}$$

$$\frac{d\overrightarrow{OM}}{dt}\Big]^{\mathcal{R}_0}_{\rfloor\mathcal{R}_0} = \frac{d\overrightarrow{OO'}}{dt}\Big]^{\mathcal{R}_0}_{\rfloor\mathcal{R}_0} + \frac{d\overrightarrow{O'M}}{dt}\Big]^{\mathcal{R}_0}_{\rfloor\mathcal{R}_0} \tag{B.2.2}$$

By applying the Varignon's theorem to the vector $\overrightarrow{O'M}$, we get :

$$\frac{d\overrightarrow{OM}}{dt}\Big]^{\mathcal{R}_0}_{\rfloor\mathcal{R}_0} = \frac{d\overrightarrow{OO'}}{dt}\Big]^{\mathcal{R}_0}_{\rfloor\mathcal{R}_0} + \frac{d\overrightarrow{O'M}}{dt}\Big]^{\mathcal{R}_0}_{\rfloor\mathcal{R}_m} + \overrightarrow{\omega}]^{\mathcal{R}_0}_{\mathcal{R}_m/\mathcal{R}_0} \times \overrightarrow{O'M} \tag{B.2.3}$$

Note that $\frac{d\overrightarrow{OM}}{dt}]^{\mathcal{R}_0}_{\rfloor\mathcal{R}_0}$ and $\frac{d\overrightarrow{O'M}}{dt}]^{\mathcal{R}_0}_{\rfloor\mathcal{R}_m}$ correspond to the absolute and relative linear velocity of the point M, defined respectively as $\overrightarrow{v}_a(M)$ and $\overrightarrow{v}_r(M)$. Further, $\overrightarrow{v}_e(M)$ represents the velocity of a point coincident with M but fixed in the mobile frame $\mathcal{R}_m$. The absolute linear velocity expressed in inertial reference frame can be expressed as :

$$\overrightarrow{v}_a(M) = \overrightarrow{v}_r(M) + \overrightarrow{v}_e(M) \tag{B.2.4}$$

Where

$$\overrightarrow{v}_r(M) = \frac{d\overrightarrow{O'M}}{dt}\Big]^{\mathcal{R}_0}_{\rfloor\mathcal{R}_m} \tag{B.2.5}$$

$$\overrightarrow{v}_e(M) = \frac{d\overrightarrow{OO'}}{dt}\Big]^{\mathcal{R}_0}_{\mathcal{R}_0} + \overrightarrow{\omega}\Big]^{\mathcal{R}_0}_{\mathcal{R}_m/\mathcal{R}_0} \times \overrightarrow{O'M} \tag{B.2.6}$$

We can differentiate the equation B.2.3 to obtain we get the linear acceleration :

$$\frac{d^2\overrightarrow{OM}}{dt^2}\Big]^{\mathcal{R}_0}_{\mathcal{R}_0} = \frac{d^2\overrightarrow{OO'}}{dt^2}\Big]^{\mathcal{R}_0}_{\mathcal{R}_0} + \frac{d}{dt}\left\{\frac{d\overrightarrow{O'M}}{dt}\Big]^{\mathcal{R}_0}_{\mathcal{R}_m} + \overrightarrow{\omega}\Big]^{\mathcal{R}_0}_{\mathcal{R}_m/\mathcal{R}_0} \times \overrightarrow{O'M}\right\} \tag{B.2.7}$$

$$\frac{d^2\overrightarrow{OM}}{dt^2}\Big]^{\mathcal{R}_0}_{\mathcal{R}_0} = \frac{d^2\overrightarrow{OO'}}{dt^2}\Big]^{\mathcal{R}_0}_{\mathcal{R}_0} + \frac{d\overrightarrow{v}_r(M)}{dt}\Big]^{\mathcal{R}_0}_{\mathcal{R}_0} + \frac{d\overrightarrow{\omega}}{dt}\Big]^{\mathcal{R}_0}_{\mathcal{R}_m/\mathcal{R}_0} \times \overrightarrow{O'M} + \overrightarrow{\omega}\Big]^{\mathcal{R}_0}_{\mathcal{R}_m/\mathcal{R}_0} \times \frac{d\overrightarrow{O'M}}{dt}\Big]^{\mathcal{R}_0}_{\mathcal{R}_0} \tag{B.2.8}$$

By applying the Varignon's theorem to the two vectors $\overrightarrow{O'M}$ and $\overrightarrow{v}_r(M)$, we get :

$$\begin{aligned}\frac{d^2\overrightarrow{OM}}{dt^2}\Big]^{\mathcal{R}_0}_{\mathcal{R}_0} = \frac{d^2\overrightarrow{OO'}}{dt^2}\Big]^{\mathcal{R}_0}_{\mathcal{R}_0} + \left\{\frac{d\overrightarrow{v}_r(M)}{dt}\Big]^{\mathcal{R}_m}_{\mathcal{R}_m} + \overrightarrow{\omega}\Big]^{\mathcal{R}_m}_{\mathcal{R}_m/\mathcal{R}_0} \times \overrightarrow{v}_r(M)\right\} + \frac{d\overrightarrow{\omega}}{dt}\Big]^{\mathcal{R}_0}_{\mathcal{R}_m/\mathcal{R}_0} \times \overrightarrow{O'M} \\ + \overrightarrow{\omega}\Big]^{\mathcal{R}_0}_{\mathcal{R}_m/\mathcal{R}_0} \times \left\{\frac{d\overrightarrow{O'M}}{dt}\Big]^{\mathcal{R}_m}_{\mathcal{R}_m} + \overrightarrow{\omega}\Big]^{\mathcal{R}_m}_{\mathcal{R}_m/\mathcal{R}_0} \times \overrightarrow{O'M}\right\}\end{aligned} \tag{B.2.9}$$

$$\begin{aligned}\frac{d^2\overrightarrow{OM}}{dt^2}\Big]^{\mathcal{R}_0}_{\mathcal{R}_0} = \frac{d^2\overrightarrow{O'M}}{dt^2}\Big]^{\mathcal{R}_0}_{\mathcal{R}_m} + 2\overrightarrow{\omega}\Big]^{\mathcal{R}_0}_{\mathcal{R}_A/\mathcal{R}_0} \times \frac{d\overrightarrow{O'M}}{dt}\Big]^{\mathcal{R}_0}_{\mathcal{R}_m} \\ + \left\{\frac{d^2\overrightarrow{OO'}}{dt^2}\Big]^{\mathcal{R}_0}_{\mathcal{R}_0} + \frac{d\overrightarrow{\omega}}{dt}\Big]^{\mathcal{R}_0}_{\mathcal{R}_m/\mathcal{R}_0} \times \overrightarrow{O'M} + \overrightarrow{\omega}\Big]^{\mathcal{R}_0}_{\mathcal{R}_m/\mathcal{R}_0} \times (\overrightarrow{\omega}\Big]^{\mathcal{R}_0}_{\mathcal{R}_m/\mathcal{R}_0} \times \overrightarrow{O'M})\right\}\end{aligned} \tag{B.2.10}$$

Note that $\frac{d^2\overrightarrow{OM}}{dt^2}\Big]^{\mathcal{R}_0}_{\mathcal{R}_0}$ and $\frac{d^2\overrightarrow{O'M}}{dt^2}\Big]^{\mathcal{R}_0}_{\mathcal{R}_m}$ correspond to the absolute and relative linear acceleration of the point M, defined respectively as $\overrightarrow{a}_a(M)$ and $\overrightarrow{a}_r(M)$. Further, $\overrightarrow{a}_e(M)$ represents the acceleration of a point coincident with M but fixed in the mobile frame $\mathcal{R}_m$. The term $\overrightarrow{\omega}\Big]^{\mathcal{R}_0}_{\mathcal{R}_m/\mathcal{R}_0} \times (\overrightarrow{\omega}\Big]^{\mathcal{R}_0}_{\mathcal{R}_m/\mathcal{R}_0} \times \overrightarrow{O'M})$ is a centripetal acceleration directed toward an axis of rotation through O'. The term $\overrightarrow{a}_c(M)$ is the Coriolis acceleration due to a velocity relative to the rotating frame. The absolute linear acceleration expressed in inertial reference frame can be written as :

$$\overrightarrow{a}_a(M) = \overrightarrow{a}_r(M) + \overrightarrow{a}_e(M) + \overrightarrow{a}_c(M) \tag{B.2.11}$$

Where

$$\overrightarrow{a}_r(M) = \frac{d^2\overrightarrow{O'M}}{dt^2}\Big]^{\mathcal{R}_0}_{\mathcal{R}_m} \tag{B.2.12}$$

$$\overrightarrow{a}_e(M) = \frac{d^2\overrightarrow{OO'}}{dt^2}\Big]^{\mathcal{R}_0}_{\mathcal{R}_0} + \frac{d\overrightarrow{\omega}}{dt}\Big]^{\mathcal{R}_0}_{\mathcal{R}_m/\mathcal{R}_0} \times \overrightarrow{O'M} + \overrightarrow{\omega}]^{\mathcal{R}_0}_{\mathcal{R}_m/\mathcal{R}_0} \times (\overrightarrow{\omega}]^{\mathcal{R}_0}_{\mathcal{R}_m/\mathcal{R}_0} \times \overrightarrow{O'M}) \tag{B.2.13}$$

$$\overrightarrow{a}_c(M) = 2\overrightarrow{\omega}]^{\mathcal{R}_0}_{\mathcal{R}_A/\mathcal{R}_0} \times \frac{d\overrightarrow{O'M}}{dt}\Big]^{\mathcal{R}_0}_{\mathcal{R}_m} \tag{B.2.14}$$

B.3 Composition of angular velocity and acceleration

We consider three frames $\mathcal{R}_0$,$\mathcal{R}_1$ and $\mathcal{R}_m$, by applying the Varignon's theorem we get :

$$\frac{d\overrightarrow{U}}{dt}\Big]^{\mathcal{R}_m}_{\mathcal{R}_1} = \frac{d\overrightarrow{U}}{dt}\Big]^{\mathcal{R}_m}_{\mathcal{R}_m} + \overrightarrow{\omega}]^{\mathcal{R}_m}_{\mathcal{R}_m/\mathcal{R}_1} \times \overrightarrow{U} \tag{B.3.1}$$

$$\frac{d\overrightarrow{U}}{dt}\Big]^{\mathcal{R}_m}_{\mathcal{R}_0} = \frac{d\overrightarrow{U}}{dt}\Big]^{\mathcal{R}_m}_{\mathcal{R}_1} + \overrightarrow{\omega}]^{\mathcal{R}_m}_{\mathcal{R}_1/\mathcal{R}_0} \times \overrightarrow{U} \tag{B.3.2}$$

From the two previous equations, we get :

$$\frac{d\overrightarrow{U}}{dt}\Big]^{\mathcal{R}_m}_{\mathcal{R}_0} = \frac{d\overrightarrow{U}}{dt}\Big]^{\mathcal{R}_m}_{\mathcal{R}_m} + (\overrightarrow{\omega}]^{\mathcal{R}_m}_{\mathcal{R}_m/\mathcal{R}_1} + \overrightarrow{\omega}]^{\mathcal{R}_m}_{\mathcal{R}_1/\mathcal{R}_0}) \times \overrightarrow{U} \tag{B.3.3}$$

By identification, we have :

$$\overrightarrow{\omega}]^{\mathcal{R}_m}_{\mathcal{R}_m/\mathcal{R}_0} = \overrightarrow{\omega}]^{\mathcal{R}_m}_{\mathcal{R}_m/\mathcal{R}_1} + \overrightarrow{\omega}]^{\mathcal{R}_m}_{\mathcal{R}_1/\mathcal{R}_0} \tag{B.3.4}$$

We can differentiate the equation B.3.4 to obtain the angular acceleration given by :

$$\frac{d\overrightarrow{\omega}}{dt}\Big]^{\mathcal{R}_m}_{\mathcal{R}_m/\mathcal{R}_0} = \frac{d(\overrightarrow{\omega}_{]\mathcal{R}_m/\mathcal{R}_1})}{dt}\Big]^{\mathcal{R}_m}_{\mathcal{R}_0} + \frac{d\overrightarrow{\omega}}{dt}\Big]^{\mathcal{R}_m}_{\mathcal{R}_1/\mathcal{R}_0} \tag{B.3.5}$$

By applying the Varignon's theorem to the vector $\overrightarrow{\omega}_{]\mathcal{R}_m/\mathcal{R}_1}$, we get :

$$\overrightarrow{\dot{\omega}}]^{\mathcal{R}_m}_{\mathcal{R}_m/\mathcal{R}_0} = \overrightarrow{\dot{\omega}}]^{\mathcal{R}_m}_{\mathcal{R}_m/\mathcal{R}_1} + \overrightarrow{\omega}]^{\mathcal{R}_m}_{\mathcal{R}_1/\mathcal{R}_0} \times \overrightarrow{\omega}]^{\mathcal{R}_m}_{\mathcal{R}_m/\mathcal{R}_1} + \overrightarrow{\dot{\omega}}]^{\mathcal{R}_m}_{\mathcal{R}_1/\mathcal{R}_0} \tag{B.3.6}$$

Bibliography

[1] H. Pasternak, S. Schilling, and S. Komann, "The steel construction of the new cargo-lifter airship hangar", pp. 173 –182, 2001. [Online]. Available: http://www.sciencedirect.com/science/article/pii/B9780080439488500163.

[2] P. W. Berg, S. Isaacs, and K. L. Blodgett, *"airborne fulfillment center utilizing unmanned aerial vehicles for item delivery"*, US Patent 9,305,280, 2016.

[3] J. Hartmann, "Conceptual design of air vehicles with hybrid lift concepts-a design space exploration", in *55th AIAA Aerospace Sciences Meeting*, 2017, p. 1625.

[4] I. Pasternak, *"flight system for a constant volume, variable buoyancy air vehicle"*, US Patent 9,016,622, 2015.

[5] R. V. Petrescu, R. Aversa, B. Akash, J. Corchado, F. Berto, M. Mirsayar, S. Kozaitis, T. Abu-Lebdeh, A. Apicella, and F. I. Petrescu, "Airlander", *Journal of Aircraft and Spacecraft Technology*, vol. 1, no. 2, 2017.

[6] A. R. Handley, *"system for controlling the lift of aircraft"*, US Patent 7,568,656, 2009.

[7] J. R. Skuza, Y. Park, H. J. Kim, and S. T. Seaman, "Feasibility study of cargo airship transportation systems powered by new green energy technologies", *Technical report. NASA Center for Aero Space Information*, 2014.

[8] A. Elfes, S. S. Bueno, M. Bergerman, and J. G. Ramos, "A semi-autonomous robotic airship for environmental monitoring missions", in *Proceedings. 1998 IEEE International Conference on Robotics and Automation (Cat. No.98CH36146)*, vol. 4, 1998, 3449–3455 vol.4. DOI: 10.1109/ROBOT.1998.680971.

[9] K. Kanistras, G. Martins, M. J. Rutherford, and K. P. Valavanis, "A survey of unmanned aerial vehicles (uavs) for traffic monitoring", in *2013 International Conference on Unmanned Aircraft Systems (ICUAS)*, 2013, pp. 221–234. DOI: 10.1109/ICUAS.2013.6564694.

[10] S. Oh, S. Kang, K. Lee, S. Ahn, and E. Kim, "Flying display: Autonomous blimp with real-time visual tracking and image projection", in *2006 IEEE/RSJ International Conference on Intelligent Robots and Systems*, 2006, pp. 131–136. DOI: 10.1109/IROS.2006.281919.

[11] Y.-G. Lee, D.-M. Kim, and C.-H. Yeom, "Development of korean high altitude platform systems", *International Journal of Wireless Information Networks*, vol. 13, no. 1, pp. 31–42, 2006, ISSN: 1572-8129. [Online]. Available: https://doi.org/10.1007/s10776-005-0018-6.

[12] Y. Yang, J. Wu, and W. Zheng, "Design, modeling and control for a stratospheric telecommunication platform", *Acta Astronautica*, vol. 80, no. Supplement C, pp. 181 –189, 2012, ISSN: 0094-5765.

[13] B. Buerge, "The suitability of hybrid vs. conventional airships for persistent surveillance missions", *48th AIAA Aerospace Sciences Meeting Including the New Horizons Forum and Aerospace Exposition. Orlando, Florida*, 2010.

[14] L. Liao and I. Pasternak, "A review of airship structural research and development", *Progress in Aerospace Sciences*, vol. 45, no. 4, pp. 83 –96, 2009, ISSN: 0376-0421. [Online]. Available: http://www.sciencedirect.com/science/article/pii/S0376042109000153.

[15] Y. Li and M. Nahon, "Modeling and simulation of airship dynamics", *Journal of Guidance, Control, and Dynamics*, vol. 30, no. 6, pp. 1691 –1700, 2007.

[16] S Gomes, "An investigationin to the flight dynamics of airships with application to the yez-2a", *PhDthesis,Cranfield Institut of Technology*, 1990.

[17] A. José and C. B.S. S. Raul de Paiva Ely, "Influence of wind speed on airship dynamics", *Journal of Guidance, Control, and Dynamics*, vol. 25, no. 6, pp. 1116 –1124, 2002.

[18] J. D. Jones S. P. Delaurier, "Aerodynamic estimation techniques for aerostats and airships", *Journal of Aircraft*, vol. 20, no. 2, pp. 120–126, 1983.

[19] S. I. Li Y. Nahon M., "Modeling and simulation of flexible airships", *AIAA Journal*, vol. 47, no. 3, pp. 592 –605, 2009.

[20] S. Bennaceur, N. Azouz, and D. Boukraa, "An efficient modeling of a flexible airships", 2006, pp. 573–582. [Online]. Available: https://hal.archives-ouvertes.fr/hal-00342772.

[21] E. Paiva, J. Azinheira, and A. Moutinho, "Erratum - influence of wind speed on airship dynamics", *Journal of Guidance, Control, and Dynamics*, vol. 31, pp. 443–444, 2008. DOI: 10.2514/1.33409.

[22] S. Bennaceur, "Modeling and control of flexible flying engines", Theses, Université d'Evry-Val d'Essonne, 2009. [Online]. Available: https://tel.archives-ouvertes.fr/tel-00465065.

[23] E. Hygounenc, I.-K. Jung, P. Souères, and S. Lacroix, "The autonomous blimp project of laas-cnrs: Achievements in flight control and terrain mapping", *The International Journal of Robotics Research*, vol. 23, no. 4-5, pp. 473–511, 2004. [Online]. Available: https://doi.org/10.1177/0278364904042200.

[24] G. A. Khoury, *Airship technology*. Cambridge university press, 2012, vol. 10.

[25] S. S. Bueno, J. R. Azinheira, J. Ramos, E Paiva, P. Rives, A. Elfes, J. R. Carvalho, and G. F. Silveira, "Project aurora: Towards an autonomous robotic airship", in *Workshop on Aerial Robotics, IEEE International Conference on Intelligent Robots and Systems*, 2002, pp. 43–54.

[26] S Samaali, A Abichou, and L Beji, "Longitudinal and horizontal stabilisation of an unmanned blimp", *International Journal of Vehicle Autonomous Systems*, vol. 5, no. 1-2, pp. 138–157, 2007.

[27] A. Moutinho and J. R. Azinheira, "Stability and robustness analysis of the aurora airship control system using dynamic inversion", in *Proceedings of the 2005 IEEE International Conference on Robotics and Automation*, IEEE, 2005, pp. 2265–2270.

[28] P. Herman and W. Adamski, "A trajectory tracking controller for vehicles moving at low speed", in *2017 25th Mediterranean Conference on Control and Automation (MED)*, IEEE, 2017, pp. 1183–1188.

[29] ——, "Nonlinear tracking control for some marine vehicles and airships", *2017 11th International Workshop on Robot Motion and Control (RoMoCo)*, pp. 257–262,

[30] P. Herman and W. Adamski, "Velocity controller for a class of vehicles", *Foundations of Computing and Decision Sciences*, vol. 42, no. 1, pp. 43–58, 2017.

[31] X. Shao-Rong, L. Jun, R. Jin-Jun, and G. Zhen-Bang, "Computer vision-based navigation and predefined track following control of a small robotic airship", *Acta Automatica Sinica*, vol. 33, no. 3, pp. 286–291, 2007.

[32] M. Gautier, "Dynamic identification of robots with power model", in *Proceedings of International Conference on Robotics and Automation*, IEEE, vol. 3, 1997, pp. 1922–1927.

[33] P. Dietmaier, "The stewart-gough platform of general geometry can have 40 real postures", in *Advances in Robot Kinematics: Analysis and Control*, Springer, 1998, pp. 7–16.

[34] M. Gouttefarde and C. M. Gosselin, "Analysis of the wrench-closure workspace of planar parallel cable-driven mechanisms", *IEEE Transactions on Robotics*, vol. 22, no. 3, pp. 434–445, 2006.

[35] C. Gosselin, "Cable-driven parallel mechanisms: State of the art and perspectives", *Mechanical Engineering Reviews*, vol. 1, no. 1, DSM0004–DSM0004, 2014.

[36] S. Kawamura, W. Choe, S. Tanaka, and H. Kino, "Development of an ultrahigh speed robot falcon using parallel wire drive systems", *Journal of the Robotics Society of Japan*, vol. 15, no. 1, pp. 82–89, 1997.

[37] M. M. Aref and H. D. Taghirad, "Geometrical workspace analysis of a cable-driven redundant parallel manipulator: Kntu cdrpm", in *2008 IEEE/RSJ International Conference on Intelligent Robots and Systems*, IEEE, 2008, pp. 1958–1963.

[38] C. GOSSELIN, "Cable-driven parallel mechanisms: State of the art and perspectives", *Mechanical Engineering Reviews*, vol. 1, no. 1, DSM0004–DSM0004, 2014. DOI: 10.1299/mer.2014dsm0004.

[39] R. Bostelman, J. Albus, N. Dagalakis, A. Jacoff, and J. Gross, "Applications of the nist robocrane", in *Proceedings of the 5th International Symposium on Robotics and Manufacturing*, 1994, pp. 14–18.

[40] T. Dallej, M. Gouttefarde, N. Andreff, R. Dahmouche, and P. Martinet, "Vision-based modeling and control of large-dimension cable-driven parallel robots", in *2012 IEEE/RSJ International Conference on Intelligent Robots and Systems*, IEEE, 2012, pp. 1581–1586.

[41] C. Fanin, P. Gallina, A. Rossi, U. Zanatta, and S. Masiero, "Nerebot: A wire-based robot for neurorehabilitation", in *ICORR'03*, HWRS-ERC, 2003, pp. 23–27.

[42] R. Nan, D. Li, C. Jin, Q. Wang, L. Zhu, W. Zhu, H. Zhang, Y. Yue, and L. Qian, "The five-hundred-meter aperture spherical radio telescope (fast) project", *International Journal of Modern Physics D*, vol. 20, no. 06, pp. 989–1024, 2011.

[43] L. M. Ulander, H. Hellsten, and G. Stenstrom, "Synthetic-aperture radar processing using fast factorized back-projection", *IEEE Transactions on Aerospace and electronic systems*, vol. 39, no. 3, pp. 760–776, 2003.

[44] J.-P. Merlet, "Marionet, a family of modular wire-driven parallel robots", in *Advances in Robot Kinematics: Motion in Man and Machine*, Springer, 2010, pp. 53–61.

[45] A. Pott, H. Mütherich, W. Kraus, V. Schmidt, P. Miermeister, and A. Verl, "Ipanema: A family of cable-driven parallel robots for industrial applications", in *Cable-Driven Parallel Robots*, Springer, 2013, pp. 119–134.

[46] P. Miermeister, M. Lächele, R. Boss, C. Masone, C. Schenk, J. Tesch, M. Kerger, H. Teufel, A. Pott, and H. H. Bülthoff, "The cablerobot simulator large scale motion platform based on cable robot technology", in *2016 IEEE/RSJ International Conference on Intelligent Robots and Systems (IROS)*, 2016, pp. 3024–3029. DOI: 10.1109/IROS.2016.7759468.

[47] J. Albus, R. Bostelman, and N. Dagalakis, "The nist robocrane", *Journal of Robotic Systems*, vol. 10, no. 5, pp. 709–724, 1993. [Online]. Available: https://onlinelibrary.wiley.com/doi/abs/10.1002/rob.4620100509.

[48] R. Yao, X. Tang, J. Wang, and P. Huang, "Dimensional optimization design of the four-cable-driven parallel manipulator in fast", *IEEE/ASME Transactions on Mechatronics*, vol. 15, no. 6, pp. 932–941, 2010, ISSN: 1083-4435. DOI: 10.1109/TMECH.2009.2035922.

[49] H. Li, X. Zhang, R. Yao, J. Sun, G. Pan, and W. Zhu, "Optimal force distribution based on slack rope model in the incompletely constrained cable-driven parallel mechanism of fast telescope", in *Cable-Driven Parallel Robots*, T. Bruckmann and A. Pott, Eds. Berlin, Heidelberg: Springer Berlin Heidelberg, 2013, pp. 87–102, ISBN: 978-3-642-31988-4. [Online]. Available: https://doi.org/10.1007/978-3-642-31988-4_6.

[50] J. Merlet and D. Daney, "A portable, modular parallel wire crane for rescue operations", in *2010 IEEE International Conference on Robotics and Automation*, 2010, pp. 2834–2839. DOI: 10.1109/ROBOT.2010.5509299.

[51] J. Lamaury and M. Gouttefarde, "Control of a large redundantly actuated cable-suspended parallel robot", in *2013 IEEE International Conference on Robotics and Automation*, 2013, pp. 4659–4664. DOI: 10.1109/ICRA.2013.6631240.

[52] J. J. Gorman, K. W. Jablokow, and D. J. Cannon, "The cable array robot: Theory and experiment", in *Proceedings 2001 ICRA. IEEE International Conference on Robotics and Automation (Cat. No.01CH37164)*, vol. 3, 2001, 2804–2810 vol.3. DOI: 10.1109/ROBOT.2001.933047.

[53] A. B. Alp and S. K. Agrawal, "Cable suspended robots: Feedback controllers with positive inputs", in *Proceedings of the 2002 American Control Conference (IEEE Cat. No.CH37301)*, vol. 1, 2002, 815–820 vol.1. DOI: 10.1109/ACC.2002.1024915.

[54] E. Ottaviano and G. Castelli, "A study on the effects of cable mass and elasticity in cable-based parallel manipulators", in *ROMANSY 18 Robot Design, Dynamics and Control*, V. Parenti Castelli and W. Schiehlen, Eds., Vienna: Springer Vienna, 2010, pp. 149–156.

[55] J. P. Merlet, "Solving the forward kinematics of a gough-type parallel manipulator with interval analysis", *The International Journal of Robotics Research*, vol. 23, no. 3, pp. 221–235, 2004. [Online]. Available: https://doi.org/10.1177/0278364904039806.

[56] B. Vujanovic, "Conservation laws of dynamical systems via d'alembert's principle", *International Journal of Non-Linear Mechanics*, vol. 13, no. 3, pp. 185 –197, 1978, ISSN: 0020-7462. [Online]. Available: http://www.sciencedirect.com/science/article/pii/0020746278900070.

[57] J. Fink, N. Michael, S. Kim, and V. Kumar, "Planning and control for cooperative manipulation and transportation with aerial robots", *The International Journal of Robotics Research*, vol. 30, no. 3, pp. 324–334, 2011. [Online]. Available: https://doi.org/10.1177/0278364910382803.

[58] I. Maza, K. Kondak, M. Bernard, and A. Ollero, "Multi-uav cooperation and control for load transportation and deployment", *Journal of Intelligent and Robotic Systems*, vol. 57, no. 1, p. 417, 2009. [Online]. Available: https://doi.org/10.1007/s10846-009-9352-8.

[59] K. Sreenath and V. Kumar, "Dynamics, control and planning for cooperative manipulation of payloads suspended by cables from multiple quadrotor robots", in *Robotics: Science and Systems*, 2013.

[60] X. Zhou, C. P. Tang, and V. Krovi, "Analysis framework for cooperating mobile cable robots", in *2012 IEEE International Conference on Robotics and Automation*, 2012, pp. 3128–3133. DOI: 10.1109/ICRA.2012.6225169.

[61] X. Zhou, C. P. Tang, and V. Krovi, "Cooperating mobile cable robots: Screw theoretic analysis", in *Redundancy in Robot Manipulators and Multi-Robot Systems*, D. Milutinović and J. Rosen, Eds. Berlin, Heidelberg: Springer Berlin Heidelberg, 2013, pp. 109–123. [Online]. Available: https://doi.org/10.1007/978-3-642-33971-47.

[62] T. Rasheed, P. Long, D. Marquez-Gamez, and S. Caro, "Available wrench set for planar mobile cable-driven parallel robots", in *2018 IEEE International Conference on Robotics and Automation (ICRA)*, 2018, pp. 962–967. DOI: 10.1109/ICRA.2018.8461199.

[63] X. Zhou, S.-k. Jun, and V. Krovi, "Tension distribution shaping via reconfigurable attachment in planar mobile cable robots", *Robotica*, vol. 32, no. 2, 245–256, 2014.

[64] A. A.K. V. Anson Michael, "Orientation workspace and stiffness optimization of cable-driven parallel manipulators with base mobility", *Journal of Mechanisms and Robotics*, vol. 9, no. 3, pp. 031 011–031011–16, 2017.

[65] S. Qian, B. Zi, D. Wang, and Y. Li, "Development of modular cable-driven parallel robotic systems", *IEEE Access*, vol. 7, pp. 5541–5553, 2019, ISSN: 2169-3536. DOI: 10.1109/ACCESS.2018.2889245.

[66] T. Rasheed, P. Long, D. Marquez-Gamez, and S. Caro, J. Lenarcic, Ed.

[67] ——, "Tension distribution algorithm for planar mobile cable-driven parallel robots", in *Cable-Driven Parallel Robots*, Cham: Springer International Publishing, 2018, pp. 268–279.

[68] F. B. Abdallah, N. Azouz, L. Beji, and A. Abichou, "Modeling and stabilization of a cable-driven parallel platform suspended by an airship", in *2017 11th International Workshop on Robot Motion and Control (RoMoCo)*, 2017, pp. 53–58. DOI: 10.1109/RoMoCo.2017.8003892.

[69] M. A. Khosravi and H. D. Taghirad, "Robust pid control of cable-driven robots with elastic cables", in *2013 First RSI/ISM International Conference on Robotics and Mechatronics (ICRoM)*, IEEE, 2013, pp. 331–336.

[70] M. A. Khosravi and H. D. Taghirad, "Robust pid control of fully-constrained cable driven parallel robots", *Mechatronics*, vol. 24, no. 2, pp. 87 –97, 2014, ISSN: 0957-4158. [Online]. Available: http://www.sciencedirect.com/science/article/pii/S0957415813002353.

[71] H. M. Irvine and H. M. Irvine, *Cable structures*. MIT press Cambridge, MA, 1981, vol. 17.

[72] N. Riehl, M. Gouttefarde, S. Krut, C. Baradat, and F. Pierrot, "Effects of non-negligible cable mass on the static behavior of large workspace cable-driven parallel mechanisms", in *2009 IEEE international conference on robotics and automation*, IEEE, 2009, pp. 2193–2198.

[73] J.-p. Merlet and D. Daney, "A portable, modular parallel wire crane for rescue operations", in *2010 IEEE International Conference on Robotics and Automation*, IEEE, 2010, pp. 2834–2839.

[74] K. Kozak, Q. Zhou, and J. Wang, "Static analysis of cable-driven manipulators with non-negligible cable mass", *IEEE Transactions on Robotics*, vol. 22, no. 3, pp. 425–433, 2006.

[75] G. Carbone, "Stiffness analysis and experimental validation of robotic systems", *Frontiers of Mechanical Engineering*, vol. 6, no. 2, pp. 182–196, 2011.

[76] L. Mikelsons, T. Bruckmann, M. Hiller, and D. Schramm, "A real-time capable force calculation algorithm for redundant tendon-based parallel manipulators", in *2008 IEEE International Conference on Robotics and Automation*, 2008, pp. 3869–3874. DOI: 10.1109/ROBOT.2008.4543805.

[77] P. H. Borgstrom, B. L. Jordan, G. S. Sukhatme, M. A. Batalin, and W. J. Kaiser, "Rapid computation of optimally safe tension distributions for parallel cable-driven robots", *IEEE Transactions on Robotics*, vol. 25, no. 6, pp. 1271–1281, 2009, ISSN: 1552-3098. DOI: 10.1109/TRO.2009.2032957.

[78] C. Gosselin and M. Grenier, "On the determination of the force distribution in over-constrained cable-driven parallel mechanisms", *Meccanica*, vol. 46, no. 1, pp. 3–15, 2011. [Online]. Available: https://doi.org/10.1007/s11012-010-9369-x.

[79] S. Kawamura, H. Kino, and C. Won, "High-speed manipulation by using parallel wire-driven robots", *Robotica*, vol. 18, no. 1, 13–21, 2000.

[80] and S. K. Agrawal, "Cable suspended planar robots with redundant cables: Controllers with positive tensions", *IEEE Transactions on Robotics*, vol. 21, no. 3, pp. 457–465, 2005, ISSN: 1552-3098. DOI: 10.1109/TRO.2004.838029.

[81] G. El-Ghazaly, M. Gouttefarde, and V. Creuze, "Adaptive terminal sliding mode control of a redundantly-actuated cable-driven parallel manipulator: Cogiro", in *Cable-Driven Parallel Robots*, A. Pott and T. Bruckmann, Eds., Cham: Springer International Publishing, 2015, pp. 179–200, ISBN: 978-3-319-09489-2.

[82] J. Lamaury, M. Gouttefarde, A. Chemori, and P. Hervé, "Dual-space adaptive control of redundantly actuated cable-driven parallel robots", in *2013 IEEE/RSJ International Conference on Intelligent Robots and Systems*, 2013, pp. 4879–4886. DOI: 10.1109/IROS.2013.6697060.

[83] F. B. Abdallah, N. Azouz, L. Beji, S. Hima, and A. Abichou, "Modeling and control of an aerial robocrane using a wire driven system", in *2018 Annual American Control Conference (ACC)*, 2018, pp. 508–513. DOI: 10.23919/ACC.2018.8431168.

[84] H. Imine, L. Fridman, H. Shraim, and M. Djemai, *Sliding mode based analysis and identification of vehicle dynamics*. Springer Science & Business Media, 2011, vol. 414.

[85] A. Benalia, M. Djemai, and J. Barbot, "Control of the kinematic car using trajectory generation and the high order sliding mode control", in *SMC'03 Conference Proceedings. 2003 IEEE International Conference on Systems, Man and Cybernetics. Conference Theme - System Security and Assurance (Cat. No.03CH37483)*, vol. 3, 2003, 2455–2460 vol.3. DOI: 10.1109/ICSMC.2003.1244252.

[86] F. B. Abdallah, N. Azouz, L. Beji, and A. Abichou, "Modeling of a heavy lift airship carrying a payload by a cable driven parallel manipulator", *International Journal of Advanced Robotic Systems (accepted)*, 2019.

[87] S. Chaâbani, "Dynamique non-linéaire d'un dirigeable flexible", Thèse de doctorat dirigée par Lerbet, Jean et Abichou, Azgal Mathématiques appliquées Evry-Val d'Essonne 2014, PhD thesis, 2014. [Online]. Available: http://www.theses.fr/2014EVRY0008.

[88] H. J. Allen and Perkins, "Estimation of the forces and moments acting on inclined bodies of revolution of high fineness ratio", *NACA RM-a9i26*, 1949.

[89] J. D. Delaurier, "Aerodynamic estimation techniques for aerostats and airships", *Journal of Aircraft*, vol. 20, no. 2, pp. 120–126, 1983.

[90] E. Hygounenc, "Modélisation et commande d'un dirigeable pour le vol autonome", Thèse de doctorat dirigée par Souères, Philippe Automatique. Robotique Toulouse 3 2003, PhD thesis, 2003. [Online]. Available: http://www.theses.fr/2003TOU30174.

[91] M. Munk, "The aerodynamic forces on airship hulls", *NACA TR-184,*, 1924.

[92] R. H. Upson and W. A. Klikff, "Application of practical hydrodynamics of airship design", *NACA TR-405,*, 1933.

[93] J. D. Hunt, "Structural analysis of aerostat flexible structure by the finite-element method", *Journal of Aircraft*, vol. 19, no. 8, pp. 674–678, 1982.

[94] F. Jelenciak, M. Gerke, and U. Borgolte, "Modelling of airship flight mechanics by the projection equivalent method", *International Journal of Advanced Robotic Systems*, vol. 12, no. 12, p. 195, 2015. DOI: 10.5772/62078. [Online]. Available: https://doi.org/10.5772/62078.

[95] H. Lamb, "Hydrodynamics. 6th ed", *NewYork: Dove*, 1945.

[96] T. Fossen, "Guidance and control of ocean vehicles", *New York : Wiley*, 1998.

[97] G. Kirchhoff, "Ueber die bewegung eines rotationskörpers in einer flüssigkeit.", ger, *Journal für die reine und angewandte Mathematik*, vol. 71, pp. 237–262, 1869. [Online]. Available: http://eudml.org/doc/148114.

[98] G. Caviglia and A. Morro, "Kirchhoff's equations for the rigid body motion revisited", *Meccanica*, vol. 52, no. 6, pp. 1485–1489, 2017. [Online]. Available: https://doi.org/10.1007/s11012-016-0476-1.

[99] Z. Y. Mueller J. Paluszek M., "Development of an aerodynamic model and control law design for a high altitude airship", in *American Institute of Aeronautics and Astronautics*, 2004.

[100] B. Y. Beji L. Abichou A., "Position and attitude control of an underactuated autonomous airship", in *International Journal of Differential Equations and Applications*, vol. 8, 2004, pp. 231–255.

[101] P. G. Thomasson, "Equations of motion of a vehicle in a moving fluid", in *Journal of Aircraft*, vol. 37, 2000, pp. 630–639.

[102] K. M. Meirovitch L., "State equations for a spacecraft with maneuvering flexible appendages in terms of quasi-coordinate", in *Applied Mechanics Reviews*, vol. 42, 1989, pp. 37–48.

[103] F. Fossen Thor I. Ola-Erik, "Nonlinear modelling of marine vehicles in 6 degrees of freedom", *Mathematical Modelling of Systems*, vol. 1, no. 1, pp. 17–27, 1995. [Online]. Available: https://doi.org/10.1080/13873959508837004.

[104] H. Y. Wu X. Moog C. H., "Modelling and linear control of a buoyancy-driven airship", in *2009 7th Asian Control Conference*, 2009, pp. 75–80.

[105] A. N., C. S., L. J., and A. A., "Computation of the added masses of an unconventional airship", in *Journal of Applied Mathematics*, 2012. [Online]. Available: https://doi.org/10.1155/2012/714627.

[106] Y. S. Qin Wang Hua Chen and L. Qiao., "Coupling dynamics analysis of the flying cable driven parallel robot", *INTERNATIONAL JOURNAL OF CIRCUITS, SYSTEMS AND SIGNAL PROCESSING*, vol. 12, pp. 181–189, 2018.

[107] C. Masone, H. H. Bülthoff, and P. Stegagno, "Cooperative transportation of a payload using quadrotors: A reconfigurable cable-driven parallel robot", in *2016 IEEE/RSJ International Conference on Intelligent Robots and Systems (IROS)*, 2016, pp. 1623–1630. DOI: 10.1109/IROS.2016.7759262.

[108] S. Lacroix, I.-K. Jung, P. Souères, E. Hygounenc, and J.-P. Berry, "The autonomous blimp project of laas/cnrs — current status", 2002, pp. 487–496. DOI: 10.1007/3-540-36268-1_44.

[109] L. Beji, A. Abichou, and Y. Bestaoui, "Stabilization of a nonlinear underactuated autonomous airship-a combined averaging and backstepping approach", in *Proceedings of the Third International Workshop on Robot Motion and Control, 2002. RoMoCo '02.*, 2002, pp. 223–229. DOI: 10.1109/ROMOCO.2002.1177111.

[110] M. A. Hammami, "On the stability of nonlinear control systems with uncertainty", *Journal of Dynamical and Control Systems*, vol. 7, no. 2, pp. 171–179, 2001, ISSN: 1573-8698. DOI: 10.1023/A:1013099004015. [Online]. Available: https://doi.org/10.1023/A:1013099004015.

[111] A. Moutinho and J. R. Azinheira, "Hover stabilization of an airship using dynamic inversion", *IFAC Proceedings Volumes*, vol. 39, no. 15, pp. 193 –198, 2006, 8th IFAC Symposium on Robot Control, ISSN: 1474-6670. [Online]. Available: http://www.sciencedirect.com/science/article/pii/S1474667016385135.

[112] W. Perruquetti and J. P. Barbot, *Sliding mode control in engineering*. M. Dekker, 2002, vol. 11.

[113] T. Floquet*, J.-P. Barbot, W. Perruquetti, and M. Djemai, "On the robust fault detection via a sliding mode disturbance observer", *International Journal of control*, vol. 77, no. 7, pp. 622–629, 2004.

[114] A. BenAbdallah, M. Dlala, and M. A. Hammami, "A new lyapunov function for stability of time-varying nonlinear perturbed systems", *Systems Control Letters*, vol. 56, no. 3, pp. 179 –187, 2007, ISSN: 0167-6911. [Online]. Available: http://www.sciencedirect.com/science/article/pii/S0167691106001459.

université PARIS-SACLAY
ÉCOLE DOCTORALE
Sciences et technologies de l'information et de la communication (STIC)

Titre : Modélisation et commande d'un robot parallèle à câbles suspendu à un dirigeable gros porteur

Mots clés : Dirigeable gros porteur, Robot parallèle à câbles, Contrôle du chargement et déchargement

Résumé :
A l'heure où le monde entier appelle à développer de nouvelles technologies de transport afin de faire face au défi écologique, des projets de dirigeables gros porteurs permettent de relever ce défi. En outre, les dernières avancées technologiques dans le domaine de l'aérospatiale ont permis de résoudre un certain nombre de problèmes responsables de l'hibernation des grands dirigeables. Ceci a donné naissance à de nouveaux types de dirigeables gros porteurs. Dans cette thèse, le modèle dynamique du dirigeable gros porteur est défini afin de concevoir un contrôleur efficient. La particularité du dirigeable présenté est sa capacité de charger et de décharger le fret en vol stationnaire. Ce dirigeable est muni d'une grue formée par un robot parallèle à câbles (RPC) permettant d'optimiser le chargement et déchargement. Nous avons concentré nos efforts dans cette thèse à l'analyse de cette phase critique. Le dirigeable gros porteur sera représenté par un système multi-corps composé de plusieurs corps reliés entre eux par des articulations.
Les contributions de la thèse sont présentées en deux parties. Dans la première partie, nous supposons qu'il n'y a pas de couplage inertiel entre le dirigeable et le RPC. Ainsi nos recherches ne concernent que le RPC en tenant compte de la mobilité de la base suspendue par des câbles considérés dans un premier temps comme idéaux, puis les phénomènes d'affaissement et de flexibilité des câbles seront pris en compte. La conception de la commande de ce système doit aussi intégrer une répartition optimale de la tension car les câbles doivent à chaque configuration rester tendus. Dans la deuxième partie, nous abordons l'analyse du système global en considérant l'effet de couplage inertiel entre la charge utile suspendue et le dirigeable. Le modèle dynamique de ce système multicorps formé par le dirigeable et le RPC peut être modélisé comme une interconnexion de sous-systèmes d'ordre inférieur. Nous supposons que le dirigeable gros porteur est un sous-système faiblement couplé. En se basant sur cette hypothèse, un contrôleur décentralisé est proposé permettant de contrôler indépendamment le dirigeable et le RPC. Les résultats des simulations numériques sont présentés et montrent la robustesse de ce contrôleur.

Title : Modeling and control of a cabel driven parallel manipulator suspended by a heavy lift airship

Keywords : Heavy lift airship, Cable driven parallel manipulator, Control of cargo loading and unloading

Abstract :
In the recent years, researchers have become increasingly interested in the development of radically new and sustainable transportation modes for both passengers and cargo. These challenges have led to study in areas of knowledge that were dormant, such as the potential of using lighter than air aircraft for cargo transportation. The focus of this thesis is the development of a control architecture that can be integrated on autonomous heavy lift airship and thereby enables safe cargo exchange process. Besides, the dynamic model of the heavy lift airship must be clarified before designing a controller. This system makes use of a Cable Driven Parallel Manipulator (CDPM), allowing the airship to load and unload cargo while hovering.
The heavy lift airship is a multi-body systems in which multiple rigid bodies are joined together. During loading and unloading process, the transferred cargo can oscillate due to airship maneuvers. On the other hand, the pendulum-like behavior of suspended load can alter the flight characteristics of the airship. The thesis contributions are presented in two parts. In the first part, we assume that there is no inertial coupling between the airship and CDPM. Hence, our research concerns only the CDPM tacking into account the base mobility at first and then the cable sagging phenomena. The control design should integrate an optimal tension distribution since cables must remain in tension.
In the second part, we address the analysis of the heavy lift airship considering the coupling effect between the suspended payload and the airship. To describe the dynamics coupling, the basic motion of one subsystem is regarded as an external disturbance input for the other one. Hence, the dynamic model of this multi-body system composed of the airship and the CDPM can be modeled as an interconnection of lower order subsystems. We assume that the heavy lift airship is a weakly coupled subsystems. Based on this assumption, we design a decentralized controller, which makes it possible to control the airship and the CDPM independently. Numerical simulation results are presented and stability analysis is provided to confirm the accuracy of our derivations.

Université Paris-Saclay
Espace Technologique / Immeuble Discovery
Route de l'Orme aux Merisiers RD 128 / 91190 Saint-Aubin, France